UNIV
LIBRARY
21/6/05
OF ADELAIDE

The University of Adelaide

Australian School of Petroleum

Geological Evaluation of the Eocene Latrobe Group in the Offshore Gippsland Basin for CO_2 Geosequestration

Robert Root
B. App. Sc., M.Sc.

Supervisor: Dr. Simon Lang

Submitted in fulfilment of the requirement
for the degree of Doctor of Philosophy

June 2005

Table of Contents

Abstract vi
Statement of Originality vii
Acknowledgements viii
List of Figures ix
List of Tables xv

Chapter 1—Introduction 1
Abstract 1
Introduction 1
AIM OF THIS STUDY 2
Environmental, Socio-economic and Political Significance 3
Sequestration Options for CO_2 5
CO_2 Geosequestration Analogues and Lessons Learned 11
Physical and Chemical Properties of CO_2 13
PHYSICAL PROPERTIES OF CO_2 13
CHEMICAL PROPERTIES OF CO_2 21
Methodology 24
CONTRIBUTIONS OF OTHER RESEARCHERS 25
DATA 26
Overview of the Gippsland Basin 27
BASIN HISTORY 30
Structure and Stratigraphy of the Central Deep Area 31
Gippsland Basin and CO_2 Storage 32

Chapter 2—Sedimentology 35
Abstract 35
Introduction 35
Methodology 36
CORE DESCRIPTION 36
PETROGRAPHY 36
ANALOGUES 38
Lithofacies Descriptions 38
Facies Associations 46
MIDDLE AND UPPER SHORFACE 46
TIDAL CHANNEL 50
LOWER SHOREFACE 55
FORESHORE, BARRIER ISLAND, BERM 59
TIDAL DELTA 60
FLUVIAL CHANNEL 63
FLUVIAL OVERBANK 66
UNDIFFERENTIATED COASTAL PLAIN 68

Shelf 69
Pore-Scale Heterogeneity 71
Petrography of Nearshore Facies 72
Petrography of Coastal/Alluvial Plain Facies 75
Petrography of Shelf Facies 77
Petrographic Interpretation 79
Implications for CO_2 Geosequestration and Geological Model Construction 84

Chapter 3—Structure and Stratigraphy 89
Abstract 89
Introduction 89
Methodology 90
Seismic Interpretation 90
Well Tie and Horizon Mistie Analysis 91
Depth Conversion 93
RMS Amplitude Mapping 95
Horizon and Fault Modelling 95
Wireline Correlation 96
Structure 96
Stratigraphy 101
Seismic-Scale Stratigraphy 101
Wireline Log-Scale Stratigraphy 109
Depositional History 113
Lower M. diversus and L. balmei Palaeo-geography 116
Middle and Upper M. diversus Palaeo-geography 118
P. asperopolus Palaeo-geography 120
Lower N. asperus Palaeo-geography 122
Middle and Upper N. asperus Palaeo-geography 123
Implications for CO_2 Geosequestration and Geological Model Construction 124

Chapter 4—Analogues and Geostatistics 128
Abstract 128
Introduction 128
Horizontal and Vertical Data Density and Distribution 130
Depositional Environments and Spatial Continuity 131
Semi-Variograms 133
Categorical and Continuous Variables 134
Madograms 138
Modelling Madograms and Semi-Variograms 139

Methodology 141
Results 144
FLUVIAL ENVIRONMENTS 152
NEARSHORE ENVIRONMENTS 154
DELTAIC ENVIRONMENTS 156
VERTICAL SEMI-VARIOGRAMS 160
Discussion 161
VERTICAL SEMI-VARIOGRAMS 161
HORIZONTAL SEMI-VARIOGRAMS 162
STRATIGRAPHY AND PRESERVATION POTENTIAL 165
APPLICABILITY OF ANALOGUE MADOGRAMS AND SEMI-VARIGRAMS TO GEOLOGICAL MODELS 166

Chapter 5 –Seal Evaluation 169
Abstract 169
Introduction 169
Methodology 171
SEAL CAPACITY 171
SEAL GEOMETRY 173
SEAL INTEGRITY 175
Results 175
SEAL CAPACITY 175
SEAL GEOMETRY 186
SEAL INTEGRITY 189
Discussion of Seal Potential 192
TOP SEAL POTENTIAL 192
FAULT SEAL POTENTIAL—EMPIRICAL EVALUATION 193

Chapter 6—Geological Model Construction 197
Abstract 197
Introduction 197
Methodology 198
PETROPHYSICS 198
Model Geometry 199
GRID CELL SIZE 199
GRID ORIENTATION 203
ZONES 205
LAYERS 206
Attributes 208
DEPTH 210
VOLUME 210

FACIES 211
POROSITY 217
PERMEABILITY 225
WATER SATURATION 228
TEMPERATURE 233
PRESSURE 236
SALINITY 238
FAULT PROXIMITY 241
CO_2 COMPRESSIBILITY AND EXPANSION 243
Volumetrics 245
STRUCTURAL TRAPPING 249
GAS TRAPPING / RESIDUAL CO_2 250
MINERALOGICAL TRAPPING 250
DISSOLUTION 250

Chapter 7—Conclusions and Recommendations 255
Abstract 255
Introduction 256
Summary of Numerical Flow Simulation 256
Conclusions Relating to Geosequestration of CO2 in the Gippsland Basin 261
General Conclusions Relating to Geosequestration of CO2 264
Recommendations for Further Work 265

References Cited 269

Appendix I—Eastern Australasian Basin Symposium II Conference Paper 284

Appendix II—Geometry of Reservoirs and Seals (EXCEL file) on CD
Appendix III—Biostratigraphic Picks (EXCEL file) on CD
Appendix IV—Core Sample Depths and Analyses (Excel File) on CD
Appendix V—Well Locations and Basic Data (EXCEL file) on CD
Appendix VI—Well Temperature Data (EXCEL file) on CD
Appendix VII—Well Salinity Data (EXCEL file) on CD
Appendix VIII—Well Checkshot Data (EXCEL file) on CD
Appendix IX—Petrographic Point Count Data (EXCEL file) on CD
Appendix X—X-ray Diffraction Data (EXCEL file) on CD
Appendix XI—Core Analysis Data (EXCEL file) on CD
Appendix XII—Geological Model (GEOCARD file) includes wells, well markers, surfaces, grids, and; attributes on CD

Abstract

A geological evaluation of the Eocene Latrobe Group in the offshore Gippsland Basin was carried out to assess the technical feasibility of CO_2 geosequestration, which is a practical solution for reducing greenhouse gas emissions to the atmosphere.

The study area is characterised by a regional anticline plunging to the east-south-east with large-scale internal architecture comprising transgressive, retrogradationally stacked stratigraphy that dips gently landward and is unconformably truncated by overlying sealing units. The primary reservoir/aquifer targets for CO_2 injection are palaeo-shoreline parallel nearshore sandstone bodies characterised by high porosity and permeability (average ~25% and 100s mD) and good interconnectivity. The key regional sealing unit is the Lakes Entrance Formation, which consists of mudstone and marl capable of sealing large columns of CO_2 (~750 m).

A geocellular model was constructed for volumetric estimates and numerical flow simulation of CO_2 injection and storage. Rock properties were spatially populated in the model using depositional analogues and geostatistical techniques to represent realistic geological variability.

The proposed strategy for CO_2 geosequestration is to inject CO_2 outside four-way structural closure to allow up-dip fluid migration to the north then west governed by the structure of regional sealing units. This approach is associated with several advantages including: structural trapping in depleted hydrocarbon fields along the migration path; CO_2 migration perpendicular to stratigraphy to retard the rate of up-dip migration; and the leveraging of unconventional trapping mechanisms including residual gas trapping behind the mobile CO_2 plume and dissolution of CO_2 into formation water. Probabilistic estimates of CO_2 capacity utilising the proposed strategy indicate that 1395 – 2575 Mtonnes could be sequestered.

Numerical flow simulation of CO_2 injection at 10 Mtonnes/yr for 20 years showed that the proposed strategy was technically feasible with an expected arrival time of CO_2 at the first hydrocarbon field along the migration path 20 – 200 years after the end of injection, depending on the level of permeability heterogeneity. The key trapping mechanism was structural trapping in the short term and dissolution of CO_2 into formation water in the long term. After 2000 years ~40% of the injected CO_2 was dissolved in the formation water and CO_2 had not reached the westernmost hydrocarbon field indicating considerable extra capacity.

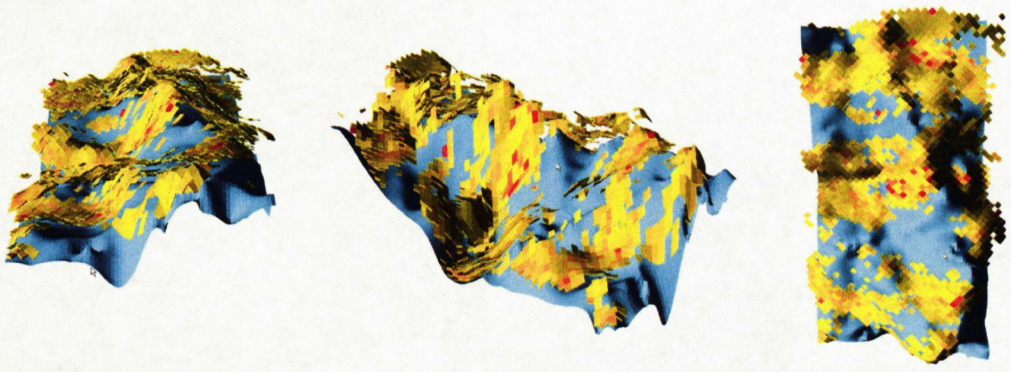

NAME: ROBERT ROOT PROGRAM: DOCTOR OF PHILOSOPHY

This work contains no material which has been accepted for the award of any other degree or diploma in any university or other tertiary institution and, to the best of my knowledge and belief, contains no material previously published or written by another person, except where due reference has been made in the text.

I give consent to this copy of my thesis, when deposited in the University Libraries, being available for photocopying and loan.

SIGNATURE: DATE: 24/4/07

Acknowledgements

I would particularly like to thank Simon Lang (ASP), Catherine Gibson-Poole (ASP), Jochen Kassan (Whistler Research), and John Bradshaw (Geoscience Australia) all of whom were exceptionally generous with their time, help, and ideas towards the completion of this study. Working with the APCRC GEODISC research group has been a unique pleasure. Thank-you to the management, particularly Andy Rigg and Peter Cook, and all of the researchers.

Special thanks to Geoscience Australia and the Victorian Department of Natural Resources and Environment for the provision of resources and data. GeoVisual and Schlumberger are thanked for technical support and software. From ChevronTexaco, Roger Bartlett and Seb Leigh were very generous in allowing me time off work to complete this thesis and Ian Taggart and Kemal Anbarci provided useful engineering input. Finally, the companies that sponsored this research are sincerely thanked for their support: BP, BHP Billiton, ChevronTexaco, TotalFinaElf, Shell, Woodside, and the Australian Greenhouse Office.

My sincere thanks to the following people who were instrumental in the completion of this study:

ASP
Nathan Ceglar
Ghazi Krishan
Richard Hillis
Jurgen Streit
Ric Daniel
John Kaldi
Maureen Sutton
Janet Hart
Takeshi Nakanishi
Tobi Payenberg
Scotty Mildren
Jerry Meyer
Rosalie Pollock
Aaron Cummings
Lester Davies

Geoscience Australia
Paula Cronin
Jane Blevin
Frank Brasil
Mark Webster
Paul Wilson
Victoria Mackie
Jenny Maher
Eddie Resiak

CSIRO (Perth)
Valorie Roy
Jim Undershulz
Claus Otto
Don Sherlock

CSIRO (Melbourne)
Jonathan Ennis-King
Lincoln Paterson

GeoVisual
Steve Tyson

Saros Group
Tim O'Sullivan

BHP Billiton
Mitch Ellis
Simon Horan

Victorian Department of Natural Resources and Environment
Kathy Hill
Bob Harms
Dee Ninis
Tania Bennell

Independent Consultants
Lynton Spencer
Alan Partridge

Schlumberger
Tom Kivior
Tony Hayball

List of Figures

Chapter 1—Introduction

Figure 1.1	Global mean temperature anomalies.	**3**
Figure 1.2	Temperature, CO_2 concentration and methane concentration 420,000 yrs before present.	**4**
Figure 1.3	Estimated global capacity of CO_2 sinks.	**6**
Figure 1.4	Seismic section showing the effect of subsurface CO_2 at Sleipner Vest Field in the North Sea.	**11**
Figure 1.5	Phase diagram for carbon dioxide.	**13**
Figure 1.6	Changes with depth in the density of CO_2 and the viscosity ratio between water and CO_2.	**14**
Figure 1.7	Conceptual comparison of CO_2 geosequestration in a depleted/disused field scenario and CO_2 geosequestration in a saline aquifer scenario.	**15**
Figure 1.8	Simulation of CO_2 injection, Frio Sandstone, Texas.	**17**
Figure 1.9	The effect of reservoir heterogeneity on CO_2 storage capacity in the Frio Sandstone, Texas.	**17**
Figure 1.10	Graph showing the influence of injection rate on two-phase flow behaviour and storage efficiency.	**18**
Figure 1.11	Flow simulation of CO_2 injection at Sleipner Vest Field.	**18**
Figure 1.12	Measured relative permeability of CO_2 from core flood experiments.	**20**
Figure 1.13	CO_2 solubility in water plotted against pressure at various reservoir/aquifer temperatures.	**21**
Figure 1.14	Simulation of CO_2 injection in a homogeneous reservoir at 930 and 3330 years after injection with CO_2 dissolution in formation water.	**22**
Figure 1.15	Workflow applied for geological model construction in this study.	**24**
Figure 1.16	Regional structure of the Gippsland Basin.	**27**
Figure 1.17	Gippsland Basin stratigraphy.	**28**
Figure 1.18	Map of the Gippsland Basin showing major structural features and the locations of oil/gas fields.	**29**
Figure 1.19	Conceptual NW-SE cross-section of the Gippsland Basin.	**31**
Figure 1.20	Map of Australia showing the results of source-sink matching for CO_2 storage.	**33**

Chapter 2—ESSCI Sedimentology

Figure 2.1	Tarwhine 1, 2665.78-2665.99: Pebble-cobble conglomeratic sandstone with normal grading and parallel stratification.	**40**
Figure 2.2	Whiting 1, 2685.59-2685.77: Fine- to medium-grained cross-bedded and ripple cross-laminated sandstone.	**40**
Figure 2.3	Tarwhine 1, 2667.79-2667.91: Fine- to medium-grained, conglomeratic, cross-bedded sandstone overlain by parallel stratified sandstone.	**40**
Figure 2.4	Fortescue 1, 2425.22-2425.35: Very fine- to fine-grained, parallel stratified sandstone with *Arenicolites*, *Planolites*, *Thalassinoides*, and *?Skolithos* burrows.	**41**
Figure 2.5	Luderick 1, 1855.50-1855.63: Swash-stratified upper shoreface sandstone with mild bioturbation.	**41**
Figure 2.6	Fortescue 1, 2421.66-2421.96: Swash-stratified sandstone with moderate bioturbation.	**41**

Figure 2.7	Fortescue 1, 1853.64-1853.67: *Ophiomorpha* burrow.	**41**
Figure 2.8	Seahorse 2, 1505.60-1505.72: Medium- to coarse-grained poorly consolidated sandstone with an *Ophiomorpha* burrow.	**41**
Figure 2.9	Luderick 1, 1839.42-1839.58: Large vertical burrow interpreted as *Diplocraterion* burrow in fine-grained sandstone.	**42**
Figure 2.10	Whiting 1, 2685.40-2685.52: Very fine- to fine-grained ripple cross-laminated and wavy bedded sandstone and small irregularly shaped, mud-filled, horizontally or obliquely oriented burrows (*Planolites*).	**44**
Figure 2.11	Fortescue 1, 2434.35-2434.47: Heavily bioturbated sandstone, siltstone and mudstone with little resolvable primary structure.	**44**
Figure 2.12	Seahorse 2, 1503.42-1503.55: Bioturbated, interbedded very fine-grained sandstone and mudstone.	**44**
Figure 2.13	Wrasse 1, 2597.24-2597.36: Calcareous mudstone.	**44**
Figure 2.14	Wrasse 1, 2750.50-2750.72: Moderately bioturbated glauconitic sandstone.	**45**
Figure 2.15	Marlin 4, ~2249.20m: Faulted and fractured mudstone.	**45**
Figure 2.16	Key for graphic logs.	**46**
Figure 2.17	Core description for Fortescue 2.	**49**
Figure 2.18	Core description for Fortescue 2 (continued).	**50**
Figure 2.19	Core description for Snapper 5.	**52**
Figure 2.20	Core description for Seahorse 2.	**53**
Figure 2.21	Core description for Wirrah 1.	**54**
Figure 2.22	Core description for Fortescue 1.	**57**
Figure 2.23	Core description for Luderick 1.	**58**
Figure 2.24	Holocene barrier island setting, Bethany Bay, Delaware.	**60**
Figure 2.25	Core description for Marlin 4.	**62**
Figure 2.26	Core description for Barracouta 5.	**63**
Figure 2.27	Core description for Tarwhine 1.	**65**
Figure 2.28	Core description for Whiting 1.	**66**
Figure 2.29	Core description for Veilfin 1.	**68**
Figure 2.30	Core description for Marlin 1.	**70**
Figure 2.31	Petrographic image for Barracouta 5.	**73**
Figure 2.32	Petrographic image for Luderick 1.	**73**
Figure 2.33	Petrographic image for Seahorse 2.	**74**
Figure 2.34	Petrographic image and SEM images for Fortescue 2.	**74**
Figure 2.35	Petrographic image for Snapper 5.	**75**
Figure 2.36	Petrographic image for Fortescue 1.	**75**
Figure 2.37	Petrographic image for Marlin 4.	**75**
Figure 2.38	Petrographic image for Tarwhine 1.	**76**
Figure 2.39	Petrographic image and SEM image for Veilfin 1.	**77**
Figure 2.40	Petrographic image and SEM images for Whiting 1.	**77**
Figure 2.41	Petrographic image for Wrasse 1.	**78**
Figure 2.42	Quartz, feldspar, and rock fragment diagram for the petrographic samples described in this study.	**80**
Figure 2.43	Porosity and permeability plotted against depth.	**82**
Figure 2.44	Routine core analysis porosity and permeability.	**83**
Figure 2.45	Width plotted against length for depositional facies of the study interval.	**87**
Figure 2.46	Thickness plotted against width for depositonal facies of the study interval.	**88**

Chapter 3—ESSCI Structure and Stratigraphy

Figure 3.1	Visualisation of the BaseSeal surface and intersecting seismic lines.	**91**
Figure 3.2	Comparison of 1974 vintage line (left) with a 1994 vintage line (right) at a line intersection.	**92**

Figure 3.3	Seismic coverage in the study area and colour-coded, average mistie at line intersections for BaseSeal and Horizons 1 - 4.	**92**
Figure 3.4	Two-way time plotted against depth for checkshots used in this study.	**94**
Figure 3.5	RMS amplitude plotted against coal thickness as a proportion of interval thickness.	**95**
Figure 3.6	Time structure map showing fault traces at Horizon 4 and at the BaseSeal horizon.	**97**
Figure 3.7	Seismic section from the Swordfish 1, Salmon 1, Veilfin 1 area to Snapper Field.	**98**
Figure 3.8	Major structural features of the study area.	**100**
Figure 3.9	West to east seismic line showing the Gippsland Basin ESSCI structure.	**101**
Figure 3.10	BaseSeal depth structure map.	**103**
Figure 3.11	Horizon 1 depth structure map.	**103**
Figure 3.12	Horizon 2 depth structure map.	**104**
Figure 3.13	Horizon 3 depth structure map.	**104**
Figure 3.14	Horizon 4 depth structure map.	**105**
Figure 3.15	West to east cross-section showing only seismic interpretation flattened on the BaseSeal surface.	**106**
Figure 3.16	Seismic interpretation with the sequences separated and Wheeler diagram.	**107**
Figure 3.17	Stratigraphic cross-section along depositional dip.	**111**
Figure 3.18	Stratigraphic cross-section along depositional strike.	**112**
Figure 3.19	Methodology for palaeo-geographic reconstruction.	**114**
Figure 3.20	RMS seismic amplitude in the study area.	**115**
Figure 3.21	Conceptual stratigraphic cross-section.	**117**
Figure 3.22	Conceptual palaeo-geography map for the Lower *M. diversus* and *L. balmei* interval.	**118**
Figure 3.23	Palaeo-geographic map for the Middle and Upper *M. diversus* stratigraphic interval.	**119**
Figure 3.24	Seismic line in the Marlin Canyon area.	**120**
Figure 3.25	Palaeo-geographic map for the *P. asperopolus* stratigraphic interval.	**121**
Figure 3.26	Palaeo-geographic map for the Lower *N. apserus* stratigraphic interval.	**122**
Figure 3.27	Palaeo-geographic map for the Middle to Upper *N. asperus* stratigraphic interval.	**124**
Figure 3.28	Seismic line from the Swordfish 1, Salmon 1, Veilfin 1 area to Snapper Field.	**125**
Figure 3.29	Seismic line showing a fault south of Sworfish-1 that is associated with significant displacement and propagates into sealing lithologies.	**126**

Chapter 4—Analogues and Geostatistics

Figure 4.1	Estimated ratios of horizontal to vertical anisotropy from various depositional environments	**130**
Figure 4.2	Directional experimental semi-variograms for porosity in the Gippsland Basin Study area.	**132**
Figure 4.3	Example of categorical facies variables and systems tracts identified on wireline logs.	**137**
Figure 4.4	Madograms along depositional strike and dip generated from a barrier island setting, Gelliondale area, SE Victoria.	**139**
Figure 4.5	Madograms along depositional strike and dip generated from a barrier island setting, Galveston Island area, Texas coast.	**140**
Figure 4.6	Locations of analogues used in this study.	**142**
Figure 4.7	Example facies map for trained madogram generation.	**143**
Figure 4.8	Depositional environment and scale of investigation for analogues used in this study.	**144**

Figure 4.9	Analogue madograms and semi-variograms for fluvial environments of deposition.	**153**
Figure 4.10	Analogue madograms and semi-variograms for nearshore wave-dominated environments of deposition.	**155**
Figure 4.11	Analogue madograms and semi-variograms for deltaic environments of deposition.	**157**
Figure 4.12	Analogue madograms and semi-variograms for various environments of deposition.	**158**
Figure 4.13	Generalised madograms and semi-variograms for particular kinds of depositional environments based on analogue data.	**159**
Figure 4.14	Vertical experimental semi-variograms calculated from petrophysical porosity and permeability data in the study area.	**160**
Figure 4.15	Conceptual example of the changes in a madogram for fluvial channel facies with respect to stratigraphic position (systems tract).	**166**

Chapter 5—Seal Evaluation

Figure 5.1	Typical geometry of sealing facies represented in the study area.	**174**
Figure 5.2	Map of regional sealing facies.	**176**
Figure 5.3	MICP curves for regional sealing facies within the study area.	**177**
Figure 5.4	MICP curves for intraformational seals of the upper Latrobe Group within the study area.	**178**
Figure 5.5	MICP curves for intraformational seals of the upper Latrobe Group within the study area cont...	**179**
Figure 5.6	MICP curves for intraformational seals of the upper Latrobe Group within the study area cont...	**180**
Figure 5.7	MICP curves for intraformational seals of the upper Latrobe Group within the study area cont...	**181**
Figure 5.8	MICP curves for intraformational seals and reservoirs.	**182**
Figure 5.9	MICP curves for upper Latrobe Group intraformational seals and reservoirs cont...	**183**
Figure 5.10	Threshold pressures plotted against facies type.	**184**
Figure 5.11	Threshold pressure for different depositional facies represented in the study area.	**185**
Figure 5.12	Analogue data of lateral extent for fine-grained facies of various depositional environments.	**187**
Figure 5.13	Comparison of seal geometry for different sealing units of the study area.	**189**
Figure 5.14	Rock compressibility and ductility for different lithologies in the study area.	**189**
Figure 5.15	Comparison of seal integrity for different sealing units of the study area.	**191**
Figure 5.16	Values for seal capacity, seal geometry, and seal integrity are multiplied to calculate seal potential. Plots are provided for each component.	**191**
Figure 5.17	West to east seismic line at Snapper Field.	**194**
Figure 5.18	West to east seismic line at Barracouta Field.	**194**
Figure 5.19	Southwest to northeast seismic line in the area near Tarwhine 1.	**195**
Figure 5.20	Modern day Gippsland bathymetry with SNIFFER survey and SAR data.	**196**

Chapter 6—Geological Model Construction

Figure 6.1	Grid cell size used in the geological model.	**201**
Figure 6.2	Comparison of grid cell size and width to length aspect ratios of depositional facies.	**202**
Figure 6.3	Comparison of grid cell size and thickness to width aspect ratios of depositional facies.	**202**

Figure 6.4	Conceptual flow lines showing flow paths parallel to the orientation of grid cell faces.	**204**
Figure 6.5	Geological model grid orientation.	**205**
Figure 6.6	Layering styles that can be applied within zones of the geological model.	**207**
Figure 6.7	Examples of layering relationships within the geological model.	**208**
Figure 6.8	Histogram of the CentreDepth attribute.	**210**
Figure 6.9	Histogram of cell volume attribute.	**211**
Figure 6.10	Categorical facies attributes representing lower shoreface-shelf, nearshore, and alluvial-coastal plain facies tracts in each zone of the geological model.	**213**
Figure 6.11	Scatter plot and histograms of porosity and permeability for facies measured from routine core analysis compared with histograms of porosity and permeability of facies from attributes in the geological model.	**215**
Figure 6.12	Facies used in the geological model, shown with reference to stratigraphic unit.	**216**
Figure 6.13	Histogram of log analysis porosity at the wells.	**217**
Figure 6.14	Spatial distribution of porosity at various layers in the geological model.	**222**
Figure 6.15	Six realizations of porosity with the grid sliced along NE and NW trending axes.	**224**
Figure 6.16	Scatter plot of attributes $KatWell_{arithmetic}$ and $KatWell_{harmonic}$.	**226**
Figure 6.17	Scatter plot of log permeability versus porosity at the wells.	**226**
Figure 6.18	Realisations of permeability distribution in the geological model using absolute permeability attributes generated from the harmonic mean and arithmetic mean of petrophysical permeability measurements at the wells.	**228**
Figure 6.19	Scatter plot of effective porosity and water saturation based on quantitative log analysis from wells in the study area.	**229**
Figure 6.20	Histograms of expected water saturation within structural closures in the study area assuming CO_2 charge.	**232**
Figure 6.21	Horner plot temperatures plotted against depth for wells within the study area.	**234**
Figure 6.22	Spatial distribution of temperature attribute within the geological model.	**236**
Figure 6.23	Spatial distribution of pressure attribute within the geological model.	**237**
Figure 6.24	Quantitative log analysis salinity (NaCl equivalent) versus depth in the upper Latrobe Group.	**239**
Figure 6.25	Histogram of salinity attribute (NaCl equivalent).	**239**
Figure 6.26	Various ranges of salinity displayed in the geological model.	**239**
Figure 6.27	Fault planes from which the proximity to fault attribute was calculated.	**242**
Figure 6.28	Spatial distribution of CO2ExpansionFactor attribute within the geological model.	**244**
Figure 6.29	Spatial distribution of the CO_2 capacity attribute within the geological model.	**247**
Figure 6.30	Probabilistic distribution of CO_2 capacity with no contribution from unconventional trapping mechanisms (dissolution, gas trapping & mineralogical trapping).	**252**
Figure 6.31	Probabilistic distribution of CO_2 capacity with estimated contributions from unconventional trapping mechanisms (dissolution, gas trapping & mineralogical trapping).	**253**
Figure 6.32	Tornado plot showing the impact of uncertainties on CO_2 capacity based on probabilistic estimates.	**254**

Chapter 7—Conclusions and Recommendations

Figure 7.1	One realisation of a reservoir flow simulation of the upper Latrobe Group ESSCI for 20 years, 200 years and 2000 years after CO_2 injection ceases.	**258**
Figure 7.2	Proportion of dissolved CO_2 over time for the base case model and three different permeability realisations.	**258**

List of Tables

Chapter 1—Introduction

Table 1.1	Global capacity estimates for geosequestration.	**7**
Table 1.2	Capacities of various ESSCI types in Australia.	**8**

Chapter 2—ESSCI Sedimentology

Table 2.1	Petrographic analyses carried out for this study.	**37**
Table 2.2	Upper Latrobe Group lithofacies.	**38**
Table 2.3	Relative abundance of lithofacies and facies associations.	**71**
Table 2.4	X-ray diffraction results for selected samples.	**78**
Table 2.5	Description of facies used in the geological model.	**85**

Chapter 3—ESSCI Structure and Stratigraphy

Table 3.1	Stratigraphic surfaces and units utilised in this study.	**108**

Chapter 4—Analogues and Geostatistics

Table 4.1	Geostatistical analogue locations and references.	**143**
Table 4.2	Analogue madograms and semi-variogram characteristics for different depositional environments.	**145**
Table 4.3	Generalised characteristics of vertical experimental semi-variograms for different facies.	**161**
Table 4.4	Vertical reservoir heterogeneity for different depositional environments.	**162**
Table 4.5	Horizontal directions of maximum and minimum spatial variance for different geological model zones.	**167**

Chapter 5—Seal Evaluation

Table 5.1	CO_2 column heights calculated from MICP data for depositional facies in the study area.	**186**
Table 5.2	Lateral extent of sealing units in the study area.	**188**
Table 5.3	Seal integrity for different sealing facies of the study area.	**190**

Chapter 6—Geological Model Construction

Table 6.1	Zones and surfaces in the Gippsland Basin ESSCI geological model.	**206**
Table 6.2	Attribute data included in the Gippsland Basin ESSCI geological model.	**208**
Table 6.3	Categorical facies attributes in the Gippsland Basin ESSCI geological model.	**212**
Table 6.4	Temperature data.	**233**
Table 6.5	Z-factors and gas expansion factors applied to the Gippsland Basin ESSCI geological model.	**245**
Table 6.6	Ranges for probabilistic CO_2 capacity estimates.	**251**

Chapter 1—Introduction

Abstract

Anthropogenic emissions of greenhouse gases to the atmosphere, particularly CO_2, have had a measurable impact on global climate over the last century. Presently, the most technically and economically feasible option for the storage of large volumes of CO_2 is geological storage (geosequestration). There are several options for geosequestration in Australia, including storage of CO_2 in depleted and disused hydrocarbon fields and utilisation of CO_2 for enhanced oil recovery and for enhanced coal bed methane recovery, but in terms of available storage capacity, geosequestration in deep saline aquifers is the most favourable option.

CO_2 behaves differently than hydrocarbon at reservoir conditions in terms of flow behaviour and chemical behaviour. CO_2 is soluble in water and can react chemically with some mineralogical rock components, which are key factors in assessing the technical feasibility of CO_2 geosequestration. Other important factors include the rate and direction of CO_2 migration, the style of multiphase flow, and pore pressure behaviour. These factors are controlled by many variables including: reservoir and seal geometry, internal reservoir heterogeneity at large and small scales, pressure/temperature conditions, the composition of the reservoir rock, and type/chemistry of the formation fluids. Operational controls such as injector well location and injection rate are also critical variables. Because of the complexity of the interrelated variables involved, numerical simulation is required to develop a predictive understanding of CO_2 behaviour in the subsurface.

The upper Latrobe Group in the Gippsland Basin 'central deep' area was chosen as a potential site for geosequestration because of its proximity to stationary emitters of CO_2, good data density and coverage, favourable regional seal potential, and good reservoir properties. The purpose of this study is two-fold:

- *To conduct reservoir characterisation and geological model construction for numerical simulation of CO_2 injection and storage to assess the technical feasibility of CO_2 geosequestration in the offshore Gippsland Basin 'central deep' area*
- *To identify the differences in methodology for constructing a geological model for CO_2 storage and traditional methodologies for constructing reservoir models for petroleum exploration and production (E&P) including natural gas storage.*

Introduction

Geosequestration has received increasing attention in the last decade as a bridging technology to reduce greenhouse gas emissions to the atmosphere while economic alternatives to fossils fuels are developed. Subsurface injection and long-term geological storage, or 'geosequestration', of carbon dioxide is a practical technology

with potential to reduce global greenhouse gas emissions. This study focuses specifically on the offshore Gippsland Basin in southeast Australia as an opportunity for geosequestration of CO_2. Before addressing the environmental, socio-economic and political drivers for geosequestration, critical technical questions associated with geosequestration need to be outlined:

- What is the volume of carbon dioxide that can be safely stored?
- What is the likely direction and rate of carbon dioxide movement/migration?
- What is the likely residence time of CO_2 in the subsurface?

Although well-developed petroleum exploration and production (E & P) techniques for reservoir characterisation and the construction of geological models are utilised in this study, some modifications to conventional workflows and methodologies are necessary when reservoir characterisation and geological model construction are applied to CO_2 geosequestration specifically. The construction of a geological model for CO_2 storage has different objectives and requires a different approach to the construction of a geological model for petroleum E & P, including natural gas storage, for the following reasons:

- Chemically and physically CO_2 behaves differently to hydrocarbon and saline water/brine at reservoir conditions.
- The stored CO_2 does not to have to be recovered in the foreseeable future.
- The behaviour of the CO_2 in the sub-surface has to be simulated thousand of years into the future at least.
- Very large volumes of fluid typically need to be stored.
- Reservoir models representing very large areas are generally required.
- The environmental, social, and health and safety risks associated with the possibility of uncontrolled release of CO_2 must be considered in addition to traditional commercial risk.

Aim of this Study

The aim of this study is to geologically characterise the Eocene upper Latrobe Group of the Gippsland Basin 'central deep' area and to construct a geological model as part of a technical evaluation for CO_2 geosequestration. A predictive understanding of subsurface CO_2 behaviour will be developed through integrated reservoir/aquifer characterisation, geological model construction, and numerical flow simulation to

develop a conceptual strategy for geosequestration. Critical questions regarding CO_2 storage capacity and subsurface residence/migration time will be addressed, and key risks and uncertainties will be identified. A second objective is to develop general conclusions and recommendations regarding the method applied to reservoir characterisation and geological model construction for CO_2 geosequestration.

Environmental, Socio-economic and Political Significance

In the last decade increasing evidence has come to light that anthropogenic greenhouse gas emissions, and particularly CO_2 emissions to the atmosphere, have had a measurable impact on global temperature (Zillman 2001). The rise in global mean temperature this century is thought to be between ~0.3°C – 0.6°C (Halmann & Steinberg 1999, Rochelle *et al.* 1999; Fig. 1.1).

A 'business as usual' scenario may result in a rise of global temperature by an average of 2°C in the next century (Halmann & Steinberg 1999). Although changes in the magnitude of global temperature in the geological past are thought to have been of greater or similar magnitude, the current rate of temperature increase may be unprecedented. The rate of climate change, rather than the magnitude of climate change, may be the most important factor for affecting global ecosystems (Rochelle *et al.* 1999). The rapid increase in the atmospheric concentration of CO_2 over the last century appears to exceed natural variation over the last 420,000 years (United States Department of Energy 2002; Fig. 1.2).

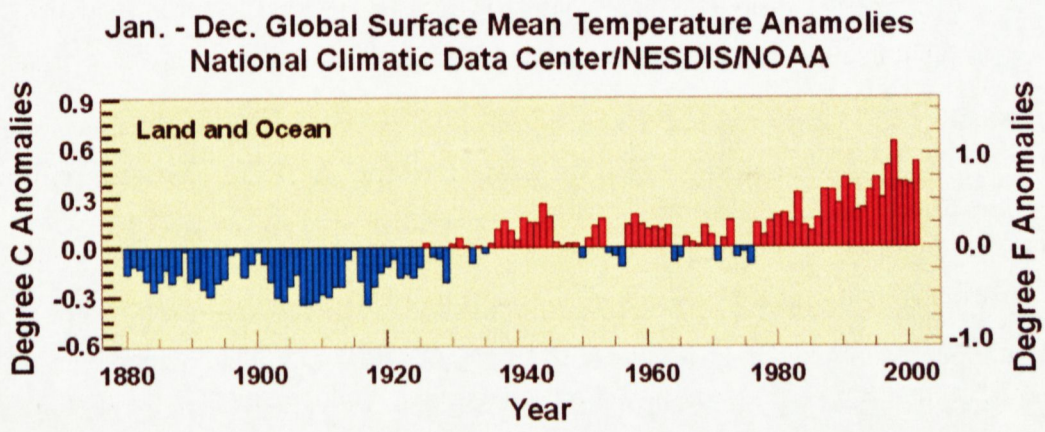

Figure 1.1 — Global temperature anomalies show a rise in global mean surface temperature of approximately 0.6°C during the last century (figure modified from the National Oceanic and Atmospheric Administration 2002).

The most important contributor to anthropogenic global warming is CO_2 emissions to the atmosphere as a result of fossil fuel consumption. Between one-half and two-thirds of the anthropogenic contribution to global temperature increase is thought to stem from CO_2 emissions (Rochelle *et al.* 1999, van der Meer *et al.* 2001, Halmann & Steinberg 1999). Energy consumption results in the release of 22 gigatonnes per year (Gt/yr) of CO_2 to the atmosphere globally, accounting for 85% of anthropogenic CO_2 emissions (Rochelle *et al.* 1999). The limiting factor for continued use of fossil fuel energy in the future is not likely to be scarcity of fossil fuels, but rather the atmosphere's limited ability to absorb carbon without inducing negative effects like global warming (Lenstra & Van Engelenburg 2001).

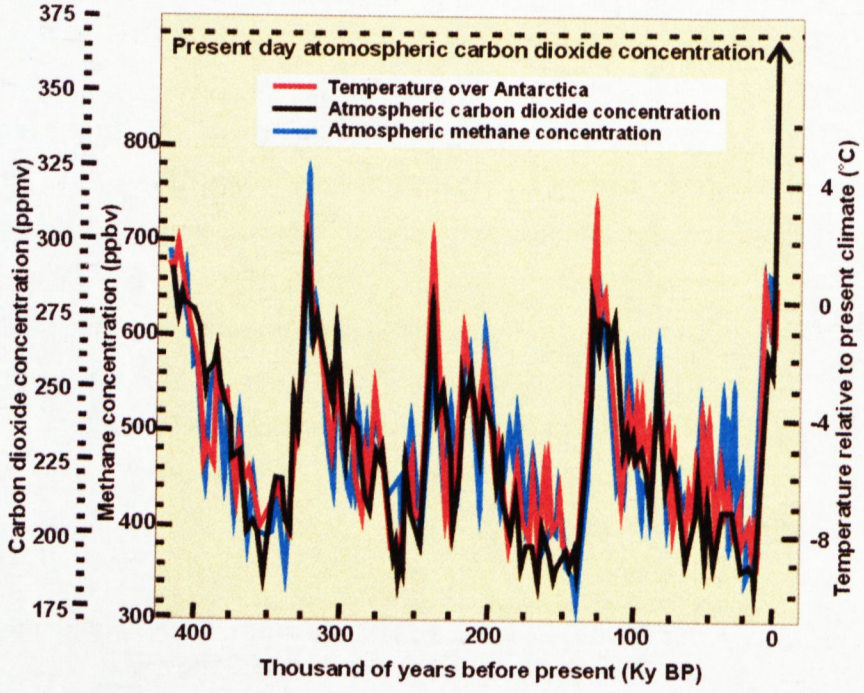

Figure 1.2 — Temperature, CO_2 concentration and methane concentration over the past 420,000 yrs before present. The present day level of atmospheric carbon dioxide is highlighted for comparison (~370 ppmv). Figure modified from the National Oceanic and Atmospheric Administration (2002).

Arguably, the most attractive option for reducing global greenhouse gas emissions is adopting alternative renewable energy sources; however, most countries are likely to remain dependent on fossil fuels well into the 21st century (Bachu *et al.* 1994, Eliasson 2001). A rapid move away from fossil fuels is not likely to be achievable without serious disruption to the global economy (Kaarstad 2002). As a result, emissions reductions from improved energy efficiency, from use of renewable energy sources, and from non-CO_2 mitigation strategies will not be sufficient to meet Kyoto

protocol targets in most developed countries. New technologies must be implemented and existing technologies must be refined in terms of reducing anthropogenic CO_2 emissions if we are to have a significant impact on atmospheric levels of CO_2 (Klara *et al.* 2003). In this respect, geosequestration of CO_2 may be viewed as a 'bridging technology' to stabilise atmospheric levels of CO_2 while more environmentally sustainable methods of energy generation are developed and implemented.

In Australia, Kyoto Protocol emissions targets are not likely to be met unless new solutions for the 'greenhouse problem' are found. Currently, Australia's projected emissions of greenhouse gases for the period of 2008 – 2012 are 111% of 1990 levels. Emissions in 1998 are equal to 117% of 1990 emissions if extensive land clearing within Australia in 1990 is not used in calculating 1990 CO_2-e emissions. The Kyoto Protocol target is 108% of 1990 emissions over the 2008 – 2012 period (The Australian Greenhouse Office 2002).

Although Australia is not a signatory to the Kyoto Protocol presently, government regulation of carbon emissions to the atmosphere appears likely for the near future. For the Australian energy industry, solutions to greenhouse gas emissions, and particularly CO_2 emissions, must be found now in anticipation of governmental enforcement of greenhouse gas emissions limits.

The Commonwealth of Australia is presently examining the feasibility and implications of greenhouse gas emissions trading in Australia. Additionally, the government has agreed in principle to award carbon credits to companies that take action to mitigate CO_2 emissions before the official implementation of a carbon credit trading scheme (The Australian Greenhouse Gas Office 2002). Clearly, emissions trading will be a direct economic incentive for Australian industry to reduce CO_2 emissions to the atmosphere.

Sequestration Options for CO_2

Sequestration options for CO_2 that are currently available, other than the earth's atmosphere, include:

- Ocean
- Biomass (e.g. trees and soils, algae)
- Mineral immobilisation (e.g. mineral carbonate)

- The earth's crust (geosequestration).

In practice, no single option for CO_2 sequestration is likely to be sufficient to stabilise or reduce the atmospheric levels of greenhouse gases. Ideally, a number of sequestration methods should be employed in parallel with global reduction of emissions to maximise the effectiveness of measures to mitigate global warming. However, the degree to which a single sequestration option will be effective is dependent on its particular technical, economic, environmental and political advantages and limitations.

The ocean is by far the largest potential sink for CO_2 with an expected long residence time (Fig. 1.3). The amount of CO_2 that would be required to double the present day atmospheric concentration would change the oceanic concentration by less than two percent (Herzog 1999). However, ocean storage is limited for a number of reasons (Bachu 2000, Gale 2002a, Gale 2002b): there is uncertainty associated with the behaviour of CO_2 in the deep ocean and uncertainty regarding the effect of CO_2 on the marine environment (Johnston & Santillo 2002). Additionally, the economics of CO_2 transport associated with ocean sequestration may be prohibitive. Most significantly, the environmental, societal, and legal implications of ocean sequestration are likely to be considered unacceptable globally (Bachu 2000, Bachu et al. 1994, Gale 2002b).

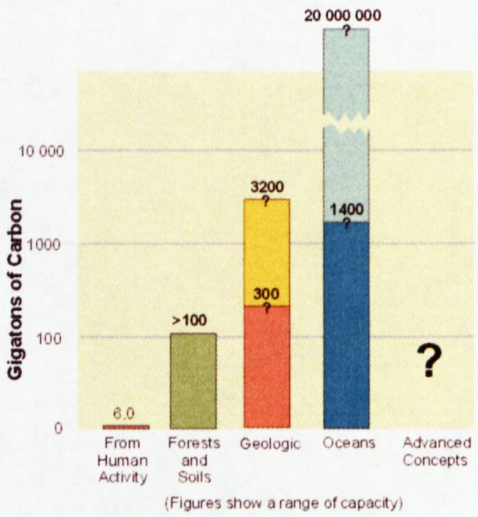

Figure 1.3 — Estimated global capacity of CO_2 sinks in gigatons of carbon (figure modified from the United States Department of Energy 2002).

Other sequestration options are also limited by economic and technical considerations. Sequestration of CO_2 in biomass is limited by uncertainty regarding

CO_2 residence times and by competition for land use (Bachu 2000, Bachu et al. 1994). Mineral immobilisation of CO_2 is primarily limited by high costs associated with the large quantity of mineral base required, and by slow reaction kinetics at normal pressures and temperatures (Freund 2001, Bachu *et al.* 1994).

Among the methods of CO_2 sequestration that are available, geological sequestration is thought to be the most technically and economically feasible. Residence times of CO_2 in the subsurface are likely to be very long and estimates of global geological capacity for CO_2 are considerable (Gale 2002b, Bachu 2000, Bachu *et al.* 1994, Bachu and Gunter 1999, Holloway 1997, Gunter & Perkins 1993, Studlick *et al.* 1990).

Estimates of the global total capacity for geological storage range from ~200 – 1100 Gt of CO_2 if a structural trap is required (Hendricks and Blok 1993, Hendricks and Blok 1995, Holloway 1997). However, a structural trap is not necessarily required for geosequestration of CO_2—CO_2 can be injected into very large (10s – 100s km^2), horizontal or gently dipping aquifers where the residence/migration time of the CO_2 is very long (1000s – 1,000,000 yrs; Bachu *et al.* 1994). Because of the very long residence time of CO_2 in some aquifers without four-way structural closure, the CO_2 is 'trapped' in the reservoir/aquifer for practical purposes. Consequently, global estimates of CO_2 capacity in the world's sedimentary basins must be markedly increased (Table 1.1). Estimates of global capacity for geological CO_2 sequestration are associated with considerable uncertainty, but total capacity is thought to be sufficient for several hundred years of global emissions (Holloway 1997).

Table 1.1: Global capacity estimates for geosequestration (from Gale 2002a).

Storage Option	Global Capacity	
	Gt CO_2	% of emissions to 2050
Depleted oil and gas fields	920	45
Deep Saline Aquifers	400 - 10,000	20 – 500
Unminable coal seams	20	<2

The various options for geological storage of CO_2 in Australia have been reviewed in Bradshaw & Rigg 2001; Cook *et al.* 2000; Rigg & Bradshaw 2001 and Rigg *et al* 2001. Risked assessment of 65 potential sites for CO_2 storage showed that sufficient pore volume for ~743,000 million tonnes (Mt) of CO_2 exists in Australia. This pore volume capacity is sufficient to store more than 1600 times the Australian annual CO_2

emissions based on 1998 emissions estimates (Bradshaw *et al.* 2002b, Bradshaw & Rigg 2001; Table 1.2). The options for geosequestration of CO_2 in Australia include:

- Storage in deep unused brackish or saline water-filled reservoir rocks
- Storage in depleted oil and gas reservoirs
- Storage in deep, unminable coal seams
- Storage in large voids or cavities in salt beds salt domes or bedded carbonates
- Use of CO_2 for enhance oil recovery (EOR); and use of CO_2 for enhanced coal bed methane recovery (ECBMR).

Table 1.2: Capacities of various ESSCI* types in Australia (from Bradshaw *et al.* 2002b).

Primary Trap Type	No. of ESSCIs	Secondary Trap Types	Total Risk Capacity (TCF)	Million Tonnes CO_2	No. of 1998 yrs emissions (= 8.5 TCF or 456 Mt)	% of total	% of No. of ESSCIs
ECBM	2	-	<1	24	<<1	<<1%	3%
Structural	28	14	567	30,395	67	4%	43%
Stratigraphic	7	5	296	15,905	35	2%	11%
Hydrodynamic (saline aquifers)	28	24	12,979	696,322	1527	94%	43%
Mineralogical		2					
TOTALS	65	45	13,842	742,646	1629	100%	100%

*** ESSCI = Environmentally Sustainable Site for CO_2 Injection.**

Few depleted/disused hydrocarbon reservoirs are presently available for CO_2 storage in Australia. However, more will become available as mature hydrocarbon assets are depleted. Depleted/disused hydrocarbon reservoirs are attractive for CO_2 storage because they have proven containment potential for a fluid less dense than water (i.e. oil or hydrocarbon gas), and because they are generally associated with large/comprehensive datasets (well data and seismic) that permit rigorous assessment of their technical viability for CO_2 storage. However, the total volume of CO_2 that can be stored in depleted/disused hydrocarbon fields in Australia is small by comparison with the volume of CO_2 that can be stored in saline aquifers. An additional challenge for the near term is that hydrocarbon fields are typically not available for CO_2 storage until they have been depleted—in some cases

simultaneous hydrocarbon production and CO_2 injection may damage or minimise the hydrocarbon resource.

ECBMR opportunities exist in Australia currently because of abundant coal-rich basins, and are described by Bradshaw *et al.* (2002a). However, like depleted/disused hydrocarbon reservoirs, the volume of CO_2 that can be stored through ECBMR is relatively small by comparison with the amount of CO_2 that can be stored in saline aquifers. Similarly, opportunities for CO_2-EOR may be available in Australia, particularly where heavy oil and/or tight reservoir exist*. Despite relatively small capacities for CO_2 storage, the use of CO_2 for both EOR and ECBMR has the potential to generate income that will offset the cost of CO_2 geosequestration projects. EOR and ECBMR opportunities are likely to be locally important in Australia for niche markets, but limited in terms of reducing Australia's total greenhouse gas emissions (Bradshaw *et al.* 2002a).

For Australia, disposal of CO_2 in deep unused brackish or saline water-filled reservoir rocks may be the most feasible option for geological CO_2 storage (Cook *et al.* 2000). The total volume of CO_2 that can be stored in saline reservoirs is much greater than the volume of CO_2 that can be attributed to any of the other geological storage options (Table 1.2). Additionally, key technical uncertainties like storage efficiency and pressure limitations (addressed later in this chapter) are less important in the case of saline aquifer geosequestration because a much larger pore volume is generally available for CO_2 than in the case of depleted/disused hydrocarbon field geosequestration.

Commonly saline aquifer geosequestration opportunities utilise residence/migration time traps, discussed previously, rather than conventional four-way closures, but are still thought to have potential for long residence time and large capacity. For example, simulation of CO_2 storage in the Petrel Sub-basin, Northwest Shelf Australia, indicated that ~ 400 tcf (21,500 Mt) of CO_2 could be stored permanently, without utilising a four-way structural or stratigraphic trap (Ennis-King & Paterson 2001).

Despite the considerable advantages of CO_2 storage in saline aquifers there are also disadvantages. For example, the containment risk associated with CO_2 storage in aquifers is unproven unless a non-hydrostatic pressure gradient has been maintained

in the aquifer (Lindeberg 1997, Kaarstad 2002). Additionally, saline aquifers are generally characterised by a paucity of well and seismic data, so technical uncertainty may be higher and/or the cost associated with data acquisition and interpretation for rigorously characterising aquifer and seal prior to CO_2 injection may be higher than in the case of a depleted/disused hydrocarbon field.

The prospect of utilising residence time/migration traps for CO_2 naturally leads to the question: how long must the CO_2 remain in the subsurface to be considered effective as a mitigation strategy? Presently there is considerable interest around the issue of target geosequestration residence time (Lindeberg 2002), which is a legislative, social and political issue as well as technical and environmental. However, there appears to be growing consensus in the scientific community around the 1000 – 10,000 year timeframe as a reasonable residence time expectation. A number of lines of thought lead to this conclusion:

- If CO_2 geosequestration is to be an effective carbon mitigation strategy, CO_2 leakage to the atmosphere must not exceed trivial amounts over a time span of 100s of years (Hawkins 2002).

- Simulation studies show that the vast majority of CO_2 is likely to be immobile in the subsurface or dissolved in formation water after ~1000 – 10,000 yrs (e.g. Flett *et al.* 2003, Ennis-King & Paterson 2001).

- Residence time expectations greatly in excess of natural climatic cyclicity (e.g. ~100,000 yr eccentricity or ~20,000 yr precession cycles) may be unreasonable.

- Technical forecasts are associated with greater uncertainty as their prediction timeframe increases. Major unpredictable geological events, such as a tectonic re-adjustment, are likely to occur over very long, 'geological' time spans (> one million years?).

* CO_2 injection both decreases oil viscosity and swells oil in addition to provided pressure maintenance and conventional gas sweep.

CO_2 Geosequestration Analogues and Lessons Learned

Although geological storage of CO_2 is a relatively new concept, most of the required technology has been developed by the petroleum industry over the past few decades. Several petroleum industry projects that involve fluid injection and storage in the subsurface around the globe serve as good analogues for various aspects of CO_2 geosequestration.

The Statoil CO_2 sequestration project at Sleipner Vest Field in the North Sea is the only saline aquifer CO_2 geosequestration project with significant operational history (Fig. 1.4). CO_2 geosequestration at In Salah in Algeria has begun recently. There are several other planned CO_2 storage projects utilising saline aquifers and depleted/disused hydrocarbon fields including the Snovit project in Norway, and the Gorgon project in Australia, as well as a number of pilot/trial CO_2 storage projects (e.g. Frio Sandstone Project in Texas & Vacuum Field in New Mexico). However, because of the relative immaturity the CO_2 storage industry, it is useful to identify analogues from other industries and other kinds of projects.

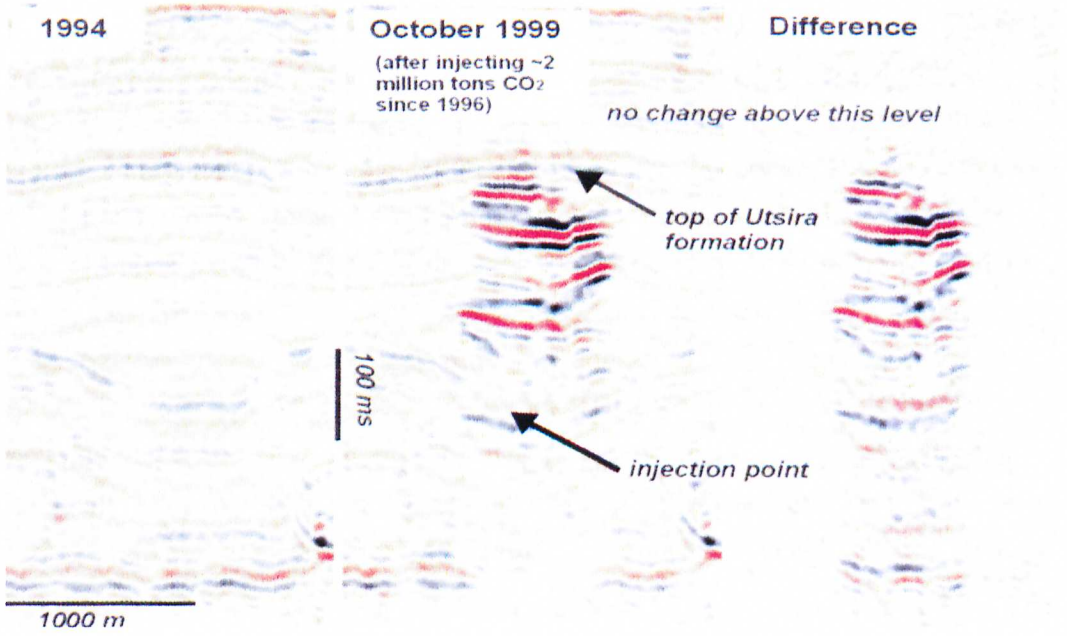

Figure 1.4 — Seismic section showing the effect of subsurface CO_2 at Sleipner Vest Field in the North Sea. Pre-injection (Left), post-injection (Middle) and the difference (Right) between pre- and post-injection seismic character is shown (figure courtesy of StatOil).

A number of EOR operations provide good analogues for disused/depleted hydrocarbon field storage, for example, the Weyburn Project in Saskatchewan, Canada (Wilson *et al.* 2001) and Rangely Weber Field in Colorado (Stevens *et al.* 2001, Bowker & Shuler 1991). Additionally, numerous hydrocarbon gas storage projects over several decades in North America and Europe have proven that geological storage of gas can be safe and effective. Notably, studies by Benson (2003) and Perry (2003) addressed analogues and identified lessons learned from other projects and industries as well as from natural CO_2 accumulations that can be applied to CO_2 storage. More than 40 acid gas injection projects have been carried out in Canada over the last 15 years, which also serve as useful analogues (Bachu *et al.* 2001). Acid gas has a considerable H_2S component* so it is more corrosive than CO_2 and it is toxic.

The risks associated with geological CO_2 storage are reasonably well understood largely because of analogous industries and practices. The greatest technical risk associated with geological CO_2 storage is the uncontrolled release of CO_2 either from failure at the injection well or pre-existing well penetrations, or from CO_2 leakage to the surface or seabed by way of an unforeseen subsurface migration pathway (Holloway 1997).

Studies of natural gas storage suggest that well penetrations are the most likely conduits for gas leakage to surface (Perry 2003). However, leakage of stored gas via geological conduits, particularly faults and fractures has also occurred. A key lesson learned from a number of analogous industries to CO_2 storage is that inadequate subsurface reservoir/aquifer characterisation resulting in inappropriate reservoir/aquifer selection or inappropriate injection/storage strategies is a key root cause of containment failures (Benson 2003). Despite the fact that CO_2 is neither toxic nor flammable, uncontrolled CO_2 release to the surface could represent an environmental and safety risk because high atmospheric and soil gas concentrations of CO_2 have adverse consequences for the health of animals (including humans) and plants.

* Acid gas is a by-product of 'sweetening' sour oil or gas and consists of a mixture of H_2S and CO_2.

Physical and Chemical Properties of CO_2

A number of physical and chemical characteristics of CO_2 at reservoir conditions influence feasibility of geosequestration including:

- Flow behaviour of CO_2 at reservoir conditions
- Dissolution of CO_2 into formation water
- Chemical reactions between CO_2 and mineralogical components of the aquifer/reservoir rock.

PHYSICAL PROPERTIES OF CO_2

Above 31.1°C and 7.38 MPA, CO_2 is in a supercritical phase. Supercritical CO_2 (SC CO_2) has a density that is similar to a liquid, but behaves as a gas because it fills all of the available pore volume and has a viscosity similar to that of a gas (Fig. 1.5). Because of its compressibility, storage of SC CO_2 is more efficient than storage of gaseous CO_2 by >100 times at typical reservoir conditions (Rochelle *et al.* 1999).

The sharp density increase associated with the phase change of CO_2 will occur at depths between 500 m – 1000 m in typical sedimentary basins (Ennis-King & Paterson 2001). The density difference between SC CO_2 and water is generally in the range of 0.3 – 0.7 g/cm^3 at aquifer/reservoir conditions. Consequently, SC CO_2 will (initially) rise through a water column (Holloway *et al.* 1996).

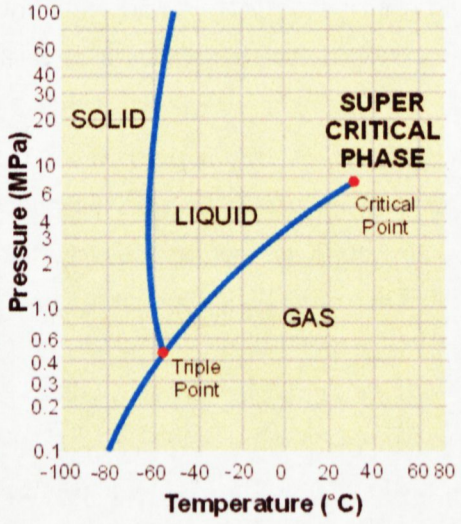

Figure 1.5 — Phase diagram for carbon dioxide (figure modified from Bachu 2000).

A key issue with regard to the volume of CO_2 that can be stored in a particular reservoir or aquifer is the percentage of the available pore volume that is filled by CO_2

(storage efficiency). The percentage of pore volume that SC CO_2 will occupy in the subsurface is a function of the ability of SC CO_2 to displace the *in situ* formation fluids. The areal efficiency of SC CO_2 displacing water improves with depth because the viscosity difference between the gaseous and liquid phase decreases with depth. However, the displacement efficiency of SC CO_2 at reservoir/aquifer depths that are likely to be utilised for CO_2 storage is unfavourable (Fig. 1.6).

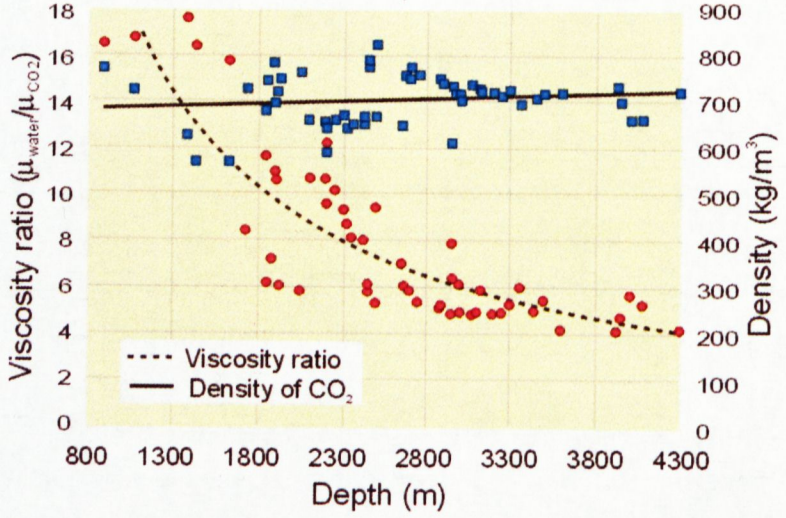

Figure 1.6—Changes with depth in the density of CO_2 and the viscosity ratio between water and CO_2. The density difference between CO_2 and water is virtually independent of depth. However, the viscosity difference between CO_2 and water decreases with increasing depth (figure modified from Holloway *et al.* 1996).

The implication of inefficient displacement of water is that CO_2 may take advantage of only a small percentage of the pore volume that would theoretically be available within a structural closure or along a migration path. For example, where CO_2 is injected into conventional structures with four-way closure the CO_2 may not fill all of the pore volume encompassed by the structural closure because of poor displacement efficiency. Instead, the CO_2 front may remain close to the top seal surface and migrate to the structural spill point before all of the pore space encompassed by the structural closure is filled (van der Meer 1992; Fig. 1.7).

Early simulation studies of geosequestration suggested very poor storage efficiency of CO_2 where only a very small percentage of the available pore volume was filled (e.g. van der Meer 1992, van der Meer 1995). However, more recent simulation indicated that storage efficiency varies in the range of 13% – 68% of pore volume depending on the characteristics of the geosequestration site and the prevailing

displacement mechanism and two-phase flow behaviour (Holt *et al.* 1995). Additionally, empirical data from CO_2-EOR suggests that CO_2 is stored in >20% of the total pore volume (Holt *et al.* 1995, Gale 2002a).

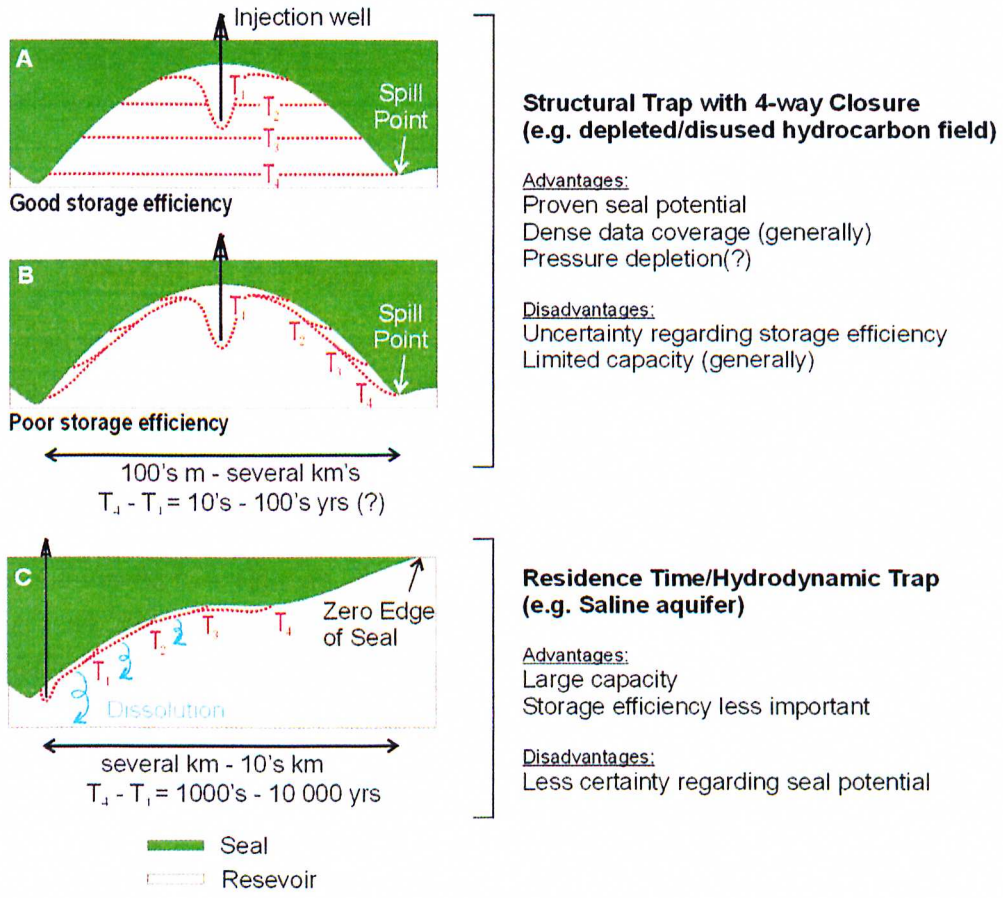

Figure 1.7—Conceptual comparison of CO_2 geosequestration in a depleted/disused field scenario (A & B) and CO_2 geosequestration in a saline aquifer scenario (C). The conceptual positions of CO_2 front with time are provided (represented by red, dotted lines). In the saline aquifer scenario (C), uncertainty regarding storage efficiency is less important because of the large available pore volume.

The storage efficiency of injected CO_2 is variable and is dependent on a number of 'site specific' factors, including (Doughty *et al.* 2002):

- Two-phase flow behaviour
- Trap structure/geometry
- Reservoir heterogeneity
- Porosity.

During CO_2 injection and storage two-phase flow is generally dominated by two competing flow behaviours: 'gravity override' and 'viscous flow'. The relative importance of these two kinds of two-phase flow behaviours is likely to influence storage efficiency as well as migration rate and direction. Flow dominated by gravity override is characterised by CO_2 rising buoyantly through the water column because of the density difference between formation water and SC CO_2. Consequently, low permeability barriers and seals to vertical fluid flow are typically important. The regional dip and geometry of the seal/reservoir interface, or the 'base seal surface', will be a major control on the behaviour of the injected CO_2 in a scenario where gravity override is the dominant flow mechanism.

In contrast, flow dominated by viscous forces may be characterised by permeability channelling in which SC CO_2 flows along high permeability pathways. The degree of reservoir heterogeneity and the injection pressure are important controls on the resulting flow pattern. Where reservoirs are characterised by a low degree of reservoir heterogeneity and low injection pressures gravity override will tend to be the dominant flow pattern. As the level of reservoir heterogeneity and injection pressure increases, viscous forces become more dominant and the flow pattern of the SC CO_2 becomes dependent on the correlation length of permeability in the direction of flow (Holt *et al.* 1995, Ennis-King & Paterson 2001).

In practice, the pressure gradient will decrease with distance from the injection well, and after injection ceases, so a combination of the viscous forces and gravity override is likely to occur in most CO_2 storage scenarios. Moreover, the period over which injection occurs will generally represent a small fraction of the total CO_2 storage timeframe (1000s – 10,000s yrs) so gravity forces are likely to be the dominant control in the long term (Lindeberg 1997).

The simulation results in Figure 1.8 from Doughty *et al.* (2002) show the subsurface distribution of gas saturation results from SC CO_2 taking advantage of high permeability pathways due to reservoir heterogeneity as it rises to the top of the reservoir/aquifer. The storage efficiency, and consequently the CO_2 capacity, increases with greater reservoir heterogeneity and as viscous flow become more dominant (Fig. 1.9). However, in some cases storage efficiency is decreased as viscous flow becomes more dominant (Fig. 1.10). The relationship of two-phase flow

behaviour and storage efficiency is dependent on the specific site and geosequestration strategy.

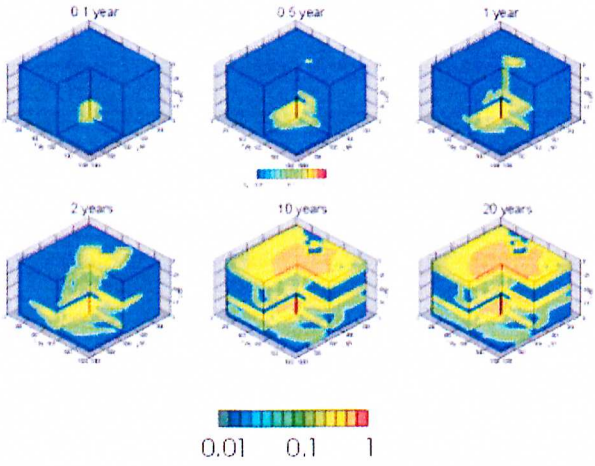

Figure 1.8—Simulation of CO_2 injection from Doughty *et al.* (2002). CO_2 saturation is represented by the colour bar.

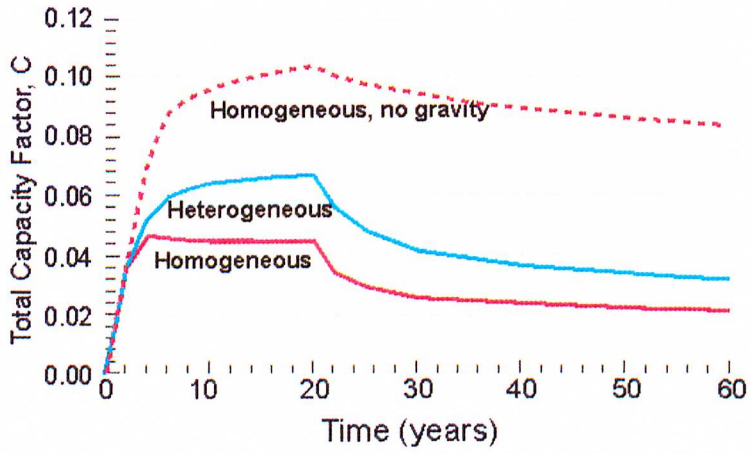

Figure 1.9—The effect of reservoir heterogeneity on CO_2 storage capacity in the Frio Sandstone, Texas (figure modified from Doughty *et al.* 2002).

The importance of reservoir heterogeneity for the subsurface behaviour of CO_2 is evident at Sleipner Vest in the North Sea, where CO_2 has been injected since 1996. Shale layers that act as intra-reservoir seal/baffle units markedly affect the pattern of CO_2 distribution in the reservoir/aquifer by creating a tortuous path for the vertical migration of SC CO_2. This is illustrated by reservoir simulation conditioned by time-lapse 3D seismic monitoring (Torp and Gale 2002, Obdam *et al.* 2002, van der Meer *et al.* 2001; Fig. 1.11). Simulation results indicate that SC CO_2 initially migrates

upward until a shale unit is encountered that acts as a barrier to vertical migration and induces lateral migration of the SC CO_2 towards a local structural high. The seal is breached when the SC CO_2 concentration (or column) builds up sufficiently at the structural high (van der Meer *et al.* 2001).

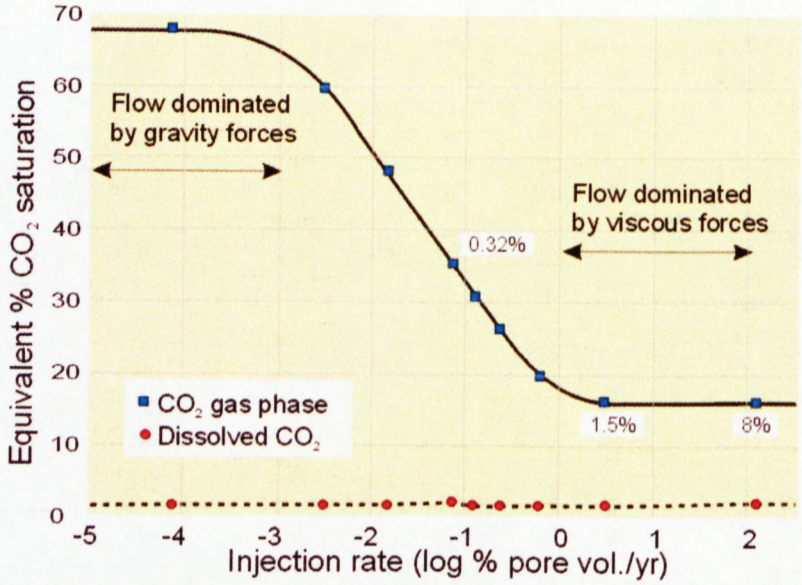

Figure 1.10—Graph showing the influence of injection rate on two-phase flow behaviour and storage efficiency. CO_2 saturation increases as injection pressure increases and viscous flow becomes more dominant (figure modified from Holloway *et al.* 1996).

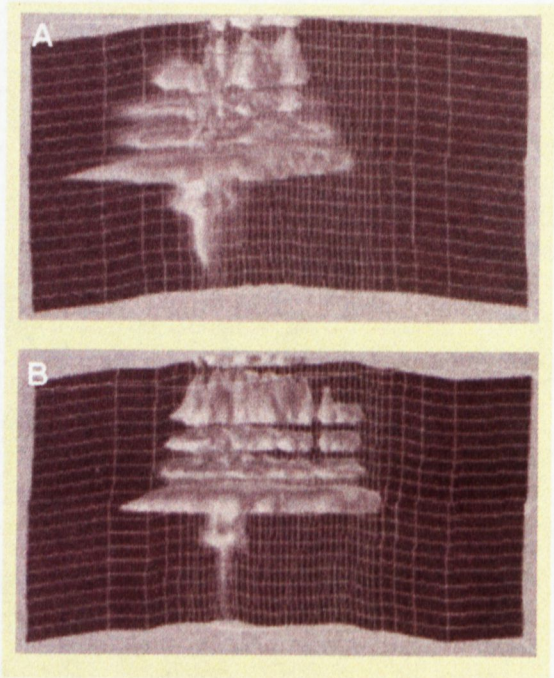

Figure 1.11—Numerical flow simulation of CO_2 injection at Sleipner Vest Field, which has been history matched with time lapse 3D seismic reflection data. Two perpendicular cross-sections of a simulation result are shown (A & B). Intra-reservoir shale units that act as barriers to vertical SC CO_2 migration (figure from van der Meer *et al.* 2001).

Of the parameters that influence the ratio of viscous flow and gravity-dominated flow, only the injection pressure is controlled by the operator. The maximum allowable reservoir pressure, which is generally defined by the difference between the hydrostatic pressure gradient and the fracture gradient of the reservoir/aquifer, is the main control on injection pressure. Because the injection pressure is limited by the fracture gradient of the reservoir/aquifer dramatic changes to the injection rate for the purpose of improving storage efficiency will be limited in practice without increasing injection well count. Careful selection of the reservoir/aquifer and selection of injector well locations, target injection zones, well design, and completion strategies may be the primary opportunities to maximise storage efficiency.

The structure, pore volume and storage efficiency of CO_2 governs the total CO_2 capacity, as discussed previously. However, in closed hydraulic systems the reservoir/aquifer pressure is another primary control on the volume of CO_2 that can be injected. Injection of CO_2 into limited aquifer systems or depleted/disused depletion-drive hydrocarbon fields will result in significantly greater pressure increases than CO_2 injection into very large or 'infinite' aquifer systems. In the case of closed hydraulic systems there is a limited volume of fluid (and rock) to buffer pressure increase.

Obdam *et al.* (2002) suggested that up to a five-fold increase in storage capacity could be achieved (in some geosequestration scenarios) if reservoir pressure can be increased to leak-off pressure. However, CO_2 containment risk increases with significant pressure increase because the risk of mechanical failure of faults, fractures and rock is greater when formation pressure is significantly altered. Additionally, high aquifer/reservoir pressure requires greater compression for injection, which impacts on project cost. Consequently, the difference between hydrostatic pressure and fracture (leak-off) pressure for a given aquifer/reservoir is a key characteristic that affects suitability of a site for CO_2 geosequestration. Obdam *et al.* (2002) suggests that aquifer pressure can be increased by 1.35 times leak-off pressure at depths between 0 m and 1000 m, and 2.4 times leak-off pressure at depths between 1000 m and 5000 m, as a general rule.

In general, the uncertainty regarding storage efficiency and pore pressure increase is less important where a residence/migration time trap within a very large saline aquifer is utilised because a large volume of interconnected pore space is generally available. Where a residence/migration time trap is utilised for CO_2 storage the rate and direction of SC CO_2 migration may be the most important factor for evaluating

feasibility for CO_2 geosequestration. The rate of CO_2 migration is important because no subsurface migration path is infinite. In the absence of structural closure the terminus of the flow path may defined by the zero edge of the regional seal, bubble point pressure/volume/temperature (PVT) conditions for CO_2, or some location thought to be associated with adverse consequences if contacted by migrating CO_2 (e.g. hydrocarbon reserves/resources or existing well penetrations).

Some general conclusions can be drawn for selecting appropriate residence/migration time traps. A gently dipping seal/reservoir interface and a low rate of hydrodynamic flow will result in a low rate of SC CO_2 migration. Low SC CO_2 migration rates are favourable in the context of CO_2 storage because residence time is likely to be longer. As a result, reservoirs/aquifers of moderate permeability may be preferable to high permeability reservoirs/aquifers for CO_2 storage (Bachu *et al.* 1994).

Residual CO_2 left along the migration path is another important factor for assessing the viability of a residence/migration time trap. The proportion of residual CO_2 behind the migrating plume is a function of relative permeability and the capillary properties of the aquifer/reservoir rock (Fig. 1.12). Residual CO_2 or trapped gas may represent a significant proportion of the injected volume (30% – 50%), particularly where long migration paths are utilised and where rock properties are favourable for gas trapping (Ennis-King and Paterson 2001, Flett *et al.* 2003). A percentage of the total volume of SC CO_2 will also dissolve into the formation water, which is described below.

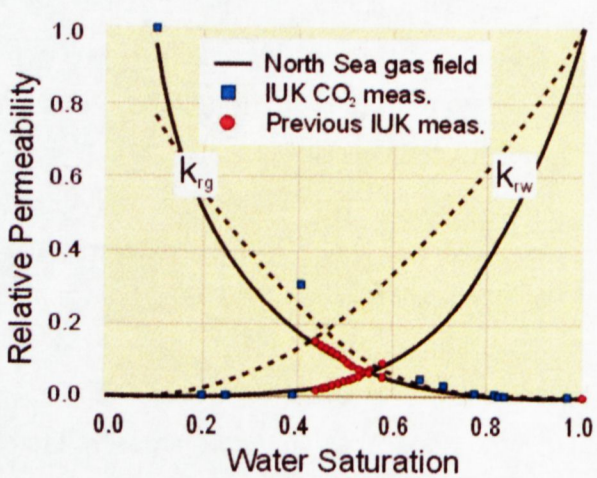

Figure 1.12—Measured relative permeability of CO_2 from core flood experiments. Two data sets for relative permeability of CO_2 are provided (blue and red). Figure modified from Holloway *et al.* 1996.

CHEMICAL PROPERTIES OF CO_2

Carbon dioxide is soluble in water. Solubility increases with increasing pressure and decreases with increasing temperature and salinity (Fig. 1.13). Most simulation studies show that over the lifetime of injection (tens of yrs) virtually all SC CO_2 will be in the free gaseous phase (Holloway *et al.* 1996); however, given a long enough timeframe, dissolved CO_2 in formation water will be the dominant form of storage (Gale 2002a). The solubility of CO_2 in 1 molar (M) brine is 41 – 48 kg/m^3 and 24 – 29 kg/m^3 in 4M brine (Ennis-King & Paterson 2001). Estimates by Bachu *et al.* (1994) and Ennis-King & Paterson (2001) indicate that 10% - 30% of the injected CO_2 can dissolve into formation water over the lifetime of injection (10 to a few 10s of years). Simulation studies suggest that complete dissolution is likely to occur over 1000s – 10,000s of years (Ennis-King *et al.* 2002).

Brackish and dilute formation waters are preferable for CO_2 storage because the solubility of CO_2 decreases with salinity. Higher solubility of CO_2 in brackish or dilute formation waters will also promote mineralogical trapping (see next section). Regardless of the salinity of formation water, the dissolution of irreducible CO_2 trapped behind the mobile plume will take longer than dissolution of 'free' CO_2 because the formation water in the proximity of the irreducible CO_2 is likely to be already saturated with respect to CO_2 (Ennis-King & Paterson 2001).

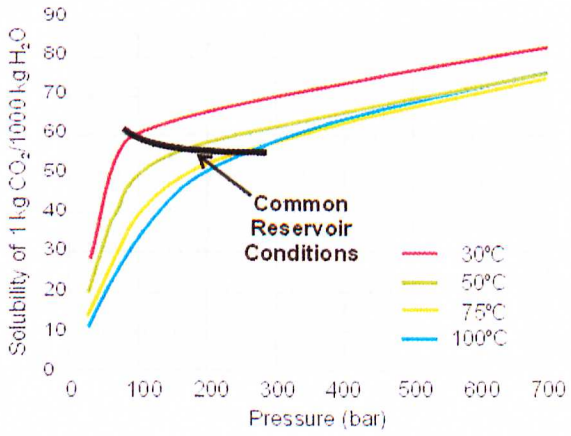

Figure 1.13 — CO_2 solubility in water plotted against pressure at various reservoir/aquifer temperatures (figure modified from Holloway *et al.* 1996).

When SC CO_2 is dissolved into the formation water the resulting polar bonded CO_2 and H_2O molecules are denser than the formation water. Consequently, a 'density inversion' is induced and dissolved CO_2 will sink in the water column (Ennis-King & Paterson 2001, Kaarstad 2002; Fig. 1.14). The pattern and direction of CO_2 migration

would probably be largely controlled by the rate and direction of hydrodynamic flow and partly by the geometry of the basal seal rather than the top seal. In the case of ESSCI sites without four-way structural closure, it is necessary to assess whether any SC CO_2 in the gaseous phase will reach the zero edge of the seal or bubble-point depth* before all of the SC CO_2 is dissolved into the formation water (Bachu *et al.* 1994, Ennis-King & Paterson 2001). This may be a critical factor for assessing the technical feasibility of CO_2 geosequestration in many residence/migration time trap scenarios.

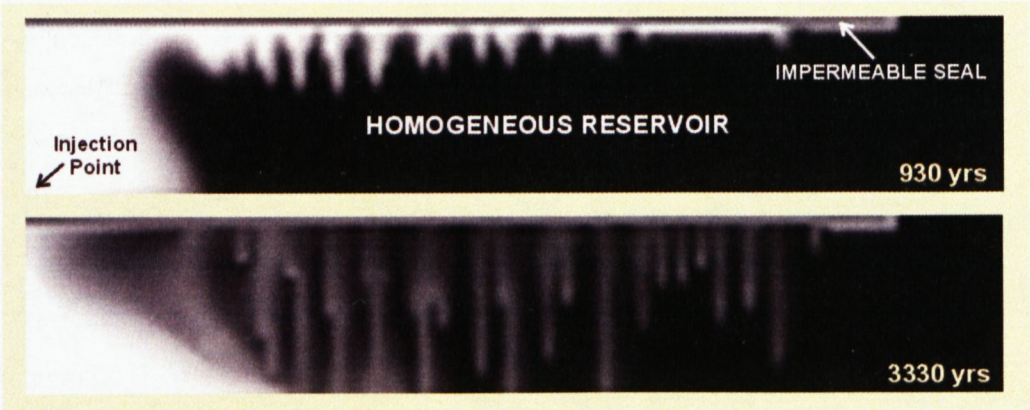

Figure 1.14 —Simulation of CO_2 injection in a homogeneous reservoir at 930 and 3330 years after injection. CO_2 is represented by white, formation rock and water by black. Viscous fingering of CO_2 dissolving into formation water is evident (figure courtesy of Jonathan Ennis-King, CSIRO).

Chemical reactions resulting in 'mineralogical trapping' can occur during CO_2 storage if appropriate mineralogy is present within reservoirs/aquifers. Mineralogical trapping describes a series of chemical reactions between formation rock/water and CO_2 that result in the chemical inclusion and precipitation of CO_2 within carbonate minerals. Where CO_2 is precipitated as a stable carbonate mineral the CO_2 is essentially permanently trapped in the subsurface.

In silicate reservoirs the amount of CO_2 that can be mineralogically stored by the dissolution of silicate minerals and the precipitation of carbonate minerals is limited by the availability of Ca^{2+}, Fe^{2+} and Mg^{2+} (Gunter & Perkins 1993, Bachu *et al.* 1994). As a result, reservoirs rich in basic silicate minerals are advantageous for promoting mineralogical storage of CO_2. Sodium-rich reservoirs will result in an increase in

* 'Bubble point depth' is the depth at which pressure and temperature conditions will result in phase change from supercritical CO_2 to gaseous CO_2.

bicarbonate ions within the formation water and consequently, will increase the solubility of CO_2 within the formation water* (Gunter & Perkins 1993). Even if the reservoir mineralogy is advantageous for mineralogical trapping, the reaction kinetics are thought to be relatively slow, particularly precipitation of carbonate minerals from the formation water. At Rangely Field in Colorado, which has operated as a CO_2-EOR project in a siliciclastic reservoir since 1986, there is little evidence of mineral sequestration of CO_2 (Klusman 2003). In the long term however (i.e. 1000s of years), mineralogical trapping may permanently store up to 20% of the injected CO_2 (Gale 2002b). A simplified reaction is provided showing the reaction of anorthite with CO_2 and H_2O to produce kaolinite and calcite (Bachu *et al.* 1994).

$$CaAl_2Si_2O_8 + CO_2 + 2H_2O \rightarrow Al_2Si_2O_5(OH)_4 + CaCO_3$$

(anorthite + carbon dioxide + water → kaolinite + calcite)

Chemical reactions induced by CO_2 injection may change the flow properties of the reservoir/aquifer rock. During the initial stages of injection in silicate reservoirs dissolution of reservoir rock should be the dominant process, so permeability is not likely to decrease significantly around the injector well (Gunter & Perkins 1993). Additionally, formation water will be moved away from the injector well(s) during injection, which also reduces the probability of chemical reactions altering fluid flow properties of rock in close proximity to the injector wells. Core flood experiments with CO_2 in partially carbonate-cemented silicate reservoir also suggest no net change in permeability. The permeability increase that was expected from the dissolution of carbonate cement was offset by permeability reduction from the migration of clays/fines (Bowker & Shuler 1991). However, both the dissolution/precipitation and the migration of fine-grained materials due to injection have the capacity to influence permeability. Another area of interest is the effect that chemical reactions induced by CO_2 injection will have on the sealing characteristics of sealing lithology. Little is known at present regarding the effect of chemical reactions between CO_2 and formation rock on the textural and mechanical properties of the formation rock, but it is an area of on-going research (Kirste *et al.* 2004).

* The increased 'salting out' effect, which decreases CO_2 solubility in water is more than compensated for.

Methodology

The basic methodology for the construction of 3D, stochastic geological models is well established in the petroleum industry, with numerous case studies in the literature, some of which address the Gippsland Basin specifically (e.g. Fink *et al.* 2002, Hinton *et al.* 1994, Henzell *et al.* 1984). The general methodology applied in this study is diagrammatically summarised (Figure 1.15).

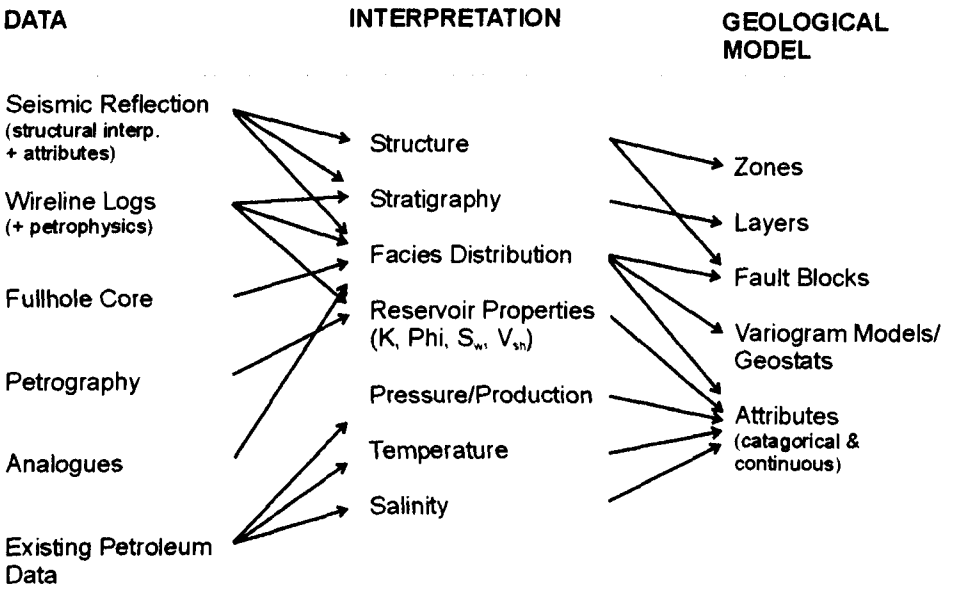

Figure 1.15—Workflow applied for geological model construction in this study.

A number of data types were integrated to produce the basic components of a geological model: zones, layers, fault blocks, statistical models and attributes. The majority of effort in constructing a geological model is associated with data collection, interpretation and manipulation to ensure internal consistency of data sets to make them suitable for the reservoir model. Much of the data used in the model was generated through various reservoir/aquifer characterisation tasks including:

- Seismic interpretation
- Wireline correlation
- Detailed core description
- Petrographic description
- X-ray diffraction
- Scanning electron microscopy

- Formation evaluation for the generation of porosity, permeability, shale volume and water saturation.

These pre-modeling tasks are associated with methodologies that are not addressed in this chapter, but are addressed instead in the methodology sections of the chapters that follow. The specific methodology applied for constructing the reservoir model is discussed in Chapter 6. For reference, the chapters which describe the methodologies for the tasks carried out in this study are listed below:

Chapter 2: ESSCI Sedimentology

- Core description
- Petrography
- Analogue selection.

Chapter 3: ESSCI Structure and Stratigraphy

- Wireline correlation
- Seismic interpretation
- Mistie Correction
- Depth Conversion
- Attribute Generation.

Chapter 4: Analogues and Geostatistics

- Geostatistical model generation (semi-variograms & madograms).

Chapter 5: Top Seal Evaluation

- Mercury Injection Capillary Pressure (MICP).

Chapter 6: Reservoir Model Construction

- Zone, layer and grid cell definition
- Conditional simulation and attribute population.

CONTRIBUTIONS OF OTHER RESEARCHERS

A number of researchers did work for this study. Specifically, Ghazi Krishan (NCPGG/Santos) point counted petrographic samples and took all of the transmitted light and scanning electron microscopy pictures included in this thesis. X-ray

diffraction was conducted at the Queensland University of Technology. Hydrodynamic study was carried out by Claus Otto, Valorie Roy, and Jim Underschulz (CSIRO Perth). MICP sample preparation and analysis was carried out by Rick Daniel (NCPGG) and Amdel. Petrophysical analysis for determination of porosity, permeability, shale volume and water saturation was carried out by Tim O'Sullivan (Saros Group). Numerical flow simulation was conducted by Jonathan Ennis-King and Lincoln Paterson (CSIRO Melbourne).

DATA

Data for this study were provided by Geoscience Australia, the Victorian Department of Natural Resources and Environment, BHP Billiton and Wiltshire Geological Services. The following data were used in this study:

- Seismic reflection lines (Geoscience Australia—GA)
- Digital wireline data (Wiltshire Geological Services)
- Seismic Navigation Data (Victorian Department of Natural Resources and Environment—VNRE)
- Conventional well data: locations, datums, well status (VNRE well completion reports—WCR)
- Checkshot data (VNRE WCRs)
- Palynological data (GA & VNRE WCRs)
- Temperature, pressure and salinity data (VNRE WCRs)
- Routine core analysis (RCA) and special core analysis (SCAL) data (VNRE WCRs).

Primary data acquisition carried out for this study included:

- Thin section preparation and analysis (Australian School of Petroleum—ASP)
- X-ray diffraction and Scanning Electron Microscopy (ASP and Queensland University of Technology)
- MICP analysis of samples from full- hole core (ASP and Amdel).

Overview of the Gippsland Basin

The Gippsland Basin is an east-west tending rift basin located off the southern coast of Victoria (Fig. 1.16) that was formed during the Early Cretaceous break-up of Australia and Antarctica. The Gippsland Basin is a fairly symmetrical rift basin bounded to the north and south by faulted terraces (Northern and Southern Strzelecki Terraces) and stable platforms (Northern and Southern Platforms). Major east – west-trending, basin-bounding fault systems—the Lake Wellington and Rosedale fault systems in the north, and the Foster and Darriman fault systems in the south—define the terraces and platforms.

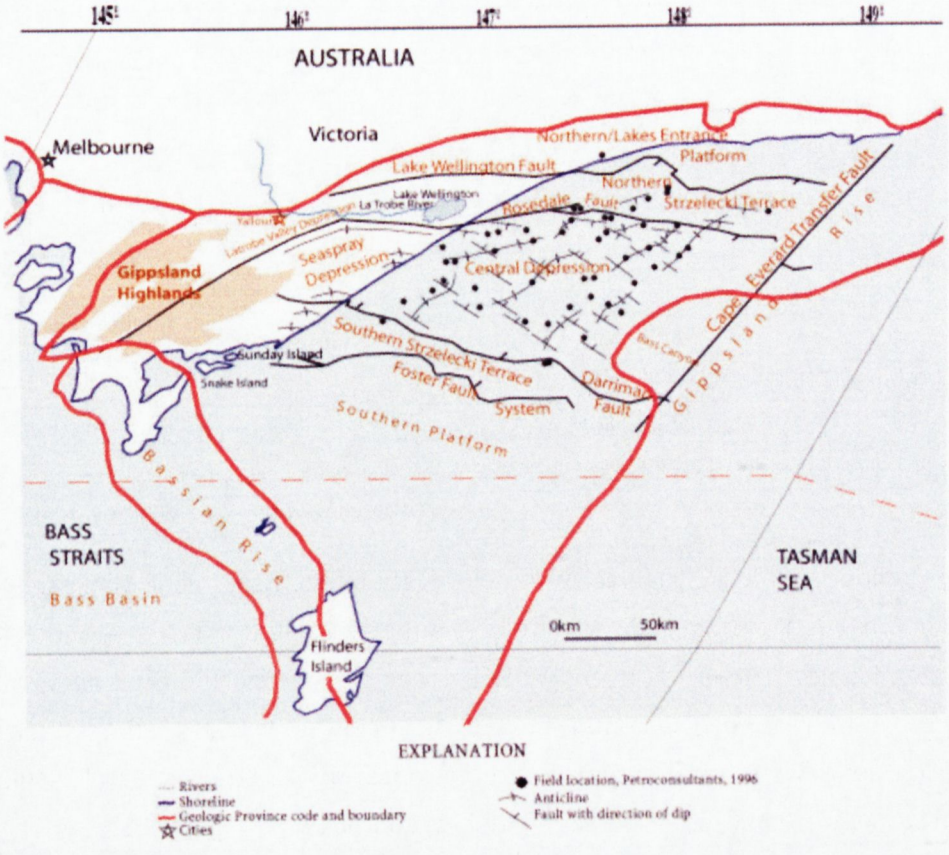

Figure 1.16—Regional structure of the Gippsland Basin (figure from Bishop 2000).

Since the mid-1960s the Gippsland Basin has been Australia's main hydrocarbon producing province with estimated reserves of 3.6 billion barrels of crude/condensate, 0.6 billion barrels of liquid petroleum gas, and 8.3 tcf of dry gas (Rahmanian *et al.* 1990). The Gurnard Formation and the Lakes Entrance Formation form a regional seal for the marginal marine reservoirs of the upper Latrobe Group. The upper Latrobe Group consists of sandstone, siltstone, mudstone and thick coal

packages, and represents the main oil and gas reservoir in the Gippsland Basin. The Gurnard and Lakes Entrance Formations consist of glauconitic sandstone, mudstone and marl. The most recent stratigraphic subdivision of the Gippsland Basin is provided in Figure 1.17 (Bernecker and Partridge 2001). Upper Latrobe Group reservoir/aquifer units evaluated in this study include parts of the Barracouta, Kingfish, Burong and Gurnard Formations. The convention adopted in this study is that stratigraphic units are referred to in terms of the spore-pollen biostratigraphic zone in which they occur (Helby *et al.* 1987).

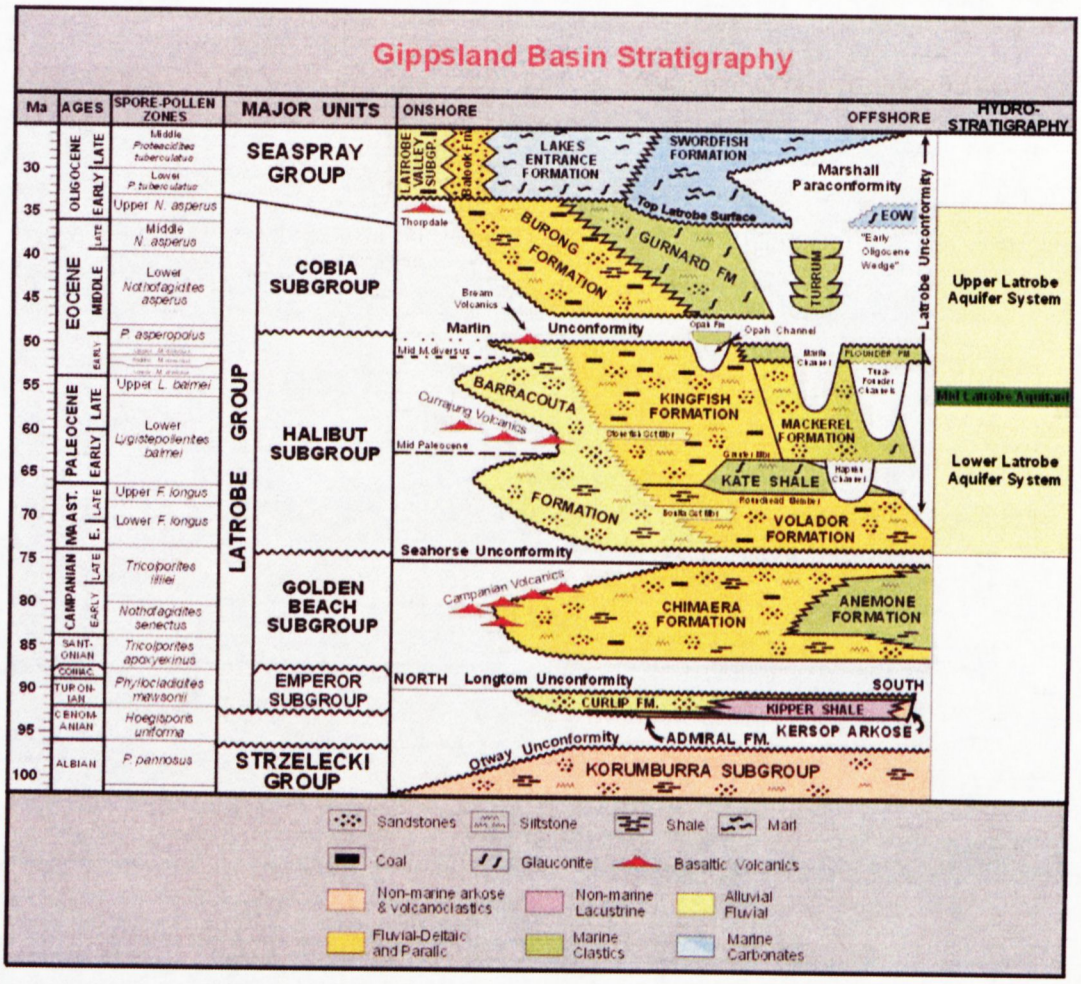

Figure 1.17 — Gippsland Basin stratigraphy. The study interval is indicated. The target for CO_2 storage is the upper Latrobe Group sandstone sealed by the Gurnard and Lakes Entrance Formations and the Marlin/Turrum submarine canyon complex. The key aquifer units are shown in the right hand track for reference. Figure from Bernecker and Patridge 2001.

The study area is located in the 'Central Deep/Depression' of the Gippsland Basin, where several producing gas and oil fields are located including Barracouta, Snapper and Marlin/Turrum Fields (Fig. 1.18).

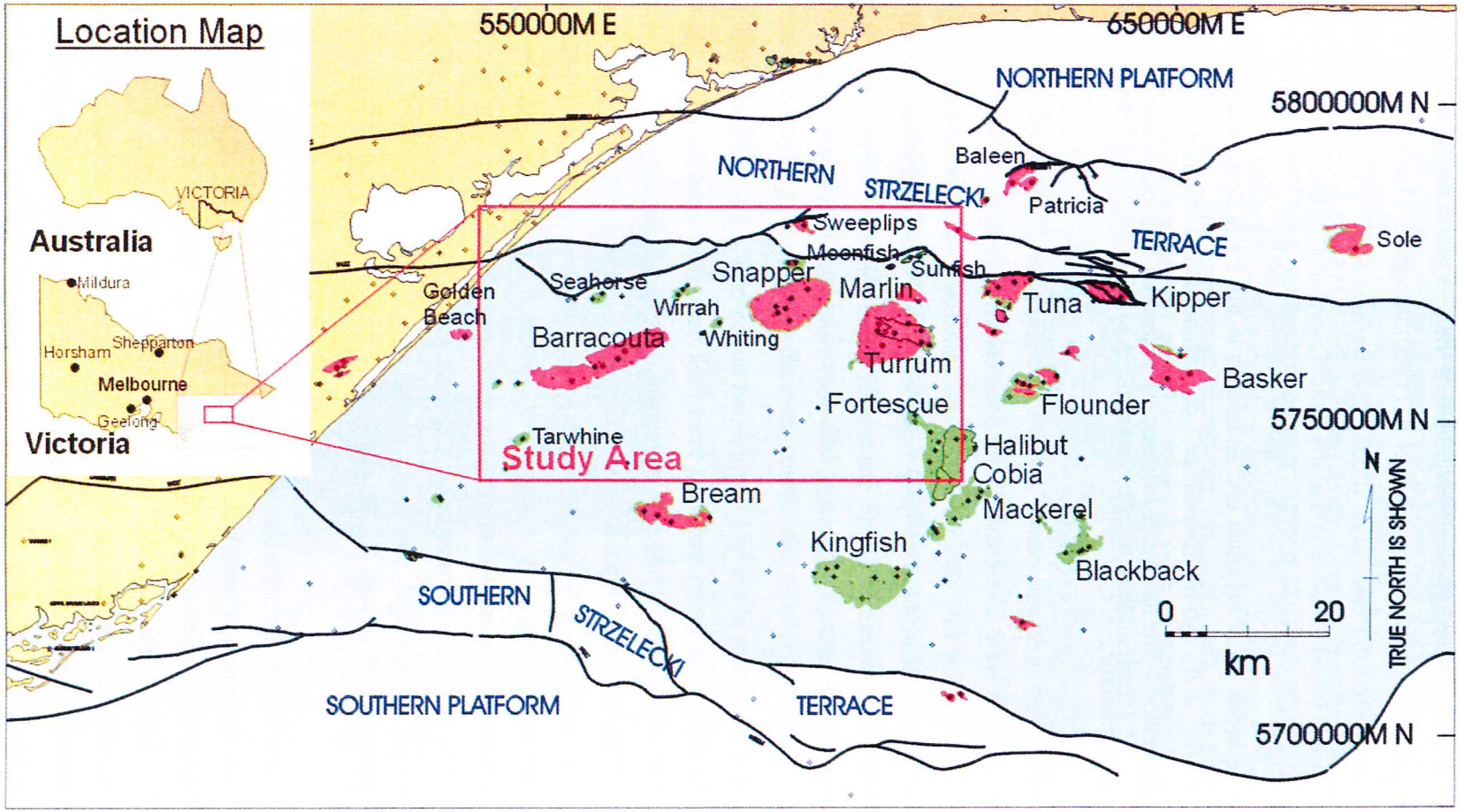

Figure 1.18 — Map of the Gippsland Basin showing major structural features and the locations of oil/gas fields (figure courtesy of the Victorian Department of Natural Resources and Environment).

BASIN HISTORY

The structural and stratigraphic development of the Gippsland Basin is described by Esso Australia Ltd (1988), Rahmanian *et al.* (1990), Megallaa (1993), Malek & Mehin (1998), Bishop (2000), Power *et al.* (2001), and Bernecker & Partridge (2001) among others. There is broad consensus that the tectonic evolution of the Gippsland Basin is essentially governed by the following regional tectonic events:

- The break-up of Australia and Antarctica in the Early Cretaceous resulted in pre-rift and syn-rift deposition of volcaniclastic sediments in alluvial depositional environments followed by extensive regional erosion during the Cenomanian.

- Rifting resumed associated with the opening of the Tasman Sea. Quartzose sediments were deposited during progressive encroachment of the sea from the southeast with periods of basaltic volcanism. Another period of regional erosion is interpreted to have occurred in the late Campanian, which may have been associated with compression and formation of the Bassian Rise that separates the Gippsland Basin from the Bass Basin to the southwest.

- After formation of the late Campanian unconformity the tectonic character of the Gippsland Basin switched from fault controlled subsidence to thermally controlled marginal sag. Up to four kilometres of Latrobe Group siliciclastic sediments were deposited with basin depocentres shifting progressively north, north-west. A transition from alluvial to nearshore marginal marine, and then to offshore fully marine shelf mudstone and glauconitic sandstone deposits is represented through the Eocene strata. The key interval of interest in this study, the Eocene upper Latrobe Group, was deposited late during the period of marginal sag and represents the last influx of major clastic deposition prior to the onset of structural inversion and regional erosion.

- Compression and inversion within the Gippsland Basin probably began in the Late Eocene and continued into the Oligocene. The transition from Latrobe Group clastic sediments to the Oligocene to Miocene limestones and marls of the Lakes Entrance and Gippsland Limestone is marked by a regional unconformity termed the 'top Latrobe surface'. This surface indicates the onset of a second period of NNE-SSW tectonic compression and mild basin inversion that has continued periodically to the present day.

Structure and Stratigraphy of the Central Deep Area

Structure in the 'central deep' area is characterised by NW – SE-trending, high-angle, normal bounding faults, many of which have been reactivated as reverse and strike-slip faults. A second synthetic fault set trends WNW – ESE and may act as linkages between the bounding NW – SE-trending faults. Most hydrocarbon accumulations in the 'central deep' area are associated with four-way closures, generally related to the regional E – W or NE – SW-trending structure (e.g. Barracouta, Snapper, Marlin, Turrum fields). Less commonly, combined structural and stratigraphic traps are formed from the angular truncation of reservoir units by submarine canyons at the upper Latrobe unconformity (e.g. Fortescue, Cobia, Halibut fields).

The stratigraphy of the upper Latrobe Group in the 'central deep' area is characterised by broadly transgressive stacking patterns and the top Latrobe angular unconformity (Fig. 1.19). Transgression is generally linked to allocyclic causal mechanisms (Rahmanian et al. 1990). Subsidence was driven by thermal sag and eustatic sea level was characterised by a punctuated rise of ~100 m (Shafik *et al.* 1998). Palaeo-climatic conditions during the mid- to late-Eocene were probably characterised by temperate climatic conditions with moderate to high rainfall (Veevers 1984).

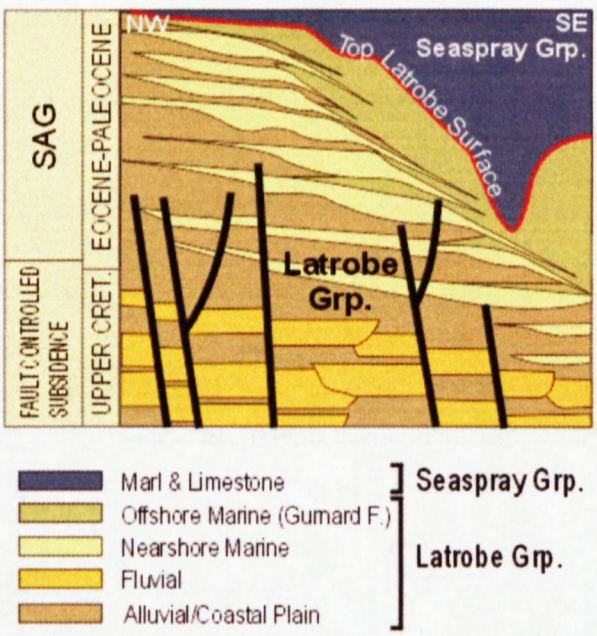

Figure 1.19—Conceptual NW-SE cross-section of the Gippsland Basin. Figure modified from Rahmanian *et al.* 1990.

Flow properties in the Gippsland Basin are influenced by primary depositional controls and by diagenetic alteration. The precipitation and secondary dissolution of carbonate cement is a strong secondary control on porosity and permeability occlusion and enhancement in some areas (Bodard *et al.* 1984). The incursion of a freshwater wedge from the present-day shoreline into the basin aquifer in combination with the position of major faults may influence the regional pattern of diagenetic alteration (Glenton 1988). Formation water salinity variations suggest that freshwater flushing occurs in the central deep area at depths down to 2400 m at least (Bishop 2000).

Gippsland Basin and CO_2 Storage

The Upper Latrobe Group ESSCI* was favourably rated in a risked regional assessment of potential CO_2 storage sites in Australia (Bradshaw *et al.* 2000, Bradshaw *et al.* 2002b). The Gippsland Basin ESSCI was deemed suitable as an ESSCI site for the following reasons:

- Proximity to stationary emitters of large quantities of CO_2
- Large estimated storage capacity for CO_2
- Dense data coverage (seismic and well data)
- Good reservoir flow properties
- Good seal potential of the regional sealing facies (Gurnard & Lakes Entrance Formations).

Twelve percent of Australia's CO_2-equivalent point-source emissions came from Southeast Victoria in 1998 (Bradshaw *et al.* 2002b). These emissions are primarily attributable to coal-fired powered stations in the Latrobe Valley (Fig. 1.20). Unproduced gas fields with high CO_2 content in the Gippsland Basin may also represent opportunities to sequester reservoir CO_2. Consequently, source to sink matching suggests that the Gippsland Basin represents the best opportunity to reduce Australia's annual CO_2 emissions with a single ESSCI option.

* ESSCI = Environmentally Sustainable Site for CO_2 Injection.

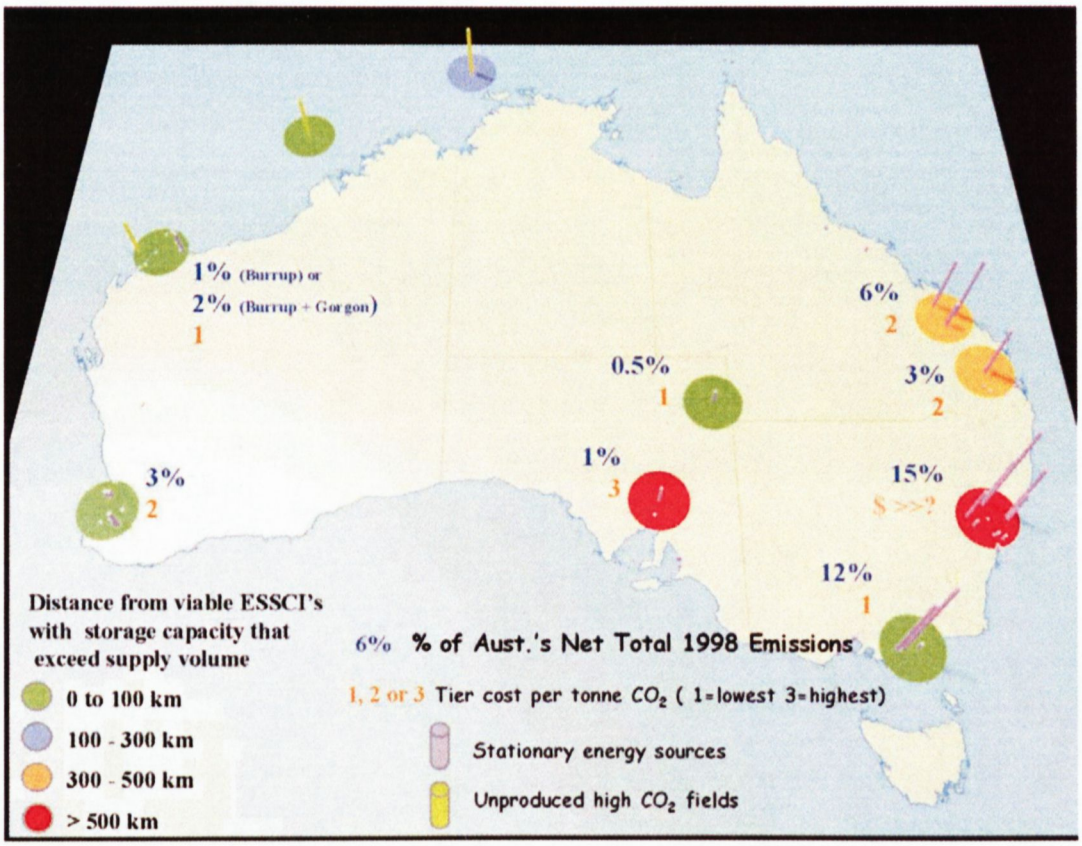

Figure 1.20—Map of Australia showing the results of source-sink matching for CO_2 storage. Point source emissions of CO_2, distance from a viable ESSCI site, and estimated economic viability is shown. Results are affected by large supply volumes, economics of scale, and storage capacity (figure from Bradshaw *et al.* 2002b).

Despite the considerable advantages associated with the Gippsland Basin as an ESSCI site, by comparison with other Australian basins the Gippsland Basin presents several relatively unique challenges that must be addressed in order to fully evaluate its potential for CO_2 storage. Among these are:

- The Gippsland Basin has an active hydrodynamic system by comparison with other Australian basins.
- Salinity ranges from brackish and dilute (~2000 ppm) to brine (>35,000 ppm).
- The Gippsland Basin is characterised by rock compositions that are likely to be reactive when CO_2 is introduced.
- Reservoir heterogeneity resulting from primary depositional controls as well as secondary diagenetic alternation is considerable.
- The area of interest in the Gippsland Basin is an active hydrocarbon province, so interference with hydrocarbon production and compromising exploration potential through CO_2 geosequestration must be considered.

In addition to addressing the unique characteristics of the Gippsland Basin, this study aims to identify and provide guidelines for addressing some of the globally applicable challenges when reservoir/aquifer characterisation and geological model construction is undertaken for geosequestration of CO_2 specifically. In particular, identifying areas where the general approach and specific workflows must diverge from well-established petroleum E & P technology may be useful regardless of geographical context.

Chapter 2—Sedimentology

Abstract

The sedimentological properties of the rock within the study area will have a significant effect on the subsurface behaviour of CO_2 in terms of its flow behaviour and in terms of its chemical behaviour. Reservoir/aquifer heterogeneity is described for rocks in the study area ranging from pore-scale heterogeneity to depositional environment-scale heterogeneity focusing on the distribution, geometry and interconnectivity of individual reservoir/aquifer and seal/barrier units as well as their flow properties.

Lithofacies suggesting a range of depositional processes were identified based on textural and compositional features in the rocks representing physical and biological influences on deposition. Based on lithofacies relationships, which indicate how depositional processes varied in space and time, a number of depositional environments were identified in the study area ranging from fluvial to nearshore marine and offshore shelfal environments.

Two key reservoir/aquifer units were identified: 1) nearshore sandbodies consisting primarily of shoreface and tidal channel sandstones characterised by good interconnectivity of individual sandbodies, relatively good compositional maturity and excellent flow properties, and; 2) fluvial channel facies characterised by lower than expected sandbody connectivity, lower compositional maturity, but also with excellent flow properties locally. The key seal/barrier facies are lower shoreface and shelf facies, which are typically heavily bioturbated and homogenized mudstone, siltstone and sandstone mixtures as well as mudstone and marl units with relatively poor flow properties.

The three groups of depositional facies described above and relevant modern and ancient analogues are utilised for construction of the geologic model. The geostatistical models selected are governed by the likely geometries and spatial distribution of depositional facies within the structural and stratigraphic framework of the geologic model.

Introduction

The sedimentology of the reservoir and seal facies is critical to the study of CO_2 geosequestration because the composition and texture of the reservoir and seal facies influence the behaviour of CO_2 in the subsurface. Porosity provides space for CO_2 to reside in the surface, and permeability controls in part the rate at which CO_2 can move through the rock. Additionally, some rock components are chemically reactive with CO_2 (e.g. carbonates, feldspars, glaucony), while other rock components are chemically inert (e.g. quartz). Reactive rock components provide an opportunity for permanent mineralogical storage of CO_2.

A hierarchical facies scheme is used consisting of lithofacies, facies associations, and environments of deposition. Understanding the environments of deposition helps us to understand the subsurface spatial arrangement of reservoir properties, such as porosity and permeability. Consequently, sedimentological characterisation of a potential ESSCI site is an important precursor to constructing a geological model.

The reservoir units of the Gippsland Basin ESSCI are Early to Late Eocene sandstones, siltstones, mudstones and coals of the upper Latrobe Group. Sealing units are Oligocene to Miocene marl, mudstone and matrix-rich glauconitic sandstone of the Gurnard Formation, the Lakes Entrance Formation, and canyon complexes (notably the Marlin Canyon in the eastern part of the study area). Intra-reservoir sealing units also exist within the upper Latrobe Group clastics.

Methodology

Core Description

Twelve full-hole cores were described in detail: Barracouta 5, Fortescue 1, Fortescue 2, Luderick 1, Marlin 1, Marlin 4, Seahorse 2, Snapper 5, Tarwhine 1, Veilfin 1 Whiting 1, and Wirrah 1. Additionally, cores from Barracouta 1, Snapper 1 and Wrasse 1 were viewed, but the condition of the core precluded detailed description.

The lithology, sedimentary and biological structures identified in core allow interpretation of lithofacies and facies associations. Graphic core descriptions were constructed. Graphic core descriptions depict lithology, grain size, sedimentary and biological structures and diagenetic alteration. The horizontal thickness and colour of the core description represents grain size. The vertical axis of the core description represents depth.

Petrography

Conventional transmitted light petrography including mineral identification and point counting was carried out by G. Krishan on 56 thin sections sampled from full-hole core. Scanning electron microscopy (SEM) and X-ray diffraction (XRD) were conducted on selected samples. SEM provided information regarding the micro-scale pore structure, and XRD provided the mineralogical compositions of reservoir and seal rock. Table 2.1 lists the samples and kinds of analyses carried out.

Table 2.1: Petrographic analyses carried out for this study (sample depths provided in Appendix IV).

Well Name	Formation	MICP	XRD	SEM	TS	PS
MICP: Mercury Injection Capillary Pressure; XRD: X-ray diffraction; SEM: Scanning Electron Microscopy; TS: Transmitted Light Thin Section; and Ps: Polished Section.						
BARRACOUTA-1	Latrobe Group				1	
BARRACOUTA-5	Latrobe Group	1			7	
FORTESCUE-1	Latrobe Group	2	1	1	4	
FORTESCUE-2	Gurnard Formation	2	2	4	4	
LUDERICK-1	Latrobe Group	1			8	
MARLIN-4	Latrobe Group	2	5		10	3
SEAHORSE-2	Latrobe Group	2	1		3	1
SNAPPER-1	Latrobe Group	1			3	
SNAPPER-5	Latrobe Group	1	1		3	1
TARWHINE-1	Latrobe Group	2	1	2	6	2
VEILFIN-1	Latrobe Group	1	2	1	2	2
WIRRAH-1	Latrobe Group	1			8	
WHITING-1	Latrobe Group		2	2	3	1
WRASSE-1	Lakes Entrance Formation	2	1		1	
TOTALS:		**18**	**16**	**10**	**63**	**10**

ANALOGUES

Analogue data were used to assess the likely geometry and orientation of reservoir and seal bodies in the subsurface, and to guide the selection of geostatistical models for reservoir model population. A literature survey was carried out that compiled >500 measurements of reservoir and seal facies geometry. Additionally, over 60 analogue semi-variogram and madograms were generated from modern and ancient analogues. The methodology for using analogues to guide the selection of geostatistical models is described in Chapter 5.

Analogues were selected that represented similar depositional environments to those that are interpreted to exist in the study area from core and wireline log data. When possible, analogues were selected from similar tectonic settings and from areas with a similar climate to the interpreted palaeo-climate during the mid – late Eocene in the Gippsland Basin.

Lithofacies Description

Lithofacies are defined by the texture and composition of sedimentary rocks. Rock texture and composition reveals the processes that were active during deposition.

Lithofacies are described and interpreted in terms of the processes that were active during deposition below.

Table 2.2: Upper Latrobe Group lithofacies.

Lithofacies Name	Description	Interpretation
Conglomerate	Pebbles, granules and cobbles; commonly in thin beds (< a few cm thick); associated with parallel stratification or cross-bedded sandstone. Clast composition includes quartz, meta-sedimentary clasts, and coal fragments. Clasts are generally well to moderately rounded and clast imbrication is common. Thicker units of conglomerate (> a few cms) may show normal, coarse-tail grading.	Deposition in currents of sufficient velocity to transport pebble-cobble sized grains. Limited evidence of deposition by debris flow (e.g. slump structures, poor sorting, lack of imbrication). The common association of conglomerate with planar stratification and cross-bedding suggests relatively high energy flow. The bed thickness of most conglomerate units suggests short-lived, high-energy events.
Parallel-stratified, very fine- to fine-grained sandstone	Sandstone showing closely spaced planar bedding surfaces approximately parallel with each other, and parallel to principle bedding surfaces. Parallel stratification is commonly associated with *Ophiomorpha* and *Diplocraterion* and other vertical and sub-vertical trace fossils. Carbonaceous chaff may be concentrated on bedding surfaces.	Bed load deposition of high flow regime currents close to a horizontal pavement (Allen 1982). Flow turbulence is dampened by high concentrations of sediment close to the substrate (Reid and Frostick 1994). Largely vertical trace fossils such as *Diplocraterion* and *Ophiomorpha* are consistent with a relatively high-energy depositional environment.
Low angle cross-bedded very fine- to fine-grained sandstone	Sets of closely spaced bedding surfaces that erosionally truncate one another, oriented at 5° to 15° to principle bedding surfaces. Lower angle dip and longer lateral extent of bedding surface by comparison with cross-bedding. Rarely a convex-up geometry was noted in bedding sets. Low angle cross-bedded sandstone is commonly vertically associated with parallel stratified sandstone. Trace fossils that are commonly associated with low angle cross-bedded sandstone include *Ophiomorpha, Thalassinoides Diplocraterion, Arenicolites, and ?Conichnus.*	High-energy depositional conditions and high flow regime currents are inferred, similar to the parallel-stratified sandstone lithofacies. Low-angle bedding truncations suggest angular erosion; a genetic link with fair-weather wave currents is commonly inferred ('beach and longitudinal bar cross bedding' of Reineck & Singh 1975). Convex-up geometries in bedding sets (hummocks) are generally associated with hummocky swaley stratification which is thought to have a genetic link with storm currents (Collinson and Thompson 1982).

Lithofacies Name	Description	Interpretation
Planar-tabular and trough cross-bedded medium- to very coarse-grained sandstone	Sandstone with sets of closely spaced bedding surfaces oriented at a 15° to 30° angle to principal bedding surfaces. The sets are between 5 cm and 20 cm in thickness and are erosionally bound by planar surfaces oriented at 0° to 15° to principle bedding surfaces (accretion surfaces). Sets may be normally graded. Cross-bedded sandstone is commonly vertically associated with ripple cross-laminated sandstone and parallel-stratified sandstone.	Bedload deposition by upper, lower flow regime currents. Both trough and planar tabular cross-bedding reflect bedload migration of dunes and sand waves though stoss side erosion and lee side deposition (Allen 2001, Conybeare & Crook 1982, Allen 1982). Trough cross-bedding is generally thought to be deposited under slightly higher flow regime, more turbulent flow conditions. As a result of increased erosion in the lee of the structure, trough cross-bedding is generally associated with three-dimensional bed forms and planar tabular cross-bedding is generally associated with bed forms of two dimensional geometry (Collinson and Thompson 1982, Allen 1982).
Structureless and graded medium-grained sandstone to conglomerate	Sandstone without resolvable sedimentary structure (structureless) or sandstone showing a systematic vertical change in grain size. All graded sandstone is normal, coarse-tail graded (mean grain size decreases up section). In some cases structureless sandstone is associated with intense bioturbation and cementation.	Both graded sandstone and structureless sandstone are interpreted to result from very high rates of deposition associated with rapidly decelerating flows. A genetic link with turbidity currents is commonly cited (Conybeare and Crook 1982, Blatt *et al.* 1991); however, massive and graded beds resulting from primary deposition are also commonly associated with high-energy fluvial deposits (Allen 1982). Structureless sandstone is also the result of intense bioturbation (Reineck & Singh 1975) and cementation. In these cases, no genetic link with rapid deposition is inferred.

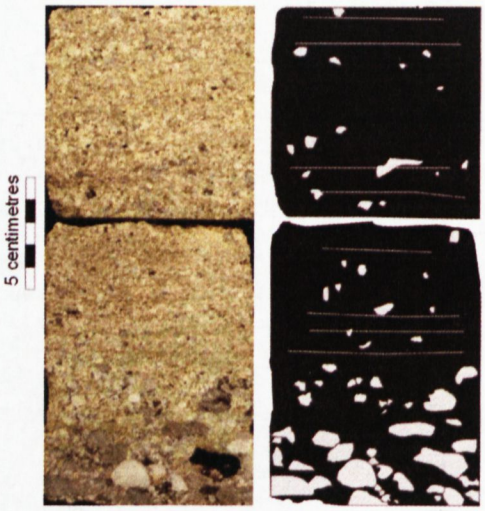

Figure 2.1 — Tarwhine 1, 2665.78-2665.99 m: Pebble-cobble conglomeratic sandstone with normal grading and parallel stratification. Interpreted as part of a fluvial channel fill.

Figure 2.2 — Whiting 1, 2685.59-2685.77 m: Fine- to medium-grained cross-bedded and ripple cross-laminated sandstone. Interpreted as part of a fluvial channel fill. Carbonaceous mud- to silt-size material is accumulated on cross-bed foresets.

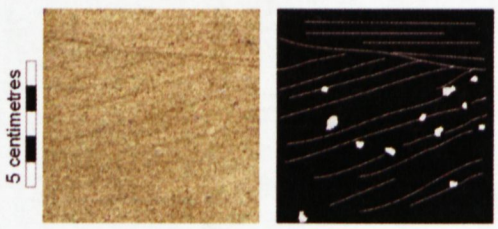

Figure 2.3 — Tarwhine 1, 2667.79-2667.91 m: Fine- to medium-grained, conglomeratic, cross-bedded sandstone overlain by parallel-stratified sandstone.

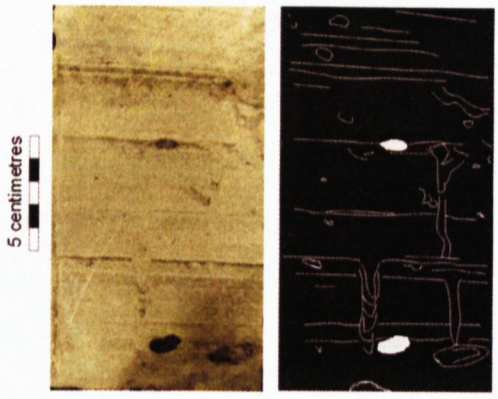

Figure 2.4 — Fortescue 1, 2425.22-2425.35 m: Very fine- to fine-grained, parallel-stratified sandstone with *Arenicolites*, *Planolites*, *Thalassinoides*, and *?Skolithos* burrows typical of a high-energy brackish-saline water assemblage. The sample is interpreted as a mid to lower shoreface sandstone.

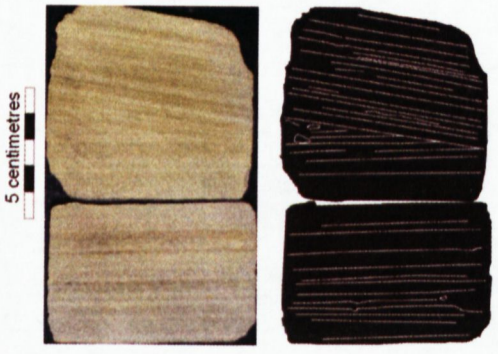

Figure 2.5 — Luderick 1, 1855.50-1855.63 m: Low angle cross-bedded upper shoreface sandstone with mild bioturbation. Low-angle bedding truncations are evident.

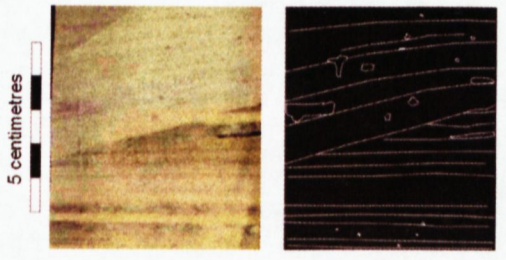

Figure 2.6 — Fortescue 1, 2421.66-2421.96 m: Low angle cross-bedded sandstone with moderate bioturbation. The convex-up geometry of the upper bedding set may be indicative of hummocky swaley stratification.

Figure 2.7 — Fortescue 1, 1853.64-1853.67 m: *Ophiomorpha* burrow with a nodular mud lining.

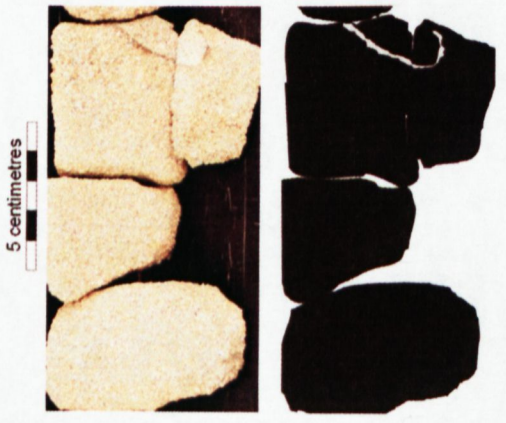

Figure 2.8 — Seahorse 2, 1505.60-1505.72 m: Medium- to coarse-grained poorly consolidated sandstone with an *Ophiomorpha* burrow in the upper part of the sample. Limited consolidation and lithification is typically associated with unusually high porosity and permeability.

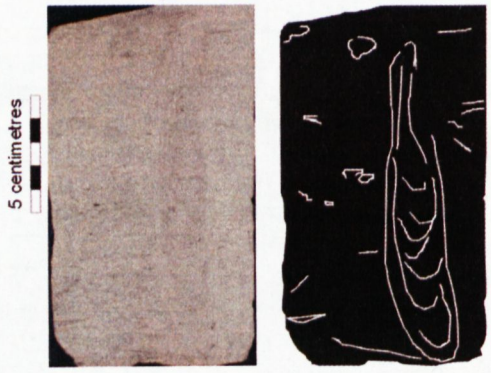

Figure 2.9 — Luderick 1, 1839.42-1839.58 m: Large vertical burrow interpreted as *Diplocraterion* in fine-grained sandstone.

Table 2.2: continued...

Lithofacies Name	Description	Interpretation
Ripple cross-laminated very fine- to medium-grained sandstone.	Sandstone with sets of bedding surfaces no greater than 5 cm in thickness that are characterised internally by closely spaced bedding surfaces inclined at an angle of between 15° and 30° to principal bedding surfaces. Where accretion surfaces exist at a relatively high angle to principal bedding surfaces (10° - 15°), the structure is identified as climbing ripple cross-lamination. Truncation of ripple cross-lamination by sub-horizontal laminae dipping in an opposing direction to the ripple cross laminae forests suggests wave ripple lamination.	Ripple cross-laminated sandstone suggests bedload deposition of sandstone under low flow regime conditions. Climbing ripple cross-lamination indicates combined deposition from bedload transport and from suspension. It is usually associated with relatively high rates of deposition and sudden reduction in flow velocity (Allen 1998). Wave ripple lamination is thought to represent erosion of ripples where the upper surface is planed by wave currents. Subsequent deposition occurs after current reversal resulting in the overlying laminae (Reinech & Singh 1975).
Very poorly sorted sandstone	Very poorly sorted sandstone is commonly characterised by very high clay content (20%-40%). Units have no resolvable bedding or grain size organization. Very poorly sorted sandstone units commonly have root traces and may be associated with small carbonate concretions and bleached horizons. Carbonaceous material is abundant in very poorly sorted sandstone.	Very poorly sorted sandstone is interpreted to result from biological 'mixing' of sedimentary layers. Root traces, bleaching and concretions are interpreted to result from soil forming processes. However, no fully developed palaeosols were identified in core.

Lithofacies Name	Description	Interpretation
Finely interbedded mudstone and siltstone to very fine-grained sandstone	Units of thin (< 2 cm) interbedded very fine-grained sandstone or siltstone and mudstone are typically characterised by ripple cross-lamination, lenticular bedding, and starved ripples, and less commonly parallel stratification. Bioturbation varies from moderate to intense and commonly consists of *Planolites* and *Diplocraterion* where individual burrows are resolvable. Soft sediment deformation features including minor slumps and folds, load casts and de-watering features may be associated with this lithofacies. Root traces and thin coal units may be present.	This lithofacies is interpreted to be deposited by periodic variations in bedload deposition and deposition by suspension. The ratio of sandstone to mudstone in most deposits indicates dominantly low-energy conditions, punctuated by short periods of bedload influx. The presence of root traces and thin coal units suggests relatively shallow water depths and emergence.
Structureless and finely laminated mudstone	Mudstone is typically laminated but may occur as structureless units that are generally associated with carbonate cementation. Individual mudstone units rarely exceed a metre in thickness. Mudstone is commonly bioturbated with *Planolites* burrows. Intensely fractured and cemented mudstone that is associated with slickensides occurs within this facies (although the occurrence of slickensides may not be facies dependent). Siderite and dolomite cementation is associated with intensely fractured rock.	Structureless and finely laminated mudstone deposits are interpreted to result from deposition by suspension in relatively low-energy depositional environments. Structureless mudstone may result from fairly rapid deposition from suspension (Collinson and Thompson 1982). Fractured and cemented rock is interpreted to represent the damage zone of a fault. Slickensides indicate displacement on fault planes.
Carbonaceous mudstone and coal	Carbonaceous mudstone and coal units may be up to several metres thick. Coal is variably cleated and commonly grades vertically into carbonaceous mudstone.	Deposition in a low-energy environment that is removed from clastic influx. In the case of carbonaceous mudstone, the rate of clastic influx may have been too great to allow true peat formation.

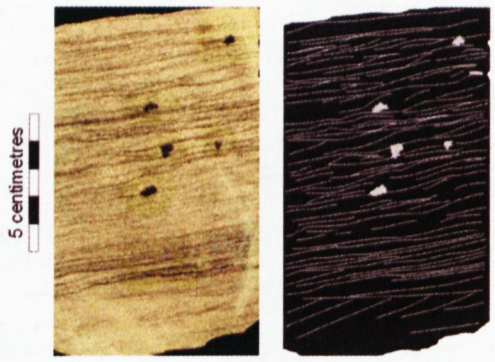

Figure 2.10 — Whiting 1, 2685.40-2685.52 m: Very fine- to fine-grained ripple cross-laminated and wavy bedded sandstone with small irregularly shaped, mud-filled, horizontally or obliquely oriented burrows (*Planolites*). Interpreted as the upper section of a fluvial channel fill.

Figure 2.11 — Fortescue 1, 2434.35-2434.47 m: Heavily bioturbated sandstone, siltstone and mudstone with little resolvable primary structure. The sample is interpreted as a lower shoreface deposit.

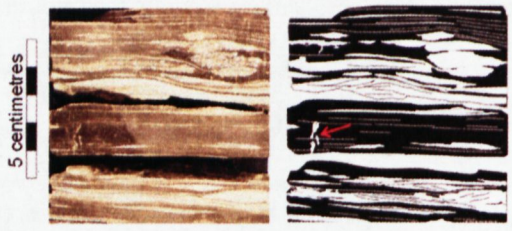

Figure 2.12 — Seahorse 2, 1503.42-1503.55 m: Bioturbated, interbedded very fine-grained sandstone and mudstone. Sandstone units are ripple cross-laminated and starved ripple bedded. Root traces exist in the mudstone units (arrow).

Figure 2.13 — Wrasse 1, 2597.24-2597.36 m: Calcareous mudstone of the Lakes Entrance Formation. The sample is interpreted as a shelf deposit.

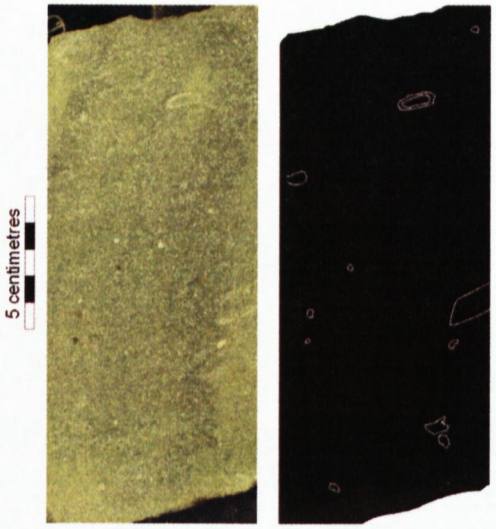

Figure 2.14—Wrasse 1, 2750.50-2750.72: Moderately bioturbated glauconitic sandstone of the Turrum Formation. The high percentage of interstitial matrix suggests that this facies will act as a barrier/seal to fluid flow. The sample is interpreted as an inner-shelf deposit.

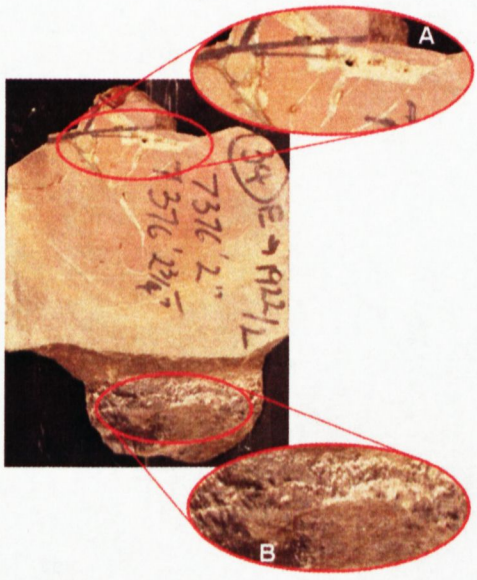

Figure 2.15—Marlin 4, ~2249.20 m: Faulted and fractured mudstone of the upper Latrobe Group. Fractures are filled with carbonate cement (A), and the mudstone is cemented throughout with dolomite and siderite cement, imparting the red colour. The fibrous mineral growth in (B) is a silken-side texture that is associated with movement along fault planes.

Facies Associations

Different kinds of lithofacies are deposited with predictable temporal and spatial patterns that result in facies associations. Facies associations reveal how depositional processes varied with time and spatially within the depositional environment. Consequently, facies associations and groups of facies associations reveal the environment in which strata were deposited. When the environment of deposition is known, relatively large-scale spatial patterns of facies can be predicted based on conceptual depositional models and analogues. The spatial patterns of facies generally allow prediction of the spatial distribution of reservoir properties, which can be 'captured' in the geological model using geostatistical techniques.

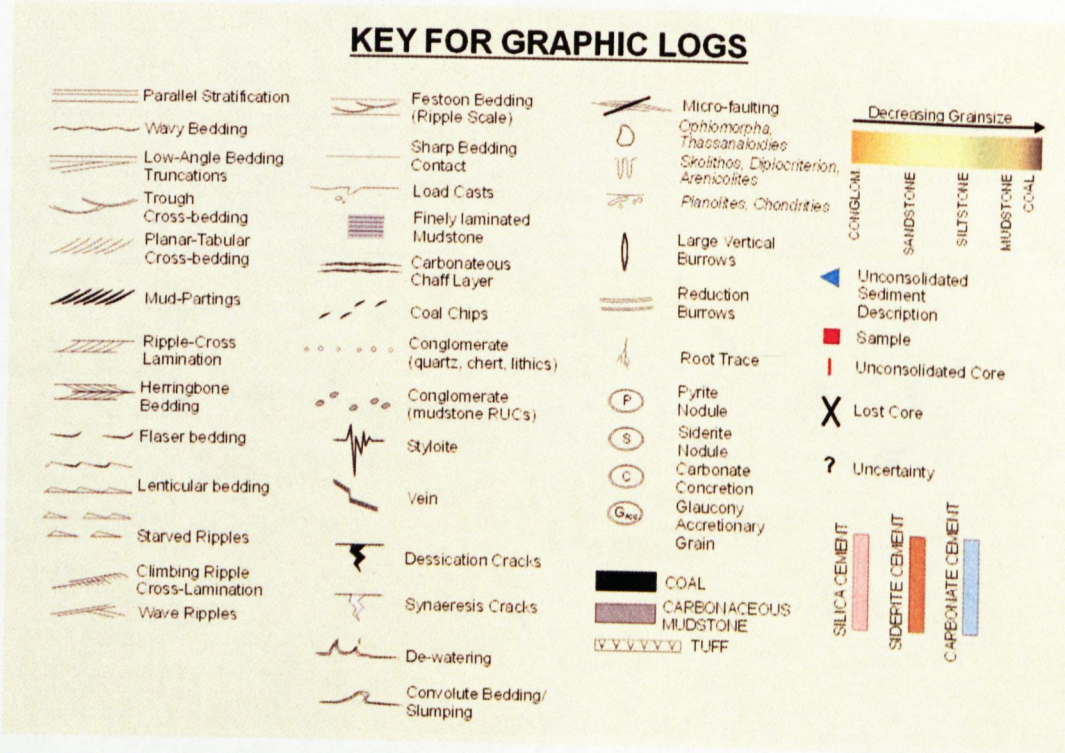

Figure 2.16—Key for graphic logs.

FACIES ASSOCIATION 1 — MIDDLE AND UPPER SHOREFACE

Description: Middle to upper shoreface deposits are characterised by very fine- to coarse-grained sandstones that are commonly parallel-stratified, low angle cross-bedded, ripple cross-laminated, and wave ripple-laminated. Stacking patterns are

typically aggradational or mildly coarsening-upwards in middle to upper shoreface successions. Both sorting and angularity are variable in shoreface sandstones, ranging from very poorly- to well-sorted and angular to sub-rounded, respectively. Parallel- and low angle cross-bedded sandstone generally has little mud or silt content, but is commonly associated with carbonaceous chaff draped on bedding surfaces.

Other structures that are common in upper to middle shoreface deposits include wavy bedding, lenticular bedding, and flaser bedding. The upper part of shoreface successions may be characterised by limited trough or planar-tabular cross-bedding. In cases where sandstone is very poorly consolidated, no primary structure may be resolvable. Upper and middle shoreface successions generally have thin interbedded mudstone or silt layers. Interbedded mudstone and siltstone layers are a few centimetres in thickness and are commonly associated with *Planolities* burrows. Thin (<3 cm) intraformational conglomerates that consist primarily of siliceous pebbles are also common in the lower part of shoreface successions. Thin conglomerate units typically have erosional bases and gradational upper contacts.

Trace fossils are abundant in middle-upper shoreface deposits and include *Ophiomorpha, Thalassinoides* and less commonly, *Diplocraterion*, *Arenicolites*, *Planolites, Palaeophycus* as well as large chevron shaped burrows up to 20 cm in length (*?Conichnus*).

Wireline log motifs of upper to middle shoreface facies are characterised by coarsening-upward gamma-ray trends (GR), with little or no separation between the neutron porosity (NPHI) and density logs (RHOB), except in gas-charged sandstones. Typically the vertical scale of coarsening-upward successions ranges from several metres to greater than ten metres.

Interpretation: The abundance of parallel and swash stratification suggests a dominant wave influence on deposition above fair weather wave base. Additionally, the trace fossil assemblage, dominated by vertical cylindrical and U-shaped dwelling burrows, is indicative of wave-dominated conditions with a sandy substrate (*Skolithos* ichnofacies assemblage; Pemberton *et al.* 1992). The dominance of vertical burrows suggests a wave-dominated environment of moderate to low energy.

Good sorting and textural maturity is typical of upper shoreface, and particularly foreshore deposits (Bjørlykke 1984), but is not evident in the shoreface facies of the upper Latrobe Group. Commonly, very poorly sorted sandstone is associated with thin coarse- to very coarse-grained sandstone or conglomerate layers that are interpreted as storm-generated beds. However, units that are interpreted to have no genetic association with storm deposition also show an unusually low level of sorting and high angularity. The relatively low level of compositional maturity may indicate a rapid rate of deposition, so time for wave action to 'clean up' sandstone was limited, and may also indicate relatively low wave energy. A rapid rate of deposition is supported by the presence of large chevron-shaped escape burrows (probably *?Conichnus*) and *Diplocraterion* burrows in shoreface deposits where the spreiten structures may suggest burrowing organisms climbing through the substrate to keep pace with aggradation (Fig. 2.9).

There is little evidence of a fluvial influence on deposition, such as fluvial distributary deposits that cut into nearshore strata, though seismic visualisation may suggest that channellised deposits and wave-dominated deltaic sediments are represented in the study interval (see Chapter 3). Deposits of unequivocal deltaic origin have not been intersected with core described in this study. Consequently, no deltaic association is inferred for the majority of wave-influenced sandstones.

Upper and middle shoreface deposits are commonly unconformably overlain by fining-upward units one to four metres in thickness that are interpreted as tidal channel deposits with indications of shallow water deposition and emergence in the upper sections. This suggests an unconformable vertical succession and missing facies. Much of the upper shoreface and the foreshore were not commonly preserved in vertical succession. Upper shoreface facies, which is typically characterised by multidirectional trough and planar tabular cross-bedding (Reineck & Singh 1975), is generally not preserved in the core that was described in this study. Instead, middle shoreface deposits are commonly overlain by tidal channel deposits followed by shallow lacustrine, lagoon and swamp/peat marsh, and undifferentiated coastal plain facies representing environments that existed landward of the coastline during deposition of the upper Latrobe Group shoreface facies. Although the depositional processes represented in the upper and middle shoreface differ, they are treated as a single facies association in this study because upper shoreface strata are rarely preserved.

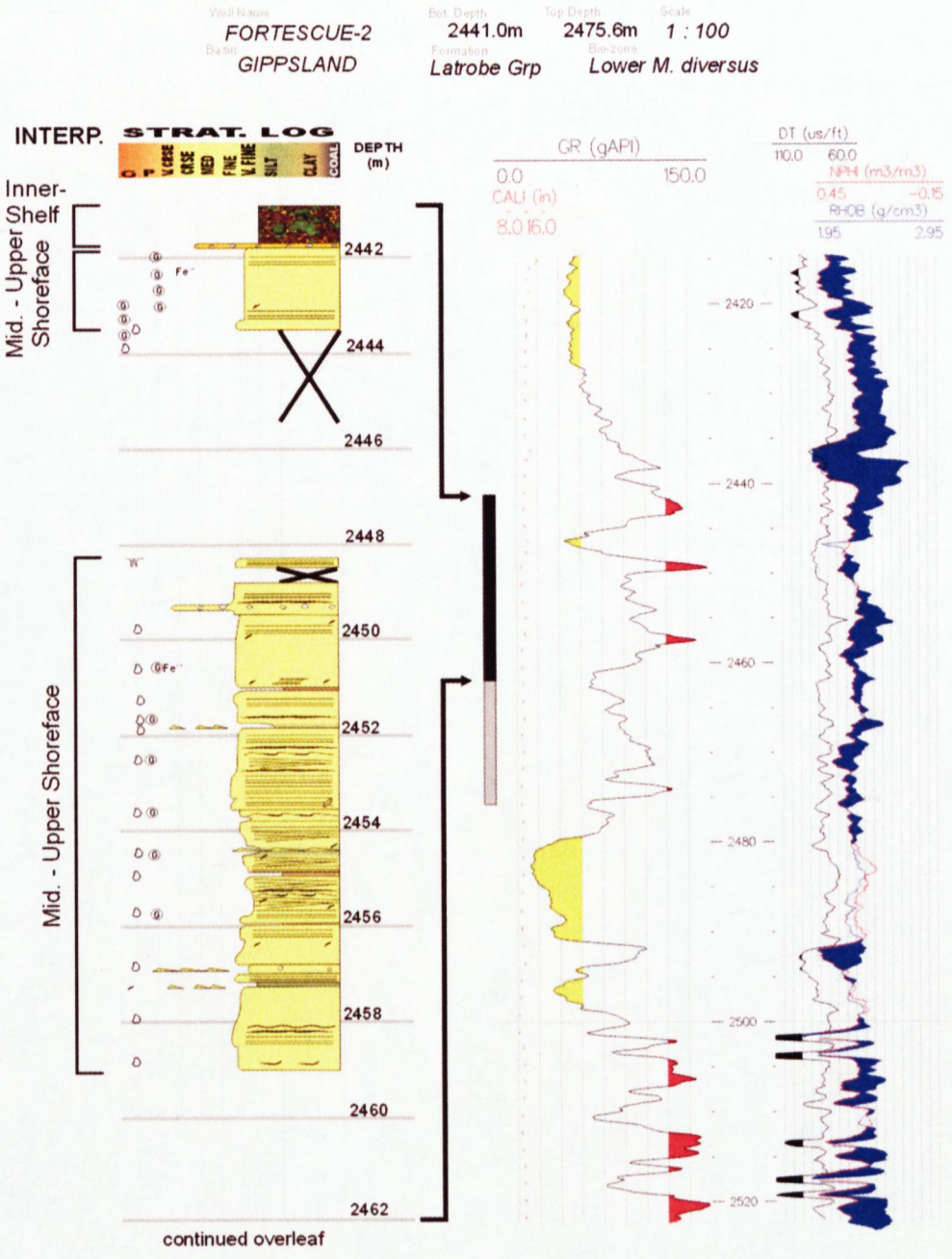

Figure 2.17—Core description for Fortescue 2 showing middle to upper shoreface facies. The inner-shelf deposit (<2442 m) is part of the Gurnard Formation. The erosional lag at 2442 m represents the 'BaseSeal' surface, which is pervasive across the study area.

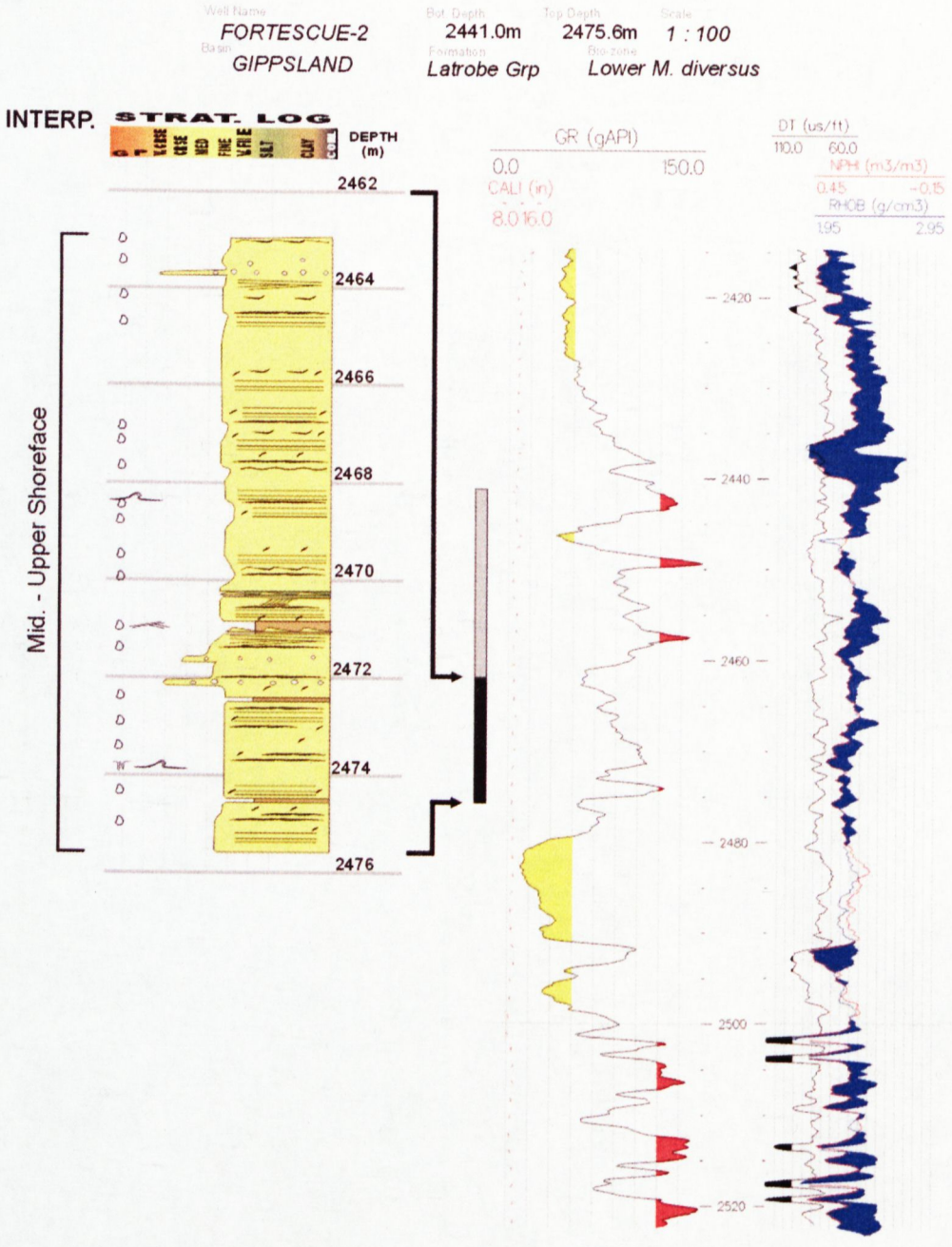

Figure 2.18—Core description for Fortescue 2 (continued). Mid-upper shoreface deposits are commonly characterised by several metres of stacked parallel and low angle cross-bedded sandstone with thin mudstone and siltstone interbeds.

Facies Association 2—Tidal Channel Deposits

Description: Middle and upper shoreface deposits are commonly unconformably overlain by fining-upward deposits of one to four metres in thickness that are interpreted to be tidal channel deposits. Tidal channel deposits are characterised by

erosive contacts at their base, associated with conglomeratic lags and parallel stratification. Ripple cross-lamination and flaser bedding are common in the upper parts of tidal channel deposits, which are finer grained and have a higher proportion of organic material than the lower part of tidal channel deposits. Siltstone or mudstone units that generally have root traces and carbonaceous mudstone or coal beds commonly overlie tidal channel deposits. Lenticular bedding and starved ripples are generally also in the upper, siltstone and mudstone dominated parts of tidal channel deposits.

Ophiomorpha burrows are common in the lower, coarser-grained parts of tidal channel deposits. Smaller vertical and sub-vertical burrows such as *Diplocraterion*, *Arenicolites*, *Planolites* and *Skolithos* become more dominant up-section, in the finer grained parts of tidal channel deposits.

Tidal channel deposits are typically represented by fining upward gamma-ray log motifs of a few metres in thickness. Negative NPHI/RHOB separation increases up-section reflecting the increasing proportion of mudstone.

Interpretation: The typical tidal channel vertical succession in the study area suggests a decrease in depositional energy and palaeo-bathymetry up-section, commonly with indications of emergence in the uppermost section (e.g. root traces). The vertical pattern is interpreted to stem from the progressive filling and lateral accretion of tidal channels similar to a fluvial meandering stream vertical succession. In regressive successions the coals and mudstone overlying tidal channel deposits represent tidal flat, back barrier lagoon and coastal plain swamp deposits.

Tidal channel deposits in modern environments are typically a few metres to a few tens of metres in thickness and commonly erode barrier island and foreshore deposits, as well as cutting into shoreface deposits. A close genetic and spatial association with flood and ebb tidal deltas is common. Typically tidal channels in the nearshore environment migrate laterally due to longshore sediment transport, cannibalising the upper sections of nearshore stratigraphic successions. The preservation potential of the upper parts of the nearshore stratigraphic succession, including foreshore, beach berm and barrier island deposits, is low and channellised deposits (tidal channel/inlet) are more typically preserved in ancient stratigraphy (Oertel *et al.* 1991, Barwis & Hayes 1979). The preservation of a particular facies is largely a function of its elevation relative to the shoreline and the areal extent of the

facies (Demarest & Kraft 1987). In the Gippsland Basin vertical successions characterised by shoreface deposits unconformably overlain by fining-upward tidal channel deposits are interpreted to be indicative of these processes.

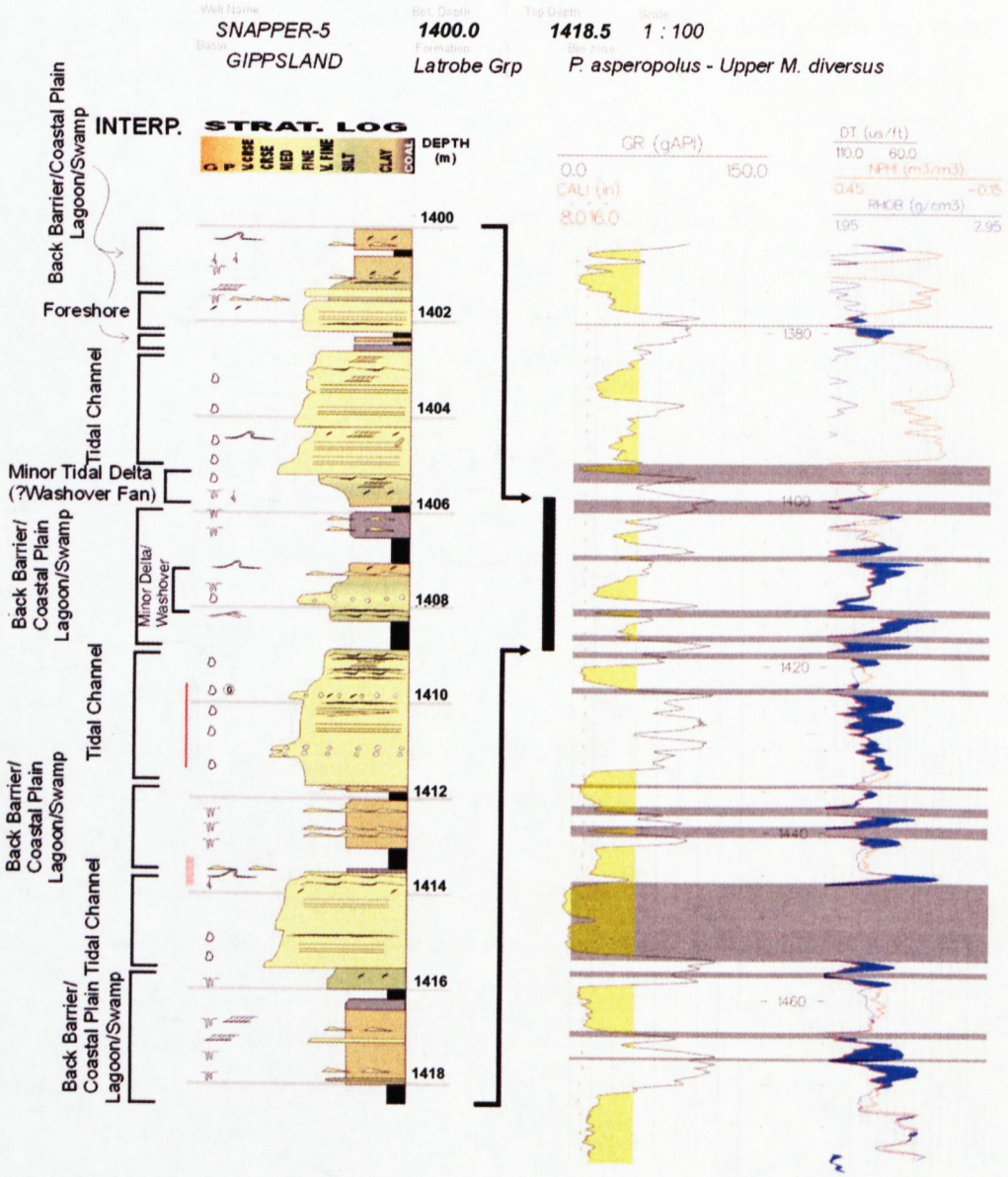

Figure 2.19—Core description for Snapper 5. Fining-upward tidal channel deposits interbedded with peat swamp and back barrier lagoonal facies.

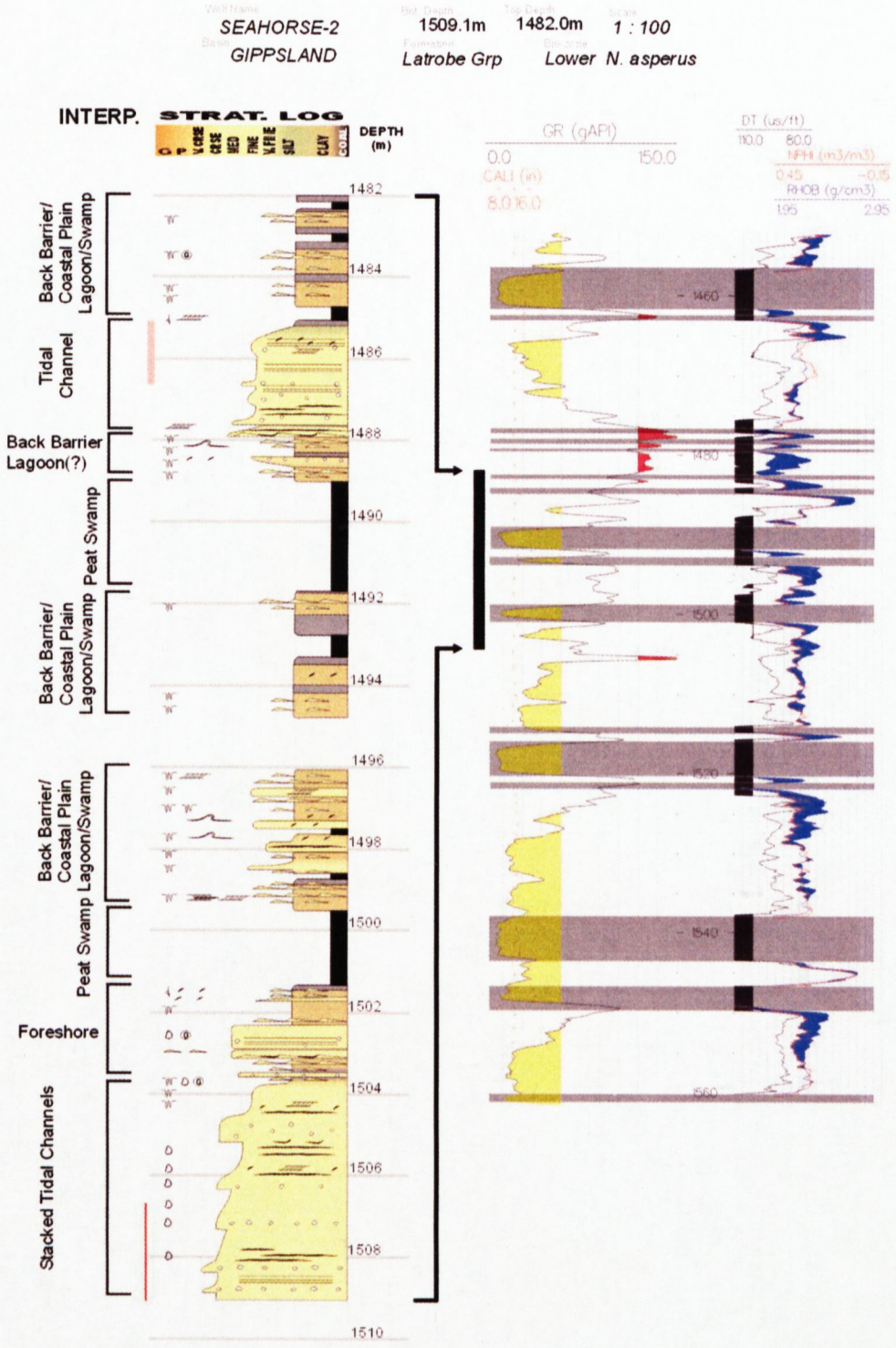

Figure 2.20—Core description for Seahorse 2. Tidal channel deposits interbedded with peat swamp and lagoonal facies. Foreshore (~1503 m) and beach berm and eolian dune deposits are not commonly preserved in the study area.

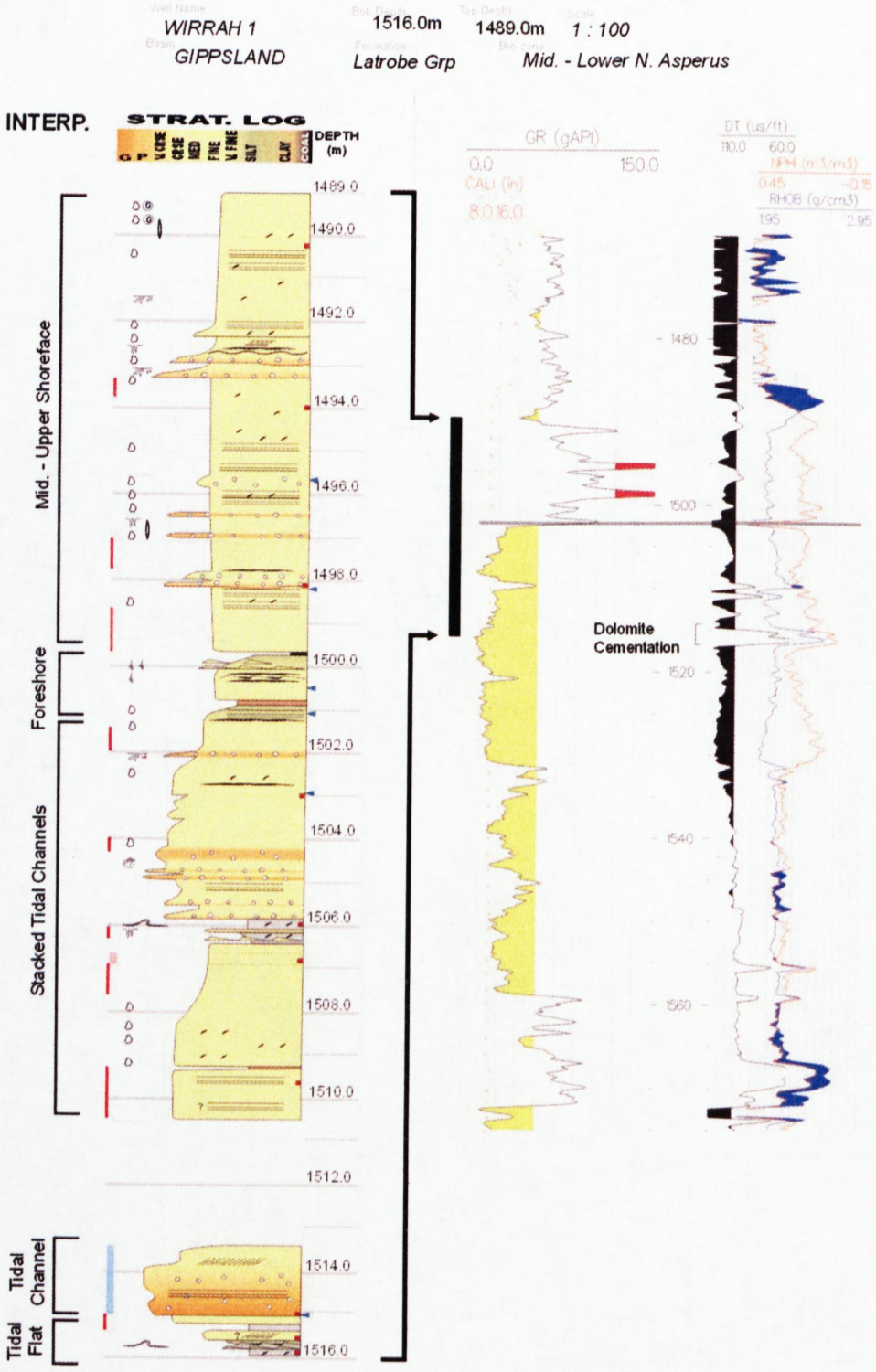

Figure 2.21—Core description for Wirrah 1 showing shoreface and tidal channel facies. The thin conglomerate units probably have a genetic association with storms.

FACIES ASSOCIATION 3—LOWER SHOREFACE

Description: Lower shoreface deposits are characterised by relatively thick successions of moderately to heavily bioturbated, siltstone and very fine- to medium-grained sandstone with parallel stratification, low angle cross-bedding, wavy bedding, layers of carbonaceous chaff and multiple thin conglomerate beds. Lower shoreface deposits have high mud matrix content in sandstone units by comparison with middle and upper shoreface deposits. Primary bedding is commonly not resolvable due to the intensity of bioturbation. Lower shoreface deposits commonly coarsen upwards into overlying middle and upper shoreface deposits. Thin mudstone units (a few centimetres in thickness) are interbedded in thick successions of parallel-laminated sandstone. Like middle and upper shoreface deposits, lower shoreface deposits are commonly associated with thin conglomerate beds. Where lower shoreface facies exist in close vertical proximity to the regional seal, burrows are commonly associated with glaucony.

Wavy bedding, wave ripples, ripple cross-lamination, flaser bedding and lenticular bedding as well as soft sediment deformation features such as flame structures and load casts are common in lower shoreface deposits. Trace fossils are commonly difficult to identify because of the intensity of bioturbation; however, *Ophiomorpha*, *Thalassinoides*, *?Rosselia*, *Planolites*, *Diplocraterion*, and *Palaeophycus* commonly exist in lower shoreface facies. Both the abundance and the diversity of trace fossils are higher in the lower shoreface facies than in the upper and middle shoreface facies.

Lower shoreface deposits are represented on wireline logs by serrated, relatively high value GR motifs that generally coarsen upward. Negative NPHI/RHOB separation is common reflecting the relatively high mud content.

Interpretation: The intensity of bioturbation in lower shoreface deposits suggests a lower energy depositional environment than is represented in middle to upper shoreface strata. A higher proportion of mudstone matrix in lower shoreface sandstone also suggests lower energy conditions. Bioturbated, muddy sandstones are typical of lower shoreface successions (Reineck & Singh 1975).

Thin interbedded conglomerate and coarse-grained sandstone layers indicate intermittent high-energy events that are interpreted as storm deposits. Low-angle

bedding truncations described from core may represent swash stratification or hummocky-swaley stratification, which is difficult to distinguish given the limited horizontal sampling area of full-hole core.

Unlike deposits of the middle and upper shoreface, lower shoreface facies is interpreted to have been deposited below fair weather wave base. The trace fossils are interpreted as a mixed *Cruziana/Skolithos* assemblage, indicative of lower energy conditions (typically greater palaeobathymetry) than the pure *Skolithos* assemblage identified in middle to upper shoreface facies (Pemberton *et al.* 1992, Bjørlykke 1984).

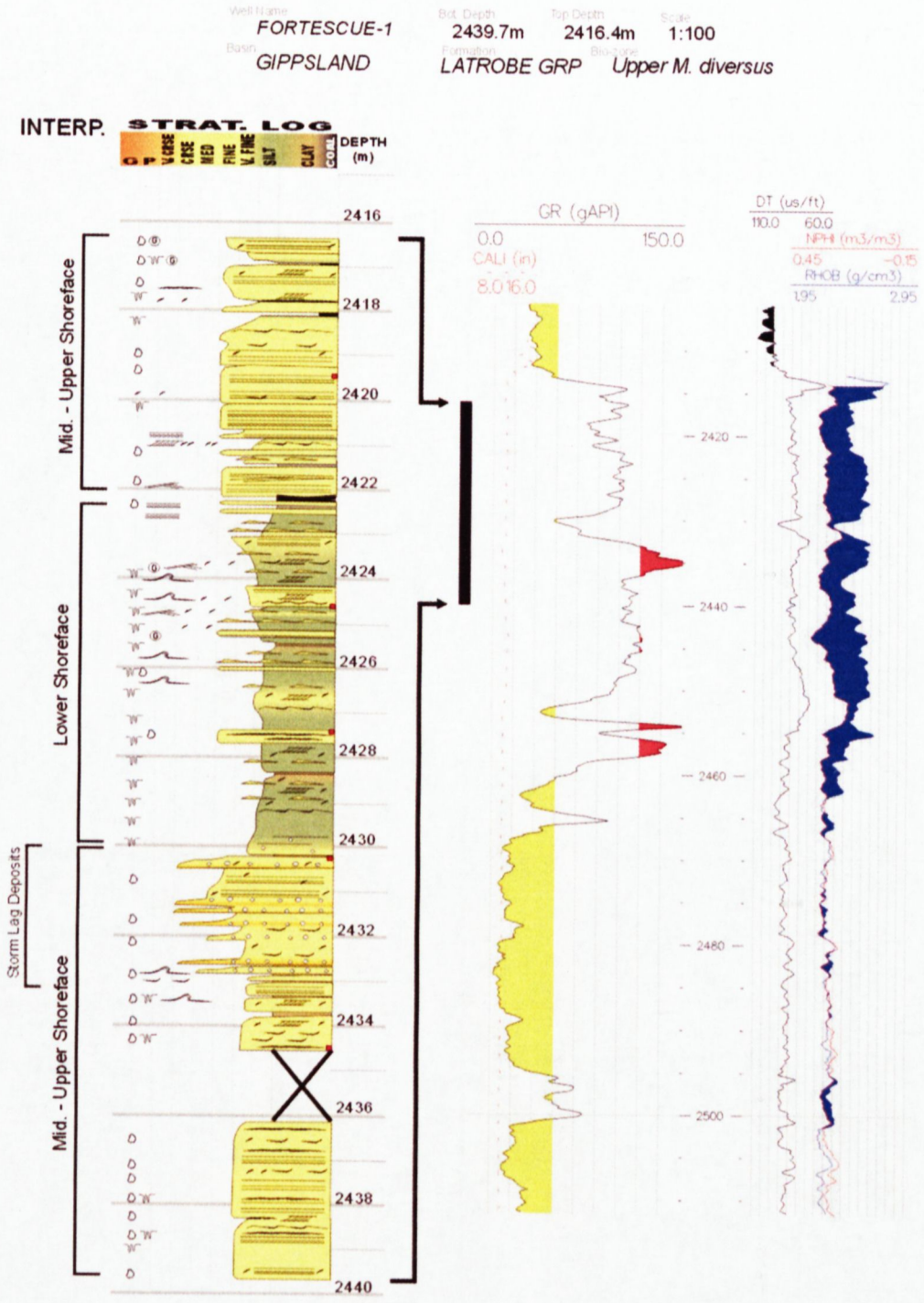

Figure 2.22—Core description for Fortescue 1. The siltstone and very fine-grained sandstone deposit between 2430 m and 2422 m is interpreted to be deposited in the lower shoreface, below fair weather wave base.

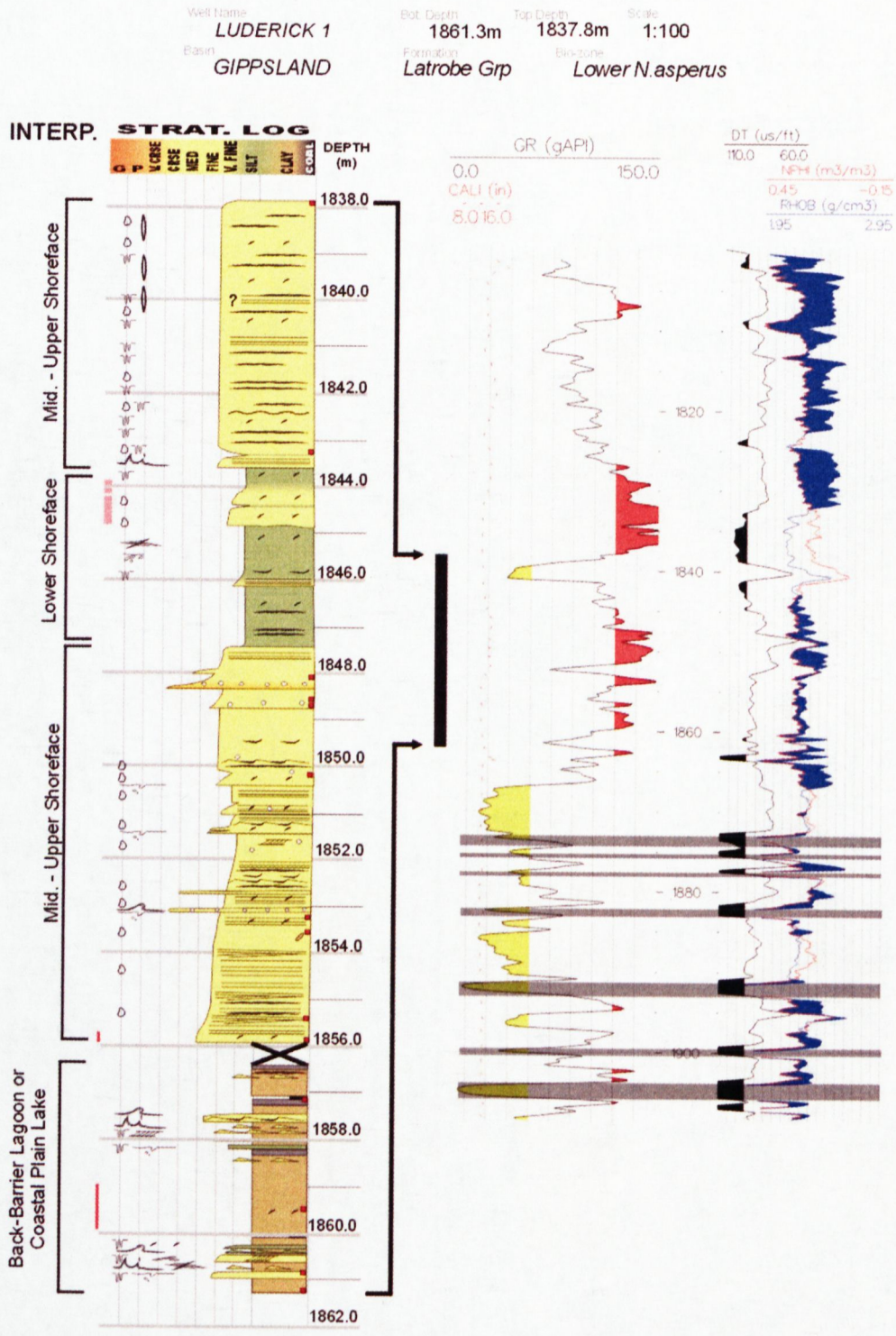

Figure 2.23—Core description for Luderick 1 showing shoreface and back barrier lagoon or lacustrine facies.

Facies Association 4—Foreshore and Beach Berm Deposits

Description: Middle to upper shoreface deposits are commonly overlain by relatively thin (<1 m) sandstone units. The thin sandstone units are interpreted as foreshore deposits, beach berm deposits that are generally not fully preserved. Parallel stratification and swash stratification are common as well as higher abundance of organic material and indications of shallow water deposition or emergence including thin coal beds, carbonaceous mudstone, and mudstone units with root traces. By comparison with shoreface deposits, bioturbation is limited in foreshore facies. Typically, sandstone of foreshore and beach berm facies is finer-grained and better sorted with lower clay content than shoreface sandstone. Generally, only *Ophiomorpha* is present in foreshore deposits. Foreshore deposits are under-represented in core by comparison with shoreface deposits.

On wireline logs foreshore deposits are usually represented in the upper-most portion of coarsening-upward shoreface successions. The foreshore facies themselves are generally characterised by higher GR values than the underlying shoreface sandstones imparting a subtle fining-upward character in the upper-most part of the overall, coarsening-upward nearshore succession (Fig. 2.26). The increase in natural radiation in foreshore deposits may be due to the higher proportion of radioactive heavy minerals and organic material.

Interpretation: The foreshore is distinguished from the shoreface because it is confined to the intertidal zone. The low abundance and diversity of trace fossils is probably due to the harshness of high energy environmental conditions within the swash zone. Indications of shallow water deposition and emergence suggest deposition in an environment more proximal than the shoreface. Additionally, greater compositional and textural maturity than underlying shoreface deposits is characteristic of foreshore deposits (Reineck & Singh 1975). Finer grain size in foreshore deposits (generally very fine- to fine-grained sandstone) than underlying shoreface deposits (very fine- to coarse-grained sandstone) is also common because wave energy and transport capacity has been limited by frictional resistance of the substrate due to shallower water depths in the foreshore.

In this study, foreshore and beach berm deposits are considered together, as all of these facies are rarely preserved and all occupy similar positions in nearshore environments. Generally, relative seal level fluctuations commonly result in the

erosion and modification of transgressive nearshore systems; barrier island and beach (foreshore) deposits have particularly low preservation potential (Reinson 1979, Barwis & Hayes 1979). It is likely that foreshore and beach berm/barrier island deposits in the study area were commonly eroded as wave base moved landward during episodic sea-level rises or as tidal channels cannibalise proximal nearshore deposits through lateral accretion. Facies that typically exist lower in the nearshore stratigraphic succession like lower–middle shoreface deposits and channellised deposits (tidal channel/inlet) tend to have the highest preservation potential. Figure 2.24 shows the spatial relationships between a foreshore/beach berm deposit and the related shoreface sands (termed 'nearshore marine sands'). The preservation potential of the shoreface sands is significantly higher than the more proximal barrier island deposit.

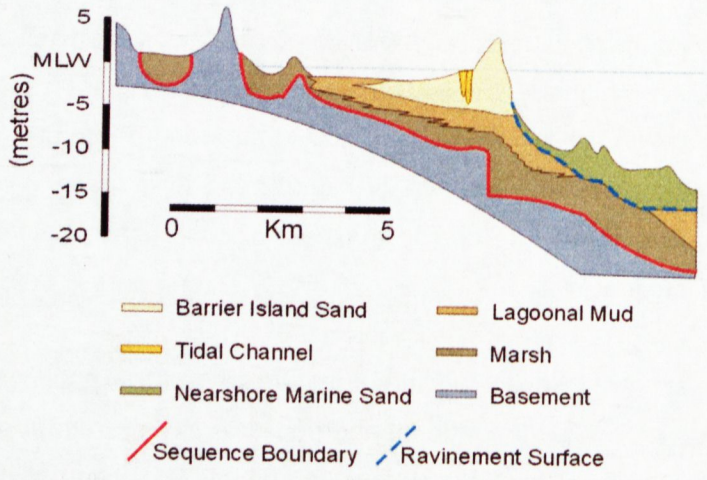

Figure 2.24—Holocene barrier island setting, Bethany Bay, Delaware (modified from Kraft 1971)

Facies Association 5—Tidal Delta

Description: Tidal delta deposits are generally coarsening-upward successions of mudstone, siltstone and very fine- to medium-grained sandstone. Coarsening-upward successions range from a metre to three metres in thickness with thin mudstone interbeds commonly separating successive coarsening-upward successions.

Common sedimentary structures in the lower sections of coarsening-upward successions are lenticular bedding, starved ripples, and wave ripple lamination as

well as soft sediment deformation features. The lower sections are dominated by mudstone and siltstone with fine interbedded sandstone units generally not exceeding a few centimetres in thickness. The upper, sandstone-dominated part of the succession is characterised by parallel stratification, ripple cross-lamination and wave ripple lamination. Bioturbation and soft sediment deformation are very common. Burrows may be associated with glaucony and ferric iron. Minor synaerisis cracks may exist in thin fine-grained units at the top of coarsening-upward successions.

Interpretation: Tidal delta coarsening-upward successions are typically accompanied by a suite of sedimentary structures that suggest an increase in depositional energy up-section. Lower energy conditions are suggested in the lower sections of coarsening-upward successions by the dominance of suspension deposits and only periodic clastic influx. In contrast, the lithology and structures of the upper sections suggest high depositional energy and abundant clastic influx by bedload transport.

The in-filling of a shallow standing body of water is suggested by the vertical succession of tidal delta deposits. Small-scale progradation is inferred for tidal delta deposits. The close vertical association with shoreface and foreshore deposits probably indicates a shallow lake or lagoon directly behind the shoreline. This may imply a barrier island depositional setting where most of the barrier has been eroded by lateral migration of tidal channels that fed ebb and flood tidal deltas. Sediment is generally derived from the shoreface or shelf and forced landward and through tidal inlets by flood tide and storm currents.

The tidal delta interpretation, as distinct from a small-scale fluvial delta (e.g. bay head delta), is favored for most deltaic deposits in the study area because of the close association between deltaic deposits and tidal channel deposits. Additionally, high to moderate bioturbation throughout the delta succession and common flaser and lenticular bedding may indicate that deposition was characterised by alternating periods of current activity and periods of relative quiescence (Reineck & Singh 1975), indicative of tidal currents. However, a bay head delta interpretation is also possible in which case sediment is delivered by a distributary network debouching into a back barrier lagoon setting from the landward side.

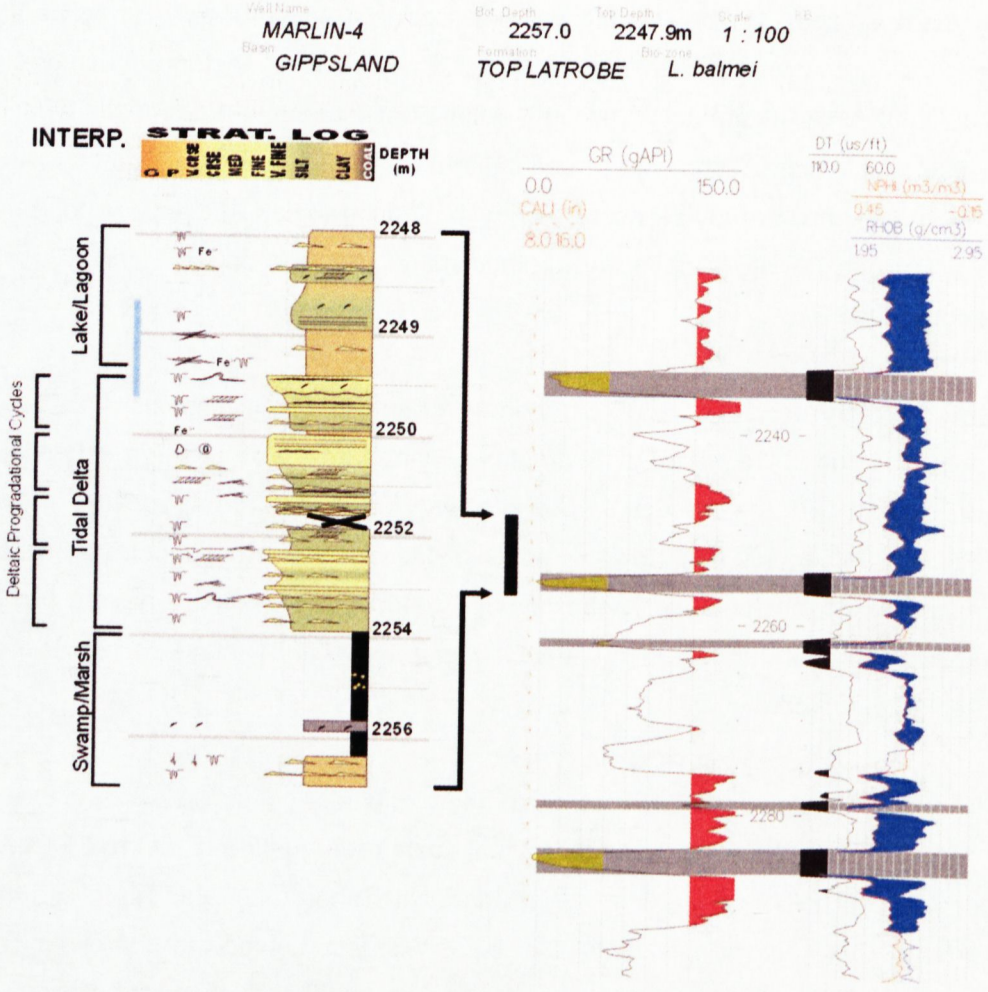

Figure 2.25—Core description for Marlin 4 showing back barrier peat swamp, tidal delta and lagoonal facies. Small-scale progradational successions are resolvable that are interpreted to be part of a small tidal delta deposit. The carbonate cemented area, indicated by the light blue bar, is associated with two faults that intersect the core.

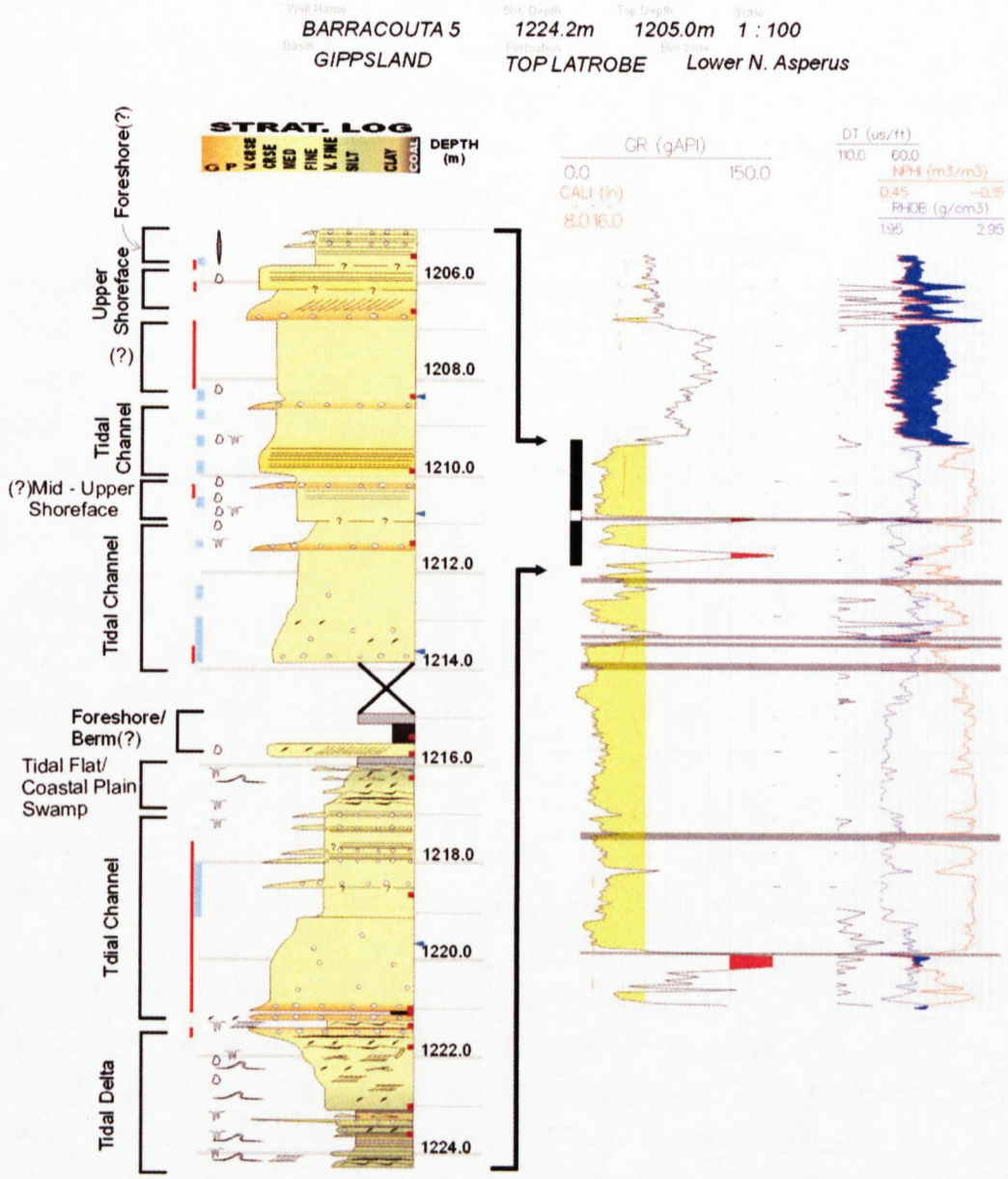

Figure 2.26—Core description for Barracouta 5. The succession is dominated by relatively coarse-grained tidal channel, shoreface and foreshore deposits. A progradational tidal deltaic deposit is resolvable between 1224.50 m and 1221.25 m.

Facies Association 6 — Fluvial Channel

Description: Fluvial channel deposits are characterised by fining-upward, trough and planar tabular cross-bedded, very fine- to coarse-grained sandstone units of one to two metres in thickness. The fining-upward succession is made up of individual fining-upward sandstone units, up to several decimetres in thickness. Parallel

stratification and layers of carbonaceous chaff are common. Sandstone units, particularly intervening shale and siltstone units, are associated with *Planolites* burrows, but the abundance and diversity of trace fossils is low. Burrows are commonly filled or ringed with glaucony. Intraformational conglomerate, consisting dominantly of pebble size siliceous clasts, is commonly associated with the basal surface of fining-upward sandstone units. Stacked successions of fining-upward sandstone units are generally capped with massive to finely laminated mudstone units that are interbedded with thin, ripple cross-laminated, lenticular bedded and starved rippled bedded sandstone units. Coal and root traces are commonly associated with the upper mudstone dominated part of the succession. Convolute bedding is the only soft sediment deformation feature that is commonly associated with fluvial channel deposits.

Fluvial channel deposits are generally represented on GR logs by serrated, fining-upward log motifs. Commonly, the fluvial channel log motif is encased top and bottom by mud-prone intervals represented by high value, serrated GR log patterns and negative separation of NPHI and RHOB logs.

Interpretation: Parallel stratification, trough cross-bedding and planar-tabular cross-bedding in the basal part of fining-upward successions indicate high flow regime and upper, low flow regime currents that are confined or semi-confined in close proximity to a horizontal pavement. The basal parts of fining-upward successions are interpreted as fluvial channel deposits consisting of individual small-scale fining-upward units that are interpreted to represent individual fluvial bar forms. Glaucony in burrows may suggest proximity to the shoreline. Channel deposits may represent part of a fluvial distributary system of the coastal plain.

The vertical pattern of sedimentary structures within the fining-upward succession indicates a decrease in flow velocity with time. The upper, finer-grained part of fining-upward successions are characterised by both bioturbation and root traces that suggest lower energy conditions with limited clastic influx, possible estuarine influence and subaerial exposure. A decrease in depositional energy up-section is characteristic of fluvial channel deposits and indicates filling and under-steepening of the channel with time. The upper lower energy part of fining-upward successions is interpreted as overbank deposits (levee and crevasse splay) or channel abandonment deposits.

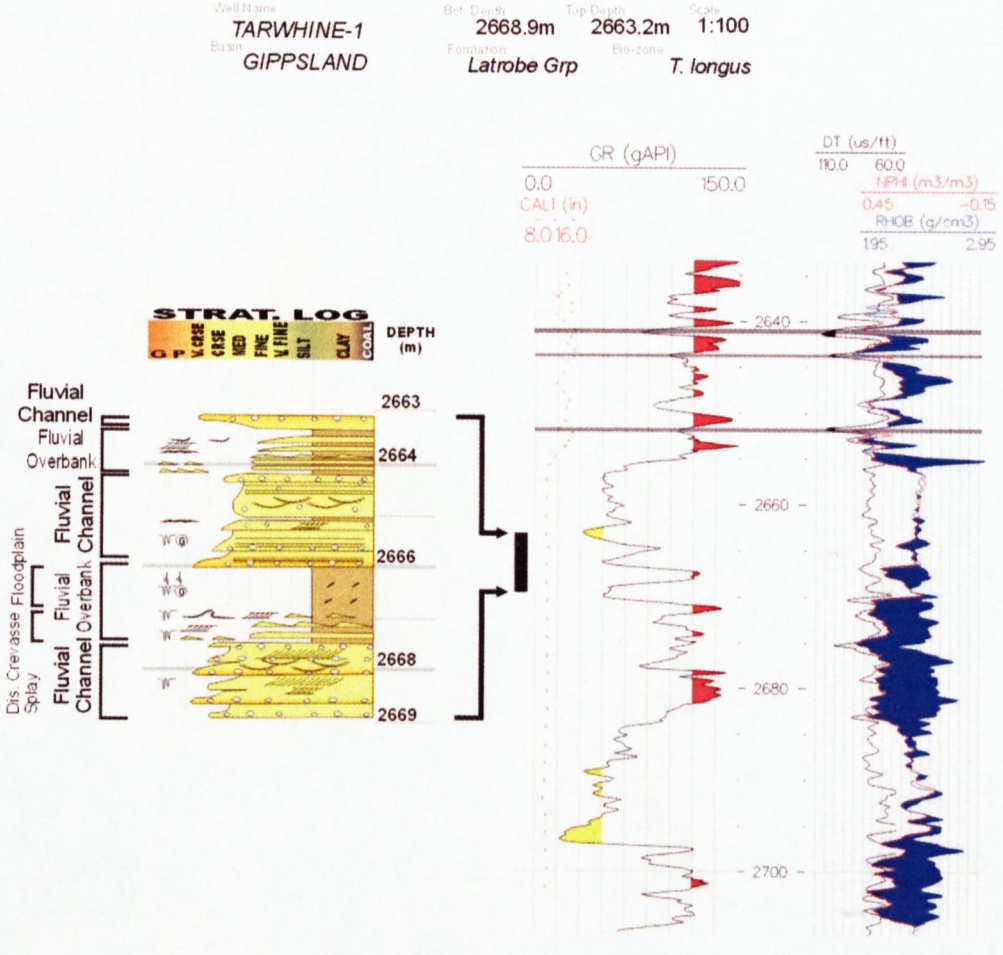

Figure 2.27—Core description for Tarwhine 1. Individual fining-upward packages of a decimetre to a few decimetres in thickness probably represent individual fluvial channel bar forms.

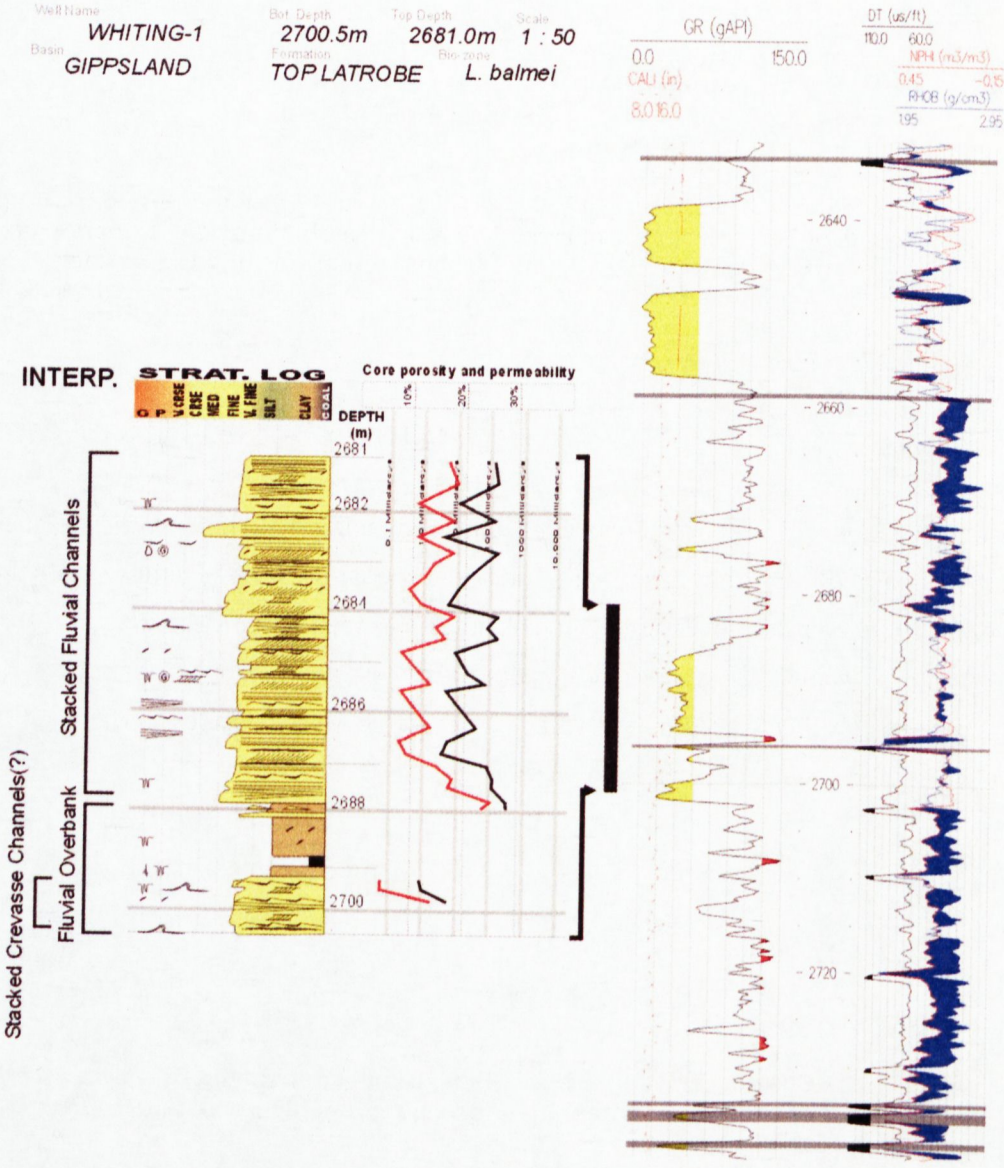

Figure 2.28—Core description for Whiting 1. Stacked fluvial channel deposits are characterised by cross-bedded fining-upward sandstone units. The presence of an *Ophiomorpha* burrow, glaucony and the relatively fine grain size may suggest proximity to the coastal plain. Fluvial distributary deposits may be represented in this core.

Facies Association 7—Fluvial Overbank

Description: Fluvial overbank deposits are characterised by successions of laminated, variably carbonaceous mudstone and siltstone with thin interbedded sandstone units. Vertical successions of fluvial overbank deposits may be several tens of metres in thickness. Interbedded sandstone units also occur, which range in thickness from approximately a metre to a few centimetres in thickness and are

generally composed of very fine- or fine-grained sandstone. Thin sandstone interbeds are generally lenticular bedded, parallel laminated, starved ripple bedded or flaser bedded. Thicker interbedded sandstone units are characterised by ripple cross-lamination, flaser bedding and a fining-upward or blocky vertical grain-size trend. Mudstone units are commonly interbedded with thin coals and may be bioturbated and/or associated with root traces. Soft sediment deformation such as flame structures, load casts and convolute bedding are common, particularly at the boundaries between sandstone and mudstone units.

Fluvial overbank deposits are characterised by serrated high value GR log motifs, with negative separation of NPHI and RHOB. Thin interbedded coals result in DT/NPHI/RHOB spikes.

Interpretation: Fluvial overbank deposits represent shallow floodplain lakes and swamps where deposition by suspension and peat growth are the dominant features. Sandstone interbeds formed from injection of bedload sediment into relatively low-energy depositional environments, probably associated with fluvial flooding events. Relatively thick, ripple cross-laminated sandstone interbeds are interpreted to represent crevasse channel facies that are dominated by confined flow in minor channels. Thinner sandstone beds interbedded with mudstone and siltstone are interpreted to represent distal, unconfined crevasse splay deposits and channel levee deposits.

Coals, carbonaceous mudstone and mudstone are all represented in the fluvial overbank environment. Their relative abundance is primarily a function of water table conditions and the amount of clastic influx. Thick coal successions are interpreted to have formed in coastal plain swamps, relatively protected from clastic sediment supply.

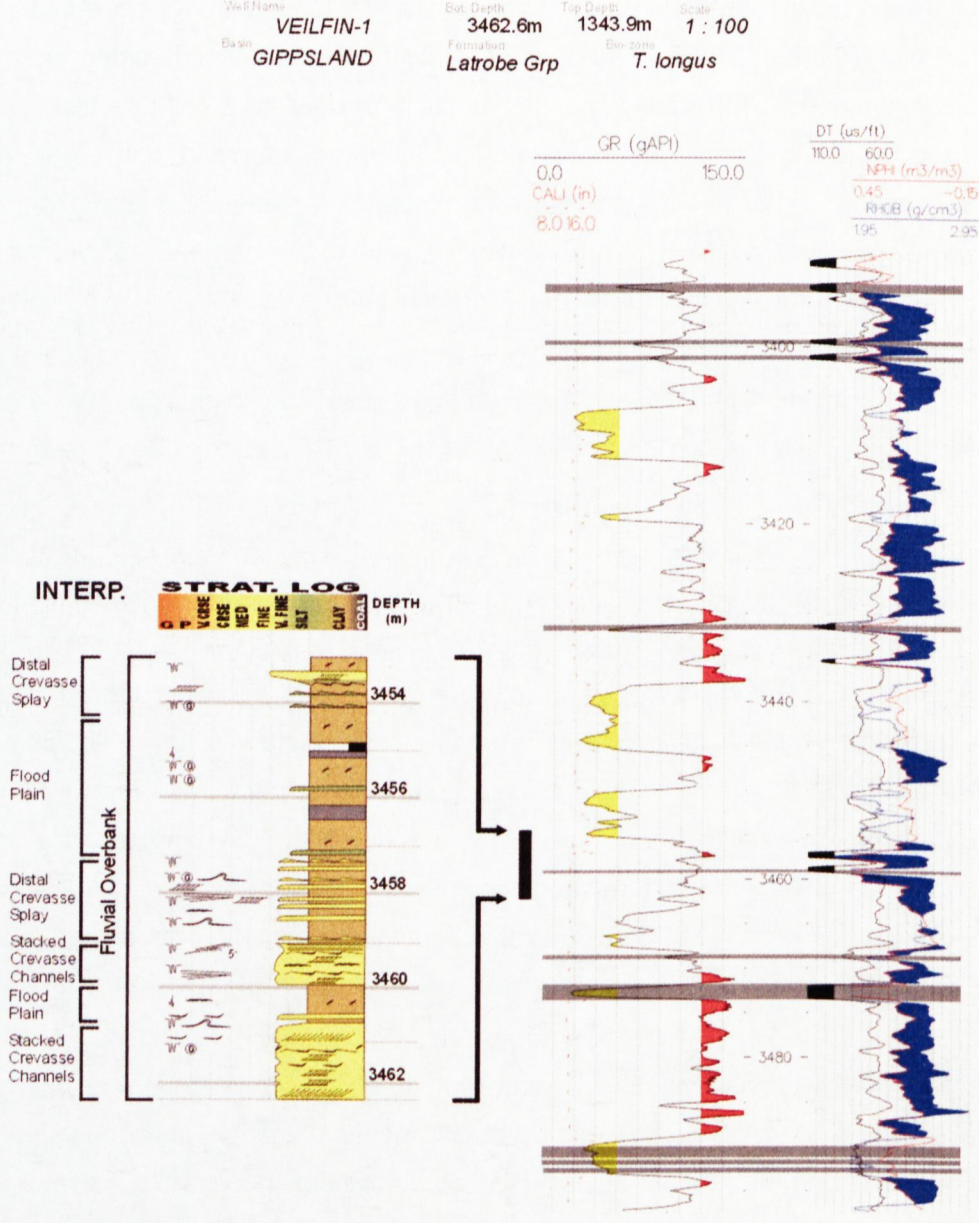

Figure 2.29—Core description for Veilfin 1. Crevasse splay deposits interbedded with floodplain deposits. Climbing ripple cross-lamination suggests rapid deposition during overbank flooding events.

Facies Association 8: Undifferentiated Coastal and Alluvial Plain

Description: Undifferentiated coastal and alluvial plain facies are characterised by heterolithic, very poorly sorted mudstone and sandstone mixtures. Principal bedding surfaces are not generally resolvable. Root traces, concretions and signs of immature palaeosol development are common. Carbonaceous material is abundant.

The very poorly sorted sandstone lithofacies and carbonaceous mudstone are the dominant components of coastal and alluvial plain facies. Vertical association with fluvial overbank deposits is common.

Undifferentiated coastal and alluvial plain facies are characterised by high value GR motifs with negative NPHI/RHOB separation.

Interpretation: The lack of primary structure in coastal and alluvial plain facies strongly suggests secondary overprint of original sedimentary fabric. Root traces, burrows and initial signs of palaeosol development like bleaching and concretions also point toward post-depositional modification of original sedimentary fabric.

Undifferentiated coastal and alluvial plain facies were produced during subaerial exposure or in very shallow water environments that were largely protected by clastic influx. Burrowing organisms and plant growth were common. The absence of thick peat accumulations may suggest that water table levels were generally too low to preserve large quantities of peat.

Undifferentiated coastal and alluvial plain facies are likely to have originally represented floodplain and other fluvial overbank facies that have been entirely reworked by organic and soil forming processes. However, the original environment of deposition for a particular unit of undifferentiated coastal and alluvial plain facies cannot be determined unequivocally due to the paucity of primary sedimentological structures.

Facies Association 9—Shelf Facies

Description: Shelf facies are characterised by thick successions of laminated and structureless mudstone and marl. Glauconitic and fossiliferous, matrix-rich sandstones are also represented in shelf facies.

Interpretation: Shelf facies are interpreted to be deposited beyond the maximum basinward limit of coarse clastic deposition (more distal than lower shoreface), and are dominated by mudstone and marl deposited from suspension. Marine fossils and

the abundance of glaucony suggest a marine environment so facies are identified as shelfal.

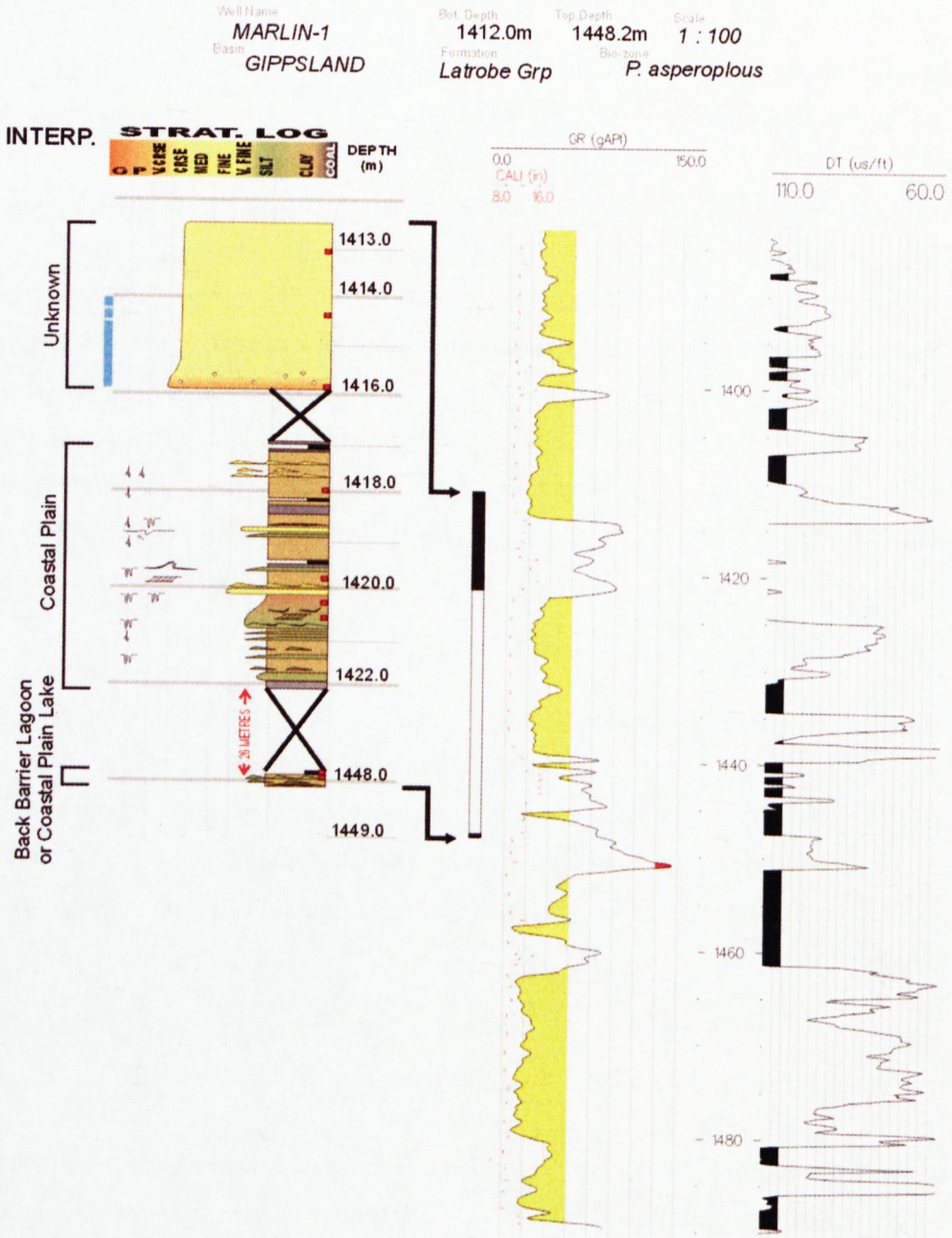

Figure 2.30—Core description for Marlin 1. The upper sandstone was essentially unconsolidated, so primarily structure and grain size trend were not easily resolvable. Consequently, no interpretation is provided for the upper sandstone.

Table 2.3 provides the relative abundance of lithofacies within facies associations. Abundant high-energy lithofacies such as conglomerate, cross-bedded sandstone and parallel-stratified sandstone occur in channellised and nearshore facies associations. These high-energy lithofacies are generally associated with good reservoir properties.

Table 2.3: Relative abundance of lithofacies within facies associations.

Horizontal= Facies Assoc. Vertical= Lithofacies	Fluvial Channel	Fluvial Overbank	Undiff. Coastal/ Alluvial Plain	Fluvial or Tidal Delta	Foreshore, Beach Berm, Barrier Island	Tidal Channel Deposits	Mid.-Upper Shoreface	Lower Shoreface	Shelf
	Proximal----------								Distal
Conglomerate	3	0	1	1	0	2	1	1	0
Parallel stratified, very fine- to fine- grained sandstone	2	1	1	2	3	2	3	3	0
Swash stratified very fine- to fine-grained sandstone	0	0	0	1	2	2	2	2	0
Cross-bedded medium- to very coarse-grained sst	3	1	0	0	1	1	2	0	0
Structureless and graded medium- to coarse-grained sandstone	2	1	1	1	1	2	2	1	0
Ripple cross-laminated very fine- to medium-grained sst.	2	3	1	3	1	2	1	2	0
Very poorly sorted sandstone	0	2	3	0	0	0	0	0	0
Finely interbedded mudstone and siltstone to v. fine sst.	1	3	1	2	0	1	0	2	1
Structureless and finely laminated mudstone	1	3	1	2	0	1	1	2	3
Carbonaceous mudstone and coal	1	2	3	1	1	1	1	0	0

3 = abundant; 2 = common; 1 = rare; 0 = absent; ?=unknown

Pore-Scale Heterogeneity

Pore-scale heterogeneity was studied through transmitted light microscope petrography, scanning electron microscopy and X-ray diffraction. All transmitted light microscopy including point counting and SEM was carried out by Ghazi Krishan (NCPGG/Santos). An interpretation is proposed based on his work.

Three facies types with unique petrographic characteristics are identified:

- **Nearshore**: including samples derived from shoreface and foreshore settings
- **Coastal/Alluvial Plain:** including fluvial channel and overbank facies
- **Shelf:** including inner-shelf, shelf and submarine canyon facies.

PETROGRAPHY OF NEARSHORE FACIES

Sandstone facies that are interpreted to have been nearshore depositional settings are typically very-poorly to well-sorted, and sub-angular with a range of mineralogical compositions. However, most nearshore samples are compositionally classified as sublitharenite to litharenite. Quartz is generally monocrystalline and rarely has embayments and stress fractures. Minor dissolution rims on quartz grains are apparent in some samples. Feldspar framework grains are dominantly orthoclase. Plagioclase only represents approximately four percent of the total feldspar in nearshore samples. Feldspar grains are commonly weathered, imparting a 'dusty' appearance, and commonly show signs of partial dissolution. 'Skeletal' feldspar grains are fairly common and may be replaced in part by kaolin or chlorite. Lithic framework grains are dominantly metamorphic rock fragments including schist fragments. Muscovite and biotite grains are also common. Trace glaucony and volcanolithic framework grains also occur in nearshore facies. The percentage of primary matrix in nearshore sandstone is generally low but ranges up to 40% locally.

Samples may be poorly lithified particularly if the samples are derived from relatively shallow locations in the basin. Evidence for mechanical compaction is limited; grain-to-grain contacts are dominantly point contacts. Additionally, there is little deformation of less mechanically stable grains such as mica and the grain packing arrangement is generally loose in nearshore samples. Primary sedimentary bedding is evident in a few samples. Bedding is resolvable because of the concentration of carbonaceous material along bedding planes and from grain size segregation between sedimentary laminae. Bedding and sorting characteristics of sandstone are disrupted by bioturbation in some cases.

Kaolin and quartz overgrowth cements are the dominant kind of authigenic clay and cement in nearshore facies sandstone of the Gippsland Basin study area. Kaolin can be seen in SEM images occluding porosity in Figure 2.31B. In lesser amounts illite/smectite may also exist in nearshore facies. Siderite, dolomite and calcite

diagenetic cement also occur variably in nearshore facies of the study area. Siderite cement may completely occlude porosity in some nearshore samples, particularly in finer grained samples of the lower shoreface. More proximal nearshore facies commonly have remnant kaolin 'floating' in pore space, suggesting some secondary porosity formed through dissolution of framework grains and authigenic clay (although clay floating in pore space may be an artefact of sample preparation in some cases).

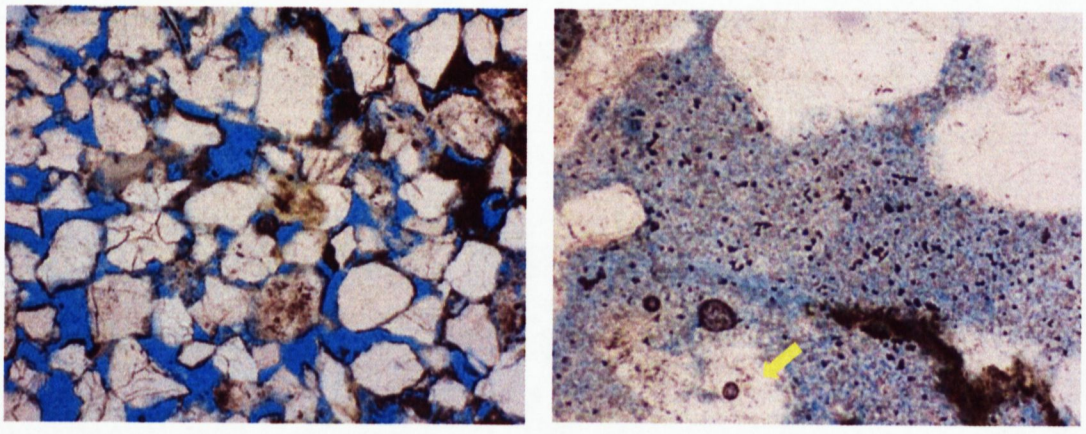

A B

Figure 2.31—Barracouta 5: Poorly consolidated shoreface sandstone. Partially dissolved feldspar and dissolution rims on quartz grains suggest secondary porosity (A). Porosity is occluded by authigenic kaolin. Replacement of a feldspar grain with kaolin is evident in the lower left of the image (arrow).

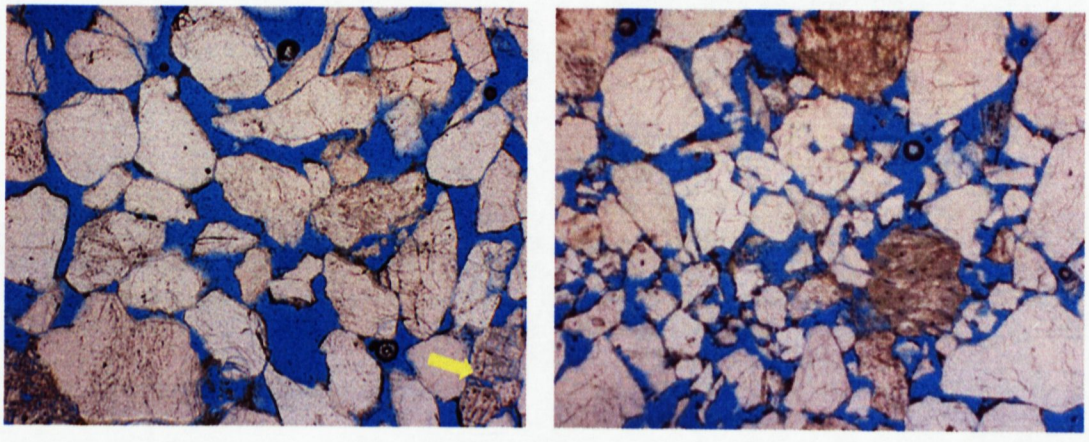

A B

Figure 2.32—Luderick 1: Poorly consolidated, high porosity, sub-angular sandstone. Well-sorted sandstone (A) and poorly-sorted sandstone (B) are shown. Partial dissolution of feldspar is evident (arrow). Framework grain composition is mostly quartz and feldspar, but lithic metamorphic clasts are also present (B).

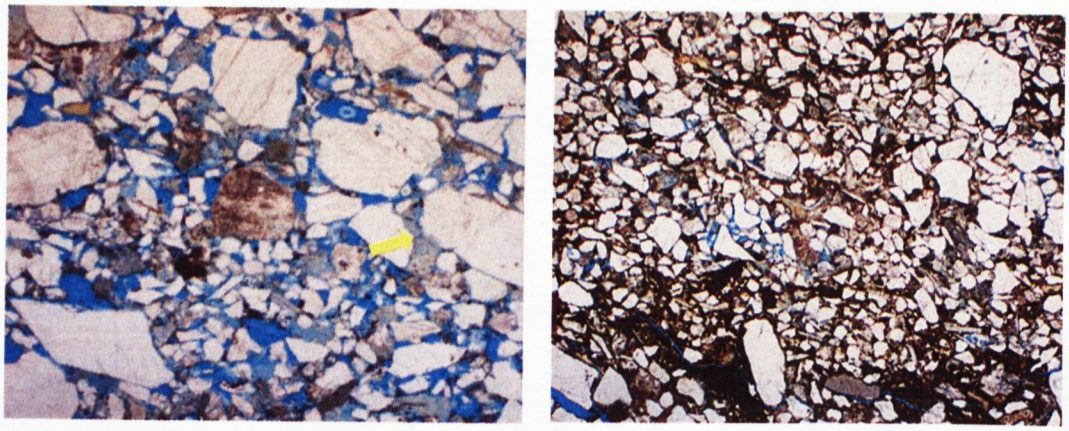

A B

Figure 2.33—Seahorse 2: Poorly sorted, matrix poor (A) and matrix rich (B) sandstone. Though primary matrix is absent in (A), kaolin can be seen occluding pore space (arrow).

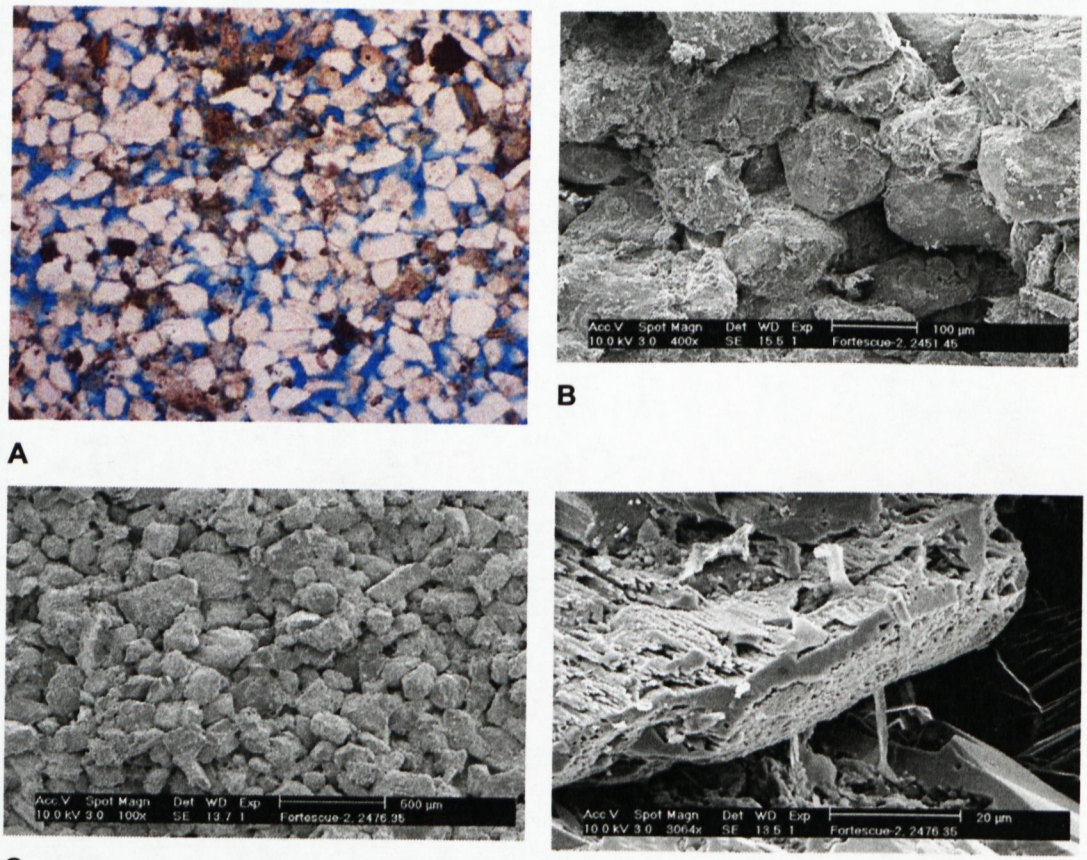

A B C D

Figure 2.34—Fortescue 2: Fine- to very fine-grained, well-sorted, middle to upper shoreface sandstone. SEM images suggest good porosity and good pore interconnectivity (B & C). 'D' shows partial feldspar dissolution.

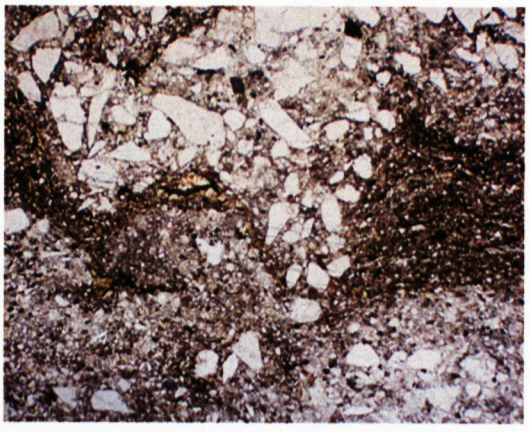

Figure 2.35—Snapper 5: Poorly sorted matrix rich sandstone. Primary texture is disrupted by bioturbation.

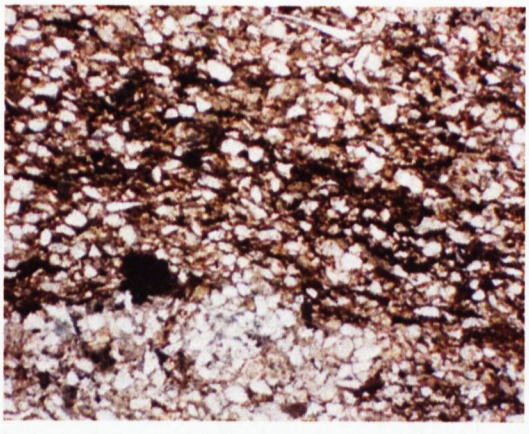

Figure 2.36—Fortescue 1: Very fine-grained, matrix rich sandstone.

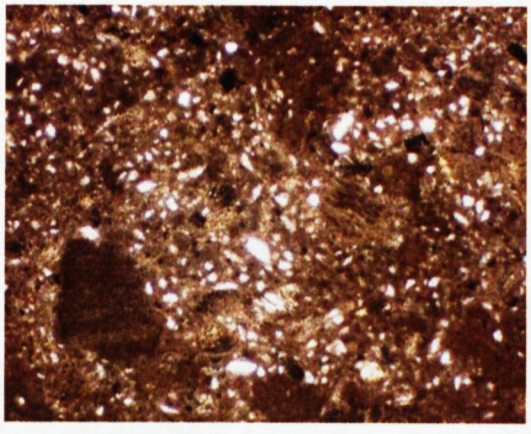

Figure 2.37—Marlin 4: Silt-mudstone seal facies. Silt and very fine-grained sandstone grains are encased in mudstone.

Petrography of Coastal/Alluvial Plain Facies

Sandstone of coastal/alluvial plain facies is typically litharenites or feldsareintes. They are generally moderately to well sorted, fine- to very coarse-grained and sub-angular to sub-rounded. Quartz grains are commonly highly stressed and polycrystalline. Well developed quartz overgrowth cement and dissolution rims are common features of quartz grains in coastal to alluvial plain facies.

Sandstone of coastal/alluvial facies is characterised by high proportions of feldspathic and lithic framework grains. Like nearshore facies, feldspar in coastal/alluvial plain facies is generally orthoclase, with plagioclase representing only approximately four percent of the total feldspar content. Feldspar grains generally show evidence of dissolution or are completely replaced by kaolin. Lithic grains are mostly metamorphic and may also show signs of partial dissolution. Lithic metamorphic grains may represent up to 30% of the total framework grain content. Mica, sedimentary rock fragments, and volcanic rock fragments are also represented in coastal/alluvial plain sandstone to a lesser degree. Primary matrix is limited in sandstone of the coastal/alluvial plain facies.

A significant volume of pore space is reduced by mechanical compaction in coastal/alluvial plain sandstone. Grain-to-grain contacts are generally straight and, more rarely, concavo-convex. Mechanically labile components are often deformed or broken between more rigid grains. Evidence of bioturbation exists in petrographic samples and laminae may be resolvable. Quartz overgrowth and kaolin are the dominant authigenic cements in coastal/alluvial plain sandstone. However, illite/smectite and chlorite are also represented in small amounts.

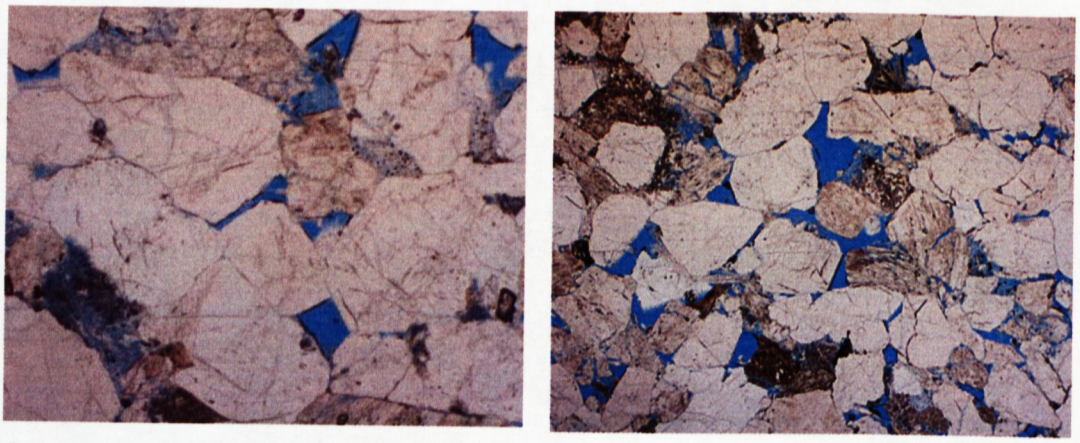

A B

Figure 2.38—Tarwhine 1: Coarse-grained fluvial sandstone. Straight grain-to-grain contacts and deformed mica grains, suggest a greater degree of compaction than is seen in nearshore samples. Quartz overgrowth cement is common.

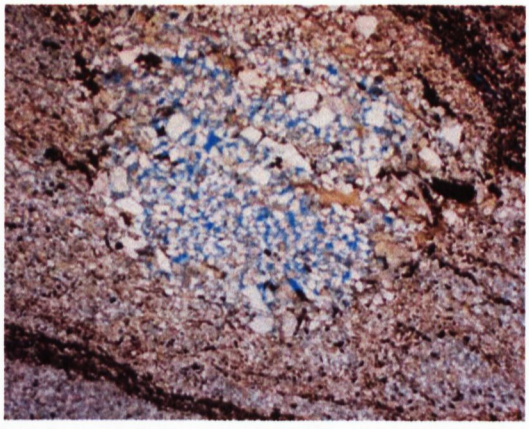

A

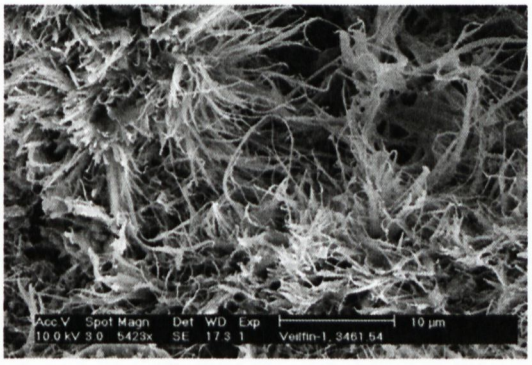

B

Figure 2.39—Veilfin 1: (A) shows a horizontal burrow in very fine-grained sandstone and siltstone of the fluvial overbank facies. Primary bedding is evident from layers with high concentrations of organic material (A). 'B' shows 'hairy' illite in sandstone pore space.

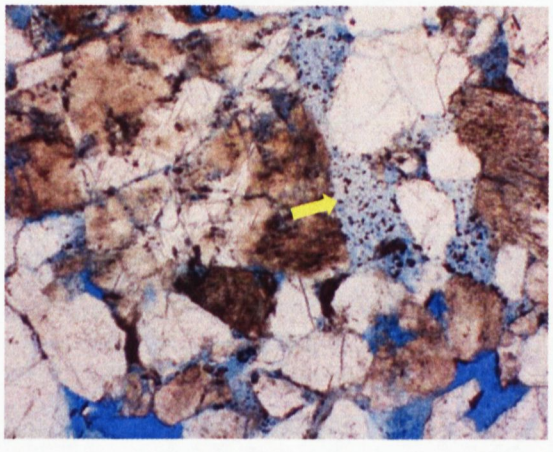

A

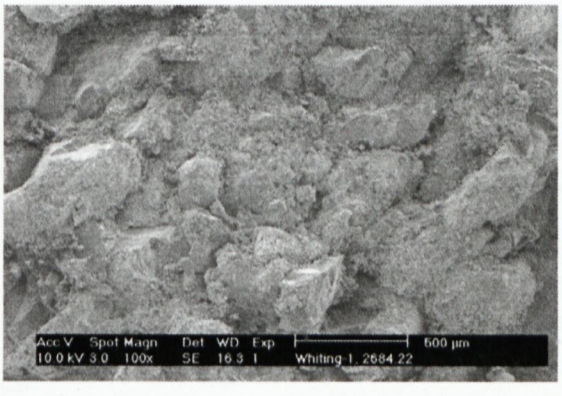

B

C

Figure 2.40—Whiting 1: Medium- to coarse-grained fluvial sandstone with kaolin cement (arrow). SEM suggests moderate degradation of reservoir quality due to kaolin (B). A close-up view of kaolin 'booklets' is provided (C).

Petrography of Shelf Facies

Few shelf facies petrographic samples were taken as mostly marls and shales are represented. Some sandstone of the inner shelf does exist however. The inner shelf sandstone is medium-grained, matrix-rich glauconitic and fossiliferous sandstone. Porosity is entirely occluded by mudstone matrix (30%). Glaucony and quartz are the only major framework grain components and are of approximately equal proportions (31% and 27% respectively).

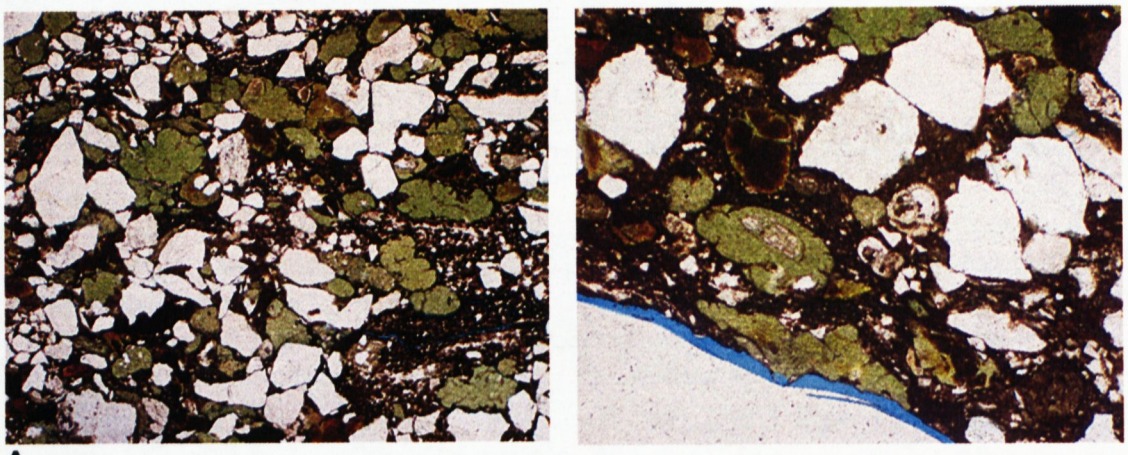

A B

Figure 2.41—Wrasse 1: Glauconitic, fossiliferous, matrix-rich sandstone of the Turrum Formation.

Table 2.4—X-ray diffraction results for selected samples.

Well Name	Depth	Quartz	Feldspar	Pyrite	Calcite	Dolomite	Siderite	Kaolin	Illite	Chlorite	I/S
Fortescue 1	2424.60	56.50%	5.20%	2.10%	0.20%	0.10%	0.00%	16.50%	19.40%	0.00%	0.00%
Fortescue 2	2451.45	76.40%	8.00%	0.00%	0.00%	0.00%	0.00%	7.80%	7.80%	0.00%	0.00%
Fortescue 2	2471.57	69.50%	11.70%	0.30%	0.00%	0.00%	0.00%	9.20%	9.20%	0.00%	0.00%
Marlin 4	2248.80	56.20%	8.50%	0.30%	0.20%	0.00%	0.00%	22.90%	11.90%	0.00%	0.00%
Marlin 4	2250.40	61.80%	12.40%	0.50%	0.00%	2.50%	2.60%	13.00%	7.20%	0.00%	0.00%
Marlin 4	2249.80	16.00%	1.60%	0.90%	0.20%	0.30%	69.60%	6.30%	5.20%	0.00%	0.00%
Marlin 4	2248.25	3.00%	0.80%	0.00%	0.10%	33.40%	60.60%	0.60%	1.50%	0.00%	0.00%
Marlin 4	2248.20	0.50%	3.20%	5.30%	0.20%	2.00%	88.60%	0.10%	0.10%	0.00%	0.00%
Seahorse 2	1486.60	25.60%	10.50%	0.00%	0.00%	39.90%	0.00%	17.00%	7.00%	0.00%	0.00%
Snapper 5	1413.92	57.30%	6.70%	0.40%	0.10%	22.20%	0.00%	10.00%	3.30%	0.00%	0.00%
Tarwhine 1	1392.10	81.00%	2.60%	0.40%	0.10%	0.20%	0.20%	12.50%	3.00%	0.00%	0.00%
Veilfin 1	3461.54	68.00%	3.00%	0.00%	0.00%	0.30%	0.60%	5.40%	12.00%	2.40%	8.30%
Veilfin 1	3453.58	58.10%	4.80%	6.50%	0.00%	0.00%	2.50%	3.60%	17.60%	6.90%	0.00%
Whiting 1	2684.22	78.60%	0.00%	0.10%	0.00%	0.10%	1.10%	14.10%	6.00%	0.00%	0.00%
Whiting 1	2682.00	74.80%	0.00%	0.10%	0.20%	0.20%	0.20%	19.90%	4.60%	0.00%	0.00%
Wrasse 1	2746.05	49.10%	8.90%	0.30%	1.40%	0.00%	1.20%	5.00%	4.70%	16.90%	12.60%

PETROGRAPHIC INTERPRETATION

Low compositional and textural maturity in sandstone of the Gippsland Basin is the result of a high proportion of feldspathic and lithic framework grains as well as a high proportion of mudstone matrix and poor sorting in many petrographic samples. The degree of compositional and textural maturity has a relationship with the part of the depositional system in which the sandstone was deposited. Sandstones deposited in more proximal areas of the depositional system have a lower compositional maturity than sandstone deposited in more distal, nearshore depositional settings.

The relationship between depositional setting and compositional maturity is expected, in the sense that sediments farther from the source area have a greater time in transport, and therefore, are subjected to a higher degree of chemical and mechanical weathering. In the Gippsland Basin, the relationship between depositional setting and compositional and textural maturity is enhanced because sediments that are deposited in relatively distal nearshore settings are likely to be subjected to wave reworking, which is an effective mechanism for enhancing compositional and textural maturity. However, even the sediments from upper shoreface and foreshore settings are unusually immature, which are characteristically subjected to the most wave energy. This may suggest a fairly local sediment source and possibly a relatively high rate of deposition.

The differing levels of compositional and textural maturity for various facies have implications for the subsurface behaviour of SC CO_2. For example, the opportunity for mineralogical trapping is different for nearshore, coastal/alluvial and shelf facies. The availability of basic cations (Fe^{2+}, Mg^{2+}, Ca^{2+}) is the limiting factor in terms of the amount of mineralogical trapping that can occur (see Chapter 1). The rock components that represent mineralogical trapping opportunities identified in this study are:

- Carbonate cement (calcite, dolomite, and siderite)
- Metamorphic and volcanic lithic framework grains (e.g. mica in schist grains)
- Glaucony
- Carbonate minerals in marl
- Plagioclase (Anorthite) framework grains.

The sealing facies may have the most appropriate mineralogy to promote mineralogical trapping because, Mg^{2+} will be available from glauconitic components and Ca^{2+} will be available from calcareous marls. However, the amount of reactant that will be available to SC CO_2 is ultimately limited because large-scale flow is not likely to occur through seal facies. The damage zones of faults in the Gippsland Basin are associated with intense siderite and dolomite cementation, which may also react with SC CO_2.

Reservoir facies also offer opportunities for mineralogical trapping in the form of carbonate cement, authigenic clay, basic lithic framework grains, and rarely feldspar. Sandstone of coastal/alluvial plain facies is characterised by lower compositional maturity than sandstone of nearshore facies. Consequently, more chemically unstable lithic and feldspathic framework grains will be available to SC CO_2 and the opportunity for mineralogical trapping is greater in coastal/alluvial plain sandstone (Fig. 2.42).

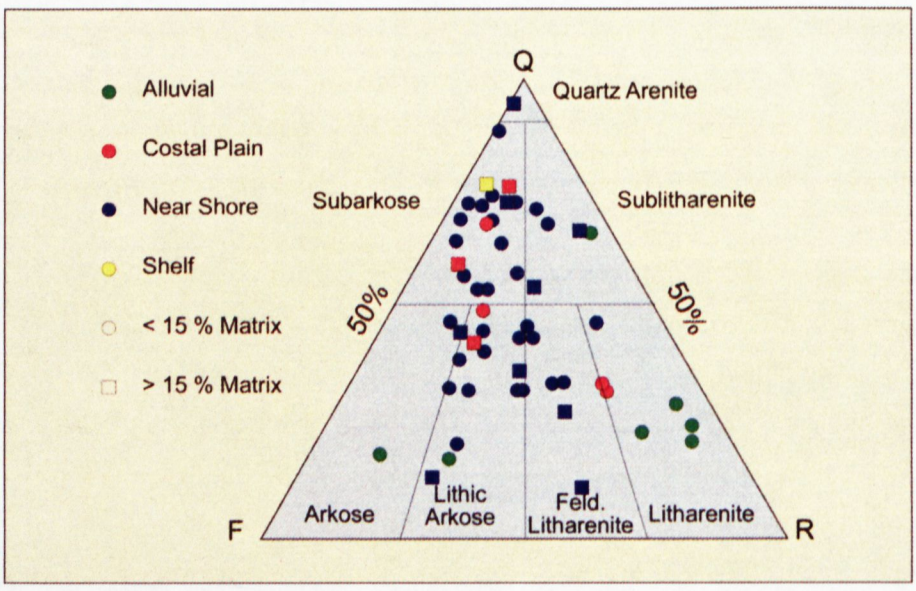

Figure 2.42—Quartz, feldspar, and rock fragment diagram for the petrographic sandstone samples described in this study. Gippsland Basin sandstones are generally compositionally immature, particularly samples from relatively proximal depositional environments. In general, sandstones with a greater proportion of lithic rock fragments (R) and feldspar (F) can be considered more chemically reactive than sandstones that consist mostly of quartz (Q).

Even in the presence of appropriate mineralogy, CO_2-rock reaction kinetics are likely to be slow, so mineralogical trapping must be regarded as a long-term trapping mechanism (see Chapter 1). The more immediate influence of pore-scale heterogeneity is the effect of textural variation on reservoir flow properties. Like

mineralogical trapping potential, the reservoir flow properties also vary between facies as a result of pore-scale textural and compositional differences between facies.

In general, porosity and permeability are higher in nearshore sandstones than in coastal/alluvial plain sandstones. At pore scale, there are a couple of reasons for this difference in reservoir properties:

- Coastal/alluvial plain sandstone samples have undergone a greater degree of compaction than nearshore sandstone samples.
- Coastal/alluvial plain sandstones have both a high proportion of authigenic clay and more evidence of dissolution than nearshore sandstone.

The disparity in the degree of mechanical compaction between facies is in part a result of sampling bias. The greater degree of mechanical compaction in coastal and alluvial plain sandstones is a function of depth of burial. Mechanical compaction is greater in coastal/alluvial plain facies in part because the coastal/alluvial plain samples used in this study were generally recovered from greater depth than the nearshore samples.

However, the higher degree of mechanical compaction in coastal/alluvial plain sandstones is not entirely a result of sampling bias. Mechanical compaction results largely from the deformation of lithic framework grains and partially dissolved feldspar framework grains between more rigid quartz grains (Fig. 2.38, A & B). Because coastal/alluvial sandstone has a greater proportion of feldspathic and lithic framework grains than nearshore sandstone, coastal/alluvial plain sandstone is generally the less mechanically stable of the two facies. Consequently, coastal/alluvial plain sandstone is likely to be more susceptible to mechanical compaction than nearshore sandstone under the same pressure/temperature conditions.

The high proportion of authigenic clay and evidence of secondary dissolution in coastal/alluvial plain sandstone stems from its relatively low compositional maturity. Lithic and feldspar grains are more susceptible to chemical alteration than quartz grains. Greater chemical alteration in coastal/alluvial plain sandstone than in nearshore sandstone results from the higher proportion of feldspar and lithic framework grains in the former. Figure 2.40 A & B shows framework grains that are altered and replaced by illite/smectite and kaolin. The effect of the alteration of framework grains is to reduce porosity, and particularly, permeability. Permeability is

affected to a greater degree than porosity because less authigenic clay is required to block pore throats than is required to completely fill porosity. The disproportionate reduction in porosity is particularly pronounced where illite and smectite exist, both of which have 'pore-bridging' structures.

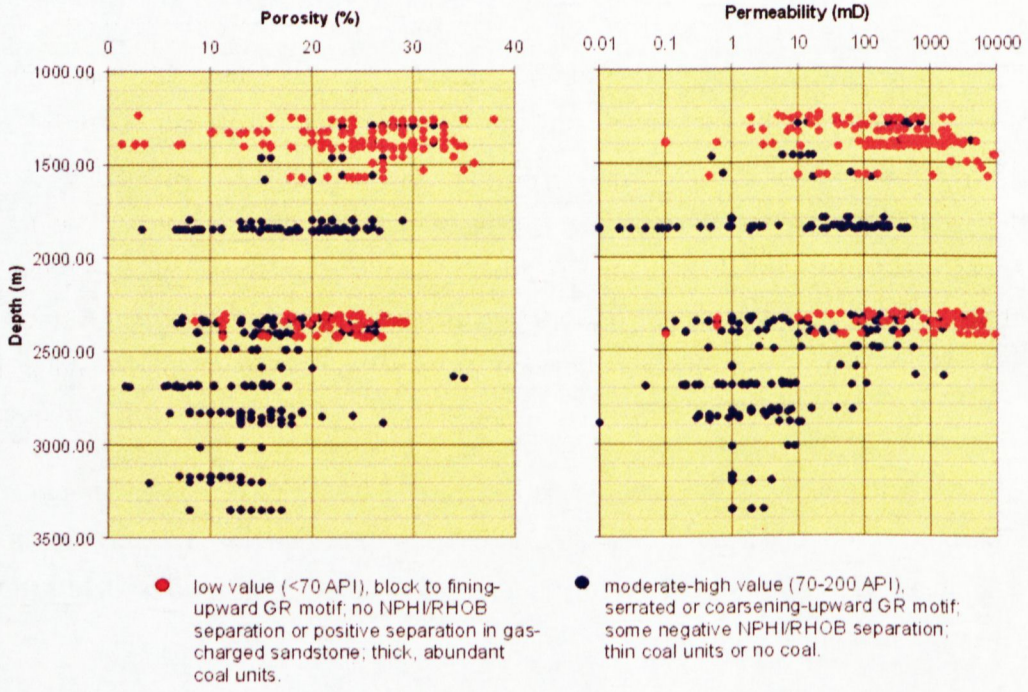

Figure 2.43—Porosity and permeability plotted against depth. Two facies identified from wireline log motif are shown.

Coastal/alluvial plain facies have more evidence of significant secondary dissolution, such as 'skeletal' feldspar grains and dissolution rims on quartz, than nearshore facies (Schmidt & McDonald 1979). For similar reasons that chemically unstable framework grains in coastal/alluvial plain sandstone are often altered to authigeneic clay, chemically unstable framework grains are also commonly dissolved. Although authigenic clay and dissolution occur for similar reasons, they are competing processes in the sense that the former reduces porosity and permeability and the latter enhances porosity and permeability. Figure 2.43 shows relatively high permeability at the 2300 m – 2500 m interval that appears discordant with the general reduction in permeability with depth. This may result from enhanced reservoir properties through secondary dissolution. Previous work also identifies secondary dissolution as a contributing factor to unusual porosity trends with depth in the Gippsland Basin (Bodard *et al.* 1984).

It is difficult to distinguish the individual effects of mechanical compaction, authigenic clay formation, and dissolution on coastal/alluvial plain sandstone. Although coastal/alluvial plain sandstone is clearly affected to a greater degree by diagenetic processes than nearshore sandstone, routine core analysis suggests that average reservoir properties are comparable between the two facies at core plug scale (< 3 cm; Fig. 2.43). The comparable average flow properties of nearshore and coastal to alluvial plain facies stems in part from sampling bias—only sandstones are sampled for routine core analysis and typically core is acquired in sandstone units, which are over-represented as a consequence. Despite the biased measurements, low porosity and low permeability 'tails' on the histograms of coastal-alluvial plain facies suggests greater pore-scale heterogeneity than is present in nearshore facies (Fig. 2.44). This is interpreted to be largely a result of a greater proportion of pore occluding authigenic clay in fluvial sandstones. Larger-scale reservoir heterogeneity between coastal/alluvial plain facies and nearshore facies is also likely to have an impact on SC CO_2 behaviour and is discussed below.

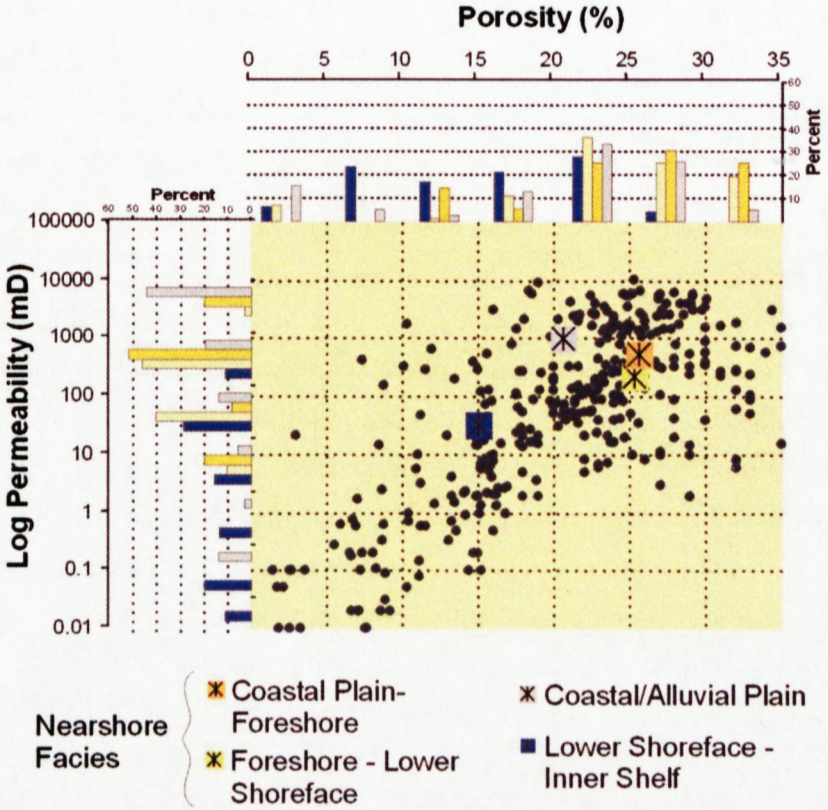

Figure 2.44—Routine core analysis porosity and permeability for the study area. Measurements are grouped according to major facies associations that exist in the study area.

Implications for CO_2 Geosequestration and Geological Model Construction

The sedimentological division of facies and the division of facies for the construction of a geological model are not identical in this study, but the facies divisions are complementary. Facies divisions must meet the following two criteria to be meaningful in the context of geological modeling for CO_2 geosequestration:

- The facies must have different fluid flow properties, in terms of the values of porosity and permeability or in terms of the likely spatial distribution of flow properties, and/or the facies must be significantly different in terms of their compositions such that the chemical behaviour of CO_2 is likely to be different between facies.
- The facies must be mappable not only with full-hole core, but from their character on wireline logs or from seismic characteristics.

The first point is self-evident; if two facies will induce similar subsurface behaviour of SC CO_2 there is no point in distinguishing between them in the reservoir model. The second point has to do with the spatial distribution of data and geostatistical population of a reservoir model (discussed in greater detail in Chapters 4 & 6). If facies are to be populated as an attribute in a reservoir model, facies must be identified at every grid cell that intersects a well bore if the well is to be used in the study. Because the paucity of well data in petroleum data sets is generally problematic, removing from the study wells in which facies distinctions from wireline logs are unclear is generally an unfavourable option. Instead, the number of facies can be reduced until their identification is possible at all of the wells. For example, it may not be possible to distinguish between crevasse splay channels and fluvial channels on wireline logs, although they can be distinguished sedimentologically in core. The most effective course of action in this situation might be to combine both facies for the purpose of reservoir modeling, provided their flow properties were not significantly different.

Although combining facies results in some loss of sedimentary detail, the practicalities of reservoir modeling are such that more than three facies are not generally used in reservoir models (Deutsch 2002). The trade-off between the capturing as much sedimentological detail as possible and minimising the computational cost (e.g. time and computing power required to build models and run flow simulation) is ultimately governed by the objectives of the study. In the context of this study, mapping detailed variations in flow behaviour over small areas is less

important than correctly characterising regional patterns of flow behaviour. Additionally, a very large area must be represented in the geological model for this study by comparison with typical geological models for hydrocarbon development/production, which generally focus on a single hydrocarbon field. For this study there is increased uncertainty regarding regional facies distributions because of relatively large areas without well control, between hydrocarbon fields particularly. Consequently, employing a relatively simple facies scheme where facies can be mapped with both well data and seismic data is useful provided the facies division captures the important aspects of reservoir/aquifer flow properties and distribution. Three facies have been identified for use in the reservoir model and are described in Table 2.5.

Table 2.5: Description of facies used in the geological model.

Model Facies	Facies Associations	Average Properties	General Comments	Strat.
Lower Shorface - Shelf	Lower Shoreface Inner-Shelf	∅ = <5% - 25% K = 0.01 mD-200 mD	Glaucony and calcareous components may be chemically reactive. Poor fluid flow characteristics. Primarily fine-grained seal facies.	Gurnard F. 'Coarse Clastics' Latrobe Group
Nearshore	Middle to Upper Shoreface Tidal Channel Foreshore Fluvial or Tidal Delta Back Barrier Lagoon/Coastal Plain Lake	∅ = 20% - 35% K = 10 mD – 10,000 mD	Moderately compositionally mature sandstone; fairly chemically inert. Good sand body interconnectivity; low reservoir heterogeneity. Clean sandstone, moderate diagenetic alteration.	
Coastal-Alluvial Plain	Fluvial Channel Undifferentiated Coastal Plain Fluvial Overbank; (crevasse splay, floodplain, floodplain lake)	∅ = <5% - 35% K = 0.1 mD – 10,000 mD	Compositionally immature sandstone; chemically reactive. Poor reservoir interconnectivity; high reservoir heterogeneity. Diagenetically altered: authigenic clay, mechanical compaction, secondary dissolution.	

Based on petrological characteristics and routine core analysis lower shoreface-shelf facies will behave dominantly as barriers to fluid flow. In contrast, coastal/alluvial plain and nearshore facies are comprised of some depositional units that have good reservoir characteristics and may be characterised as reservoir/aquifer targets. The two primary reservoir targets in the study area are: nearshore (middle to upper shoreface, tidal channel and foreshore/barrier island deposits), and fluvial channel deposits.

Reservoir properties of nearshore deposits are excellent with porosity ranging from 20% – 35% and permeability ranging from 10 mD – 10,000 mD. Unusually high porosity and permeability measurements result from uncemented and poorly consolidated nearshore deposits at shallow depths (<1200 m). However, well-lithified nearshore deposits also have good reservoir properties resulting from their relatively high textural and compositional maturity. The lack of chemically and mechanically immature framework components prevents the development of authigenic clay and the consequent occlusion of porosity and permeability. However, reservoir properties are locally reduced within nearshore deposits by carbonate cement, primarily dolomite. Pervasive cementation and significant reduction of flow properties appears to occur only in close proximity to faults.

The vertical succession of shoreface deposits in the upper Latrobe Group shows good connectivity of individual nearshore deposits and suggests that lateral connectivity may also be favorable for forming interconnected flow units. Comparison of the nearshore deposits described in core to analogues suggests widths of individual reservoir/aquifer units of between 500 m – 5000 m and lengths between 1000 m – 10,000 m (Fig. 2.44). As is typical of nearshore deposits, the direction of maximum elongation of sand bodies is expected to be parallel to the palaeo-shoreline; from N-S and from NE-SW in the upper Latrobe Group. The larger-scale facies distributions and large-scale reservoir connectivity is addressed in greater detail in Chapter 3.

Analogue data also addresses the likely geometries of depositional units that are likely to act as barriers or seals to flow in the subsurface. Back barrier lagoons and interdistributary bays and swamps as well as shelfal deposits are examples. As might

be expected, the geometry and lateral extent of fine-grained lagoonal, interdistributary bay and shelfal deposits are highly variable and can be exceptionally extensive. Fine-grained shelfal deposits, for example, are pervasive in the study area and can be seismically mapped (see Chapter 3).

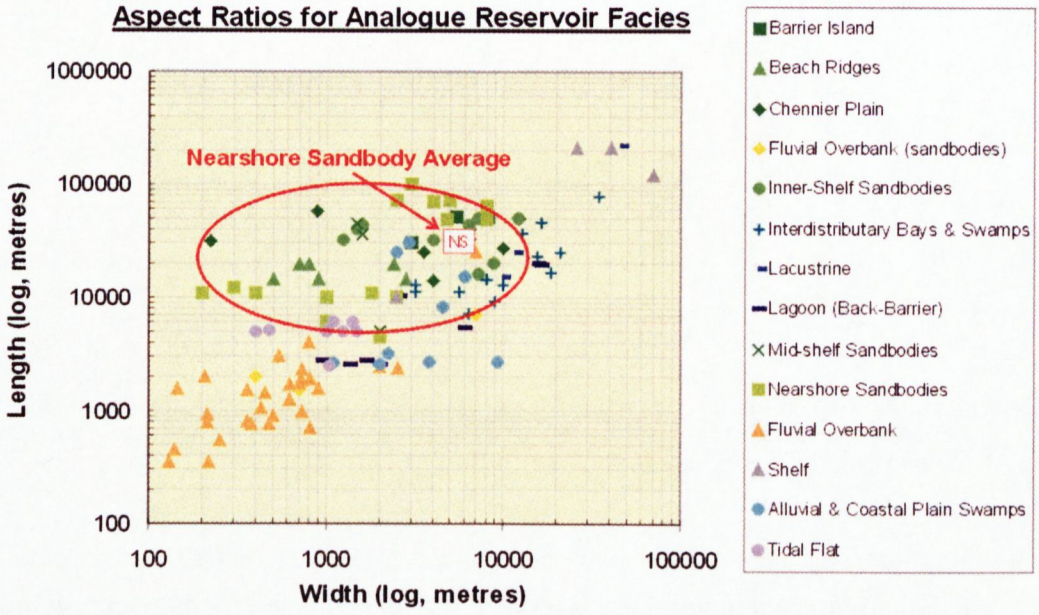

Figure 2.45—Width plotted against length for depositional facies of the study interval. Measurements are derived from modern and ancient analogues. See Appendix II for raw data and references.

Secondary reservoir/aquifer targets are fluvial channel deposits that are part of the coastal/alluvial plain facies, situated landward of the nearshore facies. Although the average reservoir properties of fluvial channel facies measured from routine core analysis are comparable with those of the shoreface and foreshore facies, fluvial facies are characterised by greater large-scale reservoir heterogeneity. Larger-scale heterogeneity is greater in fluvial facies than nearshore facies because sandstone bodies such as fluvial channels are closely spatially associated with finer-grained deposits such as floodplain shales and crevasse splays. As a result, fluvial channel facies are likely to exhibit poor vertical and lateral connectivity. Comparison with analogues suggests that individual fluvial channel facies will vary in width from 500 m – 2000 m. Analogues indicate that the orientation of fluvial channel sand bodies will be highly variable, but will generally be oriented perpendicular or oblique to the palaeo-shoreline, parallel with depositional dip.

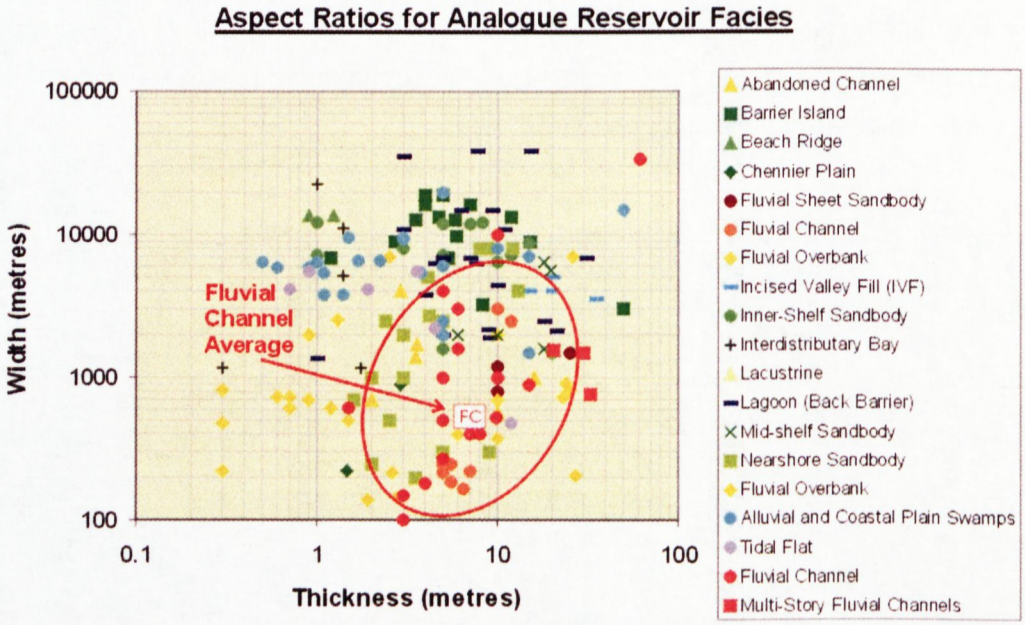

Figure 2.46—Thickness plotted against width for depositional facies of the study interval. Measurements are derived from modern and ancient analogues. See Appendix II for raw data and references.

After defining a useful facies division and the likely geometry and orientation of reservoir and seal bodies, facies must be mapped in the area of interest and reservoir/aquifer flow properties must be populated. Key aspects of mapping and populating facies are defining the structural and stratigraphic framework in which the facies reside, which is the focus of Chapter 3, and selecting geostatistical models to populate reservoir/aquifer flow properties, which is the focus of Chapter 4.

Chapter 3—Structure and Stratigraphy

Abstract

Seismic interpretation and wireline log correlation were used to map the structure and stratigraphy of the study area utilising key stratigraphic surfaces representing significant depositional and structural events. Coal-rich intervals were also seismically mapped, which helped to reconstruct the palaeogeography and spatial positions of key facies tracts in the study area.

The structure in the study area is dominated by an eastward plunging regional anticline with dip closure to the north, south and east. Several localised closures along the crest of the regional anticline contain hydrocarbon accumulations. Faults in the study area are generally near vertical features that strike to the ENE. The faults are thought to behave as barriers or baffles to lateral flow, but few of the faults propagate to the top of the reservoir/aquifer interval and into the overlying sealing units.

The stratigraphy of the study interval is dominated by a retrogradational, transgressive stacking pattern and by erosion at the BaseSeal surface, which represents the top of the reservoir/aquifer target intervals. Up vertical section, alluvial and coastal plain environments of deposition, through nearshore wave-dominated deltaic and barrier island settings into offshore shelfal settings are represented in the study interval.

The structure of the BaseSeal surface is formed by erosive events and transgressive stacking patterns in the underlying strata, and is expected to be a key control on the rate and direction of CO_2 migration. A favourable option for injection well locations based on the structure and stratigraphy of the study is the structurally low part of the regional anticline around the Salmon 1, Swordfish 1 and Cod 1 wells. This location is advantageous because it maximises distance to producing hydrocarbon fields and because it takes advantage of stratigraphic heterogeneity along the expected flow path to reduce the rate of CO_2 migration up structure.

Introduction

The structure and stratigraphy control the shape, size and internal divisions of the 'container' in which CO_2 may be injected and stored. Consequently, the quality of data and interpretation with regard to structure and stratigraphy has the potential to markedly influence uncertainty regarding the validity of the geological model as an accurate characterisation of the ESSCI site.

The interpretation of seismic data and wireline log correlation are the fundamental ways in which the structure and stratigraphy of the reservoir interval are

characterised. In this study a dense grid of 2D seismic reflection data from several surveys and vintages, and conventional wireline log suites, were used.

Critical structural and stratigraphic factors for CO_2 geosequestration include:

- The geometry of the interface between sealing and reservoir units, which is likely to control CO_2 migration over the long term
- The positions of faults and their influence on reservoir compartmentalisation and seal potential
- The effect of stratal geometry and resulting spatial facies distributions on large-scale porosity and permeability patterns in the geological model.

Methodology

SEISMIC INTERPRETATION

Seismic interpretation of the lower L. *balmei* to P. *tuberculatus* interval of the upper Latrobe Group 'Coarse Clastics' included:

- Tying wells to seismic data
- Fault mapping and fault segment assignment
- Horizon mapping
- Amplitude normalisation
- 2D amplitude visualisation and gridding
- Mistie analysis of the interpretation between different 2D lines and quality control
- Depth conversion
- 3D framework construction for the geological model.

Seismic interpretation defined the structure of the Gippsland Basin ESSCI as well as constrained the facies distributions within the Gippsland Basin ESSCI through the analysis of seismic character and amplitude visualisation. Key horizons and faults were mapped using Schlumberger products IESX and GEOVIS (Fig. 3.1).

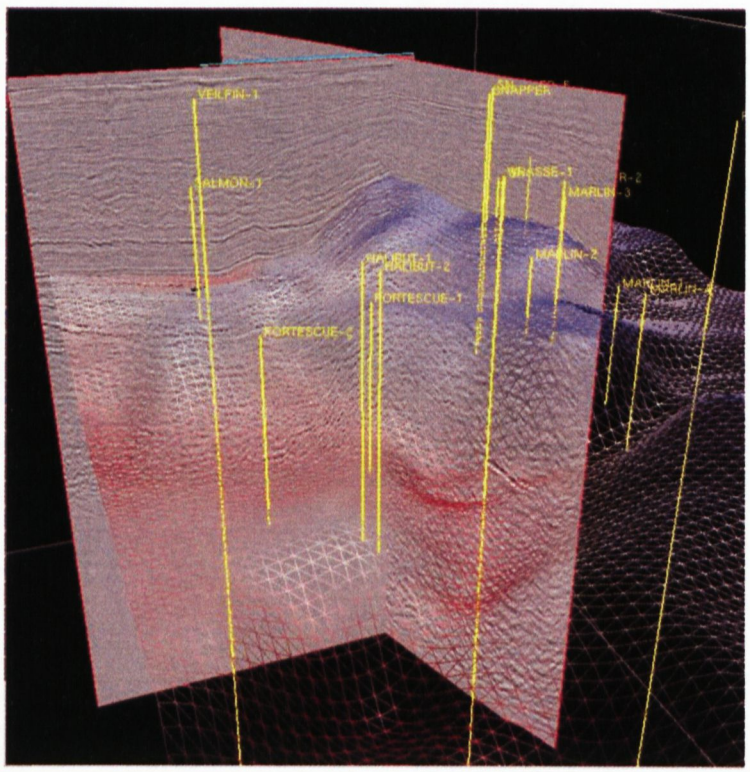
VERLPIN-1
SNAPPER-1
SNAPPER-2
SNAPPER-3
SNAPPER-4
SNAPPER-5
SNAPPER-6
SNAPPER-7
SNAPPER-8
SNAPPER-9
SNAPPER-10
SNAPPER-11
SNAPPER-12
SNAPPER-13
SNAPPER-14
SNAPPER-15
SNAPPER-16
SNAPPER-17
SNAPPER-18
SNAPPER-19
SNAPPER-20
SNAPPER-21
SNAPPER-22
SNAPPER-23
SNAPPER-24
SNAPPER-25
SNAPPER-26
SNAPPER-27
SNAPPER-28
SNAPPER-29
SNAPPER-30
SNAPPER-31
SNAPPER-32
SNAPPER-33
SNAPPER-34
SNAPPER-35
SNAPPER-36
SNAPPER-37
SNAPPER-38
SNAPPER-39
SNAPPER-40

reinterpretation was carried out where appropriate. Horizon misties typically occurred for two reasons:

- Seismic events did not match exactly in time where lines from different surveys and vintages intersected because of different acquisition and processing parameters (Fig. 3.2).
- Faults cut the horizon in close proximity to some seismic line intersections.

After the interpretation was checked, mistie corrections were run. Figure 3.3 shows colour-coded mistie estimates after static and dynamic mistie correction.

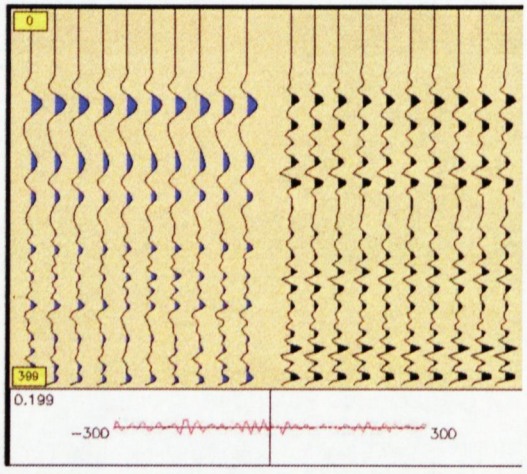

Figure 3.2—Comparison of a low frequency 1974 vintage line (left) with a higher frequency 1994 vintage line (right) at a line intersection.

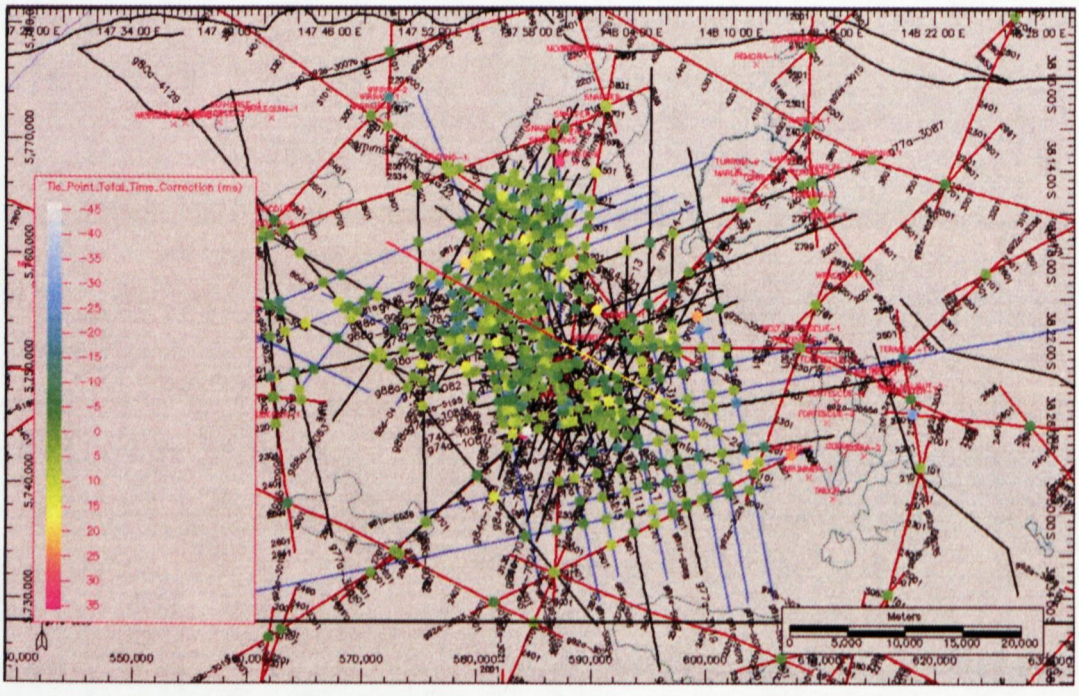

Figure 3.3—Seismic coverage in the study area and colour-coded, average mistie at line intersections for BaseSeal and Horizons 1 - 4.

DEPTH CONVERSION

Depth conversion of the seismic interpretation was carried out using a layer-cake velocity model constructed from time-depth relationships defined from seismic reflection data at well intersections and by checkshot data at the wells. Scatter point data of time and velocity were gridded, resulting in a time grid and velocity grid for each interval defined by seismic surfaces. The velocity and time grids are multiplied to give depth (seconds × metres/second = metres).

First pass depth conversion resulted in misties between depth converted seismic surfaces and well markers of up to a few hundred metres in some parts of the study area. In particular, the Salmon-Conger and the Fortescue-Cobia areas were characterised by considerable misties after first pass depth conversion. The depth errors indicated at the wells were corrected by applying bulk shifts in velocity to the checkshot data and by adding a 'pseudo-well' with velocity data between Whiting and Snapper Fields. The checkshot data used for depth conversion and the bulk shifts applied are shown in Fig. 3.4.

Considerable bulk shifts to checkshot data in some wells had to be made to achieve a match between the BaseSeal horizon and the corresponding BaseSeal marker at the wells (Fig. 3.4). The BaseSeal surface is both seismically distinctive and easily identified on wireline logs, so it was considered the most reliable time-depth pair available. Many depth conversion iterations, using various bulk shifts to checkshot two-way times, were carried out before an acceptable solution was attained. Although the horizon well intersections are considered reliable in the depth model, the depth conversion solution is not considered unique, particularly in areas with limited well control.

The uncertainty associated with depth converting the seismic interpretation is a result of several factors:

- Significant horizontal velocity gradients in the study area associated with the Gippsland Limestone and submarine channels
- Unreliable and limited time-depth data (much of the time-depth data used was several decades old and stacking velocities were not available)
- Grid spacings of several kilometres were used in the construction of velocity and time grids.

A relatively large grid spacing for the velocity model (4000 m north-south and 3500 m east-west) was used with a convergent gridding algorithm to achieve adequate coverage in areas of limited well control. The large grid spacing was a result of the large area over which the seismic interpretation existed and as a result of limited time-depth pairs in some areas.

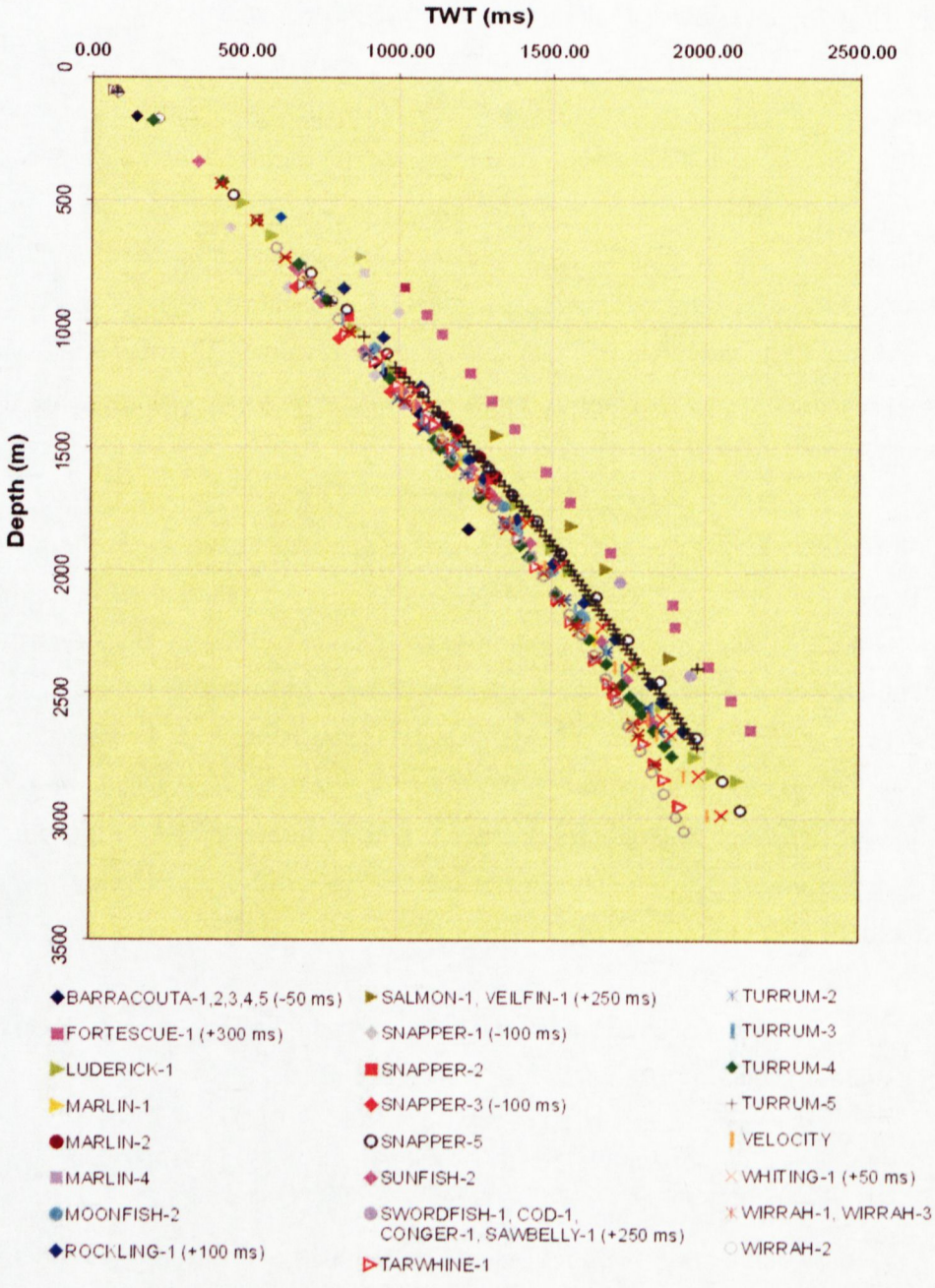

Figure 3.4—Two-way time plotted against depth for checkshots used in this study.

RMS Amplitude Mapping

Facies maps for key stratigraphic intervals of the Gippsland Basin ESSCI were constrained with root mean squared (RMS) amplitude distribution maps. A statistically significant correlation between RMS amplitude and coal distribution in the Gippsland Basin ESSCI exists if gas-charged sandstones are removed from analysis (Fig. 3.5). Determining the distribution of coal using seismic facies and RMS amplitude distribution was particularly effective for constraining the distribution of depositional facies in the study area.

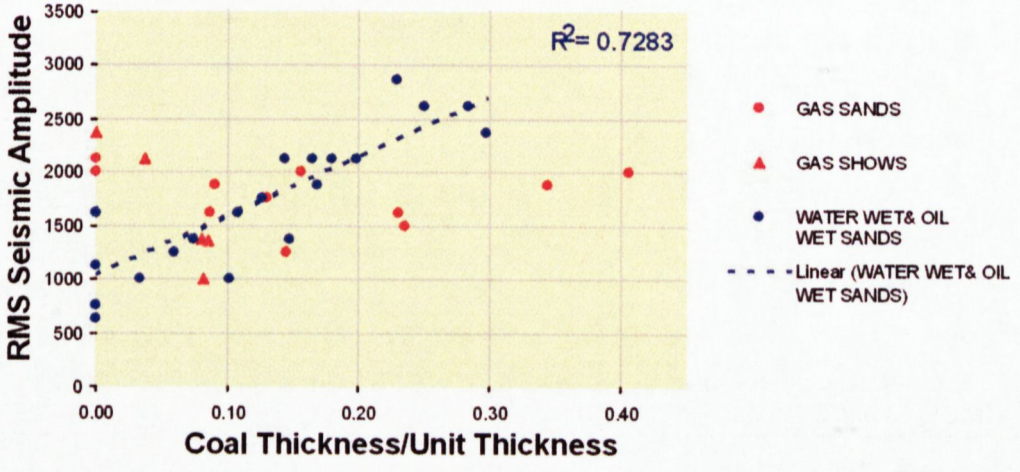

Figure 3.5—RMS amplitude plotted against coal thickness as a proportion of interval thickness. RMS amplitude has a good correlation with coal if natural gas effects are discounted.

An amplitude normalisation was run on all seismic lines used in this study in order to produce RMS amplitude distribution maps. In the absence of amplitude normalisation, the amplitude response of seismic lines from different surveys and vintages would have been considerably different resulting in unreliable maps. The RMS amplitude seismic attribute was gridded using convergent gridding to fill in areas between 2D seismic lines.

Horizon and Fault Modeling

Horizon and fault interpretations were gridded to form three-dimensional surfaces for the geological model and geomechanical assessment. The geometric relationships between various surfaces (horizons and faults) in the Gippsland Basin ESSCI were quality controlled and edited in Schlumberger's FRAMEWORK 3D. For the geological

model surface intersections must be edited because surfaces cannot cross, even on very small scales. Five seismic horizons and nine fault surfaces were selected for inclusion in the geological model.

WIRELINE CORRELATION

Key sequence stratigraphic surfaces between the *L. balmei* and *P. tuberculatus* biozones of the upper Latrobe Group were correlated between 70 wells in the study area. Core descriptions, conventional wireline log suites, seismic reflection lines, and palynological data were used for correlation. Sequence stratigraphic surfaces including sequence boundaries and various kinds of flooding surfaces (transgressive surfaces and maximum flooding surfaces) were identified based on stratigraphic stacking patterns and biostratigraphic data and correlated between wells based on criteria provided in Van Wagoner *et al.* (1990), Posamentier and Allen (1999) and Lang *et al.* (2001). The sequence stratigraphic units defined from the integration and interpretation of the data types mentioned above define packages of contemporaneously deposited lithofacies, which facilitate meaningful interpretation of depositional systems and resulting stratal geometries and architectures. Software packages used for wireline correlation were Schlumberger products WELLPIX and STRATLOG.

Structure

The structure within the study area is dominated by a regional anticline with a fold axis trending broadly WSW – ENE that plunges to the east. There is a second group of folds within the study area with fold axis orientation trending NNW – SSE. Consequently, several localised four-way closures exist along the crest of the regional anticline. Hydrocarbon accumulations defining Barracouta, Snapper and Marlin/Turrum Fields and several other smaller fields are contained within the structural closures (see Fig. 3.6). The regional anticline is characterised by three-way closure to the north, east and south.

Major bounding faults within the study area trend dominantly from northwest to southeast. A second synthetic fault set trends WSW – ENE. The faults within the study area are near vertical features within the study interval, but the dip of the faults characteristically shallows with depth.

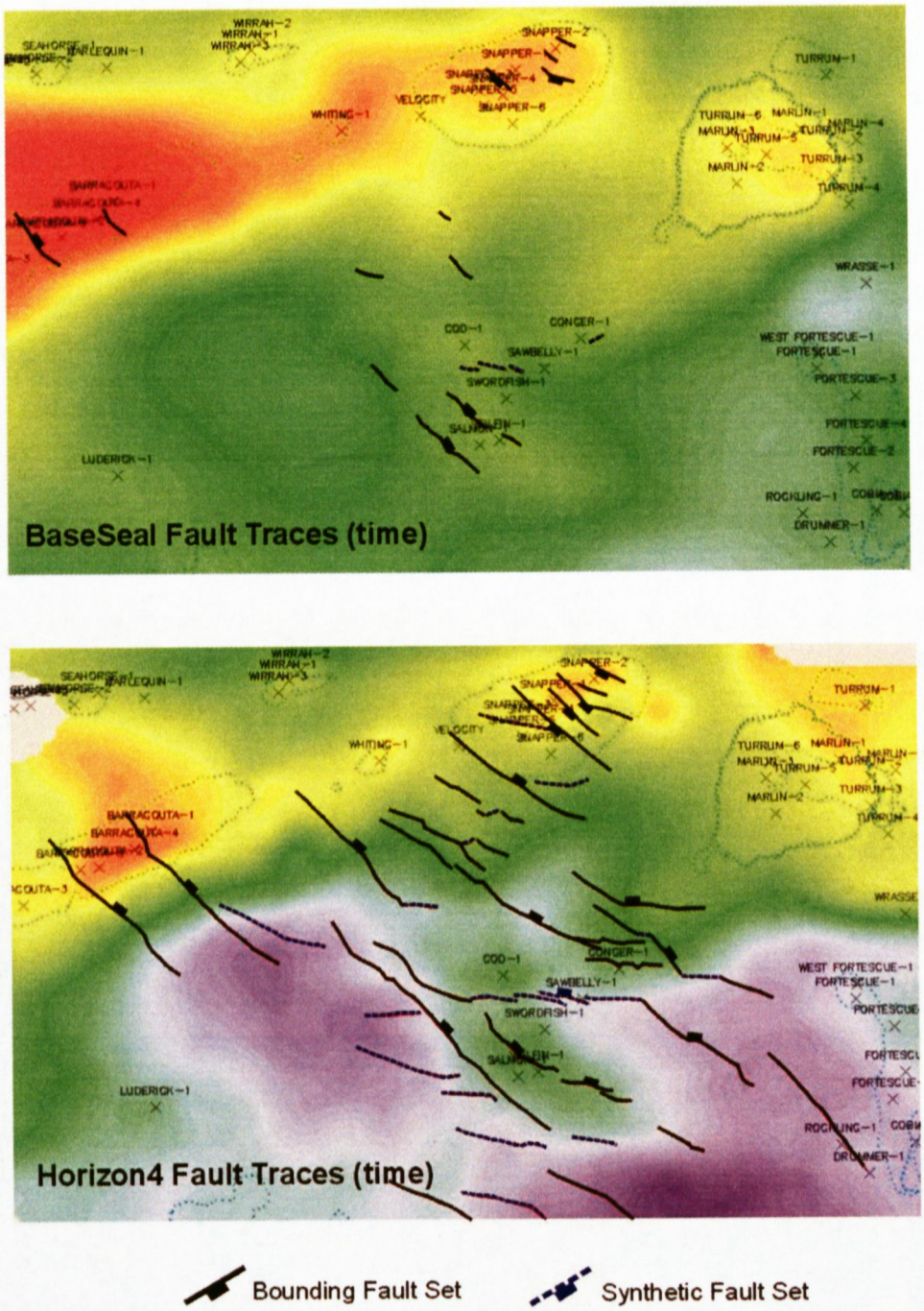

Figure 3.6—Time structure map showing fault traces at Horizon 4 and at the BaseSeal horizon. The NW-SE bounding fault set and the WNW-ESE synthetic fault set are distinguished. Note that few faults propagate through the BaseSeal surface.

The majority of faults in the study area are interpreted as reactivated normal faults. As the sense of movement on the majority of faults remains normal, the degree of basin inversion in the study area is interpreted to be limited. On-lap of sealing unit strata onto older structures suggests that the majority of basin inversion postdates

the deposition of the lower sealing units (Gurnard Formation & base of Lakes Entrance Formation; Fig. 3.1). A relatively mild degree of basin inversion has probably continued to the present day (Rahmanian *et al.* 1990). As a result of the timing and magnitude of basin inversion, few faults in the study area propagate into sealing units (Gurnard and Lakes Entrance Formations) that overlie the reservoir/aquifer targets of the upper Latrobe Group (Fig. 3.6).

Although faults that intersect the upper Latrobe Group rarely propagate significantly into the overlying Gurnard and Lakes Entrance Formations, the Gurnard and Lakes Entrance Formations are internally characterised by multiple closely spaced faults (Fig. 3.7). The faults within the sealing units are small features associated with little displacement, generally at or near seismic resolution (~30 m). It is possible that the faults within the seal units are laterally connected, forming fault/fracture networks in three dimensions. The small faults within the regional sealing units were not observed to cut the BaseSeal surface, nor do the faults propagate up to the sea floor. Additionally, no connection between the faults within sealing units and deeper faults intersecting the upper Latrobe Group has been identified at seismic scale.

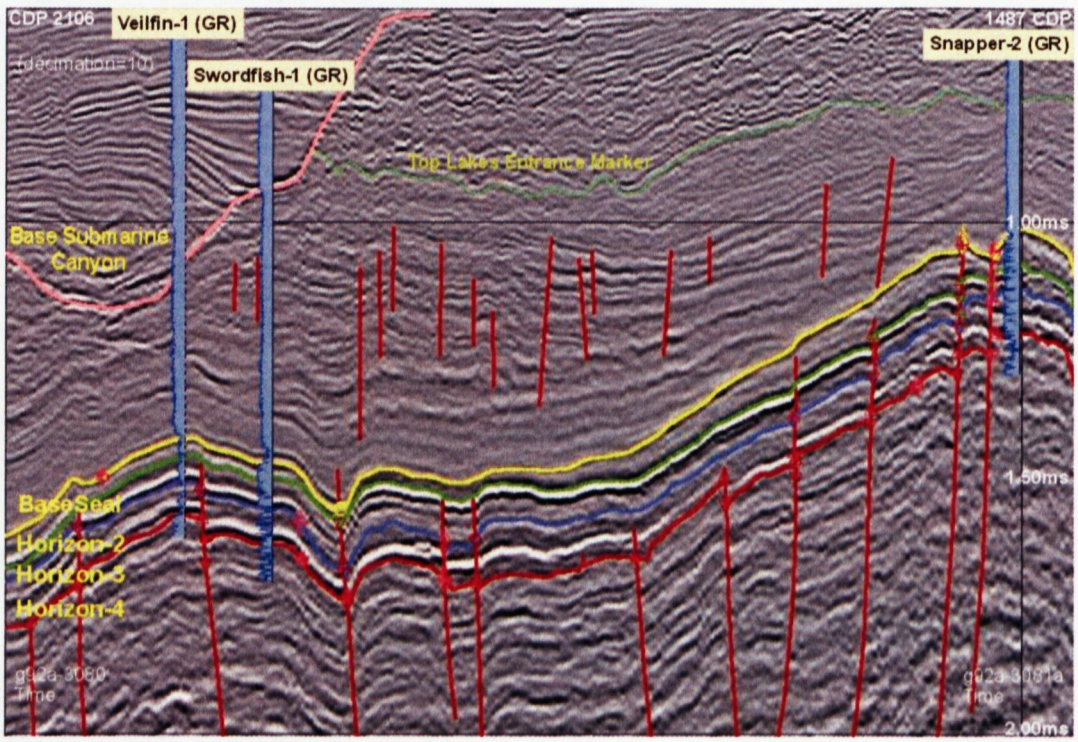

Figure 3.7—Seismic section from the Swordfish 1, Salmon 1, Veilfin 1 area to Snapper Field. Few faults (shown in red) propagate through the BaseSeal horizon (yellow) into the overlying regional seal units. Small faults can be mapped above the BaseSeal horizon within the regional sealing units.

The magnitude of displacement associated with the faults of the study area suggests fault seal potential will not be controlled by juxtaposition. The maximum throw on a fault that intersects a seal unit at the base of the seal unit (<60 m) is small by comparison with the thickness of the seal and reservoir units (100s of metres).

In general, fault displacement increases with depth through the study interval and many faults tip out (i.e. show no displacement at seismic scale) prior to reaching the BaseSeal surface. This is an important point because SC CO_2 is less dense than water and consequently, migration at base of regionally extensive impermeable units is expected to be the dominant behaviour prior to dissolution in the formation water. Therefore, in terms of fault seal affecting CO_2 flow behaviour within the top Latrobe Group the few large faults that propagate into the regional sealing units are likely to be the most important features. Nine key faults were utilised in the geological model based on the following criteria:

- The faults must occur within the area of interest and near the likely flow path of the CO_2.
- The faults must be associated with displacement greater than ~30 m.
- The faults must propagate into regional sealing units (i.e. Gurnard, Lakes Entrance, Turrum, Flounder Formations).

A fault intersected by core in Marlin 4 was associated with intense carbonate cementation in the fault damage zone (see Chapter 2). In the absence of other data, it is assumed that other faults in the study area will also be associated with heavily cemented fault rock. This assertion is supported in the literature by Glenton (1988). If faults of the study area are associated with heavily cemented damage zones the vertical and near-vertical faults of the study area may represent barriers or baffles to horizontal flow of SC CO_2.

Figure 3.8 shows the major structural features of the study area identified in this study, including:

- The fold axis of the regional anticline structure
- Fault traces for the fault sets represented in the study area as well as the position of the Rosedale Fault system
- The Marlin/Turrum submarine channel complex (discussed later in this chapter).

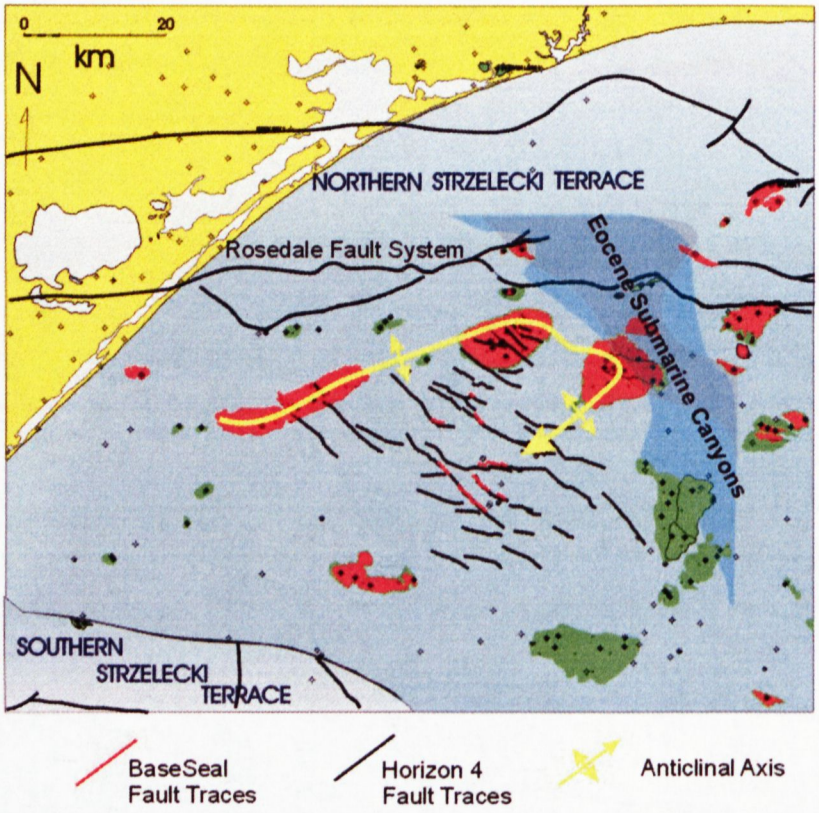

Figure 3.8—Major structural features of the study area. The axis of the regional anticline is shown, as well as fault traces at the Horizon 4 (black) and at the BaseSeal horizon (red). Green represents oil fields and red represents gas fields.

Stratigraphy

SEISMIC-SCALE STRATIGRAPHY

At sequence set scale, the study interval is characterised by a broadly transgressive stacking pattern within the upper Latrobe Group. The large-scale transgressive nature of the study interval is evident in part because of back-stepping coal-rich units, which are seismically distinctive as high amplitude reflections (Fig. 3.9). Sediment transport was from WNW – SSW during the deposition of the study interval.

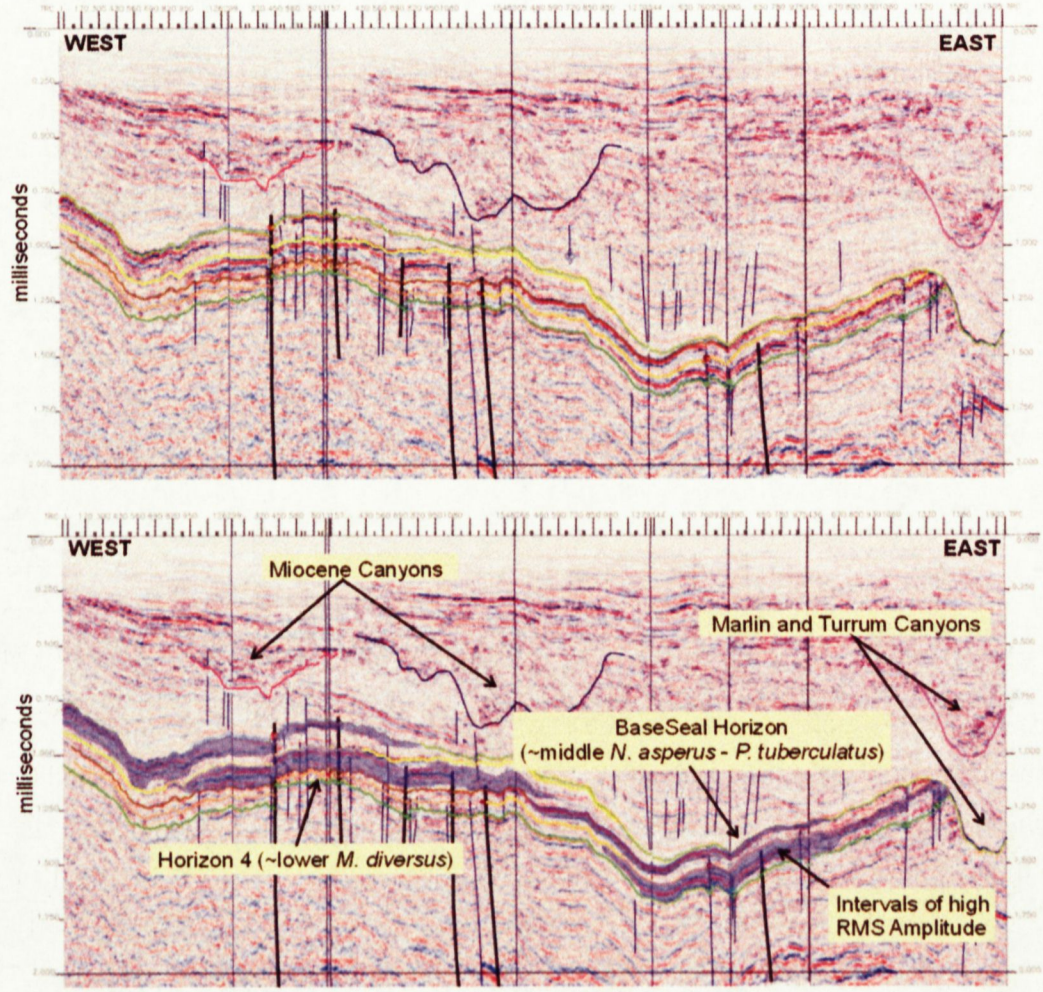

Figure 3.9 — West to east seismic line showing the Gippsland Basin ESSCI structure. Four seismic units are defined within the study interval by five horizons. These exhibit a retrogradational, transgressive character. The retrogradational geometry is also made evident by back-stepping coal-rich intervals, which are highlighted in purple. The Eocene Marlin Canyon truncates the lower seismic horizons and acts as a lateral seal.

Five seismic horizons were mapped across the study area. In order from oldest to youngest, the seismic horizons are: Horizon 4, Horizon 3, Horizon 2, Horizon 1 and BaseSeal. The mapped horizons represent seismic events that were regionally correlatable and appeared to define stratal packages of similar seismic character. For example, surfaces associated with down-lap or on-lap geometry and surfaces at which truncation of underlying units occurred were considered stratigraphically significant.

The BaseSeal surface is the youngest unconformity mapped in the study area, and truncates older horizons (Horizons 1 – 4). The older horizons are variably restricted to the western parts of the study area because of truncation by the BaseSeal unconformity and through down-lap relationships with other surfaces (Fig. 3.9).

The truncation of Horizons 3 and 4 is associated with the Marlin Canyon feature in the eastern part of the study area. The base of the Marlin Canyon is mapped as part of the BaseSeal unconformity. Core and wireline logs suggest that the Marlin Canyon is filled with low permeability strata of the Turrum Formation, and consequently, is likely to behave as a lateral seal that will prevent SC CO_2 migration to the east. However, it is possible that over the long term CO_2 in the dissolved phase may sink below the base of the geological model and migrate east beyond the Marlin Canyon. Depth structure maps are provided for BaseSeal (Fig. 3.10) and Horizons 1 – 4 (Figs 3.11 – 3.14).

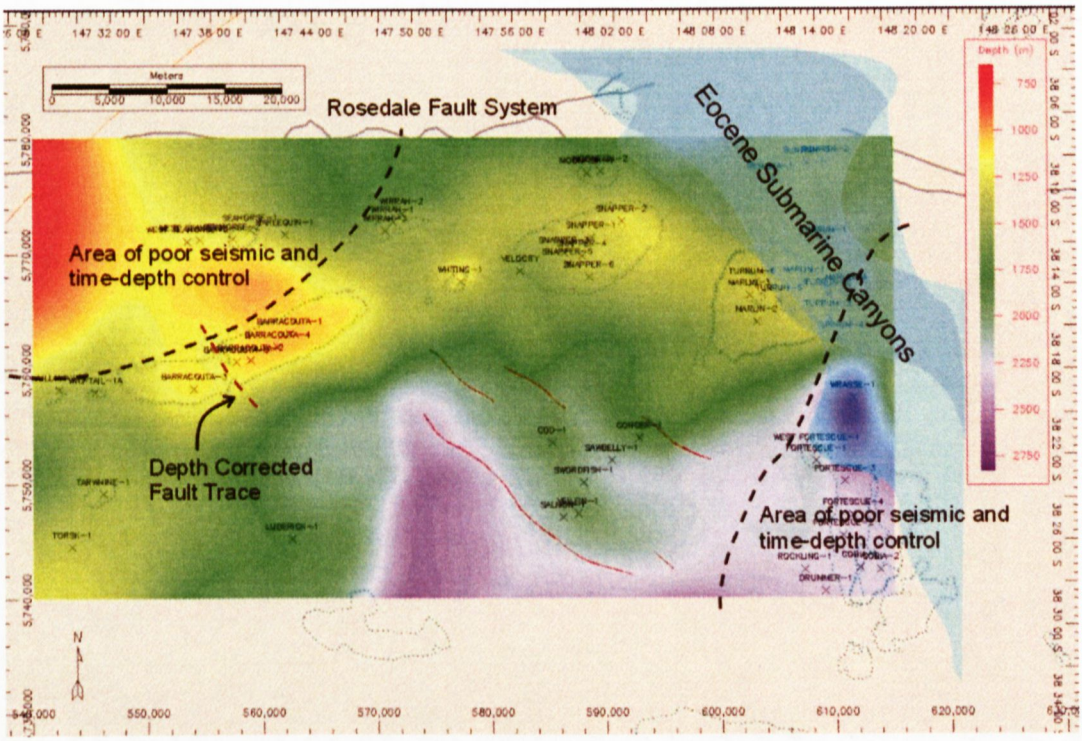

Figure 3.10—BaseSeal depth structure map. There is a paucity of seismic coverage and velocity data in certain parts of the study area, which adds to structural uncertainty in some areas. The NE and SW parts of the study area are characterised by high uncertainty.

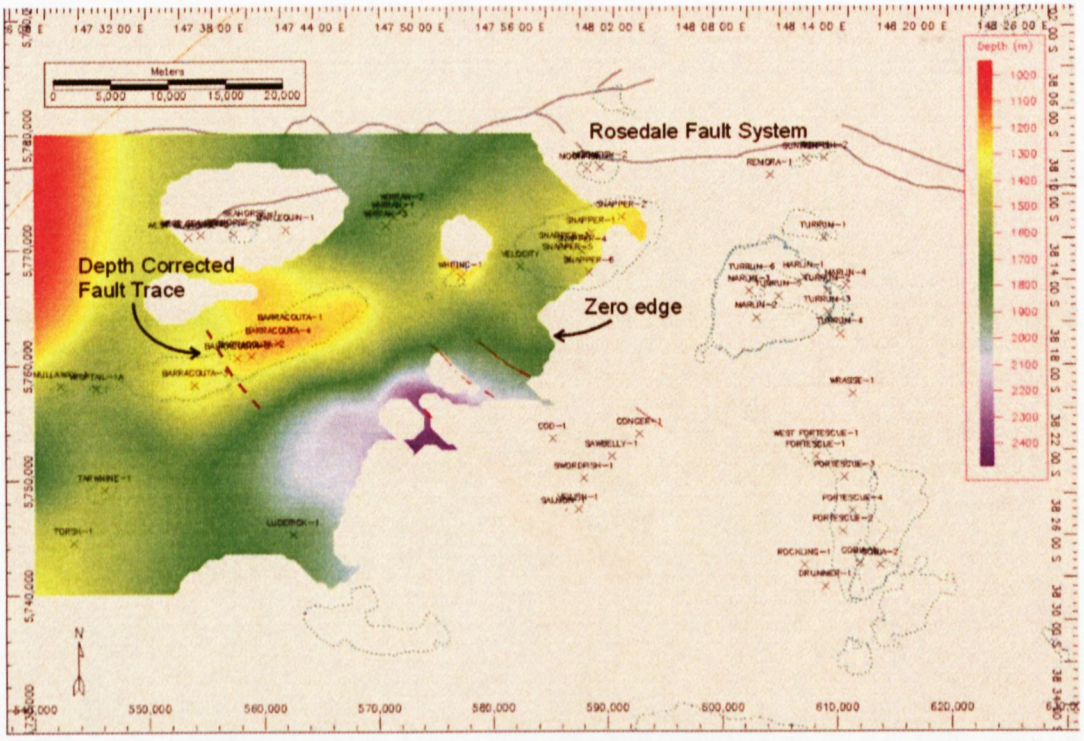

Figure 3.11—Horizon 1 depth structure map. The zero edge of the grid represents areas where the surface on-laps older strata, or areas where the surface is truncated by younger strata.

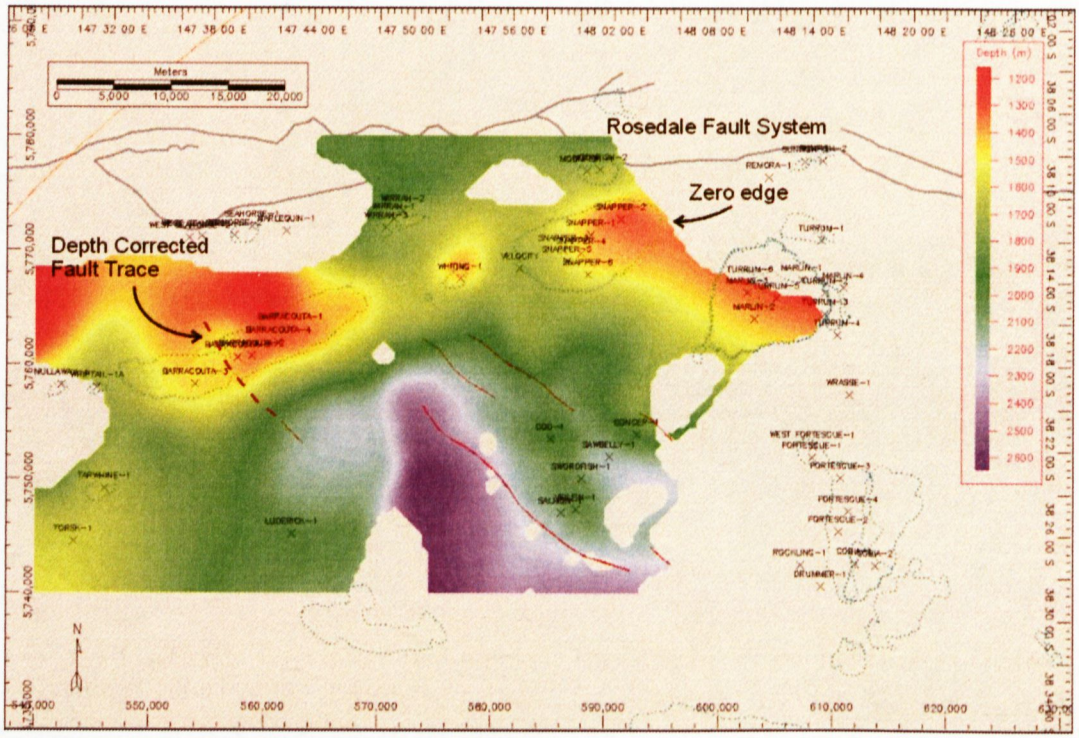

Figure 3.12—Horizon 2 depth structure map.

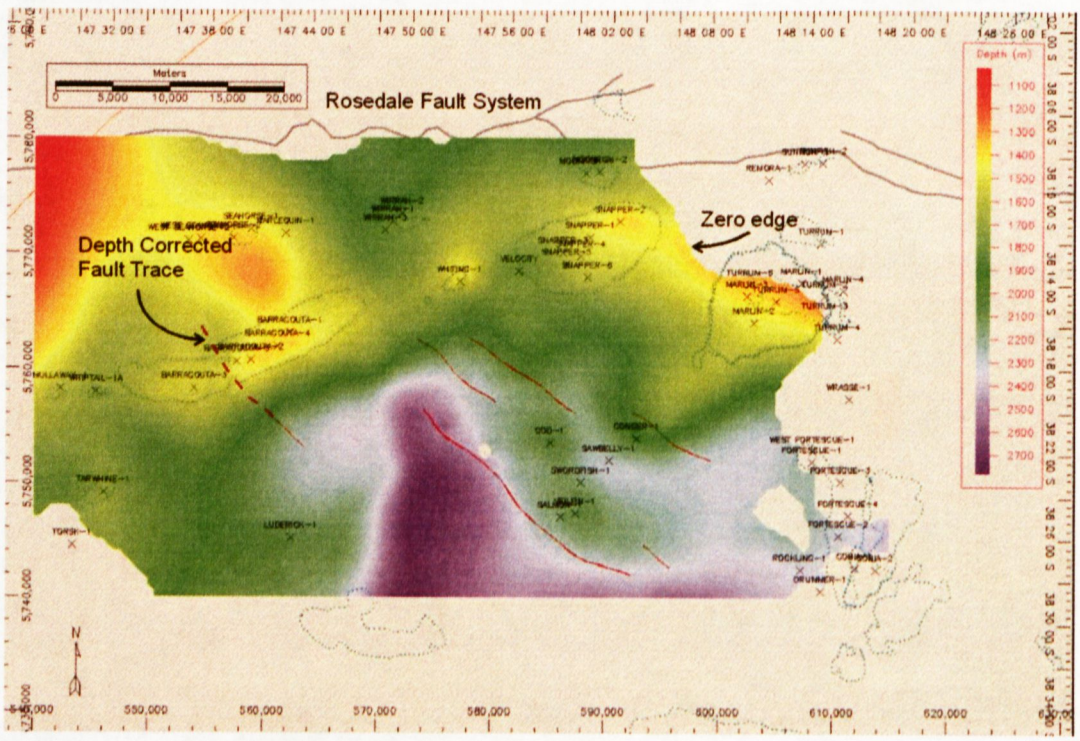

Figure 3.13—Horizon 3 depth structure map. The eastern erosional edge results from truncation by the Marlin Canyon.

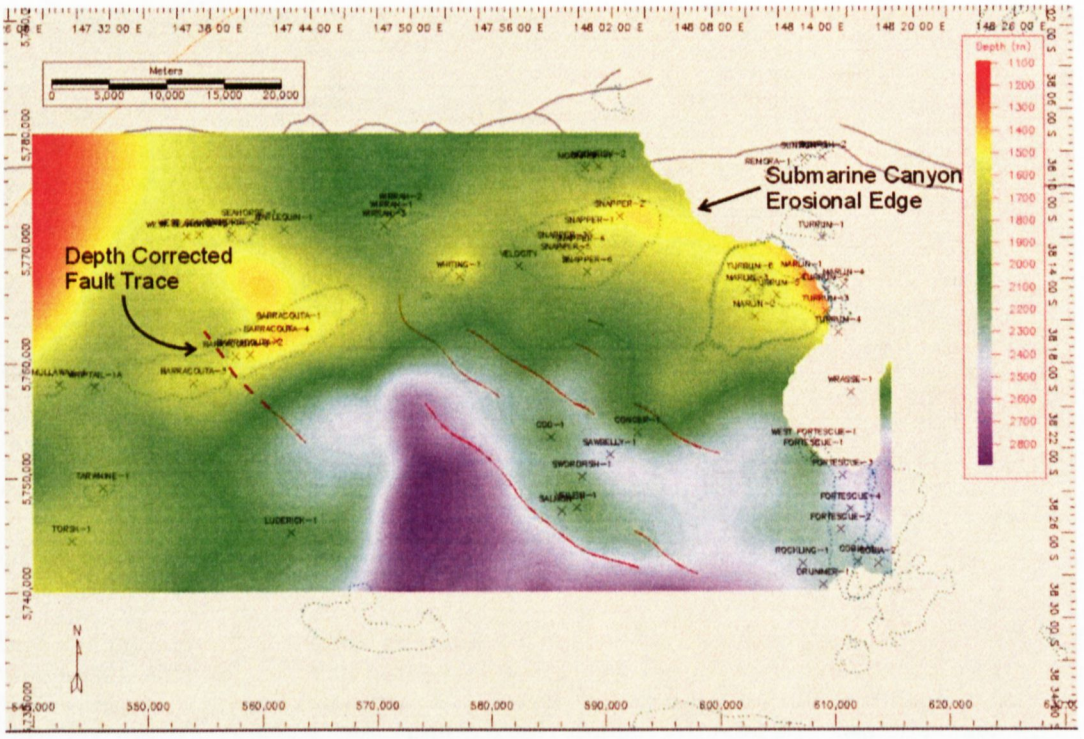

Figure 3.14—Horizon 4 depth structure map. The eastern erosional edge results from truncation by the Marlin Canyon.

All of the seismic horizons in the study area represent landward dislocations of facies tracts. Consequently, all five horizons may be characterised as flooding surfaces, associated with rises in relative sea level. In the case of four horizons (Horizon 4, 3, 2 and BaseSeal) the surfaces are also associated with regional erosion, which is suggested by seismic indications of stratal truncation and by the absence of biostratigraphic zones at wells that intersect the surfaces. These surfaces are thought to represent merged sequence boundaries and flooding surfaces where lowstand systems tract strata are completely reworked by subsequent episodes of relative sea level rise and landward migration of the shoreline. Horizon 1 is identified as a flooding surface and is not associated with resolvable evidence of erosion.

The five horizons mapped in the study area define four stratigraphic units that are named broadly after the spore-pollen biostratigraphic zone in which they occur: Middle & Upper *M. diversus*; *P. asperopolus*; Lower *N. asperus;* and Middle and Upper *N. asperus* (Fig. 3.15). In the sequence stratigraphic context, three sequences are defined, bound by sequence boundaries mapped at Horizons 4, 3, 2 and at the BaseSeal horizon. Though the Lower *N. asperus* and the Middle and Upper *N. asperus* units are mapped separately, they are interpreted to be part of the same sequence.

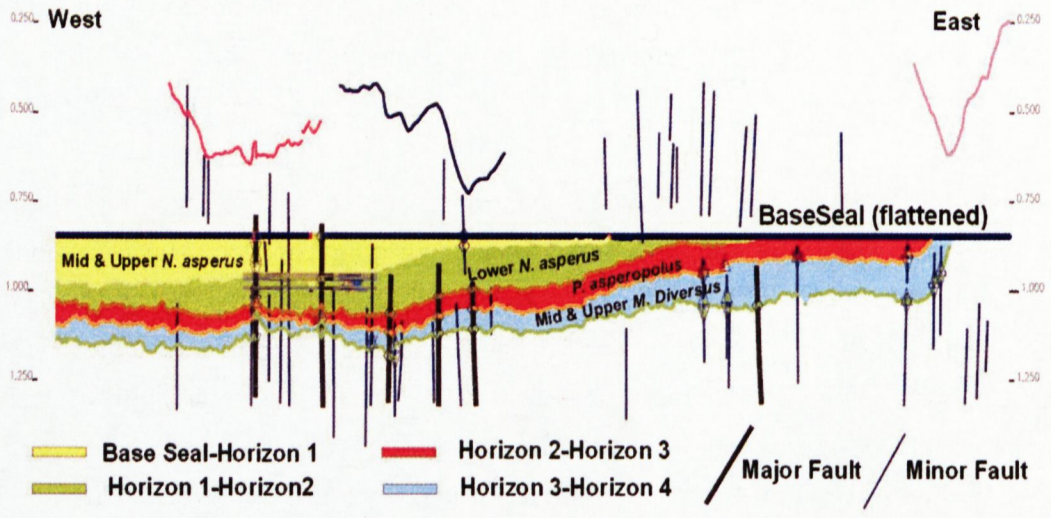

Figure 3.15—West to east cross-section showing the seismic interpretation flattened on the BaseSeal surface. Seismic horizons define four stratigraphic units (from oldest to youngest): Middle and Upper *M. diversus*; *P. asperopolus*; Lower *N. asperus;* and Middle and Upper *N. asperus*. Progressively younger stratigraphic packages sub-crop at the BaseSeal surface towards the west. The bases of several canyon features in the upper stratigraphy are also mapped.

Two particularly significant merged sequence boundary/flooding surfaces are represented by Horizon 4 and with the BaseSeal horizon. Horizon 4 separates dominantly fluvial strata below from dominantly nearshore strata above with the area of interest. The BaseSeal surface separates nearshore reservoir/aquifer targets below from sealing units above that consist predominantly of shelfal deposits. As a result the BaseSeal surface characterises the structure at the base of the regional sealing units and, consequently, is a particularly important surface for CO_2 geosequestration.

West of the study area in the onshore Gippsland Basin a lateral facies change occurs where the mudstone and marl dominated Lakes Entrance Formation changes into the sandstone dominated Balook Formation (Fig. 1.17). The point of transition is effectively the zero edge of the regional seal. The transition occurs several kilometres west of the study area, well outside the geological model boundary. In practice the uncertainty regarding CO_2 containment in the Latrobe Group would increase significantly if CO_2 were to migrate west of the model area, so the strategy selected for CO_2 injection and storage would ideally minimise this possibility.

The BaseSeal surface formed by erosion from submarine canyons and by non-deposition due to limited sediment supply to distal parts of the depositional systems. The key area of incision is associated with the Marlin Canyon in the eastern part of the study area, but seismic data also indicates some truncation of underlying stratigraphic units west of the Marlin Canyon. As a result of stratal truncation at the BaseSeal horizon and retrogradational stacking patterns, progressively younger strata subcrop to the west of the study area at the BaseSeal horizon stratigraphic level. Consequently, fluid flow up structural dip to the west also results in flow up the stratigraphy (Figs. 3.15 & 3.16). This geometric arrangement is likely to reduce large-scale E – W transmissivity.

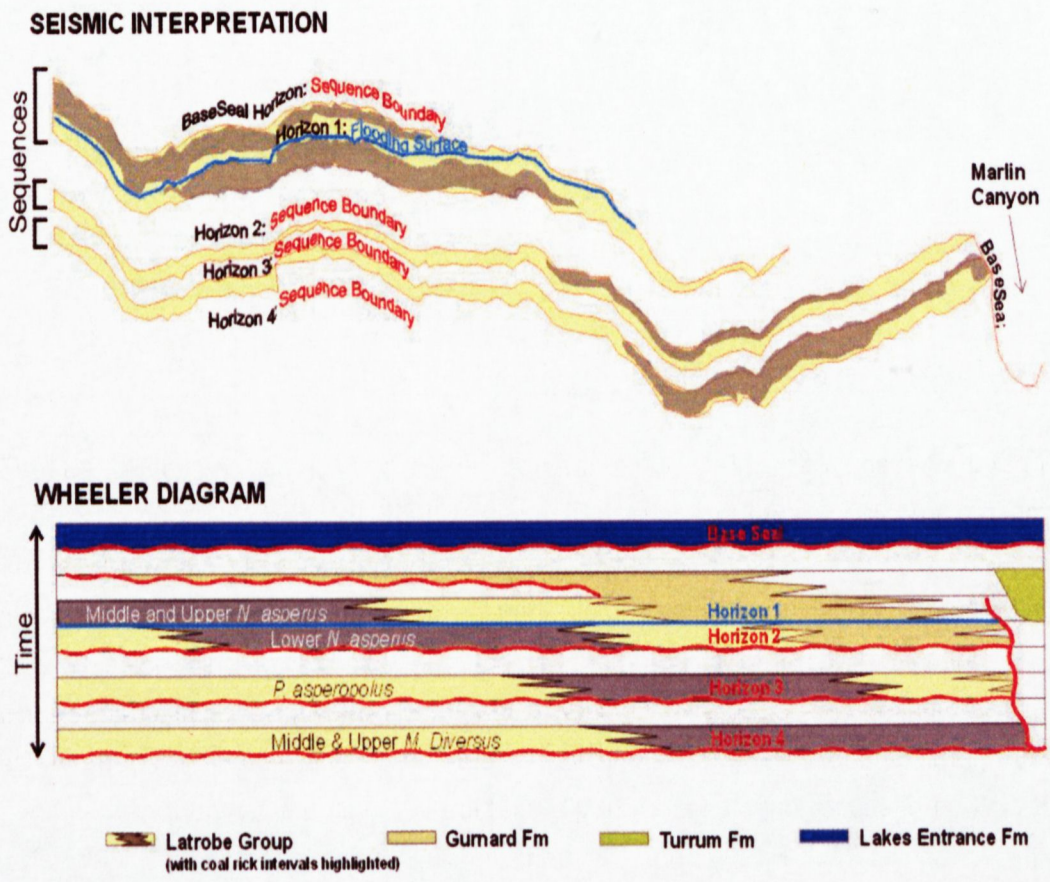

Figure 3.16—Seismic interpretation with three unconformity bound sequences separated (above) and Wheeler diagram (below). The Gurnard Fm, Turrum Fm and the Lakes Entrance Fm are shown on the Wheeler diagram in addition to the upper Latrobe Group strata.

For the purposes of geological model construction a 'phantomed' horizon of the BaseSeal horizon was translated 50 m up and a 'phantomed' horizon of Horizon 4

was translated 100 m down. These horizons define two more stratigraphic units named 'Seal' and 'Lower *M. diversus* and *L. balmei*', respectively. The stratigraphic units used for the geological model and the bounding surfaces that define them are described in Table 3.1.

Table 3.1: Stratigraphic surfaces and units utilised in this study.

Stratigraphic unit		Bounding Surfaces	
Unit Name	**Internal Architecture**	**Surface Name**	**Interpretation**
Seal	on-lap onto older structure	upper surface: **BaseSeal + 50 metres**	n/a
		bounding surface: **BaseSeal**	merged unconformity and flooding surface
Middle & Upper *N. asperus*	retrogradational stacking truncated by BaseSeal mild on-lap of older structure internal sequence boundary near base of unit (?)	bounding surface: **Horizon1**	flooding surface
Lower *N. asperus*	retrogradational stacking truncated by base seal truncates underlying units (?)	bounding surface: **Horizon2**	merged flooding surface and unconformity (?)
P. asperopolus	off-lap in west down-lap in east truncated by BaseSeal (submarine Canyon)	bounding surface: **Horizon3**	merged flooding surface & unconformity
Middle & Upper M. diversus	off-lap in west down-lap in east truncated by BaseSeal (submarine Canyon)	bounding surface: **Horizon4**	merged flooding surface & unconformity
Lower M. diversus & L. balmei	parallel reflectors (aggradational?)	lower surface: **Horizon4 + 100 metres**	n/a

WIRELINE LOG-SCALE STRATIGRAPHY

Seismically mapped horizons are the only surfaces that were 'hard wired' into the geological model. However, understanding the smaller-scale stratigraphic stacking patterns and geometry is important because it controls the way in which the reservoir/aquifer flow properties are populated in the geological model, and consequently, how reservoir heterogeneity is represented in the model. For example, if the primary direction of CO_2 migration is perpendicular to the stratigraphic strike (CO_2 migrates across stratigraphic units) the large-scale effective permeability will be lower than if the primary direction of CO_2 migration is parallel with the stratigraphic strike (CO_2 migrates along the stratigraphic units). This kind of heterogeneity is represented in the geological modeling through different kinds of layering relationships.

Sub-seismic stratigraphic division reveals that the large-scale seismically defined units can be divided into several smaller stratigraphic units based on wireline log stacking patterns and biostratigraphic control (Fig. 3.17). At log scale the stratigraphic subdivision of the Gippsland Basin is challenging because individual facies and stratigraphic units are not necessarily characterised by unique log responses. The majority of the reservoir interval consists of stacked, nearshore sandstone bodies that are difficult to delineate on wireline logs. Consequently, biostratigraphic control was used extensively in the log-scale stratigraphic subdivision of the Gippsland Basin. Fortunately, a considerable quantity of biostratigraphic data was available for the study area (see Appendix III).

The log-scale stratigraphic division is consistent with the seismic-scale stratigraphic division indicating a transgressive, retrogrational stacking pattern with stratal erosion at the BaseSeal surface, particularly in the eastern part of the study area. The seismic horizons are broadly consistent with the position of key sequence boundaries and flooding surfaces identified from wireline log stacking patterns and from biostratigraphic data (Fig. 3.17). In areas associated with thick coal successions, the seismic event representing a key stratigraphic event does not always intersect the well at exactly the same point as the wireline log pick. This is because the interface between siliciclastics and coal represents the highest impedance events in the interval and nearby events are commonly overwhelmed due to the difference in

resolution between seismic and well log data. The accuracy of the well to seismic intersections is also a function of the quality of the synthetic, which is dependent on the density and sonic logs as well as the checkshot data. The highest confidence surface in terms of seismic mapping and in terms of well to seismic tie is the BaseSeal horizon, which is distinctive both seismically and on well logs.

Thick and laterally extensive coal units were important guides for seismic mapping and wireline correlation. The formation of coal is controlled by water table and sea level as well as the precipitation and evaporation ratio. Thick coal successions are likely to form during periods of rapid sea-level rise where the rate of sea-level rise balances or slightly exceeds the peat production rate (Bohacs & Suter 1997). The relationship between relative sea level and coal formation results in coal packages that are parallel with time-equivalent surfaces, which can be correlated between wells and mapped seismically. Additionally, thick accumulations of peat form landward of the shoreline in peat swamps within the coastal plain and back barrier areas. Consequently, the distribution of coal helps to constrain the position of the palaeo-shoreline and the distribution of facies tracts within mapped stratigraphic units.

The key benefit of log-scale correlation is to yield insight into the detailed stratigraphic architecture so that the layering in the geological model can be manipulated to accurately represent it. However, the finer log-scale correlation also yields insights into the stratigraphy of the upper Latrobe Group that were not evident at seismic scales. For example, at wireline log scale 'tongues' of fluvial coastal or alluvial plain strata, represented by serrated, fining-upward log motifs, can be interpreted to prograde from the west and interfinger with nearshore strata (Figs. 3.17 & 3.18). The fluvial coastal or alluvial plain stratal packages are generally associated with sequence boundaries and may represent the remnants of late highstand and lowstand systems tract strata, which are thought to have been largely reworked by wave and tidal processes and redeposited as nearshore strata.

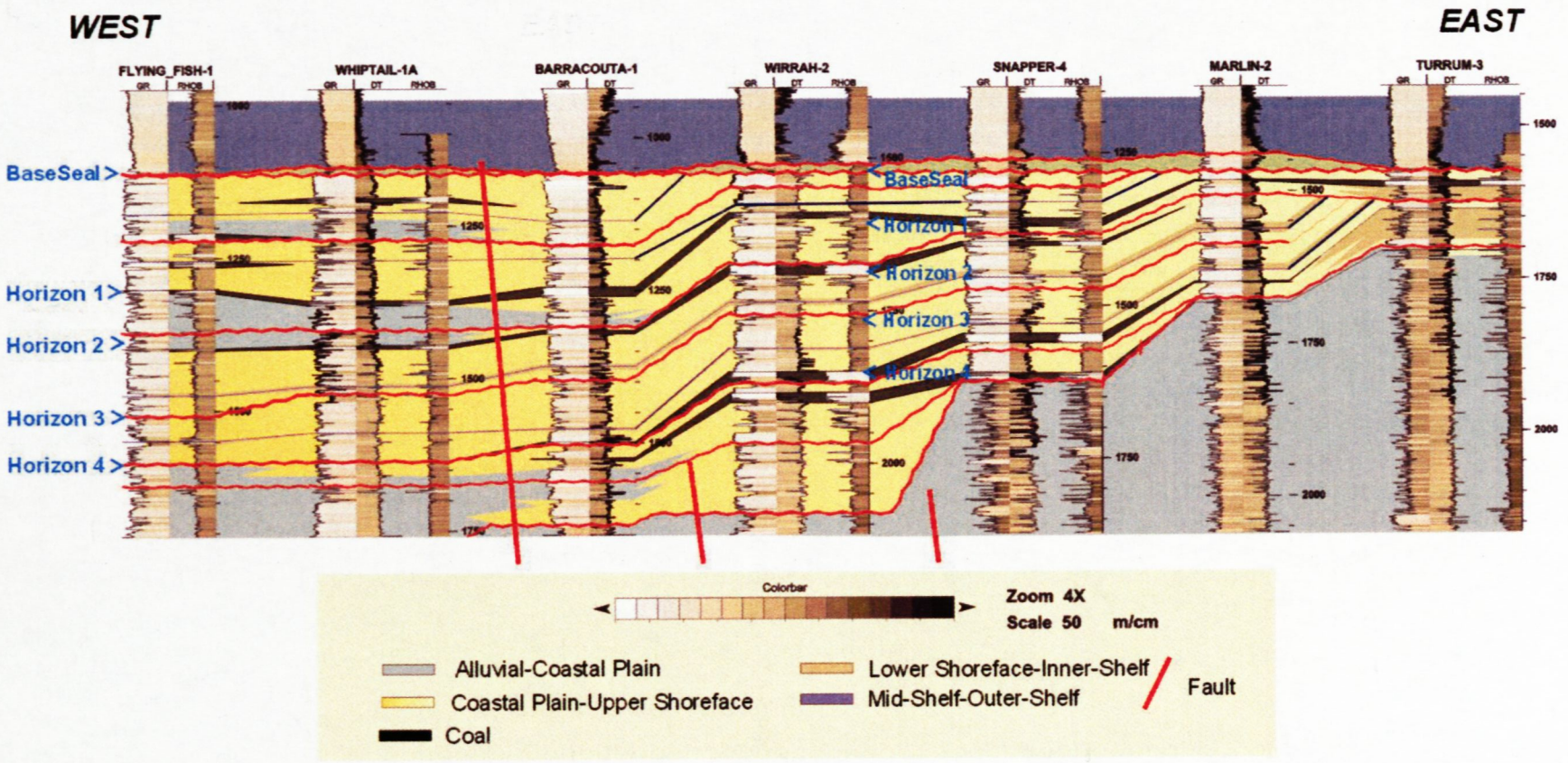

Figure 3.17—Stratigraphic cross-section along depositional dip. Sequence boundaries and flooding surfaces are correlated between wells. Strata are truncated at the BaseSeal surface in the eastern part of the study area. Wedges of coastal and alluvial plain facies (grey) are interpreted to interfinger with nearshore facies (yellow and orange). The position of the seismic horizons is shown for reference.

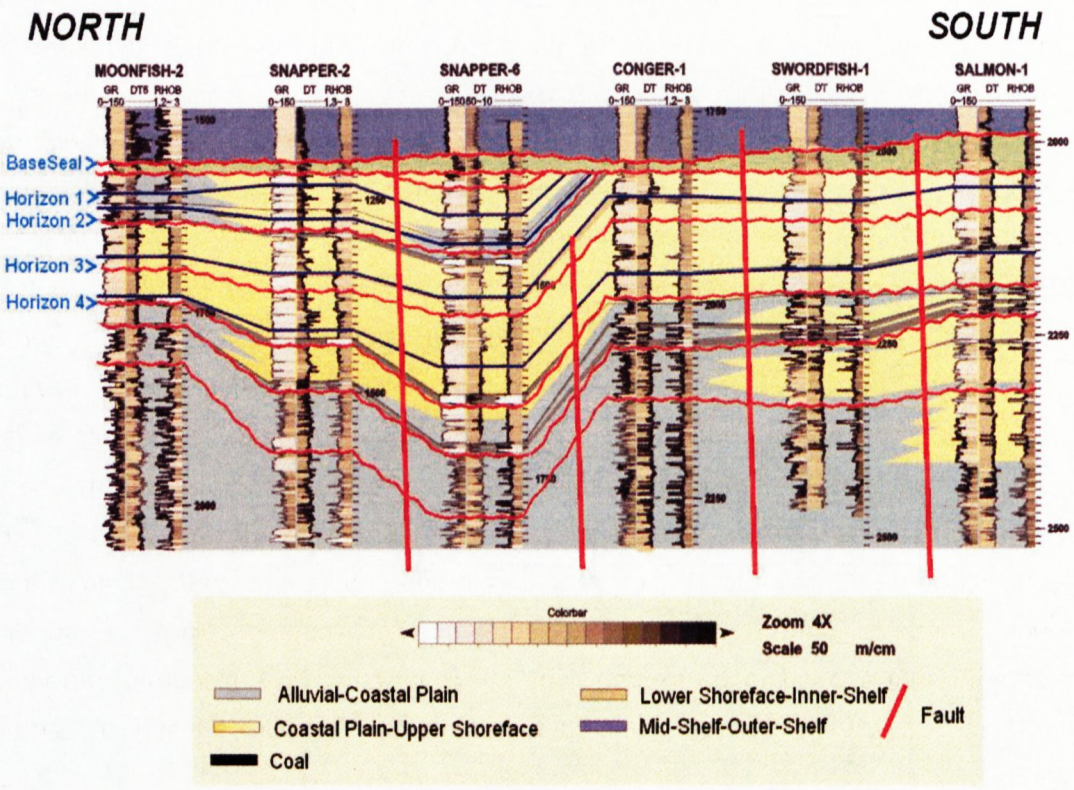

Figure 3.18—Stratigraphic cross-section along depositional strike. Sequence boundaries and flooding surfaces are correlated between wells. Alluvial and coastal plain facies (grey) below the study interval give way to nearshore faces (yellow and orange) up section.

Wireline log correlation also indicates that a thin veneer of Gurnard Formation deposits, which are thought to have been deposited in a shelf setting (see Chapter 2), overlie nearshore upper Latrobe Group strata. Based on the wireline correlation and biostratigraphic data nearshore Latrobe Group deposits appear to be truncated at the base of the Gurnard Formation suggesting an unconformable relationship between the upper Latrobe Group nearshore deposits and the Gurnard Formation shelfal deposits in some areas. The relatively sharp boundary between Latrobe Group nearshore strata and Gurnard Formation shelf strata suggests a fairly rapid landward translation of the shoreline, which may have been associated with transgressive erosion and removal of strata at the top of the Latrobe Group. Medium to coarse sand grains at the base of the Gurnard Formation in some parts of the study area were unlikely to have been transported from more distal parts of the depositional system to the shelf and may be evidence for erosion of the underlying Latrobe Group clastic deposits. The thin veneer of Gurnard Formation strata in the study area probably represents the distal equivalent of upper Latrobe Group strata deposited when the shoreline existed west of the study area (Fig. 1.17).

Depositional History

The stratigraphic division of the study interval provides a genetically meaningful framework for interpreting the depositional history (Van Wagoner *et al.* 1990). Stratigraphic division that is based on time-equivalent surfaces groups palimpsest depositional systems deposited under similar depositional conditions (i.e. similar rates of relative sea-level change and sediment supply conditions). Therefore, the spatial distribution of facies within time-equivalent stratigraphic packages can be interpreted with reference to known depositional models and modern depositional environments (Lang *et al.* 2000). The incorporation of palaeo-geographic maps for specific stratigraphic packages in geological models can contribute significantly to reducing uncertainty between wells (Dubrule & Demsleth 2001) and consequently, also contributes to accurately representing reservoir heterogeneity.

Three main sources of data were used for the interpretation of the depositional history of the study area. These are full-hole core (discussed in detail in Chapter 2), wireline logs, and seismic attributes (Fig. 3.19). The interpreted depositional history is discussed with reference to the stratigraphic units defined in Table 3.3.

At basin scale, one of the most important architectural elements contributing to reservoir heterogeneity is the position of regional facies tracts. The sedimentology and reservoir properties of major facies identified in the study area are discussed in Chapter 2. Major facies tracts are:

- Alluvial and coastal plain facies
- Nearshore facies
- Lower shoreface-shelf facies.

Amplitude maps show NNE – SSW- trending 'belts' of high RMS amplitude. The belts of high RMS amplitude are seismic responses to coal (or gas-charged sandstones) within some hydrocarbon fields and are interpreted to approximate the positions of peat-forming environments within the study area. High RMS amplitude belts move westward in progressively younger positions in the stratigraphy, reflecting the landward migration of facies tracts during transgression, which is also inferred from wireline log correlations (Fig. 3.20).

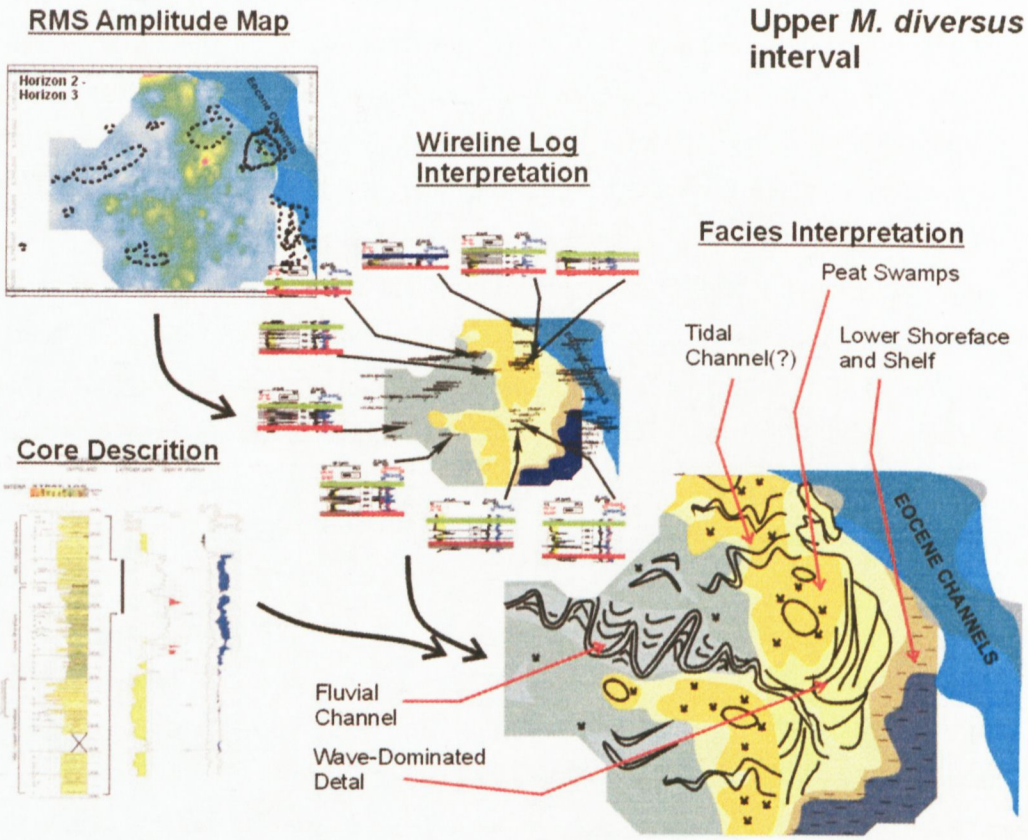

Figure 3.19—Methodology for palaeo-geographic reconstruction (more detailed maps provided in the following sections). Facies maps are constructed from seismic character, wireline logs and geological inferences regarding the environment of deposition made from core description.

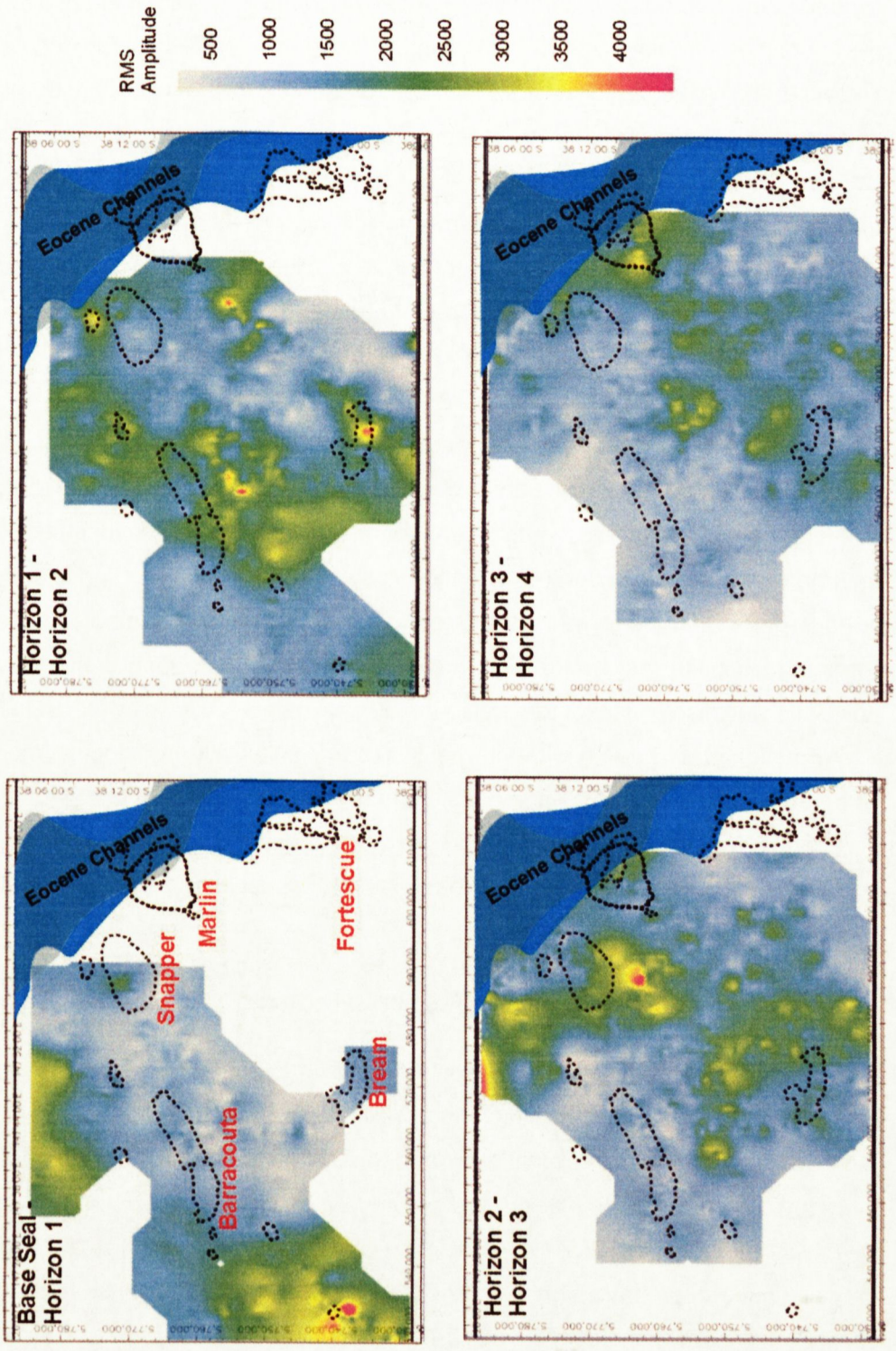

Figure 3.20—RMS seismic amplitude in the study area. High RMS amplitude, shown in green, yellow and red, is a seismic response to coal or gas-charged sandstone. Westward migration of NNW-SSE trending belts of high RMS amplitude can be seen with progressively younger positions in the stratigraphy.

The parts of the depositional system represented by the belts of high RMS amplitude are interpreted to be distal coastal plain environments, where watertable levels are highest and thick peat successions can be preserved. Back-barrier and coastal plain

swamps and marshes are generally represented in distal coastal plain environments. Nearshore environments are not characterised by prolific peat accumulation. Likewise, thick peat successions are rarely preserved in proximal coastal plain and alluvial plain environments because watertable levels are generally too low. Consequently, belts of high RMS amplitude are interpreted to separate nearshore and lower shoreface-shelf environments to the east from coastal plain and alluvial plain environments to the west. In combination with wireline log data, RMS facies maps facilitate the reconstruction of regional palaeo-geography. The position of the crosscutting Marlin Canyon is included on all facies maps for reference.

Ideally, each facies map would represent single systems tracts; however, the stratigraphic division is too coarse to delineate single systems tracts. As a result, multiple systems tracts and, consequently, many palimpsest depositional environments are represented on each facies map provided. Significantly, each stratigraphic unit does not necessarily represent a conformable succession. Stratigraphic units that may be characterised by internal sequence boundaries are noted in the discussion of depositional history below. The level of detail in the interpretation is a trade-off with the resulting complexity of the geological model (see Chapter 6). Despite the coarseness of interpretation, important regional palaeo-geographic trends can be identified in the study area. These trends have significant implications for spatial facies distributions, and consequently, spatial patterns in reservoir properties.

Lower M. diversus and L. balmei Palaeo-geography

The base of the study interval (at approximately Middle *M. diversus*) is characterised by a major flooding event resulting in a transition from deposition of dominantly fluvial facies in the alluvial and coastal plain to depositional units dominated by nearshore, marginal marine facies. As discussed previously, the flooding event is approximated by the stratigraphic position of Horizon 4. The associated rise in relative sea level may be linked to the transition from fault controlled syn-rift subsidence to thermal sag controlled post-rift subsidence near the end of the Cretaceous. The transition from fluvially dominated deposition to nearshore deposition is also identified by Rahmanian *et al.* (1990; see Fig. 3.21).

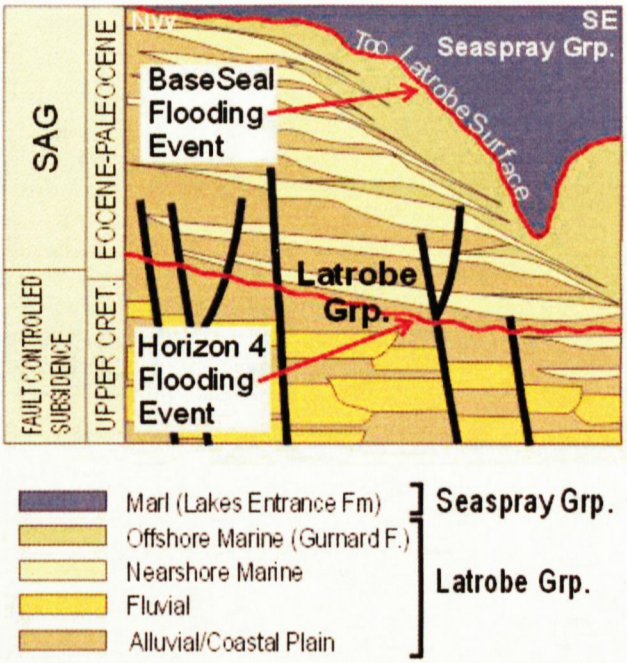

Figure 3.21—Conceptual stratigraphic cross-section. The stratigraphic positions of the Horizon 4 sequence boundary/ flooding event and the BaseSeal sequence boundary/ flooding event are shown (modified from Rahmanian *et al.* (1990).

The position of the shoreline during the deposition of the Lower *M. diversus* and *L. balmei* stratigraphic interval is interpreted to be east of the study area. Detailed reservoir characterisation has not been carried out on the Lower *M. diversus* and *L. balmei* interval as it represents the base of the geological model, and is not as important as overlying intervals in the context of CO_2 geosequestration. Based on core and wireline log interpretation the Lower *M. diversus* and *L. balmei interval* is dominated by coastal and alluvial plain facies, where fluvial channels represent the major reservoir facies (Fig. 3.22). However, wireline logs suggest that the interval consists largely of floodplain and overbank deposits (Figs. 3.17 & 3.18) and fluvial channels are likely to be relatively isolated, both vertically and laterally (Chapter 2). This suggests a high rate of aggradation in the coastal and alluvial plain, which may indicate that relative sea level rise/base level rise had already begun during deposition of the Lower *M. diversus* and *L. balmei* interval.

Following deposition of the Lower *M. diversus* and *L. balmei* interval the shoreline is interpreted to have migrated west and northwest associated with the continued rise of relative sea level.

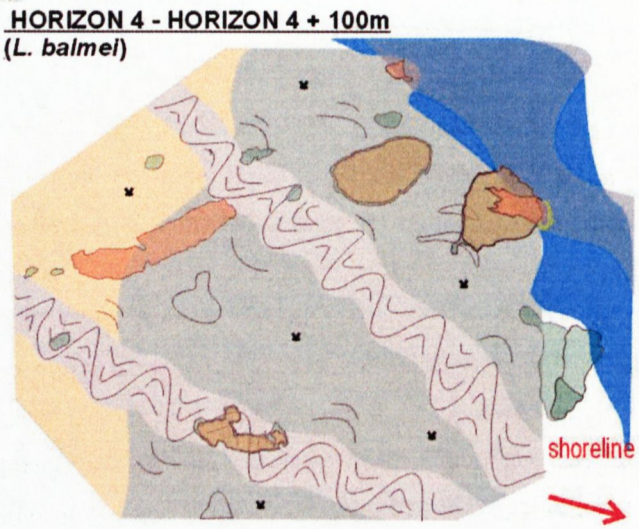

Figure 3.22—Palaeo-geographic map for the Lower *M. diversus* and *L. balmei* interval (not constrained by seismic attributes). Fluvial alluvial and coastal plain facies are the dominant facies types. Map is below the interval of interest and is diagrammatic only.

MIDDLE AND UPPER *M. DIVERSUS* PALAEO-GEOGRAPHY

During the deposition of the Middle and Upper *M. diversus* interval the shoreline is interpreted to have been situated just east and southeast of Marlin/Turrum Fields and the central deep area near Salmon 1, Conger 1, and Veilfin 1 (Fig. 3.23). Reservoir sandstones are wave-dominated, shore-parallel bodies deposited on a low-moderate energy coastline. The nearshore facies in the Middle and Upper *M. diversus* interval are represented as foreshore and middle to upper shoreface sand bodies in Figure 3.23, fed by fluvial systems from the west and northwest.

At least one episode of significant transgression is interpreted to have taken place during the deposition of the Middle and Upper *M. diversus* interval. The transgression resulted in the deposition of nearshore facies landward of the shoreline shown in Figure 3.23. Wireline logs suggest that nearshore facies were deposited as far west as Whiting Field. The possibility of a lowstand fluvial system extending to the southeast of the study area has been included in the Middle and Upper *M. diversus* facies map based on palaeo-geographic studies by Johnstone *et al.* (2001). An alternative interpretation is that submarine channels on the slope were fed by sediment from the lower shoreface.

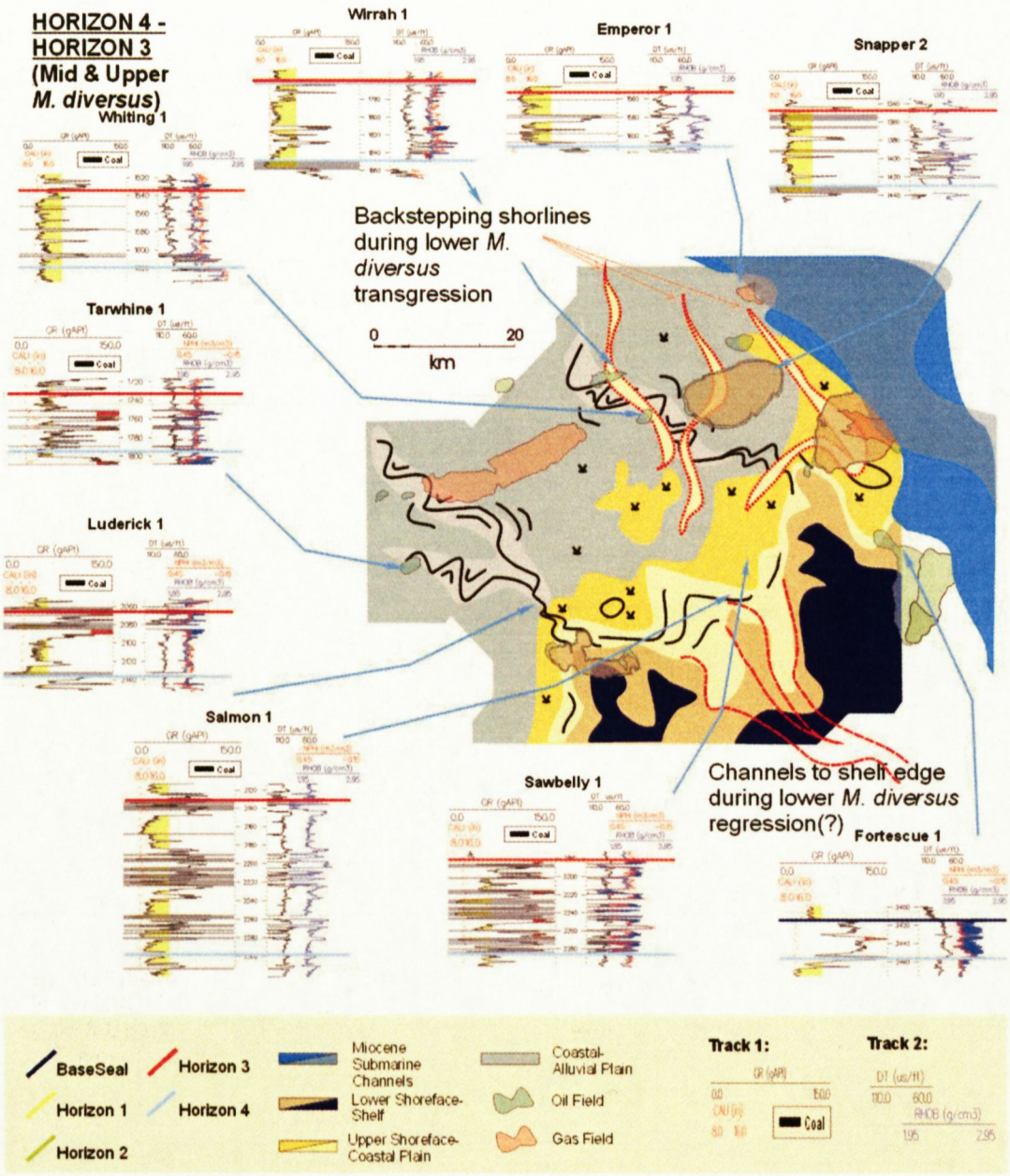

Figure 3.23—Palaeo-geographic map for the Middle and Upper *M. diversus* stratigraphic interval. Fluvial systems from the NW and W are interpreted to have fed nearshore depositional systems. At least one episode of transgression resulted in palimpsest shoreface deposits as far west as Whiting Field. Additionally, fluvial or submarine channels may have extended to the SE towards the shelf edge, possibly in response to relative sea-level fall.

The Marlin Canyon may have been initially emplaced as early as Lower *M. diversus* time associated with a considerable fall in relative sea level (Johnstone *et al.* 2001). Seismic interpretation suggests that the Marlin Canyon resulted from either mass wasting or fluvial incision from the northern Strzelecki Terrace. The internal architecture of the submarine canyons indicates that several episodes of erosion and deposition within the canyon feature may have taken place (Fig. 3.24). The Marlin

Canyon may have formed initially from fluvial incision during a fall in relative sea level or from submarine mass wasting, but strata at the base of the Marlin Canyon are part of the Turrum Formation and appear to be shelfal in origin.

The emplacement of the Marlin Canyon was associated with considerable erosion of the *P. asperopolus* and older stratigraphic intervals. The Lower *N. asperus* and *N. asperus* intervals were largely unaffected because they were restricted to the western parts of the study area during submarine canyon formation. Seismic horizons 1, 2, 3, and 4 are truncated by the BaseSeal surface to the west of, or at the Marlin Canyon complex (Fig. 3.24).

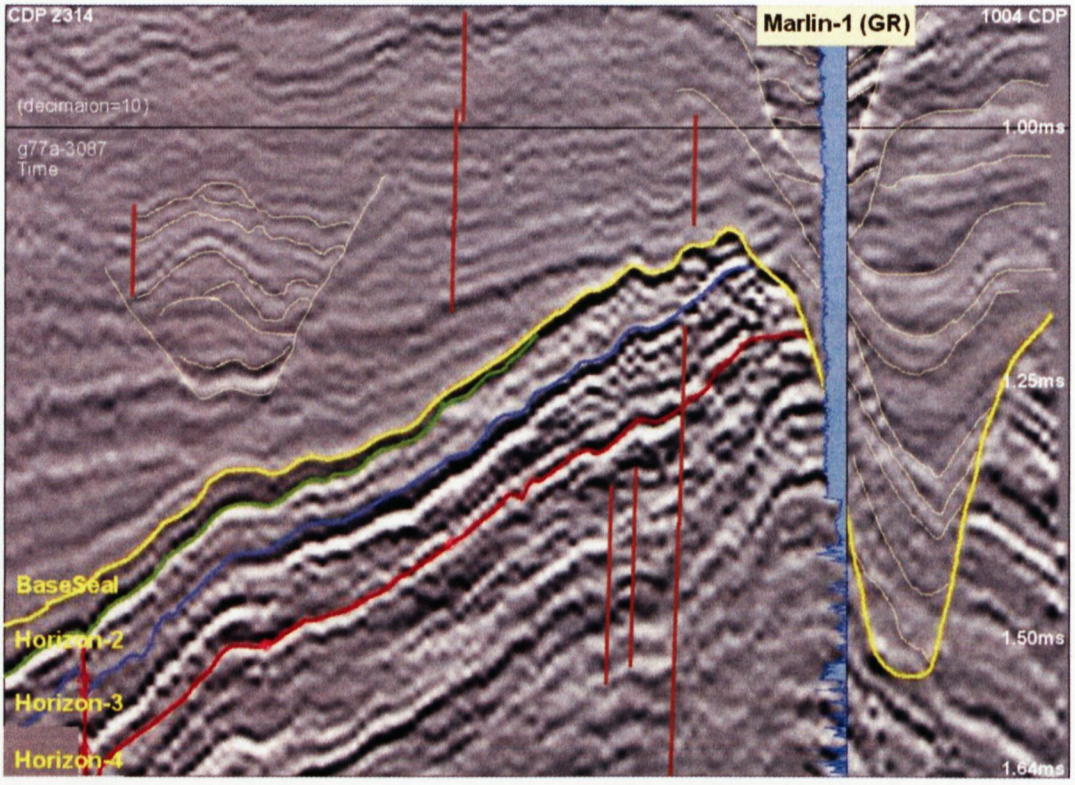

Figure 3.24—Seismic line in the Marlin Canyon area. Truncation of horizons 3 & 4 by the Marlin Canyon is evident. The internal architecture of the canyon is highlighted.

P. ASPEROPOLUS PALAEO-GEOGRAPHY

The *P. asperopolus* shoreline is northwest of the Middle and Upper *M. diversus* and is interpreted to trend NNE – SSW, by comparison with the NE-SW- trending shoreline of the Middle and Upper *M. diversus* interval. The gap in the high RMS amplitude belt in the *P. asperopolus* interval suggests that a large fluvial system cut through the back-barrier/back-berm swamps (Fig. 3.25). Consistent with this

interpretation, nearshore sandstones are depicted as part of a wave-dominated deltaic system rather than a non-fluvially influenced, foreshore-shoreface system.

Johnstone *et al.* (2001) suggest that the sediments around Barracouta Field are indicative of coastal plain deposition within the *P. asperopolus* biozone, which is consistent with the interpretation put forward in this study. The exact position of the fluvial system depicted in Figure 3.25 is poorly constrained. However, log motifs in Whiting Field, Tarwhine 1, and Luderick 1 all suggest relatively thick fluvial channel facies. The *P. asperopolus* fluvial system may have been highly mobile, or several separate fluvial depositional systems may be represented in the interval. The former possibility is represented on the facies map.

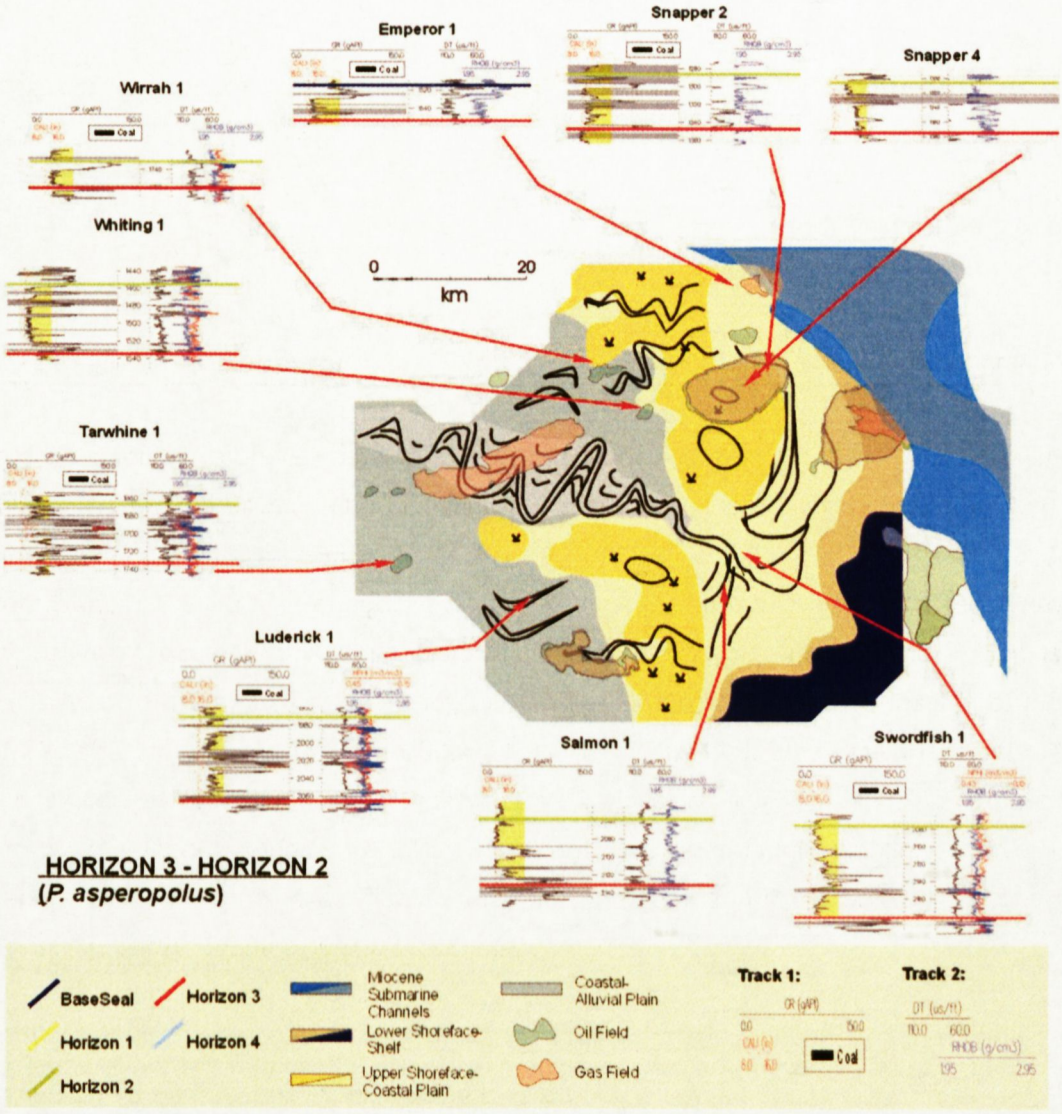

Figure 3.25—Palaeo-geographic map for the *P. asperopolus* stratigraphic interval. A wave-dominated deltaic setting is inferred for the *P. asperopolus* depositional system.

LOWER *N.ASPERUS* PALAEO-GEOGRAPHY (HORIZONS 2 – 1)

The amplitude map for the Lower *N. asperus* interval may suggest the formation of a partially protected (tidal?) embayment. Lower *N. asperus* facies are characterised by a high proportion of interbedded coal, suggesting limited clastic influx, and low energy environments onshore.

.

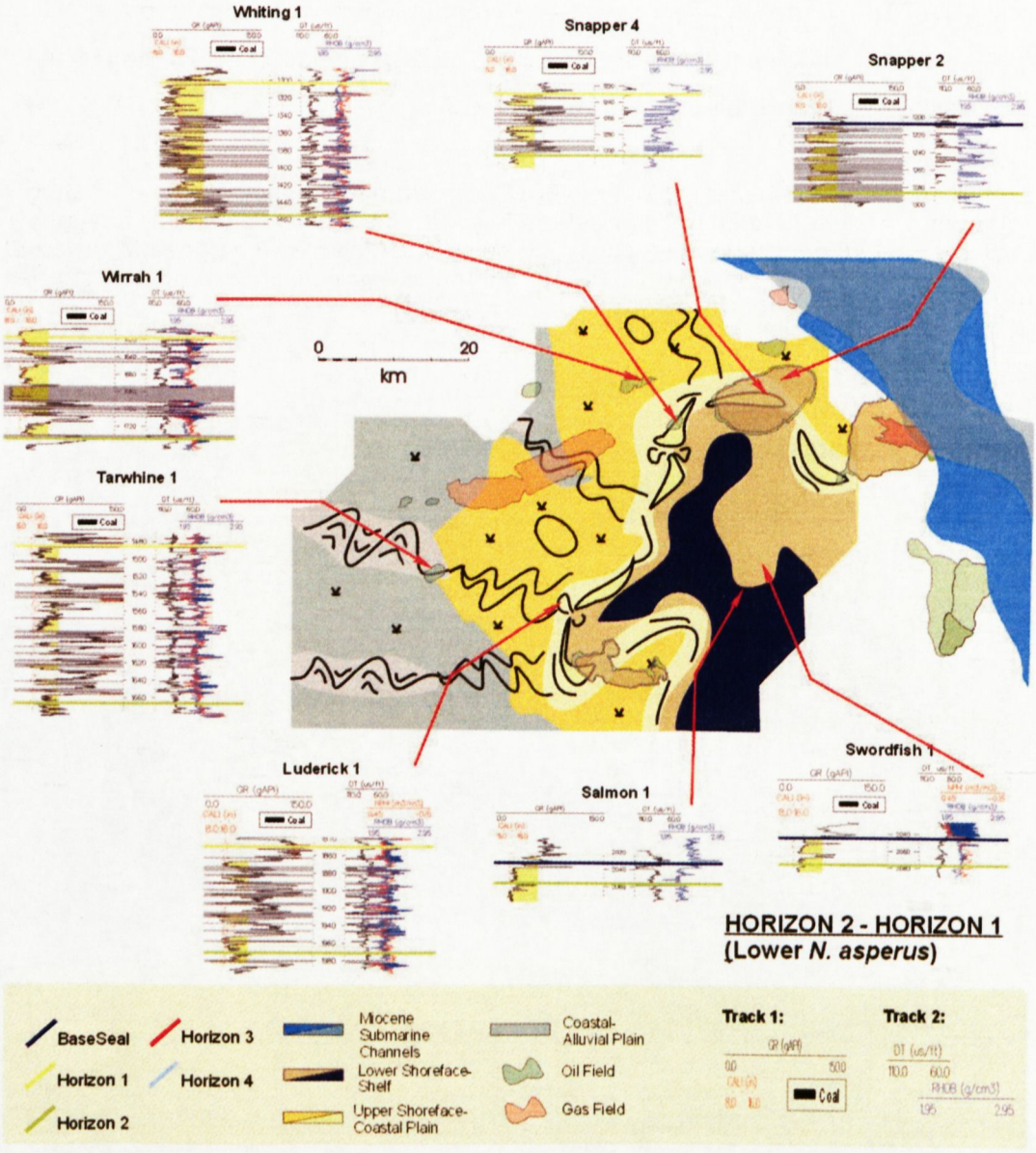

Figure 3.26—Palaeo-geographic map for the Lower *N. asperus* stratigraphic interval. The rate of transgression may have increased during deposition of the *P. asperopolus* to Lower *N. asperus* intervals. A protected embayment characterised by barrier island depositional systems is interpreted for the Lower *N. asperus* interval.

A common vertical facies association between nearshore sandstone deposits and fine-grained suspension deposits may suggest the formation of barrier island depositional environments. The fine-grained suspension deposits are interpreted to be associated with shallow back-barrier lagoon deposition. Tidally influenced facies are more common and their preservation potential is better in the Lower *N. asperus* interval, which is also a result of relatively protected back-barrier settings.

The changes in the depositional system from *P. asperopolus* to Lower *N. asperus* intervals are consistent with a rise in relative sea level resulting in transgression. Transgression in nearshore environments is commonly associated with the development of barrier island systems and a reduction in sediment delivery to coastal plain and nearshore environments due to conflicting tidal and fluvial influences. Sediment is 'trapped' in coastal plain estuaries and not delivered to the shoreline (Dalrymple *et. al* 1992, Boyd *et al.* 1992).

MIDDLE AND UPPER *N. ASPERUS* PALAEO-GEOGRAPHY (HORIZON 1 - BASESEAL)

The Middle and Upper *N. asperus* interval is characterised by continued transgression and migration of the shoreline to the northwest. As a result, Middle and Upper *N. asperus* facies within the study area are primarily lower shoreface and shelf facies. Sandstone deposits are restricted to the coastal plain and nearshore facies in the northwestern part of the study area. RMS amplitude maps suggest that the tidal embayment of the Lower *N. asperus* interval is better developed than in the Middle and Upper *N. asperus* interval—a large tidal estuary may be represented.

In addition to the depositional control on restricting Middle and Upper *N. asperus* facies to the west and northwest of the study area, seismic sections and wireline correlation suggest a degree of erosion of the Middle and Upper *N. asperus* stratigraphy during the BaseSeal sequence boundary/flooding event in the eastern part of the study area (Fig. 3.17). This suggests that any sediment delivered to the eastern parts of the study area during this period was not preserved.

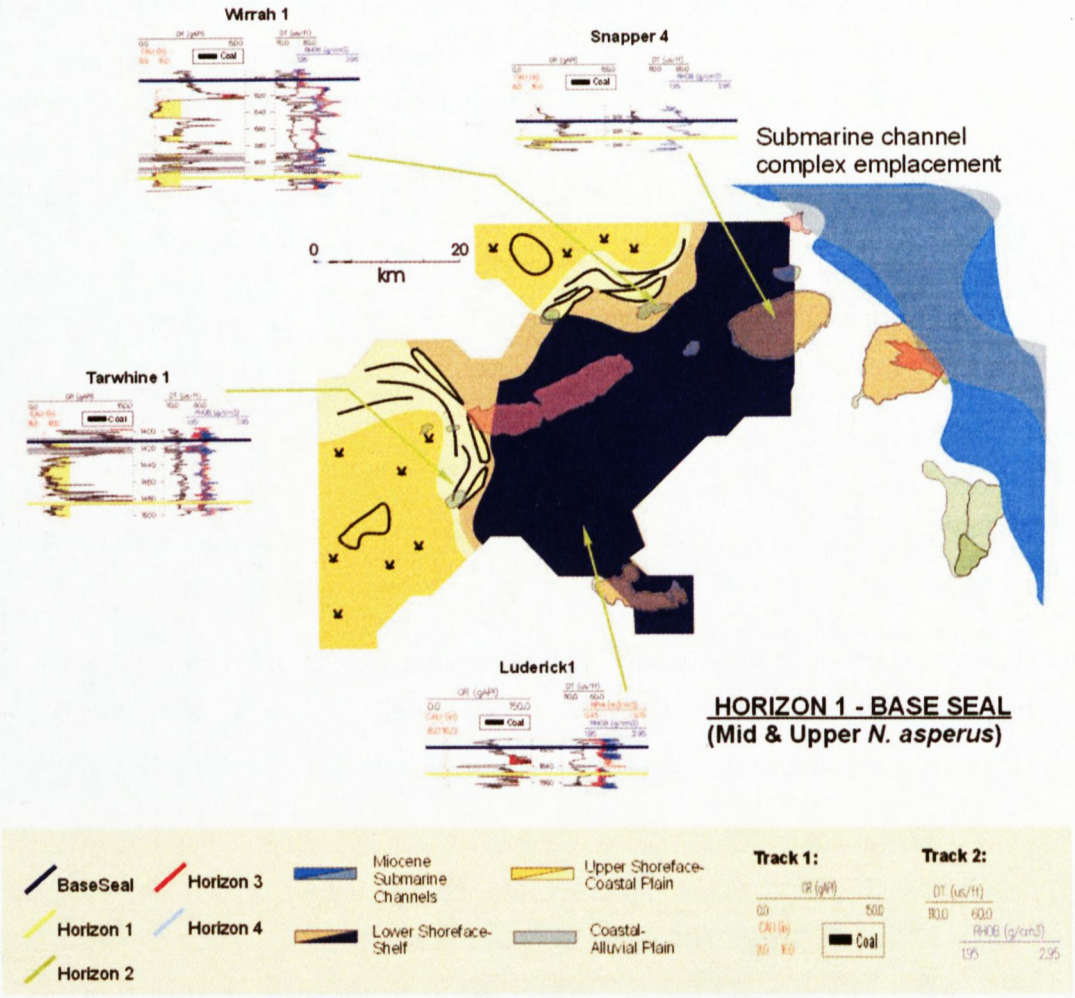

Figure 3.27—Palaeo-geographic map for the Middle to Upper *N. asperus* stratigraphic interval showing continued westward migration of the shoreline and large estuarine embayment.

Implications for CO_2 Storage and Geological Model Construction

The geometry of the BaseSeal surface is likely to play the key role in determining the rate and direction of CO_2 migration. The importance of the BaseSeal surface stems from the fact that gravity forces are likely to be the dominant flow behaviour during the majority of the time CO_2 is in the gaseous/supercritical phase prior to dissolution in the formation water. Viscous forces may only play a significant role where the pressure gradient is high—primarily in the vicinity of the injector wells (see Chapter 1). Consequently, when the SC CO_2 rises to the base of the seal unit, the migration path of the SC CO_2 is likely to be defined by the maximum dip of the BaseSeal surface. The rate of SC CO_2 migration will also be influenced by the dip magnitude of the BaseSeal surface in addition to permeability heterogeneity in the upper part of the reservoir.

Fortunately, the BaseSeal surface is the best constrained seismic horizon mapped due to the almost ubiquitous presence of high impedance shale over lower impedance coal, sandstone, siltstone, and shale of the underlying strata resulting in a characteristic strong peak response (reverse SEG polarity convention) that is easily identifiable on almost all seismic sections. Additionally, the well control for the BaseSeal surface is fairly good because virtually all wells in the study area penetrate the surface. Consequently, the geometry of critical interface between sealing units and reservoir/aquifer units is relatively well constrained in time. The key uncertainty influencing the geometry of the BaseSeal surface may be the effect of velocity variations in the over-burden for depth conversion.

If carbon dioxide were injected into the structurally low area around Salmon 1, Cod 1 and Conger 1 wells, SC CO_2 would migrate to the northeast towards Marlin/Turrum fields (Fig. 3.28) and then to the west and southwest along the axis of the regional anticline, based on the structure of the study area. Alternatively, SC CO_2 migration could be towards the north to Snapper Field depending on the exact location of injector wells.

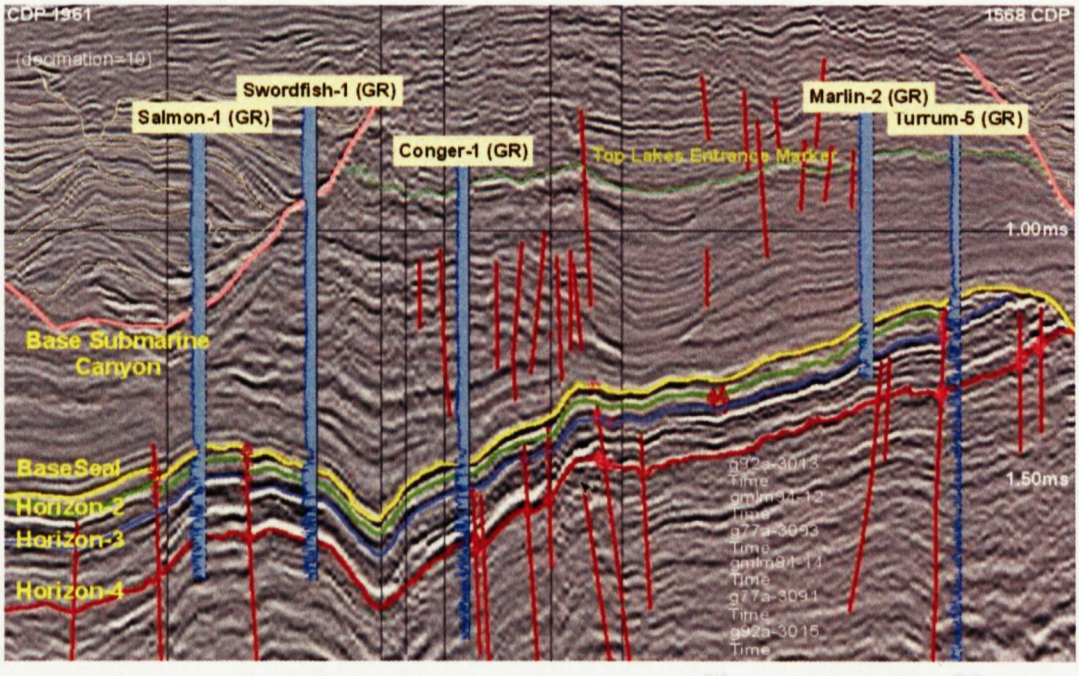

Figure 3.28—Seismic line from the Swordfish 1, Salmon 1, Veilfin 1 area to Snapper Field.

Clearly the rate of CO_2 migration and timing of CO_2 encountering existing hydrocarbon fields versus the expected date for field depletion is a significant issue (see Chapter 7). Injector locations at the structurally low area around the Salmon 1,

Cod 1, and Conger 1 wells take advantage of a relatively long stand off between injector locations and Marlin and Snapper fields. However, the structural complexity and density of faults increases in the structurally low areas so a trade-off must be made between minimising containment risk by avoiding highly faulted areas and minimising risk of contaminating hydrocarbon assets by increasing stand off from existing fields. There are several key issues here:

- The geomechanical stability of faults in proximity to the injection site and the likely increase in pore pressure at the faults as a result of CO_2 injection (Root *et al.* 2004)
- The transmissibility of E-W oriented faults in the context of altering the flow path of CO_2 up-dip towards Marlin/Turrum and Snapper fields
- The likely migration rate up-dip from the injection site, which is best assessed through geological model construction and flow simulation.

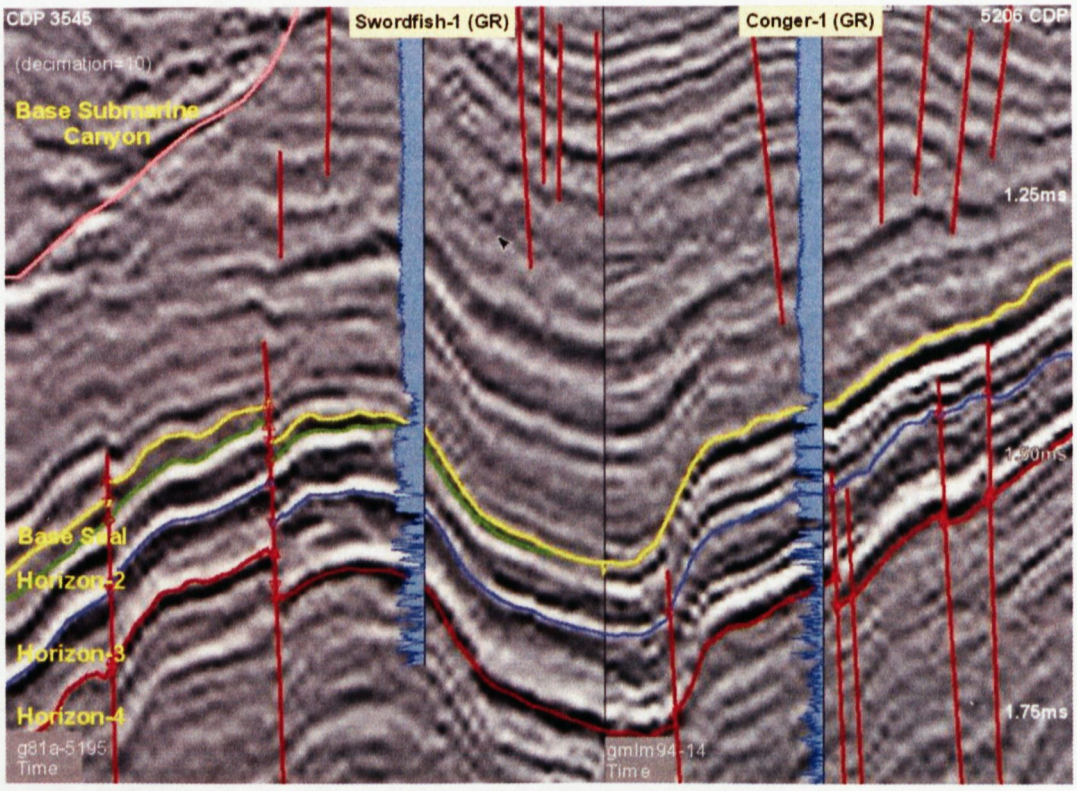

Figure 3.29—Seismic line showing a fault south of Swordfish 1 that is associated with significant displacement and propagates into sealing lithologies. Fault sets in the seal are also mapped.

In the Salmon 1, Cod 1, and Conger 1 area, the Lower *M. diversus* and *L. balmei* and Middle and Upper *M. diversus* intervals are characterised by serrated, high-value GR log motifs, suggested coastal and alluvial plain facies, dominated by floodplain and overbank fluvial facies (Fig. 3.29). It is likely that coastal/alluvial plain facies will be

characterised by relatively low permeability thickness in the Salmon 1, Swordfish 1, Cod 1 area despite the presence of localised high-permeability channellised facies. In close proximity to the injector wells high porosity and permeability is preferable to reduce injection pressure and injector well count. Consequently, if injection were to take place in the Salmon 1, Cod 1, and Conger 1 area it may be useful to inject above the *Middle and Upper M. diversus* intervals, into the nearshore sandstones of the *P. asperopolus* or Lower *N. asperus* intervals that are characterised by high net-to-gross and high porosity and permeability. Alternatively, horizontal injection wells or fracture stimulation may result in sufficient permeability for injection into the coastal-alluvial plain facies of the Middle and Upper *M. diversus* down to the *L. balmei* interval.

Nearshore sandstones within the three-way structural closure of the regional anticline in the central deep area are interconnected based on the stratigraphic model proposed herein and based on pressure data (Root *et al.* 2004). Stratigraphic compartmentalisation is not expected once CO_2 enters nearshore facies, but is considered a greater risk in fluvial facies.

The architectural arrangement of the BaseSeal unconformity and the underlying stratigraphy suggests that the interbedded low-permeability units will be oriented perpendicular to flow during the westward portion of the migration path, along the axis of the regional anticline from Marlin/Turrum fields to Barracouta. This architectural arrangement is likely to be most prominent in the upper parts of the stratigraphy (Middle and Upper *N. asperus* and *P. asperopolus*). The heterogeneity along the potential flow path of the SC CO_2 is likely to be advantageous for retarding the rate of SC CO_2 migration and possibly for improving storage efficiency (Chapter 1). Storage efficiency might be increased because low-permeability barriers and baffles to fluid flow oriented perpendicular to the CO_2 migration direction will induce some lateral migration inducing tortuosity in the flow path, and more pore space is likely to be utilised as a result.

The stratigraphy in the Gippsland Basin central deep area may represent an ideal compromise between stratigraphic compartmentalisation, which would require extra injection wells to capitalise on all of the available pore volume, and moderate levels of reservoir heterogeneity to reduce CO_2 migration rate. The influence of the combined structure and stratigraphic architecture needs to be tested through flow simulation.

Chapter 4—Analogues and Geostatistics

Abstract

Techniques such as kriging or conditional simulation for stochastically populating attributes like flow properties in geological models require descriptions of spatial variance, which are usually semi-variogram or covariance models. Horizontal experimental semi-variograms produced from well data in the Gippsland Basin ESSCI area are uninterpretable due to unfavourable data density and distribution. Unfavourable horizontal data density and distribution is typical of petroleum data sets. The problem is compounded in the case of reservoir model construction for CO_2 storage due mainly to the large areas typically represented in reservoir models for CO_2 storage. Consequently, horizontal trained madograms and semi-variograms from modern and ancient analogues are used to describe the spatial variance of facies and flow properties for different depositional environments represented in the Gippsland Basin ESSCI.

In contrast with horizontal experimental semi-variograms, vertical experimental semi-variograms in the study area are relatively well defined and can be used to characterise vertical spatial continuity of reservoir properties.

Several features of trained horizontal madograms and semi-variograms appear to be characteristic of nearshore, fluvial and deltaic depositional environments. These 'diagnostic' madogram and semi-variogram characteristics were used to guide the selection of meaningful semi-variogram models to populate porosity and permeability with sequential gaussian simulation (SGS). Porosity and permeability was populated within a deterministic framework of coastal-alluvial plain, nearshore, and lower shoreface-shelf facies that were used as classifying attributes for SGS.

Introduction

A geological model that accurately represents reservoir heterogeneity is important for simulating the behaviour of CO_2 at reservoir conditions. The degree and pattern of reservoir heterogeneity has a significant impact on the subsurface behaviour of SC CO_2. The degree and style of reservoir heterogeneity will affect the migration path of SC CO_2, the migration rate of the CO_2, and the shape of the CO_2 front. For example, the correlation length of permeability in the direction of flow, which is largely defined by the semi-variogram or covariance used in the population of a reservoir model, has a significant impact on the two-phase flow behaviour of SC CO_2 (Ennis-King and Paterson 2001). The semi-variogram is a description of the spatial continuity of a regionalised variable, which is used when attributes such as porosity and permeability are populated in a geological model with kriging or conditional

simulation. Therefore, the appropriate semi-variogram is central to realistically representing the style and degree of reservoir heterogeneity in a reservoir model.

Stochastic techniques are valuable for the construction of geological models because they facilitate realistic representations of reservoir heterogeneity, they are useful for data integration, and they allow quantification of uncertainty. However, the application of stochastic techniques in the petroleum industry is restricted to some degree by limitations of typical petroleum data sets. These limitations are generally of greater significance in the context of constructing geological models for CO_2 geosequestration because relatively large areas generally need to be represented in geological models. Consequently, the horizontal distribution of 'hard' data points in CO_2 storage scenarios is likely to be even less favourable than in conventional hydrocarbon exploration and production (E & P) scenarios for generating stochastic models.

In petroleum data sets there is generally a disparity between vertical and horizontal data resolution of several orders of magnitude. Despite the fact that sedimentary rocks are typically much more heterogeneous vertically than horizontally (Fig. 4.1), the very large difference between vertical and horizontal resolution in typical petroleum data sets makes creating accurate models of realistic heterogeneity challenging. Wireline logs and full-hole core provide very fine vertical resolution whereas horizontal resolution is generally defined by the well spacing, although integrating seismic attributes may significantly improve horizontal resolution in some cases. Unlike mining industry data sets, for which geostatistical approaches were originally developed, petroleum data sets are generally characterised by few wells and a highly irregular spatial distribution of wells, particularly within Australia. Consequently, the distribution of hard data in the horizontal plane is generally not favourable for the generation of statistical data.

One of the specific problems with unfavourable hard data distribution in the horizontal plain is that meaningful horizontal experimental semi-variograms generally cannot be generated with petroleum data sets. Typically, either the minimum spacing of wells is greater than the distance at which the maximum variance of the sample population is reached (producing a 'pure nugget' experimental semi-variogram), or there are too few wells to result in enough sample pairs of the population [$Z(Xi)$], separated by a particular distance and direction (**h**) to be statistically meaningful (Journel *pers.*

comm. 2002, Dubrule & Damsleth 2001, Kupfersberger & Deutsch 1999, Bahar & Kellkar 1998).

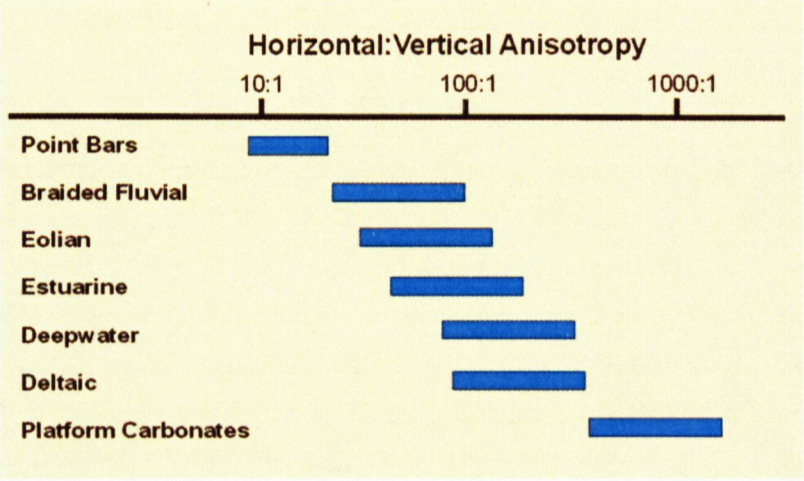

Figure 4.1—Estimated ratios of horizontal to vertical anisotropy from various depositional environments (from Deutsch 2002). Sedimentary rocks are characterised by greater anisotropy in the vertical direction than in horizontal directions. The ratio of horizontal to vertical anisotropy is in part dependent on the environment of deposition.

A previous study of analogue/trained semi-variograms that measure transmissivity and effective permeability suggest that there is no correlation between depositional environment and semi-variogram characteristics (Kupfersberger and Deutsch 1999). However, in many reservoirs, including the Gippsland Basin ESSCI, the environment of deposition can be shown to control reservoir properties (Chapter 2). For example, Liu *et al.* (2002) suggest characteristic degrees of vertical heterogeneity for specific depositional environments based on permeability and gamma-ray log data. The environment of deposition should theoretically also influence horizontal semi-variogram characteristics where there is a relationship between reservoir properties and facies. The potential utility of 'trained' semi-variograms and madograms is recognised in the literature (Pelgrain de Lestang *et al.* 2002, Deutsch 2002, Kupfersberger and Deutsch 1999); however, there is little published data at present. There remains a need for geologically based geostatistical rules for different environments of deposition (Chambers 2000).

Horizontal and Vertical Data Density and Distribution

In the Gippsland Basin ESSCI, lack of data and unfavourable data distribution renders experimental semi-variograms calculated in the horizontal plane uninterpretable. Figure 4.2 shows experimental semi-variograms of porosity. No meaningful information regarding the spatial continuity of porosity is yielded by the horizontal experimental semi-variograms. In contrast, the vertical experimental semi-

variogram has better structure due to the dense vertical sampling of wireline logs. Consequently, the vertical experimental semi-variogram provides information about the vertical spatial continuity of porosity in the study area, but the horizontal semi-variograms are inadequate.

As descriptions of horizontal spatial continuity are not attainable from experimental semi-variograms, in this study, modern and ancient analogues are used to generate 'trained' horizontal semi-variograms and madograms. Semi-variogram and madograms are produced from several modern and ancient analogues for each depositional environment represented in the Gippsland Basin ESSCI. The objective is to identify semi-variogram and madogram characteristics that are diagnostic of particular depositional environments. Diagnostic features of semi-variograms for specific depositional environments can be incorporated in semi-variogram or covariance models that are used for conditional simulation or kriging. Consequently, realistic heterogeneity for specific facies can be incorporated in the geological model of the Gippsland Basin ESSCI. This chapter focuses on characterising spatial continuity. The way in which description of spatial continuity is incorporated in attribute population through conditional simulation is discussed in Chapter 6.

Depositional Environments and Spatial Continuity

The environment of deposition typically exerts a considerable influence on the spatial anisotropy of reservoir properties such as permeability (K), porosity (∅), water saturation (S_w), and shale volume (V_{sh}). For example, a fluvial depositional environment will generally have greater variance in reservoir properties in a horizontal direction perpendicular to the average trend of channel axes than in a horizontal direction parallel with the average trend of channel axes. The greater variance in reservoir properties in a direction perpendicular to the channel axis exists because rock composition and texture typically change more significantly with distance in a direction perpendicular to the channel axis (~10^2 – 10^3 m). In contrast, in a shelf depositional environment, reservoir properties are more likely to show low variance in all horizontal directions because rock of similar composition and texture can be deposited laterally over very large areas (~10^4 – 10^6 m).

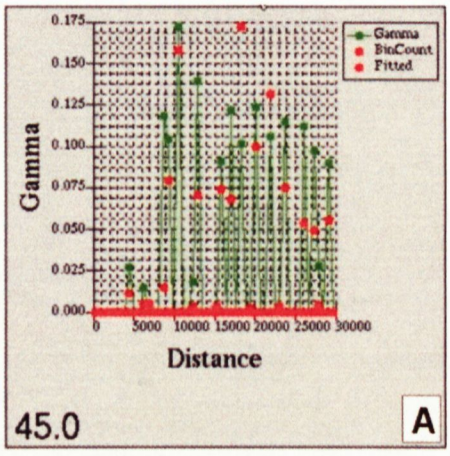

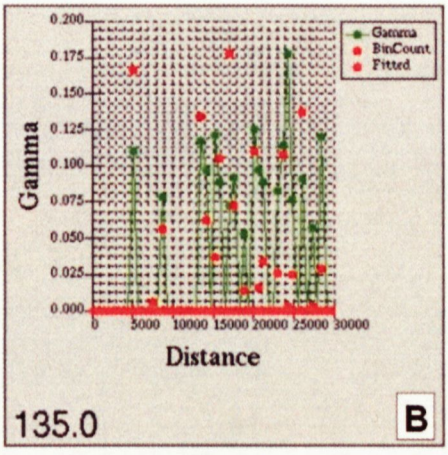

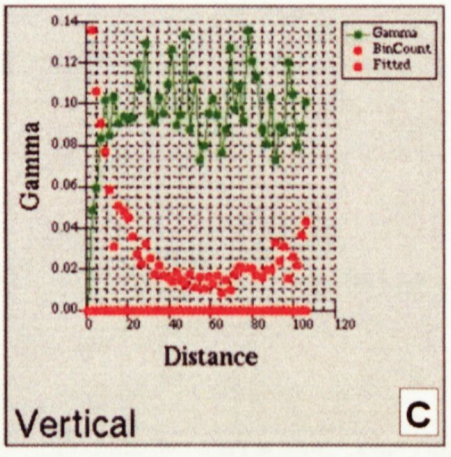

Figure 4.2—Directional experimental semi-variograms for porosity in the Gippsland Basin study area. Three experimental semi-variograms are provided. Two experimental semi-variograms are calculated within the horizontal plain at 45° (A) and at 135° (B). A vertical semi-variogram was also calculated (C).

Only the vertical semi-variogram has sufficient data pairs to be interpretable. The vertical variogram is characterised by a range between 10 m and 15 m and a sill at ~11%.

Generating meaningful stochastic models for reservoir properties is significantly more complex where secondary processes such as diagenesis or natural fracture networks control the spatial distribution of reservoir properties rather than primary depositional controls. The added complexity results because there is little evidence that an area of diagenetic carbonate alteration, for example, will have a predictable three-dimensional shape, whereas there are predictable patterns in the three-dimensional

shape of fluvial channels or barrier islands and other depositional features. However, the pattern of diagenetic alteration in a reservoir may be related to primary depositional controls that can be linked to the environment of deposition. Alternatively, the pattern of diagenesis may be controlled by the distributions of faults and fractures that may have acted as flow conduits or flow barriers for diagenetic fluid.

A comparison of routine core analysis ∅/K measurements and depositional facies in the Gippsland Basin suggests that the environment of deposition is the primary control on porosity and permeability (Fig. 2.44). A secondary control on ∅/K is carbonate cementation, which may be related to the position of major faults within the study area (see Chapters 2 & 3). Demonstrating that depositional environment is a significant control on regionalised variables such as K_v, K_h, ∅, S_w, and V_{sh} is an important precursor to selecting an approach for describing spatial continuity and the stochastic population of a reservoir model. The identification and mapping of depositional environments or facies is irrelevant in reservoirs where primary depositional characteristics such as original rock composition and texture no longer have an influence on reservoir properties.

SEMI-VARIOGRAMS

The semi-variogram is a tool for measuring the spatial continuity of a regionalised variable. The semi-variogram for regionalised variable $Z(x_i)$ is defined as:

$$\gamma(\bar{h}) = \frac{\sum_{i=1...n}^{n} [Z(X_i) - Z(X_{i+\bar{h}})]^2}{2n}$$

The semi-variogram is a continuous function of **h** that gives an indication of the correspondence between all values of a regionalised variable a distance and direction **h** apart. With most reservoir properties, the correspondence between two values in a particular direction will decrease as the distance between the two values increases. For example, two core plugs within a metre of one another are more likely to have similar porosity values than two cores plugs ten metres apart. Consequently, the value of γ will generally increase as the length of **h** increases in a particular direction.

An experimental semi-variogram (γ) is calculated from a number of vectorial lags (**h**) that are considered representative of the total sample population [$Z(x_i)$]. Ideally, several γ values are calculated in the vertical and several horizontal directions. Several horizontal directions are calculated because it is useful to identify the directions of maximum and minimum horizontal variance to properly model a regionalised variable. In practice, the direction of maximum and minimum horizontal variance will probably be parallel with depositional strike and depositional dip if primary depositional controls are the main influences on reservoir property variation. Important aspects of semi-variogram models that are required for conditional simulation or kriging are:

- Sill (C): the value of γ that represents the variance of the population
- Range (a): the length of **h** at which the sill is reached
- Nugget: the variance of the data below the minimum lag (**h**).

Generally geological modeling packages will require a value for the sill, range and nugget as well as a mathematical function that models semi-variograms in the vertical direction and in the direction of maximum and minimum variance in the horizontal plain.

Categorical and Continuous Variables

Reservoir models are conventionally populated with continuous variables such as K, ∅, S_w, and V_{sh} directly from the petrophysical interpretation at well locations. Therefore, experimental semi-variogram models that accurately represent the spatial continuity of specific reservoir properties must be generated. However, it is commonly difficult to generate statistical models that describe the horizontal spatial continuity because of the unfavourable horizontal distribution of hard data points, as discussed previously. Additionally, analogue studies very rarely measure K, ∅, S_w or V_{sh} directly.

Increasingly, petroleum geoscientists and engineers have moved towards a two-stage stochastic population of geological models, where the model is first populated with 'facies' and then the model is populated with reservoir properties within the pre-existing facies framework (Chambers 2000). Incorporating categorical 'facies'

variables (e.g. depositional facies, electrofacies, lithofacies) in the stochastic population of K, ∅, S_w and V_{sh} may allow meaningful experimental semi-variogram models to be generated from analogue data. Additionally, categorical variables representing facies provide a way to meaningfully group measurements of reservoir properties. This is associated with two significant advantages. First, many geostatistical techniques, including kriging and conditional simulation make an assumption of stationarity. Stationarity means that there will be no spatial trends of a regionalised variable within the study area—statistics such as the mean, variance or covariance are independent of location (Hohn 1999).

Most geological regionalised variables are non-stationary. For example, in the Gippsland Basin an overall degradation in reservoir properties occurs towards the east of the study area because distal non-reservoir facies are more common in the eastern parts of the study area (Chapter 3). The stationarity assumption can be honoured with geological regionalised variables by deterministically dividing data into groups where stationarity is preserved. In the Gippsland Basin, the eastward degradation in reservoir properties is still represented, but stationarity of the data is preserved by using facies variables.

The second advantage of populating reservoir properties in a reservoir model within a categorical facies framework is that the model can ensure that the spatial distribution of flow properties is compatible with the depositional model. For example, when categorical facies are used thoughtfully, it is less likely that the spatial distribution of reservoir properties will imply violations of Walter's Law, like very high permeability pathways in an area identified as a shelf depositional environment.

There are several variations on the general two-stage reservoir population technique using both categorical facies variables and continuous reservoir property variables. Both categorical facies and reservoir properties can be populated using conditional simulation. When reservoir properties are simulated, the pre-existing facies attribute is used as a classifying attribute. The classifying attributes constrain the conditional simulation such that a reservoir property from a grid cell with facies attribute '3' can only be used to populate other cells with facies attribute '3'.

Alternatively, categorical facies may be populated where specific K, ∅, S_w and V_{sh} are assigned to each facies. This approach is sometimes termed 'indicator

simulation' (GeoVisual Systems 2000). Using indicator simulation, each grid cell representing facies attribute '3' for example, will have the same value for K, ∅, S_w and V_{sh}. The approach is intrinsically limiting because variability within a particular facies is not captured. However, the approach also has several advantages including:

- The file sizes associated with reservoir models are significantly reduced because a separate K, ∅, S_w and V_{sh} attribute need not be assigned to every grid cell.
- Up-gridding and up-scaling the categorical variables results in 'pseudo-continuous' variables that populate the actual simulation grid (i.e. the reservoir properties of several categorical values are averaged in a single cell of the simulation grid).

Where the categorical variable approach described above is used, categorical variables must be assigned from core and wireline suites at each well that intersects the interval of interest. Instead of petrophysical logs, 'logs' of categorical variables are used during population of the reservoir model (Fig. 4.3). Consequently, another one of the major practical advantages of the approach is that reservoir properties can be populated in a reservoir model that has no petrophysical data or inconsistent petrophysical data, provided there is sufficient production data and routine core analysis data to accurately assign K, ∅, S_w and V_{sh} values to each categorical variable. Where facies have assigned reservoir properties it is even more important to have a strongly established relationship between facies and reservoir properties based on core analysis or petrophysics (Pelgrain de Lestang *et al.* 2002).

Although categorical variables are employed in this study, the 'indicator simulation' approach for populating categorical variables, described above, was not utilised because:

- Sufficient petrophysical data exists to use a two-stage population approach.
- The indicator simulation approach limits the variance within a particular facies unless an extremely detailed grid and facies scheme is used.
- It is unusually difficult to distinguish depositional facies from log motif alone in the upper Latrobe Group.

Though the indicator simulation approach is not used in this study it may be particularly suited to reservoir model construction for CO_2 storage because a paucity of petrophysical data and inconsistent petrophysical data are likely to be encountered when very large areas, encompassing several fields and permits, are incorporated in

a reservoir model for CO_2 storage. In addition, the reduction in computational and storage costs of geological models that use indicator simulation would be suited to CO_2 geosequestration studies, also because very large geological models typically need to be built.

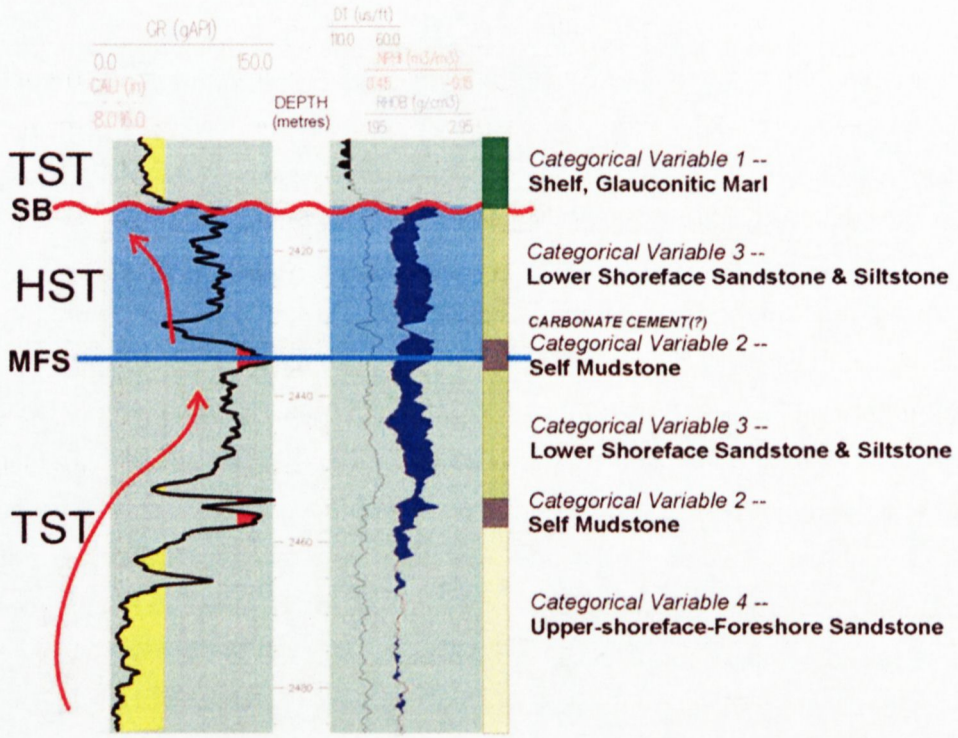

Figure 4.3—Facies (right-hand track) and systems tracts identified on wireline logs. The facies are categorical variables that are commonly populated in geological models prior to flow properties.

The approach used in this study for incorporating both categorical facies variables and continuous reservoir property variables in the reservoir model is to deterministically populate the facies attribute within the reservoir model, and then populate reservoir properties using conditional simulation. Seismic attributes, wireline log suites and core, where available, were used to produce deterministic facies maps (Chapter 3). The facies maps were used to populate each zone (defined by seismic horizons) of the geological model with a deterministic spatial distribution of facies attributes. Conditional simulation was then carried out using facies as a classifying attribute.

The degree of deterministic control on attribute population is dependent on the data quantity and quality, and the confidence in the geological interpretation. Too much

deterministic input may reduce the opportunity to realistically access the uncertainty in the geological model. Following this logic the Gippsland Basin ESSCI reservoir model is populated with three categorical facies variables that can be identified with a relatively high degree of confidence from seismic, wireline and core data. These are:

- Alluvial and coastal plain
- Nearshore
- Lower shoreface – shelf.

The rationale for choosing the three facies above is provided in Chapter 2. The major considerations were uniqueness in terms of reservoir properties, confidence in identification, and reducing complexity in the geological model.

MADOGRAMS

Where the spatial continuity of a categorical variable such as lithofacies is to be determined rather than a continuous variable, points where the lithofacies of interest exists are assigned '1' and points where the lithofacies does not exist are assigned '0'. Consequently, the following expression must return either one or zero:

$$\left|Z(X_i) - Z(X_{i+\vec{h}})\right| = 1 or\ 0$$

There are only two possible results for a particular length and direction of **h**—the value of the categorical variable is the same at Xi and $Xi\text{-}\vec{h}$ (and '0' is returned) or the value of the categorical variable is different at Xi and $Xi\text{-}\vec{h}$ (and '1' is returned). Consequently, γ need not represent one half the squared difference of the sum of $Z(Xi) - Z(Xi\text{-}\vec{h})$ and a variant of the semi-variogram equation called a 'madogram' may be used instead:

$$\gamma(\vec{h}) = \frac{\sum_{i=n\ldots1}^{n} \left|Z(X_i) - Z(X_{i+\vec{h}})\right|}{n}$$

When using the madogram equation to determine the spatial anisotropy of a particular facies, γ is equal to a value between 0 and 1. When γ is equal to 1 all data pairs separated by **h** have different values, and when γ is equal to 0 all data pairs separated by **h** have the same value. Therefore, the value of γ may be viewed as a representation of the probability that points separated by **h** will have the same categorical variable (facies).

MODELING MADOGRAMS AND SEMI-VARIOGRAMS

An experimental semi-variogram or madogram is applicable to specific lengths and directions of **h**, but techniques for stochastic population such as conditional simulation and kriging require γ for all possible lengths and directions of **h** (i.e. all possible pairs of $Z(Xi)$ & $Z(Xi-\vec{h})$ in the population). Consequently, a mathematical function must be fitted to the semi-variogram. Positive functions that asymptotically approach a fixed value are commonly used (e.g. gaussian, spherical, and exponential functions). In practice however, any definite, positive function of **h** is acceptable provided the function 'fits' the experimental data. In some cases a function representing the sum of two or more simple models called a 'nested model' is required to appropriately fit the experimental data; for example: $\gamma(\mathbf{h}) = \gamma_1(\mathbf{h}) + \gamma_2(\mathbf{h})$.

In some cases experimental semi-variograms will show oscillations or systematic variations in γ values with changing **h** in a given direction. Oscillations in semi-variograms are sometimes termed the 'hole effect' (Hohn 1999). In general, this effect results from a consistent spacing in a particular direction of some feature that influences the value of the regionalised variable in the study area. Nested equations incorporating sine or cosine expressions are typically used to represent the hole effect. Two examples of analogue madograms and fitted models used in this study are provided below in Figures 4.4 and 4.5.

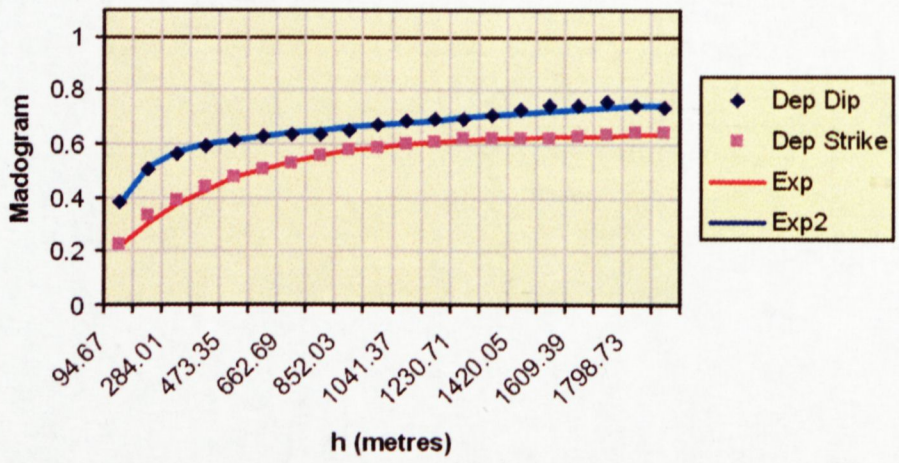

Figure 4.4—Madograms along depositional strike and dip generated from a barrier island setting, Gelliondale area, SE Victoria. Two exponential functions were used to fit the data.

In Figure 4.4 a standard exponential equation is used for the madogram parallel with depositional strike:

$$\gamma(h) = \left(1 - e^{-h/400}\right) + 0.1$$

A nested equation is used for the madogram parallel with depositional dip:

$$\gamma(h) = 0.55\left(1 - e^{-h/90}\right) + 0.325\left(1 - e^{-h/2000}\right)$$

Figure 4.5 is another example of two madograms parallel with depositional dip and depositional strike from a barrier island setting. The scale of analysis is significantly greater than that of the madograms in Figure 4.4.

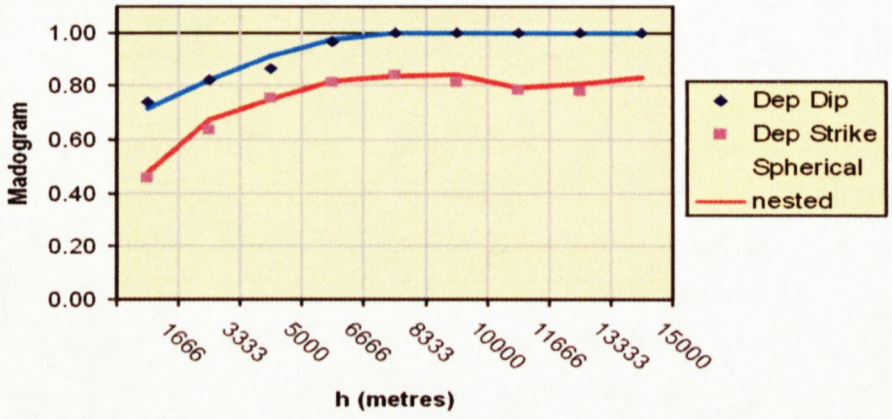

Figure 4.5— Madograms along depositional strike and dip generated from a barrier island setting, Galveston Island area, Texas coast. Spherical and nested functions were used to fit the data.

In Figure 4.5 a nested equation incorporating a hole effect (sine expression) models the madogram along depositional strike:

$$\gamma(h) = 0.82\left(1 - e^{-h/1900}\right) + \frac{\sin 3h}{15}\left(1 - e^{-h/25000}\right)$$

A gaussian equation models the madogram along depositional dip:

$$\gamma(h) = 0.4\left(\frac{3h}{2(8500)} - \frac{h^3}{2(8500^3)}\right) + 0.6 \qquad for\ h \le 8500$$

$$\gamma(h) = 1 \qquad for\ h > 8500$$

Methodology

Modern analogues and outcrop analogues from depositional environments that were deemed similar to the depositional environments represented in the Gippsland Basin ESSCI area were used in this study to generate statistical models of spatial variability. Selection of suitable modern analogues was governed primarily by:

- The interpreted depositional environment
- The quality and quantity of published data on the area
- Palaeo-climatic condition
- Tectonic setting during deposition of the strata to which the analogue is applied
- The scale of the reservoir model to which the analogue is applied.

Analogues for the upper Latrobe Group were sought that represent primarily wave-dominated nearshore depositional environments and fluvio-deltaic systems. Ideally, depositional systems in rift/post-rift settings and passive margins characterised by temperate climatic conditions were considered preferable. The scale of analogue studies that were used focused primarily on scales of ~10 km, because the reservoir model for CO_2 storage is very large by necessity.

The selection of analogues used in this study was also governed by the availability of detailed facies maps (Fig. 4.6). Consequently, the Gulf Coast region in the United States is probably over-represented. The most appropriate analogues for the Gippsland Basin are probably the Southeast Victorian Coast in Australia and the Atlantic Coast analogues in the United States.

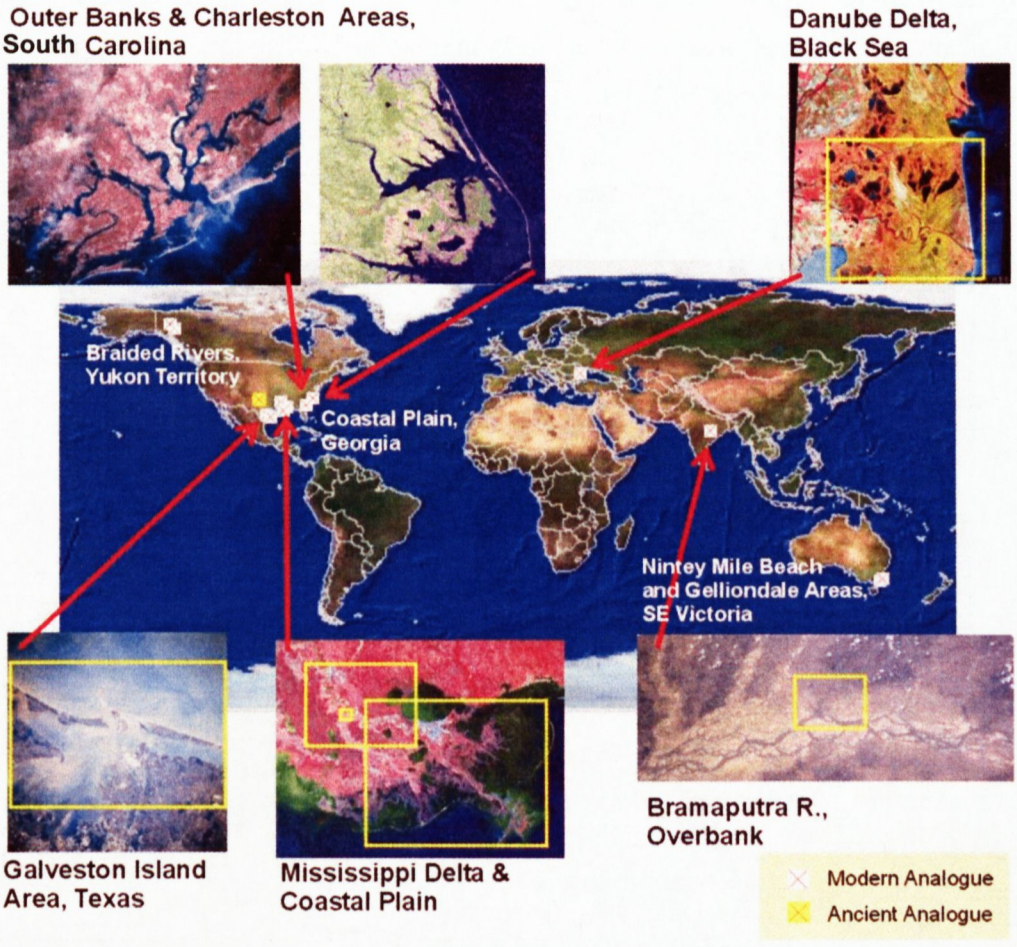

Figure 4.6—Locations of analogues used in this study.

Madograms were constructed from published facies maps of modern and ancient depositional environments. Each facies was assigned a number and a 2D grid was constructed that represents the horizontal distribution of facies. A series of simple nested conditional statements was then used to calculate the experimental madogram for each facies represented in the grid. The conditional statements used for facies 'G' are provided below.

1) IF $Z(X_l)$ OR $Z(X_l+h_1) \neq$ G, RETURN [null value]

2) IF $|Z(X_l)-Z(X_l+h_1)| = 0$, RETURN 0

3) IF $|Z(X_l)-Z(X_l+h_1)| = 1$, RETURN 1

4) average values IF $\neq$ [null value]

5) repeat steps 1-4 for h_2, h_3, h_4, etc…

Sixty-two experimental madograms and experimental semi-variograms were calculated from 15 published facies maps (Table 4.1). The depositional environments

represented by the madograms include barrier island settings, wave-dominated and fluvially-dominated deltaic settings, and braided and meandering fluvial settings. The madograms and semi-variograms were manually fitted with mathematical functions.

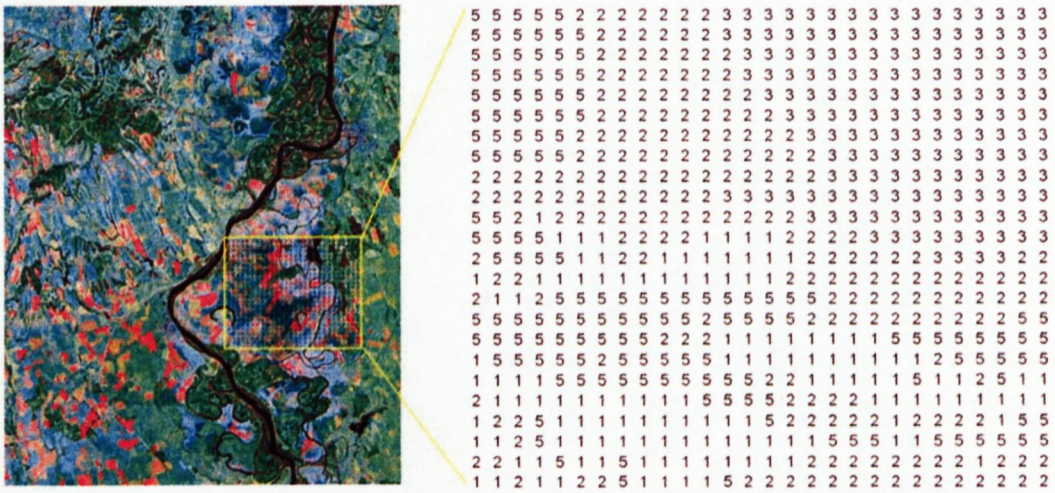

Figure 4.7—Example facies map for trained madogram generation. Madograms were produced from facies maps of various depositional environments in modern and ancient settings. Each facies is assigned a number and location on a grid. The madogram is then calculated from the grid.

Table 4.1: Geostatistical analogue locations and references.

#	Area	Country	Region	Depositional Environment	Analogue Type	Reference
1	Brahmaputra River	India		Braided River + Overbank	modern	Coleman (1969)
2	Slims River	Canada	Yukon Territory	Braided River	modern	Miall (1996)
3	Donjek River	Canada	Yukon Territory	Braided River	modern	Miall (1996)
4	Gelliondale Area	Australia	SE Victoria	Barrier Island	modern	Jenkins (1968)
5	Miss. Point Bar	United States	Mississippi	Meandering Fluvial	modern	Saucier (1967)
6	Mississippi Overbank	United States	Mississippi	Meandering Fluvial, Overbank	modern	Farrell (1987)
7	Snake and Sunday Is.	Australia	SE Victoria	Barrier Island/ Chennier Plain	modern	Jenkins (1968)
8	Little Creek Meander	United States	Mississippi	Meandering Fluvial	modern	Werren (1989)
9	Gulf Coast Chennier	United States	Louisiana	Chennier Plain	modern	Gould & McFarlan(1959)
10	Galveston Island	United States	Texas	Barrier Island	modern	McCubbin (1982)
11	Danube Delta	Romania	Black Sea	Wave Dominated Delta	modern	Wright & Colemen(1976)
12	Booch Sandstone	United States	Oklahoma	Fluvially Dominated Delta	ancient	Busch (1971)
13	Continental Shelf	United States	Texas	Shelf	modern	Shideler (1978)
14	Mississippi Delta	United States	Mississippi	Fluvially Dominated Delta	modern	Fisher (1969)
15	Coastal Plain	United States	Georgia	Coastal Plain	modern	Markewich *et al.* (1992)

Figure 4.8 shows the 15 analogues used in this study plotted by scale of analysis (maximum **h** length) and depositional environment. Scales of maximum **h** between 10^4m and 10^5m are of the greatest utility for this study because of the large area represented by the reservoir model. However, descriptions of small-scale spatial continuity in various depositional environments are important as well.

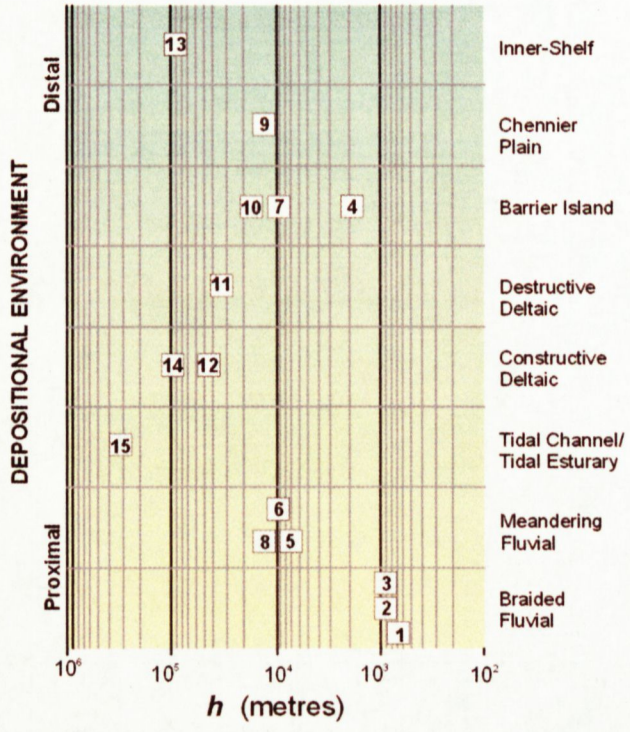

Figure 4.8—Depositional environment and scale of investigation for analogues used in this study.

Results

There are several characteristics of analogue madograms and semi-variograms that are specific to certain kinds of depositional environments. In particular fluvial, wave-dominated nearshore and deltaic depositional environments are identified as having specific madogram and semi-variogram characteristics. The analogues used and characteristics of their madogram and semi-variogram are provided in Table 4.2.

Table 4.2: Analogue madograms and semi-variogram characteristics for different depositional environments.

#	Area	Facies	Variable	Direction	Function Type	Lag (m)	Max. Lag (m)	n	Range (m)	Sill (γ)	Nugget (γ)	Model Function
1	Brahmaputra River	Braided Channel	Facies	Dip	m*	55.6	722.3	2113	520	0.41	0.08	$\gamma(\bar{h}) = 0.75\left(1 - e^{\left(-3\bar{h}/280\right)^2}\right) + 0.25$
1	Brahmaputra River	Braided Channel	Facies	Strike	m	55.6	722.3	2029	400	1.0	0.2	$\gamma(\bar{h}) = 0.43\left(1 - e^{-3\bar{h}/450}\right)$
1	Brahmaputra River	Crevasse Splay	Facies	Dip	m	55.6	722.3	2141	410	0.77	0.24	$\gamma(\bar{h}) = 0.7\left(1 - e^{-3\bar{h}/450}\right) + 0.075$
1	Brahmaputra River	Crevasse Splay	Facies	Strike	m	55.6	722.3	2153	480	0.98	0.32	$\gamma(\bar{h}) = 0.82\left(1 - e^{-3\bar{h}/285}\right) + 0.15$
1	Brahmaputra River	Levee	Facies	Dip	m	55.6	722.3	1253	~750	1.0	0.20	$\gamma(\bar{h}) = 0.45\left(1 - e^{\left(-3\bar{h}/285\right)^2}\right) + 0.25$
1	Brahmaputra River	Levee	Facies	Strike	m	55.6	722.3	1707	420	0.7	0.23	$\gamma(\bar{h}) = \left(1 - e^{-3h/520}\right) + 0.02$
2	Slims River	In-Channel Sand Bars	Facies	Dip	m	133.3	933.3	649	>1000	>0.7	0.61	n/a
2	Slims River	In-Channel Sand Bars	Facies	Strike	m	133.3	933.3	757	>1000	>0.7	0.60	n/a
3	Donjek River	In-Channel Sand Bars	Facies	Dip	m	133.3	1067	334				$\gamma(\bar{h}) = 0.9\left(1 - e^{-\bar{h}/175}\right) + \frac{\cos 5\bar{h}}{15} + 0.08$

* 'M' represents a madogram function and 's-v' represents a semi-variogram function.

#	Area	Facies	Variable	Direction	Function Type	Lag (m)	Max. Lag (m)	n	Range (m)	Sill (γ)	Nugget (γ)	Model Function
3	Donjek River	In-Channel Sand Bars	Facies	Strike	m	133.3	1067	510				$\gamma(\bar{h}) = 0.9\left(1-e^{-\bar{h}/115}\right)+\frac{\cos 1.56\bar{h}}{10}$
3	Donjek River	In-Channel Sand Bars+Active Channels	Facies	Dip	m	133.3	1067	454				$\gamma(\bar{h}) = 0.75\left(1-e^{-\bar{h}/155}\right)+0.05$
3	Donjek River	In-Channel Sand Bars+Active Channels	Facies	Strike	m	133.3	1067	818				$\gamma(\bar{h}) = 0.93\left(1-e^{-\bar{h}/175}\right)$
4	Gelliondale Area	Mangrove Swamps	Facies	Dip	m	94.7	1893	43371	500 & >2000	~0.7	0.3	$\gamma(\bar{h}) = 0.6\left(1-e^{-\bar{h}/115}\right)+0.2\left(1-e^{-\bar{h}/2000}\right)$
4	Gelliondale Area	Mangrove Swamps	Facies	Strike	m	94.7	1893	44307	~1000 & >2000	~0.65	0.15	$\gamma(\bar{h}) = 0.41\left(1-e^{-\bar{h}/182}\right)+0.52\left(1-e^{-\bar{h}/1750}\right)$
4	Gelliondale Area	Sand Ridges	Facies	Dip	m	94.7	1893	51146	500 & >2000	~0.7	0.3	$\gamma(\bar{h}) = 0.55\left(1-e^{-\bar{h}/90}\right)+0.325\left(1-e^{-\bar{h}/2000}\right)$
4	Gelliondale Area	Sand Ridges	Facies	Strike	m	94.7	1893	52144	1050 & >2000	0.65	0.18	$\gamma(\bar{h}) = \left(1-e^{-\bar{h}/400}\right)+0.1$
4	Gelliondale Area	Swamps	Facies	Dip	m	94.7	1893	19109	>2000		0.2	$\gamma(\bar{h}) = 0.85\left(1-e^{-\bar{h}/1200}\right)+\left(\cos\frac{\bar{h}}{140}\left(1-e^{-\bar{h}/35000}\right)\right)+0.175$
4	Gelliondale Area	Swamps	Facies	Strike	m	94.7	1893	21768	>2000		0.12	$\gamma(\bar{h}) = 0.8\left(1-e^{-\bar{h}/1200}\right)+0.1$

#	Area	Facies	Variable	Direction	Function Type	Lag (m)	Max. Lag (m)	n	Range (m)	Sill (γ)	Nugget (γ)	Model Function
5	Miss. Point Bar	Point Bar	Facies	Dip	m	566	6792	5961				$\gamma(\vec{h}) = 1 - e^{-3\vec{h}/5000}$
5	Miss. Point Bar	Point Bar	Facies	Strike	m	566	6792	5788				$\gamma(\vec{h}) = 1 - e^{-3\vec{h}/6850}$
5	Miss. Point Bar	Swamps	Facies	Dip	m	566	6792	2295				
5	Miss. Point Bar	Swamps	Facies	Strike	m	566	6792	2160				
6	Mississippi Overbank	Crevasse Splay	Facies	Dip	m	658	9867	1082	7500	1.0	0.10	$\gamma(\vec{h}) = 0.95\left(\frac{3\vec{h}}{2(7500)} - \frac{0.5\vec{h}^3}{7500^3}\right) + 0.05,\ for\ \vec{h} \le 7500$
												$\gamma(\vec{h}) = 0.95,\ for\ \vec{h} > 7500$
6	Mississippi Overbank	Crevasse Splay	Facies	Strike	m	658	9867	1834	6200	1.0	0.27	$\gamma(\vec{h}) = 0.8\left(\frac{3\vec{h}}{2(6500)} - \frac{0.5\vec{h}^3}{6500^3}\right) + 0.2,\ for\ \vec{h} \le 6500$
												$\gamma(\vec{h}) = 1,\ for\ \vec{h} > 6500$
6	Mississippi Overbank	Levee	Facies	Dip	m	658	9867	4000	4800	0.87	0.30	$\gamma(\vec{h}) = 0.8\left(1 - e^{-\vec{h}/1450}\right) + 0.1$
6	Mississippi Overbank	Levee	Facies	Strike	m	658	9867	3757	4100	0.82	0.57	$\gamma(\vec{h}) = 0.4\left(1 - e^{-3\vec{h}/3000}\right) + 0.425$
6	Mississippi Overbank	Point Bar	Facies	Dip	m	658	9867	4283	~2700 & >10000	>0.90	0.17	$\gamma(\vec{h}) = 0.2\left(1 - e^{-\vec{h}/1000}\right) + \left(1 - e^{-\vec{h}/11500}\right) + 0.055$
6	Mississippi Overbank	Point Bar	Facies	Strike	m	658	9867	4306	~4000 & >10000	>0.90	0.13	$\gamma(\vec{h}) = 0.88\left(1 - e^{-3\vec{h}/6500}\right) + 0.2\cos\frac{1.5\vec{h}}{2250}\left(1 - e^{-\vec{h}/15000}\right)$
7	Snake and Sunday Islands	Barrier Island Sand	Facies	Dip	m	402.3	9253	58650	4500	0.45	0.15	$\gamma(\vec{h}) = 0.4\left(1 - e^{-\vec{h}/150}\right) + 0.175\left(1 - e^{-\vec{h}/9500}\right) + 0.02$

#	Area	Facies	Variable	Direction	Function Type	Lag (m)	Max. Lag (m)	n	Range (m)	Sill (γ)	Nugget (γ)	Model Function
7	Snake and Sunday Islands	Barrier Island Sand	Facies	Strike	m	402.3	9253	67163	~3500 & >9300	~0.50	0.01	$\gamma(\bar{h}) = 0.35\left(1-e^{-\bar{h}/1350}\right)+0.17\left(1-e^{-\bar{h}/10000}\right)+0.02$
8	Little Creek Meander*	n/a	Sand Percent	Dip	s-v	753	10542	3E+05	2700	32	10	see below...
												$\gamma(\bar{h}) = 35\left(1-e^{-3\bar{h}/2000}\right)+5\left(1-e^{-3\bar{h}/15000}\right)+2\sin 1.5\bar{h}-7$
8	Little Creek Meander*	n/a	Sand Percent	Strike	s-v	753	10542	2E+05	5200	46	26	$\gamma(\bar{h}) = 19\left(1-e^{-\bar{h}^3/2500^2}\right)+27$
9	Gulf Coast Chennier	Chennier	Facies	Dip	m	1000	12000	2881	6000	0.44	0.20	$\gamma(\bar{h}) = 0.3\left(1-e^{-\bar{h}/2500}\right)+0.175$
9	Gulf Coast Chennier	Chennier	Facies	Strike	m	1000	12000	3532	>12000	?~0.3	0.22	$\gamma(\bar{h}) = 0.1\left(1-e^{-\bar{h}/1800}\right)+\sin\frac{0.5\bar{h}}{350}\left(1-e^{\bar{h}/150000}\right)+0.2$
10	Galveston Island	Back Barrier Lagoon	Facies	Dip	m	1666	15000	593	11500	1.0	0.45	$\gamma(\bar{h}) = 1-e^{-\bar{h}/2250}$
10	Galveston Island	Back Barrier Lagoon	Facies	Strike	m	1666	15000	474	7000	0.68	0.25	$\gamma(\bar{h}) = 0.35\left(1-e^{-\bar{h}^2/4500^2}\right)+0.325$
10	Galveston Island	Barrier Island Sand	Facies	Dip	m	1666	15000	1223	9500	1.0	0.22	$\gamma(\bar{h}) = 0.75\left(1-e^{-\bar{h}^2/4000^2}\right)+0.25$
10	Galveston Island	Barrier Island Sand	Facies	Strike	m	1666	15000	613	~7000	0.32	0.10	$\gamma(\bar{h}) = 0.33\left(1-e^{-\bar{h}/2500}\right)$
10	Galveston Island	Swamps	Facies	Dip	m	1666	15000	946	9000	1.0	0.65	$\gamma(\bar{h}) = 0.4\left(\frac{3\bar{h}}{2(8500)}-\frac{\bar{h}^3}{2(8500^3)}\right)+0.6,\ for\ \bar{h}\le 8500$

#	Area	Facies	Variable	Direction	Function Type	Lag (m)	Max. Lag (m)	n	Range (m)	Sill (γ)	Nugget (γ)	Model Function
												$\gamma(\vec{h}) = 1,\ for\ \vec{h} > 8500$
10	Galveston Island	Swamps	Facies	Strike	m	1666	15000	1353	~10000	0.80	0.35	$\gamma(\vec{h}) = 0.82\left(1 - e^{-\vec{h}/1900}\right) + \frac{\sin 3\vec{h}}{15}\left(1 - e^{-\vec{h}/25000}\right)$
11	Danube Delta	Fluvial Sst.	Facies	Dip	m	1505	22575	859	7500 & >23000	0.86	0.55	$\gamma(\vec{h}) = 0.5\left(1 - e^{-3\vec{h}/6000}\right) + 0.05\left(1 - e^{-3\vec{h}/85000}\right) + 0.35$
11	Danube Delta	Fluvial Sst.	Facies	Strike	m	1505	22575	1642	7500 & 23000	0.98	0.62	$\gamma(\vec{h}) = 0.6\left(1 - e^{-3\vec{h}/3500}\right) + 0.1\left(1 - e^{-3\vec{h}/25000}\right) + 0.3$
11	Danube Delta	Marsh/Swamp	Facies	Dip	m	1505	22575	2409				
11	Danube Delta	Marsh/Swamp	Facies	Strike	m	1505	22575	4486				
11	Danube Delta	Sand Ridges	Facies	Dip	m	1505	22575	1489	>14000	0.82	0.53	$\gamma(\vec{h}) = 0.55\left(\left(1 - e^{-\vec{h}/3000}\right) + \frac{\cos 1.5\vec{h}}{15}\right) + 0.325$
11	Danube Delta	Sand Ridges	Facies	Strike	m	1505	22575	3119	11000	0.85	0.50	$\gamma(\vec{h}) = 0.4\left(\left(1 - e^{-\vec{h}/5500}\right) + \frac{\cos 1.5\vec{h}}{15}\right) + 0.5$
11	Danube Delta	Shoreface/Lwr Deltaic Plain	Facies	Dip	m	1505	22575	1828	>14000	>0.90	0.12	$\gamma(\vec{h}) = 0.9\left(1 - e^{-\vec{h}/17500} + \frac{\sin 2\vec{h}}{17}\right)$
11	Danube Delta	Shoreface/Lwr Deltaic Plain	Facies	Strike	m	1505	22575	3067	>23000	>0.60	0.05	$\gamma(\vec{h}) = 0.9\left(\frac{3\vec{h}}{2(18000)} - \frac{\vec{h}^3}{2(18000)^3}\right),\ for\ \vec{h} \le 18000$
												$\gamma(\vec{h}) = 0.9,\ for\ \vec{h} > 18000$
12	Booch Sandstone	distributary channel	Sst. Thick.	Dip	s-v	2119	31782	12359	11000 & >32000	>5000	1000	$\gamma(\vec{h}) = 3700\left(1 - e^{-3\vec{h}/15000}\right) + 1500\left(1 - e^{-3\vec{h}/150000}\right)$

#	Area	Facies	Variable	Direction	Function Type	Lag (m)	Max. Lag (m)	n	Range (m)	Sill (γ)	Nugget (γ)	Model Function
12	Booch Sandstone	distributary channel	Sst. Thick.	Strike	s-v	2119	31782	13380	13500	~3800	1500	see below...
												$\gamma(\vec{h}) = 1000\left(1-e^{-3\vec{h}/5500}\right)+1800\left(1-e^{-3\vec{h}/55000}\right)+150\left(\frac{\sin 1.5\vec{h}}{17}\right)+150$
13	Continental Shelf		Grain Size	Dip	s-v	7143	78573	1943	>79000	>1.4	1.2	see below...
												$\gamma(\vec{h}) = 0.6\left(1-e^{-3\vec{h}/40000}\right)+0.25\left(1-e^{-3\vec{h}/600000}\right)-0.05$
13	Continental Shelf		Grain Size	Strike	s-v	7143	78573	2802	>79000	>0.7	1.0	$\gamma(\vec{h}) = \frac{0.8\vec{h}}{110000}-0.1$
14	Mississippi Delta	Bays, Lagoons, Interdistrib. Lakes	Facies	Dip	m	6900	96600	2352	50000	0.95	0.57	$\gamma(\vec{h}) = 0.6\left(1-e^{-3\vec{h}/28000}\right)+0.35$
14	Mississippi Delta	Bays, Lagoons, Interdistrib. Lakes	Facies	Strike	m	6900	96600	2452	55000	0.95	0.50	$\gamma(\vec{h}) = 0.65\left(1-e^{-3\vec{h}/32000}\right)+0.3$
14	Mississippi Delta	Fluvial Channel Belt	Facies	Dip	m	6900	96600	2801	27000 & > 100000 (?)	1.0(?)	0.62	$\gamma(\vec{h}) = 0.46\left(1-e^{-3\vec{h}/15000}\right)+.25\left(1-e^{-3\vec{h}/150000}\right)+0.3$
14	Mississippi Delta	Fluvial Channel Belt	Facies	Strike	m	6900	96600	3251	27000	0.85	0.63	$\gamma(\vec{h}) = 0.4\left(1-e^{-3\vec{h}/15000}\right)+0.05\left(1-e^{-3\vec{h}/150000}\right)+\frac{\cos 2\vec{h}}{35}+0.4$
14	Mississippi Delta	Prodelta and Shelf	Facies	Dip	m	6900	96600	1573	67000	1.0	0.28	$\gamma(\vec{h}) = 0.88\left(1-e^{-3\vec{h}/57500}\right)$

#	Area	Facies	Variable	Direction	Function Type	Lag (m)	Max. Lag (m)	n	Range (m)	Sill (γ)	Nugget (γ)	Model Function
14	Mississippi Delta	Prodelta and Shelf	Facies	Strike	m	6900	96600	1705	97000	0.88	0.18	$\gamma(\vec{h}) = \left(\frac{3\vec{h}}{2(20000)}\right) - \left(\frac{\vec{h}^3}{20000^3}\right)$ for $\vec{h} \le 20000$
												$\gamma(\vec{h}) = 1$ for $\vec{h} > 20000$
14	Mississippi Delta	Swamps and Marshes	Facies	Dip	m	6900	96600	5467	24000	0.75	0.52	
14	Mississippi Delta	Swamps and Marshes	Facies	Strike	m	6900	96600	6258	28000	0.72	0.50	
15	Coastal Plain	Tidal Channels	Facies	Dip	m	13407	2E+06	4104				
15	Coastal Plain	Tidal Channels	Facies	Strike	m	13407	2E+06	5049				

Fluvial Environments

At scales of 10^3 – 10^4 m, fluvial channel facies typically have low variance along depositional dip, parallel with the general orientation of channel bodies, and higher variance with a well-defined sill along depositional strike. Similarly, the range along depositional dip is generally longer than the range along depositional strike. A hole effect may be evident along depositional strike if there is a consistent spacing of channels or channel belts. The ratio between the value of the sill for madograms parallel with depositional dip to the value of the sill parallel with depositional strike (C_{strike}/C_{dip}) is a function of the degree of channel sinuosity. Very sinuous channel patterns result in a lower C_{strike}/C_{dip} ratio, and may also induce a hole effect along depositional dip.

At relatively coarse scales of analysis (10s km), overbank facies such as crevasse splays and levee deposits tend to show a similar pattern to fluvial channel deposits with the direction of minimum variance parallel with depositional dip, but the sill values and the overall variance tends to be higher than in-channel fluvial facies. Unlike in-channel facies, the range of overbank facies along depositional strike is commonly longer than the range along depositional dip. Additionally, the ratio of sill values along depositional dip and strike (C_{strike}/C_{dip}) are consistently lower than in channellised facies.

At more detailed scales of analysis (10^1 – 10^2 m), the geometry, orientation and spacing of depositional elements within fluvial channels control the character of the semi-variogram. In general however, the direction of maximum variance remains parallel with depositional strike—probably because the pattern of elongation of most in-channel bars is parallel to depositional dip. However, generalisations regarding the semi-variogram character for different fluvial styles (e.g. braided, anastomosing, meandering) at detailed scales are difficult to make based on the data collected in this study.

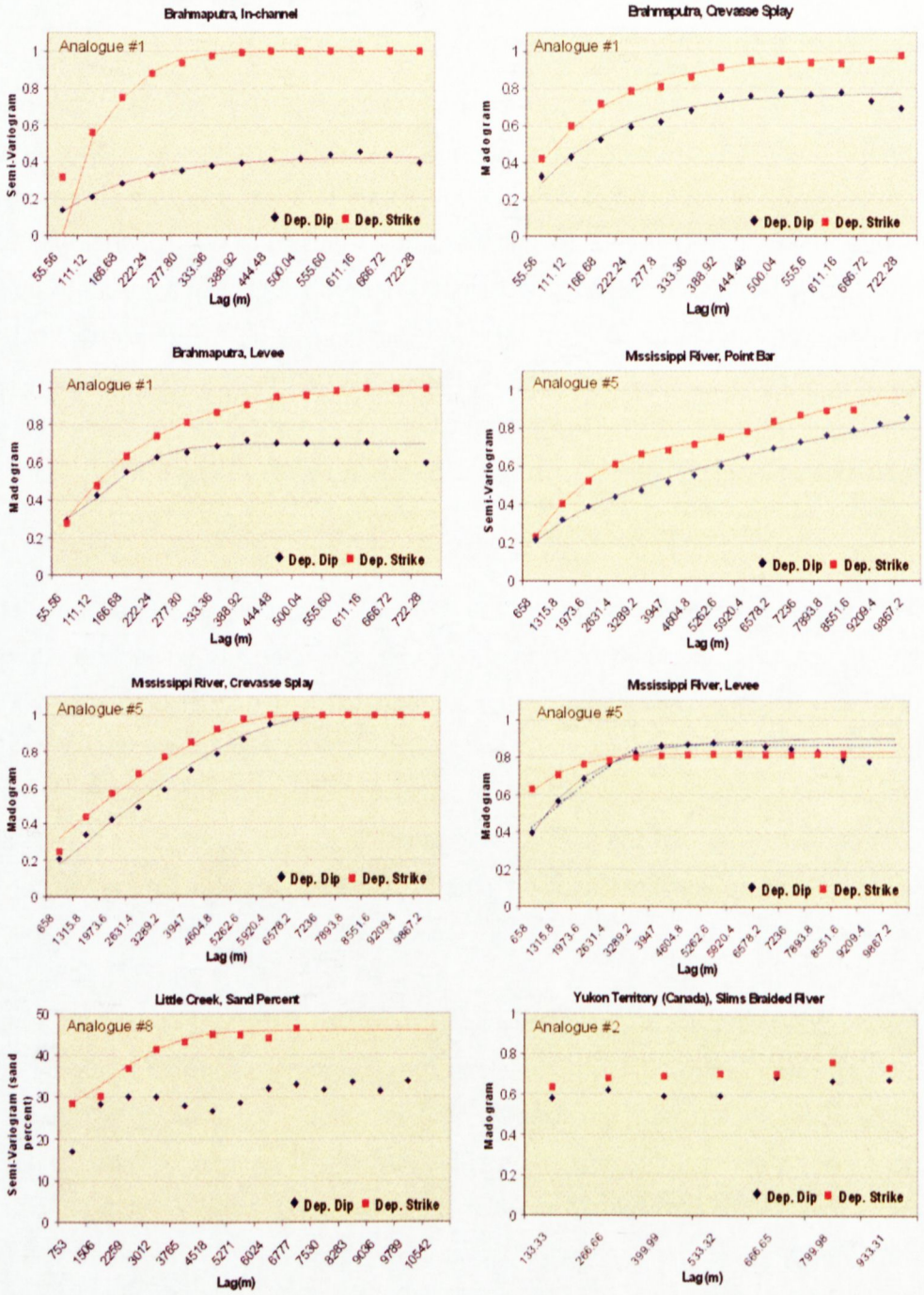

Figure 4.9—Analogue madograms and semi-variograms for fluvial environments of deposition.

NEARSHORE ENVIRONMENTS

In nearshore non-fluvial wave-dominated environments, the direction of minimum variance is along depositional dip and the direction of maximum variance is along depositional strike. Consequently, nearshore, wave-dominated depositional environments tend to be characterised by C_{strike}/C_{dip} ratios of less than one, whereas fluvial depositional environments tend to be characterised by C_{strike}/C_{dip} ratios of greater than one. This relationship generally holds between scales of 10^2m – 10^5m, but the C_{strike}/C_{dip} ratio and the horizontal anisotropy ratio increase with more detailed scales of investigation. The range along depositional strike in nearshore, wave-dominated settings is generally considerably longer than the range along depositional dip. At more detailed scales, the horizontal anisotropy ratio $(a_{min.,horizontal}/a_{max.,horizontal})^*$ tends to decrease and nested equations are generally required to model madograms and semi-variograms accurately, particularly along depositional strike.

The value C_{strike}/C_{dip} ratio in nearshore wave-dominated settings varies significantly as a function of the specific kind of depositional environment represented. For example, barrier islands tend to be characterised by a low C_{strike}/C_{dip} ratio and chennier plains are characterised by higher C_{strike}/C_{dip} ratios. A hole effect is common along depositional dip. The 'horizontal' anisotropy ratio $(a_{min.,horizontal}/a_{max.,horizontal})$ shows significant variation between nearshore, wave-dominated facies and fluvial facies as well. Generally horizontal anisotropy ratios are greater in nearshore, wave-dominated settings. At coarse scales of analysis particularly, a well-defined sill is rare along depositional strike in wave-dominated nearshore settings, suggesting the range is larger than one half the extent of the study area along depositional dip or strike.

Semi-variograms of nearshore environments are commonly best modeled with nested equations because two ranges can be incorporated in the function. Generally a range of several hundred metres and a range of several thousand metres are required to appropriately model the analogue semi-variogram or madogram.

* The anisotropy ratio is generally the range in the direction of minimum variance divided by the range in the direction of maximum variance. In a geologic context this is usually a horizontal range divided by the vertical range. The phrase, 'horizontal anisotropy ratio' refers to the ratio of the minimum to maximum ranges in the horizontal plane only.

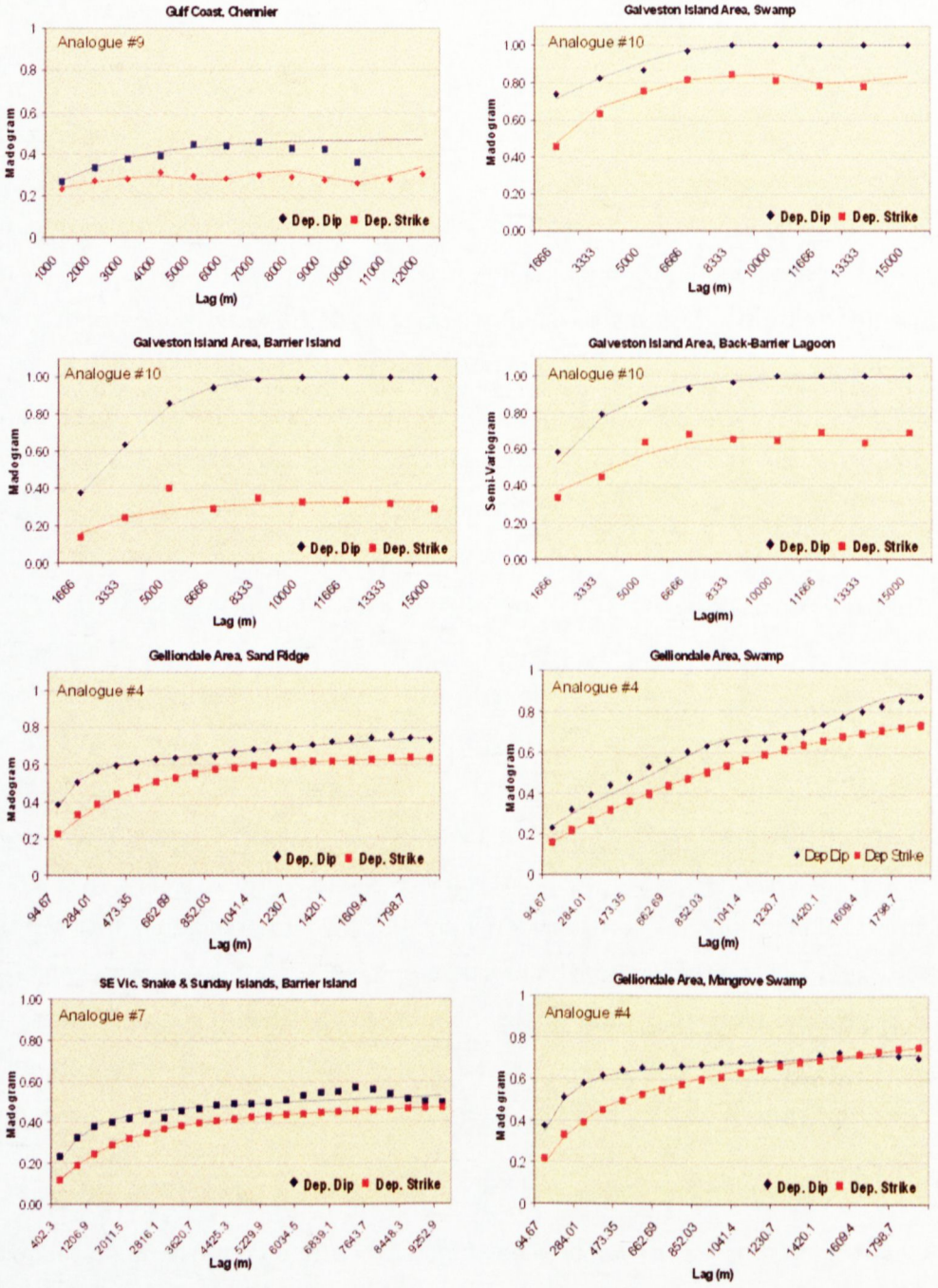

Figure 4.10—Analogue madograms and semi-variograms for nearshore wave-dominated environments of deposition.

DELTAIC ENVIRONMENTS

Deltaic environments are characterised by high variance in all horizontal directions and little variation in sill and range values along depositional dip and along depositional strike. Low spatial continuity was a common characteristic for all deltaic facies analysed. In general, there is little difference between sill values along depositional dip and depositional strike. However, wave-dominated destructive deltas may be more likely to have a direction of maximum variance along depositional dip and fluvially dominated, constructive deltas may be more likely to have a direction of maximum variance along depositional strike.

A general trend that appears to be independent of environment of deposition is that the value of the nugget, the sill and generally the range, increases as the scale of investigation increases. In a related way, the nugget, sill, and range will tend to increase as the number of facies represented in a depositional environment increases. However, this will not necessarily hold true in a depositional environment characterised by high spatial order—an environment characterised by two facies may still have a higher nugget, sill and range than an environment characterised by six facies.

The characteristics of alluvial, nearshore and deltaic depositional environments that are considered characteristic are graphically summarised in Figure 4.13.

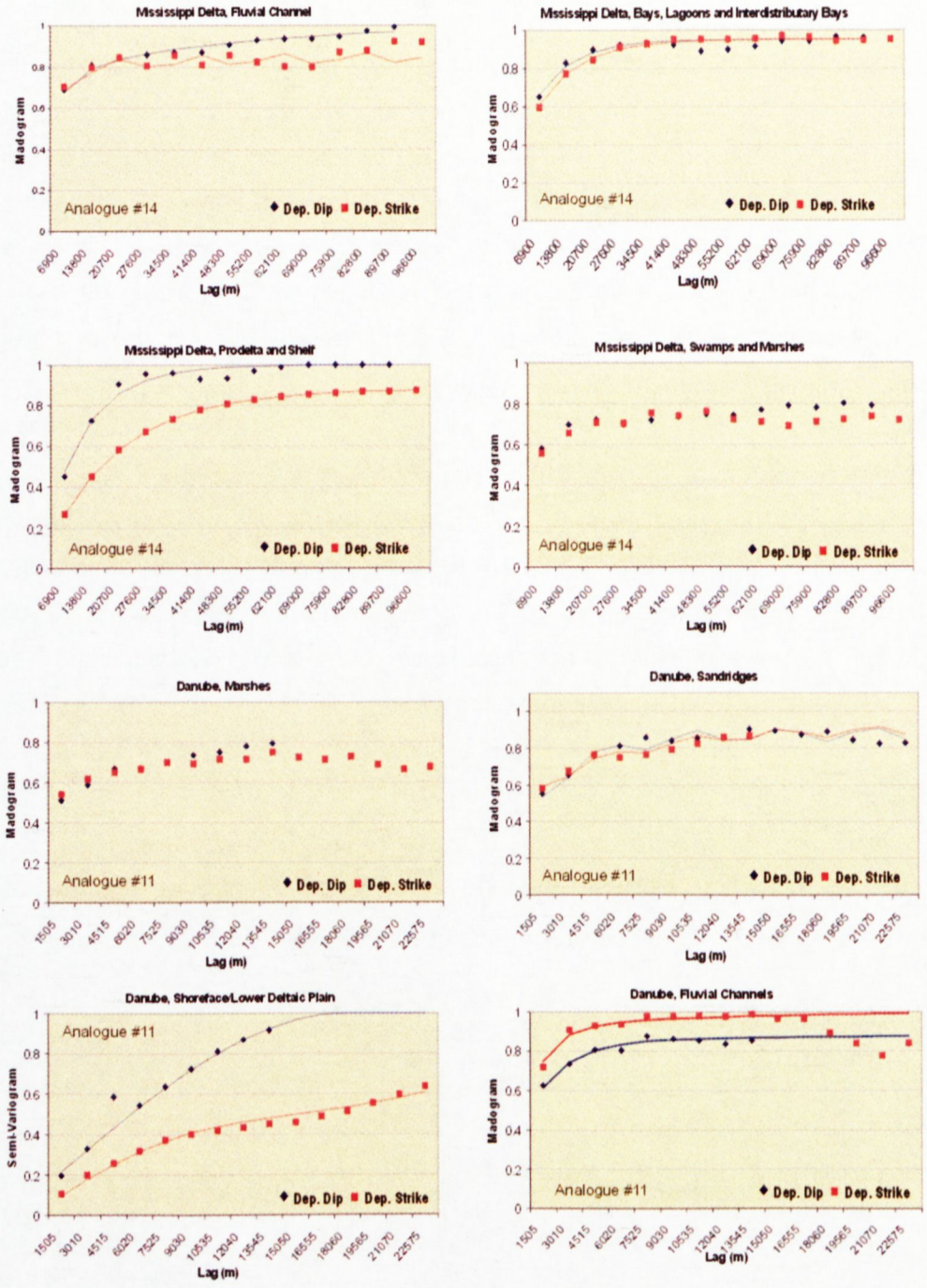

Figure 4.11—Analogue madograms and semi-variograms for deltaic environments of deposition.

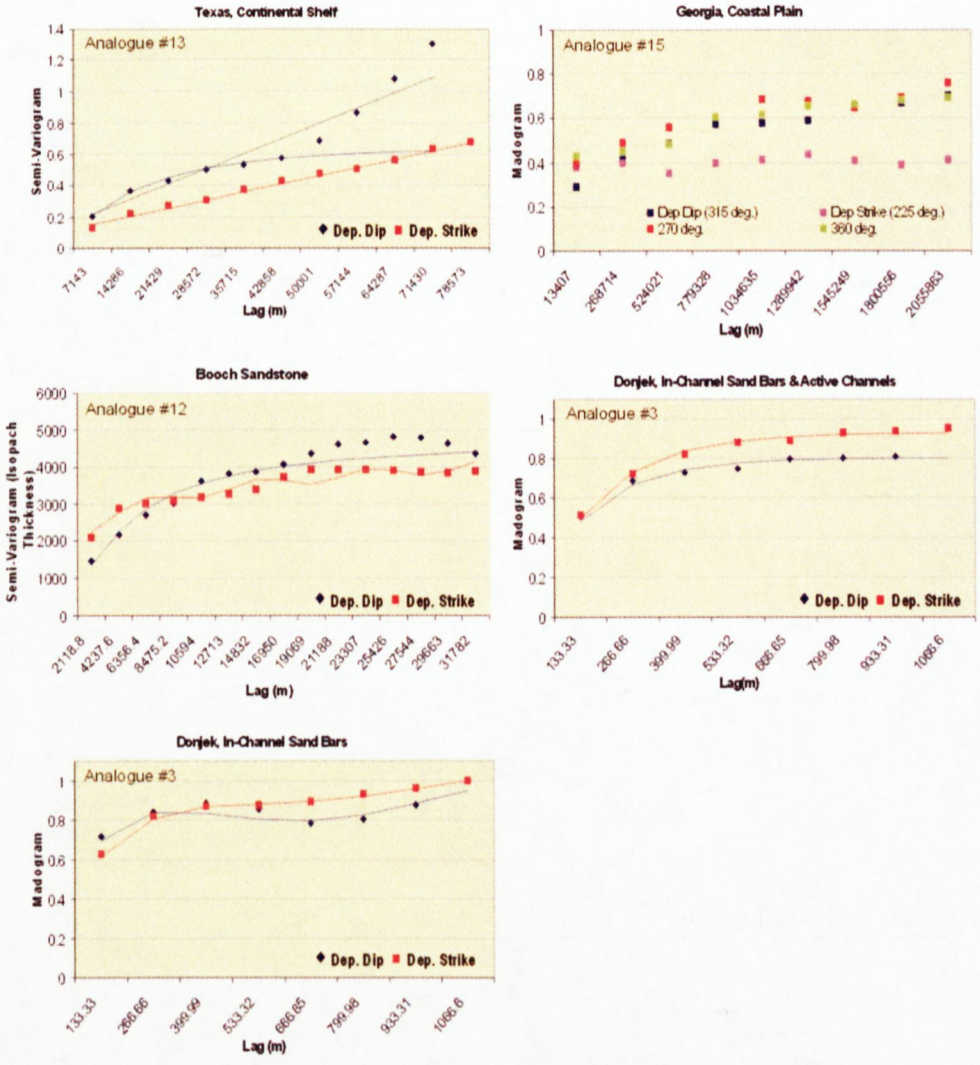

Figure 4.12—Analogue madograms and semi-variograms for various environments of deposition.

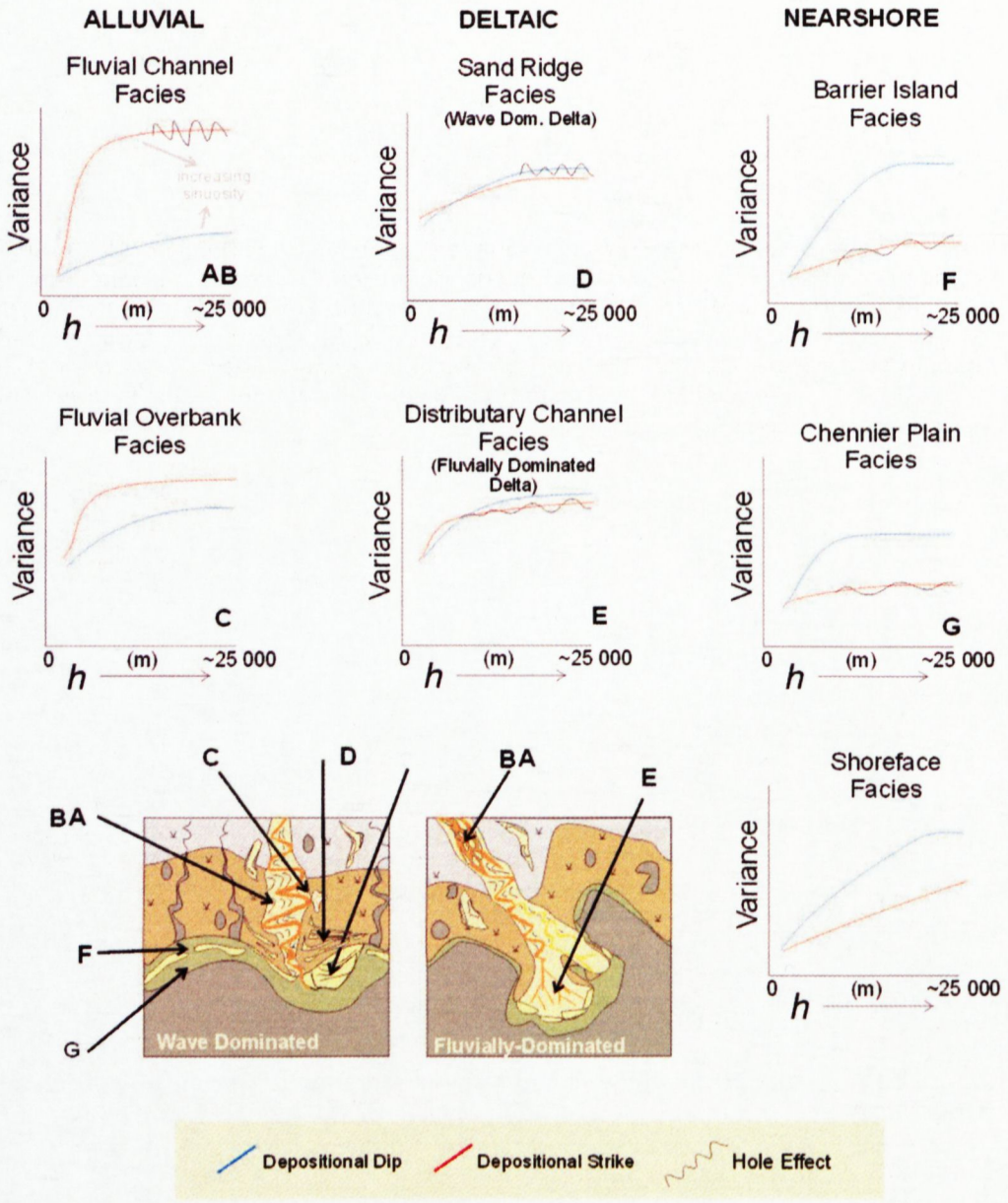

Figure 4.13—Generalised madograms and semi-variograms for particular kinds of depositional environments based on analogue data. Only one scale of analysis is shown here, 0 – 25,000 m with lag increments of ~2000 m. However, the data suggests that madogram characteristics also vary with the scale of analysis. Several semi-variogram and madogram characteristics appear to be diagnostic of specific depositional environments, discussed in greater detail in the text.

VERTICAL SEMI-VARIOGRAMS

As discussed previously, vertical experimental semi-variograms calculated from well data are usually sufficient to characterise the spatial continuity of reservoir properties in the vertical direction. Vertical experimental semi-variograms were calculated for coastal-alluvial plain facies, nearshore facies, and lower shoreface-shelf facies in the Gippsland Basin ESSCI area and are provided in Figure 4.14.

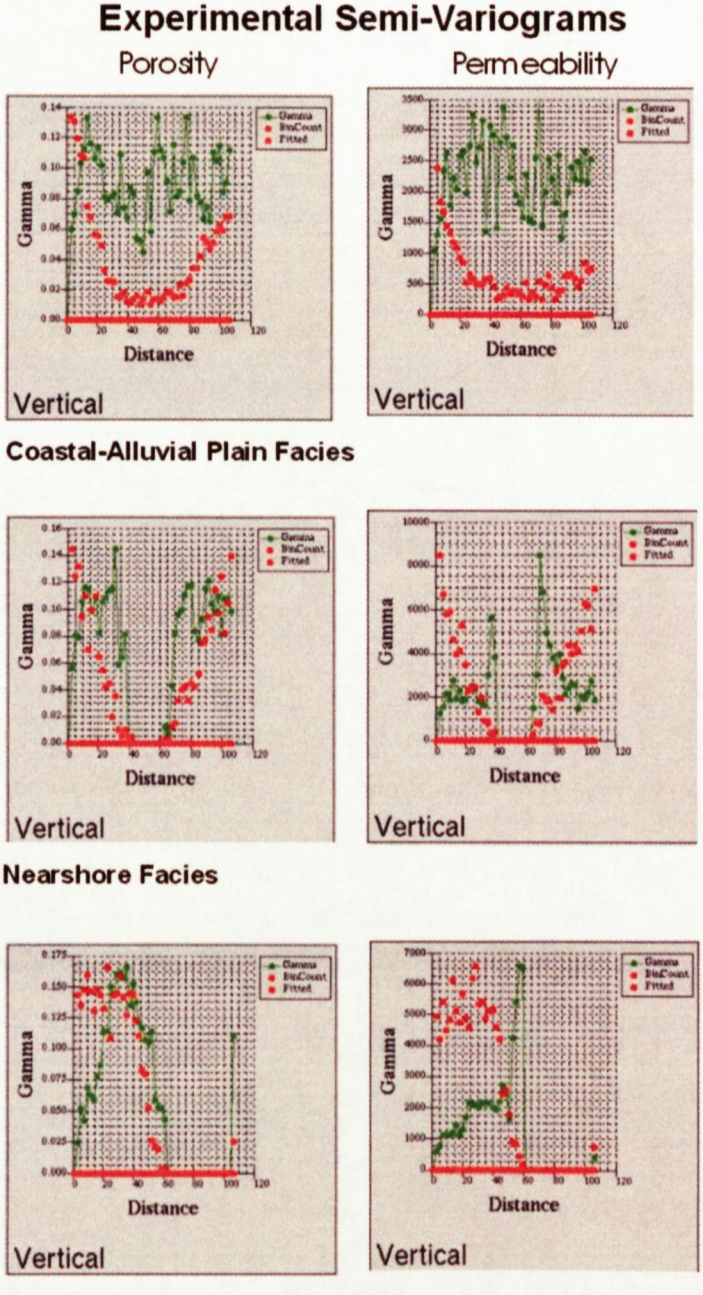

Figure 4.14—Vertical experimental semi-variograms calculated from petrophysical porosity and permeability data in the study area. The semi-variogram is represented by green dots.

Vertical experimental semi-variograms of porosity and permeability in the study area are interpretable, but are influenced by artefacts of the data sets. Severe drops in the semi-variogram of porosity and permeability at 40 and 60 metres is an artefact of the data set, which is related to the thickness of the reservoir units in which the semi-variograms were calculated. The artefacts do not represent 'real' characteristics of spatial continuity that should be represented in the reservoir model.

By ignoring artefacts of the data set that are evident in the vertical experimental semi-variograms, some conclusions regarding the spatial continuity of porosity and permeability in coastal-alluvial plain, nearshore and lower shoreface-shelf facies can be drawn. These are summarised in Table 4.3.

Table 4.3: Generalised characteristics of vertical experimental semi-variograms for different facies.

	Coastal-Alluvial Plain		Nearshore		Lower Shoreface-Shelf	
	Porosity	Permeability	Porosity	Permeability	Porosity	Permeability
Range	13 m	13 m	10 m	9 m	30 m	25 m
Sill	9%	2200 mD	11%	2100 mD	~15%	2050 mD
Nugget	4.5%	900 mD	4%	600 mD	1%	<100 mD

Discussion

Vertical Semi-Variograms

The semi-variograms used in this study for conditional simulation with alluvial-coastal plain, nearshore and lower shoreface-shelf classifying attributes are relatively straight forward as they have been calculated from petrophysical data at the wells. Levy index parameter estimates of vertical heterogeneity in various depositional environments (Liu *et al.* 2002; Table 4.4), suggest that shoreface depositional environments are the most vertically heterogeneous, and braided fluvial depositional environments the least. The experimental semi-variograms derived in this study do not show a significant difference in vertical heterogeneity between coastal-alluvial plain facies (dominated by fluvial facies) and nearshore depositional environments (dominated by shoreface and foreshore facies). Experimental semi-variograms from this study suggest the range is marginally greater in coastal-alluvial plain facies than nearshore facies and the nugget and sill values are also marginally greater. Broadly, the difference in vertical heterogeneity between the coastal-alluvial plain facies and

nearshore facies is negligible based on the experimental semi-variograms. Lower shoreface–shelf facies show greater vertical homogeneity with respect to porosity and permeability than other facies types.

Table 4.4: Vertical reservoir heterogeneity for different depositional environments (from Liu *et al.* 2002)

Depositional Environments	Levy Index Parameter	Scaling Range	Up-scaling Index	Log Types	# of Wells	Oil Field and Basins
Shoreface	1.12±0.10	0.3-5.6	18	gamma-ray	5	Flounder, Gippsland Basin
Meandering Fluvial	1.37±0.12	0.3-2.6	9	gamma-ray	10	Moomba, Cooper-Eromanga
Deltaic	1.35±0.15	0.3-7.9	26	gamma-ray	9	Challis, Timor Sea
Submarine Fan	1.51±0.10	0.3-13.4	45	gamma-ray	10	Cossack, Goodwyn and Wanaea, NW Shelf
Braided Fluvial	1.72±0.42	0.3-5.2	17	gamma-ray	13	Stratton, Texas
Shoreface	1.05±0.10	0.1-1.8	18	permeability	1	Griffin Field NW Shelf
Meandering Fluvial	1.3±0.1	0.2-2.0	10	permeability	1	Gidgealpa, Cooper Eromanga
Braided Fluvial	1.4±0.15	0.2-2.5	12.5	permeability	outcrop	Hawkesbury Sandstone, Syndey Basin
		0.2-4.5	22			

Horizontal Semi-Variograms

Two factors significantly influence the character of the madograms or semi-variograms that are generated from analogue data. These factors are the environment of deposition and the scale of investigation.

Depositional Environment

Use of analogues to create geostatistical models suggests that some madogram and semi-variogram characteristics are diagnostic of specific kinds of depositional environments. Many of the semi-variogram and madogram characteristics are expected, based on qualitative knowledge of depositional architecture. For example, the fact that maximum variance is along depositional strike in fluvial environments and along depositional dip in wave-dominated environments is not surprising.

However, some of the characteristic features of semi-variograms and madograms may not be expected based purely on a qualitative knowledge of depositional architecture. For example, a hole effect along depositional strike in many of the nearshore semi-variograms is not an entirely intuitive result. Regardless of whether semi-variogram and madogram features are intuitive, based on geological knowledge, it is useful to quantify which particular aspects of depositional architecture are important for characterising the spatial continuity of a depositional environment at a particular scale of analysis.

A commonly held conception is that an appropriate semi-variogram model can be selected if the size and shape of facies within the depositional environment is well constrained. For example, in-channel fluvial facies will have a semi-variogram range along depositional strike that will approximate the average width of the fluvial channel. The data in this study suggest that a simple relationship between facies size and shape, and madogram and semi-variogram characteristics is generally not valid. The spacing of channels along depositional strike, variations in the orientation and sinuosity of fluvial channels and facies variability within the fluvial channel all influence spatial continuity in a particular direction in addition to the size and shape of a particular facies element. A more rigorous description of spatial continuity of facies is required to produce a valid madogram or semi-variogram models.

Scale of Investigation

The characteristics of madograms and semi-variograms are not scale independent. For example, at more detailed scales of analysis (max. $\mathbf{h} < 10^3$m) it is more difficult to identify semi-variogram and madogram characteristics that are diagnostic of particular depositional environments. This may be because the spatial distribution of facies at very detailed scales of analysis is probably dominantly controlled by autocyclic processes that are similar in many depositional environments. However, at larger scales of analysis, large-scale trends in facies distribution are evident and tend to reflect large-scale controls on deposition. The shapes and orientations of large-scale depositional elements, therefore, tend to show greater consistency within particular depositional environments. For example, the orientation of a single fluvial channel can vary greatly (± 270° for highly sinuous environments), whereas the orientation of the large-scale channel belt is commonly structurally controlled and tends to be fairly consistent.

The better relationship between madogram and semi-variogram characteristics at larger scales of analysis is probably because the effect of large-scale controls on facies distribution is resolvable. For example, semi-variograms representing nearshore environments consistently have the direction of minimum variance parallel to depositional strike, whereas in proximal alluvial settings the direction of minimum variance is consistently parallel with depositional dip. This relationship results from wave influence being dominant in nearshore settings and fluvial influence being dominant in the alluvial plain. Deltaic settings are characterised by relatively low anisotropy ratios and high facies variance in directions parallel with both depositional dip and depositional strike. The low anisotropy ratios and high variance in deltaic environments probably reflect conflicting fluvial and basinal influences and increased channel bifurcation in deltaic settings.

The scale of investigation influences the character of semi-variograms or madograms for two main reasons. First, from a practical perspective facies maps of very large areas generally do not represent the same level of detail that is represented by facies maps of smaller areas. Secondly, there may be some heterogeneity that is not represented by large facies maps because the heterogeneity is below the resolution of the shortest length of **h**.

The second reason that the scale of investigation influences the character of semi-variograms and madograms is that different scales of facies architecture are represented by different scales of madograms and semi-variograms. For example, a small-scale madogram in a fluvial environment may be mostly controlled in the shapes and orientation of in-channel sandbars. A larger scale madogram is likely to reflect the size and orientation of the channel itself. Different scales of depositional architecture are sometimes reflected in a single madogram or semi-variogram. For example, many of the nearshore variograms are characterised by two ranges—one of a few hundred metres and the other of several thousand metres. The large-scale range seems to reflect the size and orientation of nearshore composite sand bodies that are oriented parallel to the shoreline for long distances (e.g. barrier islands, shoreface sand ridges etc...). The small-scale range appears to be a response to individual component sand bodies like dunes or shoreface sand ridges that make up a large-scale barrier island or shoreface. As a result of the multiple scales of heterogeneity most nearshore sand bodies are best modeled by nested equations.

Stratigraphy and Preservation Potential

Preservation potential of particular facies cannot be properly represented in madograms or semi-variograms from analogue modern depositional environments. However, preservation potential plays an important role in the horizontal distribution of facies within reservoirs. Preservation potential is largely controlled by changes in the rate of accommodation creation and sediment supply during and after deposition. Therefore, the part of the stratigraphy to which an analogue madogram or semi-variogram is applied affects the characteristics of the madogram or semi-variogram.

A relatively complete record of a single depositional system is only likely to be preserved where the rate of accommodation creation was high. Where the rate of accommodation creation was low, depositional systems are not likely to be completely preserved with all the geometries and facies distributions that are observed in modern depositional environments. Therefore, the madograms and semi-variograms that are generated from modern depositional environments are more applicable to stratigraphic packages within the transgressive systems tract and early highstand systems tract. Although the same depositional environment may be represented within the lowstand systems tract and late highstand systems tract, the distribution of facies is likely to be somewhat different.

In the case of the upper Latrobe Group, few lowstand systems tracts, characterised by the lowest ratio of accommodation to sediment supply, are interpreted to be preserved. For example, fluvial lowstand systems tracts are characterised by the preferential preservation and amalgamation of channellised facies. Consequently, the variance may be lower and the range longer in a semi-variogram of a lowstand systems tract fluvial system than it would be in a transgressive or early highstand systems tract fluvial system. The expected changes in the character of a semi-variogram with respect to stratigraphic position are provided in Figure 4.15.

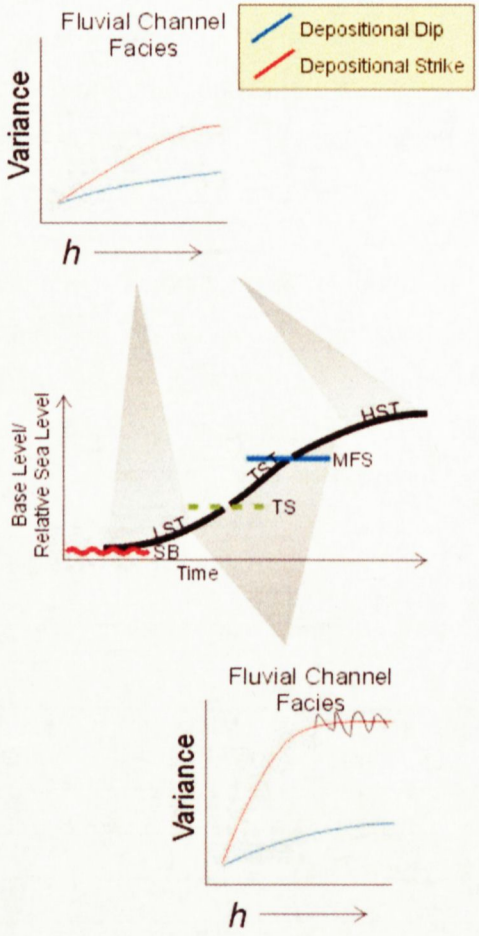

Figure 4.15—Conceptual example of the changes in a madogram for fluvial channel facies with respect to stratigraphic position (systems tract). The early LST and late HST are characterised by the lowest ratio of accommodation to sediment supply and therefore have a similar madogram character. The late LST, TST and early HST are characterised by relatively high ratios of accommodation creation to sediment supply resulting in different madogram characteristics.

Applicability of Analogue Madograms and Semi-Variograms to Geological Models

The most obvious application of analogue madograms and semi-variograms is where facies are populated in the reservoir models through conditional simulation or kriging. In the case of this study however, facies were populated deterministically so reservoir properties were populated with conditional simulation using facies as a classifying attribute.

The relationship between facies and reservoir properties suggests that an analogue madogram or semi-variogram for facies has utility for populating reservoir properties, but the exact madogram or semi-variogram is not likely to be applicable. For example, the sill and nugget value will change depending on the particular reservoir property being populated and the range will vary to reflect variation in reservoir

properties within a particular facies. However, the general characteristics of the semi-variogram or madogram do appear to be diagnostic of particular depositional environments. Particularly, the pattern of changes in semi-variogram and madogram characteristics from one depositional environment to another is expected to be widely applicable.

To populate the geological model with an attribute, semi-variogram models are required in the vertical direction and the horizontal directions of maximum and minimum spatial variance. The horizontal directions of maximum and minimum spatial variance were determined based on the interpreted orientation of the shoreline for different stratigraphic intervals, summarised in Table 4.5:

Table 4.5: Horizontal directions of maximum and minimum spatial variance for different geological model zones.

Zone	Facies	Minimum Variance	Maximum Variance
Middle & Upper N. asperus	Nearshore	035°	125°
	Lower Shoreface-Shelf	035°	125°
	Coastal-Alluvial Plain	118°	028°
Lower *N. asperus*	Nearshore	028°	118°
	Lower Shoreface-Shelf	028°	118°
	Coastal-Alluvial Plain	103°	013°
P. asperopolus	Nearshore	013°	103°
	Lower Shoreface-Shelf	013°	103°
	Coastal-Alluvial Plain	134°	044°
Middle & Upper *M. diversus*	Nearshore	044°	134°
	Lower Shoreface-Shelf	044°	134°
	Coastal-Alluvial Plain	134°	044°
Lower *M. diversus & L.. balmei*	Coastal-Alluvial Plain	134°	044°

Changes in shoreline orientation with time are reflected in the directions of maximum and minimum spatial variance (Chapter 3). Palaeo-shoreline parallel orientations (north-north-east) represent the direction of minimum spatial variance for nearshore facies and lower shoreface to shelf facies, but represent the direction of maximum spatial variance for coastal and alluvial plain facies. This is the expected pattern of spatial variance suggested by the analogue data.

Also consistent with the analogue data the maximum spatial variance (sill value) differs for the depositional facies represented in the geological model. Lower shoreface and shelf strata are characterised by the lowest sill values for a particular attribute, and coastal and alluvial plain facies are characterised by the highest sill values. For example, with respect to porosity the sill values are 10%, 13% and 15% for lower shoreface and shelf facies, nearshore facies and coastal and alluvial plain facies respectively.

The ranges assigned to semi-variogram models for the horizontal directions of maximum and minimum spatial variance were also governed by the analogue data. Lower shoreface and shelf facies were characterised by the longest ranges, up to 20,000 m in the direction of minimum spatial variance, whereas nearshore facies were assigned values between 10,000 m and 15,000 m. The shorter ranges were applied to nearshore facies in the upper stratigraphic intervals (Lower and Middle *N. asperus* and Upper *N. apserus* zones) where barrier island depositional settings are interpreted to be dominant rather than wave-dominated deltaic settings. Analogue data also suggests that the difference between range values for the horizontal directions of maximum and minimum spatial variance are likely to be greater in the barrier island setting, indicative of greater variance along depositional dip. Coastal and alluvial plain facies were characterised by the shortest ranges of only 8000 m and 4000 m in the direction of minimum and maximum spatial variance respectively.

The semi-variogram models used in the geological model were selected based not only the analogue data but also by trial and error: populating attributes with a particular semi-variogram model and then inspecting the resulting spatial distribution of the attribute to ensure that the distribution makes sense geologically and is consistent with the conceptual depositional models outlined in Chapter 3. For example, rapid pressure communication over relatively long distances is a characteristic of the upper Latrobe Group nearshore facies (Root *et al.* 2004), so a fairly laterally extensive interconnected network of moderate and high porosity and permeability values within the nearshore facies makes sense. The spatial distribution of attributes including porosity, permeability and categorical facies attributes within the geological model is addressed in greater detail in Chapter 6.

Chapter 5—Seal Evaluation

Abstract

Where aquifers are utilised for CO_2 storage the ability of the seals to contain fluids less dense than water is untested so seal evaluation is required. Several fine-grained, low permeability units of the upper Latrobe Group were evaluated in terms of their seal capacity, seal geometry and seal integrity by way of mercury injection capillary pressure measurements, seismic mapping, wireline log correlation, and using analogue data.

The Lakes Entrance Formation is considered to have excellent seal potential because it can hold back large columns of supercritical CO_2 (~750 m) and because it is regionally extensive across the study area. The localised structural closures in the study area do not exceed ~250 m, so the Lakes Entrance Formation is likely to be an effective top seal for CO_2 geosequestration. However, the calcareous parts of the Lakes Entrance Formation are more brittle than a pure siliciclastic mudstone, which may be the reason for relatively dense networks of low displacement faults in some parts of the formation.

Some fine-grained units within the upper Latrobe Group will also hold back large columns of CO_2, but are restricted in terms of lateral extent so they are likely to induce a tortuous migration path as CO_2 moves up-dip rather than hold back large columns of CO_2. The capacity of sealing units within the upper Latrobe Group is greater where sealing units were deposited in relatively distal depositional environments, probably due to very low silt and sand content. An exception to this general rule is the Gurnard Formation, interpreted to have been deposited in a shelfal environment, which is not likely to hold back SC CO_2 columns of more than a few tens of metres in some locations.

Dissolved gas content in seawater near the seabed may be an indication of hydrocarbon leakage from the subsurface, and consequently may be used as an empirical test of seal potential. High methane and ethane readings in the seawater near the Rosedale Fault System in the northernmost part of the study area may suggest that fault leakage is presently occurring. However, areas with indications of current hydrocarbon leakage are not on the expected CO_2 migration path.

Introduction

Seal potential is critical to technical evaluation for CO_2 storage because top seals are untested in most potential ESSCI scenarios. Depleted/disused hydrocarbon fields are an exception because the sealing units have previously held back a column of hydrocarbon. However, where an aquifer residence/migration time trap is employed seal potential is unknown unless the aquifer/reservoir has maintained a non-hydrostatic pressure gradient (Lindeberg 1997, Kaarstad 2002). In Australia

particularly, the majority of capacity for geological storage of CO_2 is associated with aquifer residence/migration time traps.

A second reason that seal potential is critical to the technical feasibility of CO_2 storage is that uncontrolled release is not associated with economic risk alone. There may also be environmental and social costs associated with the uncontrolled release of CO_2. Additionally, there is a risk that the uncontrolled release of CO_2 may constitute a safety risk (Holloway 1997), but a significant safety risk due to leakage is improbable where offshore reservoirs and aquifers are utilised for geosequestration. However, leakage of CO_2 to the sea floor could potentially adversely impact marine ecosystems.

The highest risk of uncontrolled CO_2 release is probably at surface during gas processing and compression. Once in the aquifer/reservoir there are three main ways CO_2 could be unintentionally released:

- Technological failure at the injection well or leakage via an existing well along the migration path of the CO_2
- Open fractures/fracture networks (e.g. the damage zone of faults)
- Top seal breach.

Only top seal potential for the Gippsland Basin ESSCI study area is evaluated in this study, although some empirical conclusions about fault seal potential are drawn. A geomechanical fault seal evaluation was carried out in parallel with this study to assess the risk of vertical leakage along fault planes and damage zones (Root et al. 2004). As mentioned previously, juxtaposition relationships of faults do not pose a fault seal risk in the study area due to the limited displacement of faults by comparison with the thickness of sealing units (Chapter 3). Evaluation of existing well penetrations to the upper Latrobe Group, some of which are several decades old, should be considered a prerequisite for CO_2 injection and storage (Benson 2003, Perry 2003), but is not addressed in this study.

Unlike migration time and capacity, top seal potential cannot be quantitatively estimated through flow simulation with the technology presently available. Consequently, top seal evaluation is carried out independently of the reservoir model. A seal evaluation technique originally developed in the petroleum industry is utilised

herein (Kaldi & Atkinson 1997, Kivior *et al.* 2002). Seal potential is considered as the product of three factors:

- Seal capacity: the hydrocarbon column that can be held by the seal
- Seal geometry: areal extent and thickness of the seal
- Seal integrity: mechanical properties of the seal (propensity for the development of fluid conducting fractures).

In the case of CO_2 geosequestration the approach must be slightly more complex; unlike hydrocarbon CO_2 is not chemically inert and conventional seal evaluation technologies do not incorporate changes in the sealing properties of rocks due to chemical reaction with CO_2 (Wildenborg & van der Meer 2002). However, it is difficult to predict the impact of CO_2/rock reactions on rock texture and particularly sealing properties. Little detailed information is presently available regarding the kinds of CO_2/rock reactions that are likely to take place at reservoir conditions and little is known about the reaction rates. However, some general conclusions can be drawn from knowledge of reactive and inert mineralogy (see Chapters 1 & 2). Additionally, the impact of CO_2/rock reactions is the subject of on-going research (Kirste *et al.* 2004).

Methodology

Seal Capacity

Like hydrocarbon, SC CO_2 is significantly less dense than water (0.3 – 0.7 g/cm^3 at typical reservoir/aquifer conditions) and will rise to the top of a water-filled reservoir and concentrate under low permeability sealing layers. In this way, supercritical CO_2 remains trapped below the less permeable sealing layer until buoyancy pressure exerted on the seal by the column of SC CO_2 exceeds the capillary pressure of the seal. Buoyancy pressure (*Pb*) on the seal is a function of the column height (*h*), and the density of SC CO_2 (ρ_{CO2}) and formation water (ρ_{fw}). As the column height increases, the buoyancy pressure on the seal increases:

$$Pb = h(\rho_{fw} - \rho_{CO2})0.433$$

It is useful to determine the maximum column height of SC CO_2 that can be held by a particular sealing lithology before its capillary pressure is exceeded (hB_{max}), which is a measure of the seal capacity.

The capillary pressure (Pc) of a seal is a function of the interfacial tension between the wetting and non-wetting phase (σ), wettablility (θ), and the radius of the largest pore throats in the seal rock (R). The relationship is described by (Downey 1984):

$$Pc = \frac{2\sigma \cos\theta}{R}$$

Capillary pressure, and consequently the maximum column height that can be held by a seal (h_{max}), can be determined by conducting mercury capillary injection pressure (MICP) measurements on samples of the sealing lithology. MICP is a process by which a sample of the sealing lithology is placed in a sealing chamber into which mercury is introduced to surround the sample. The pressure in the chamber is raised incrementally, which eventually forces the mercury through the sample. The volume of mercury injected at each pressure is a measure of mercury saturation in the sample (Schowalter 1979). In the air/mercury system, air is the wetting phase and mercury is the non-wetting phase.

However, for geosequestration, the focus is on SC CO_2/formation water systems, where formation water is the wetting phase and SC CO_2 is the non-wetting phase, rather than air/mercury systems. The conversion from the air/mercury system to the formation water/SC CO_2 system is made using the following relationship:

$$P_{Cfw/CO2} = P_{Ca/m} \frac{\sigma_{fw/CO2} \cos\theta_{fw/CO2}}{\sigma_{a/m} \cos\theta_{a/m}}$$

...where $P_{Cfw/CO2}$ is capillary pressure in the formation water/SC CO_2 system, $P_{Ca/m}$ is capillary pressure in the air/mercury system, $\sigma_{fw/CO2}$ is formation water/SC CO_2 interfacial tension, $\sigma_{a/m}$ is the air/mercury interfacial tension, $\theta_{fw/CO2}$ is the contact angle in the formation water/SC CO2 system, and $\theta_{a/m}$ is the contact angle in the air mercury system.

The capillary pressure has two components, which can be measured from MICP: the capillary entry pressure (*Pe*) and the threshold pressure (*Pth*). Where the buoyancy pressure is greater than the entry pressure, hydrocarbons enter the seal, and where the buoyancy pressure is greater than the threshold pressure, a continuous hydrocarbon filament is present through the seal (Kivior *et al.* 2002). The seal is breached when the entry pressure is reached. The maximum SC CO_2 column height that can be supported by a seal can be calculated using the threshold pressure:

$$h_{\max} = \frac{Pth - Pth_{res}}{(\rho_{fw} - \rho_{CO2})0.433}$$

The maximum column height supported by a particular sealing unit is given by the threshold pressure of the seal unit (*Pth*) minus the threshold pressure of the reservoir (Pth_{res}) divided by the buoyancy pressure exerted on the seal [$(\rho_{fw}-\rho_{CO2})0.433$].

MICP analysis on 18 samples was conducted specifically for this study on both seal and reservoir samples at NCPGG and Amdel. Twenty-two additional open file MICP data were used (Victorian Department of Natural Resources open file well completion report database), which were originally acquired by ESSO Australia Ltd.

SEAL GEOMETRY

Seal geometry of thick regional sealing units can be mapped from seismic interpretation and from wireline log correlation. However, thin sealing lithologies are below seismic resolution, so direct measurement of their lateral extent and distribution is difficult and can often only be inferred between wells. Where sealing lithologies are below seismic resolution, estimates of their likely lateral extent are made from published analogue measurements of seal geometry (Fig. 5.1). The assumption is made that the environment of deposition influences the resulting lateral extent of the sealing unit. For example, it is reasonable to assume that prodelta shale will be more laterally extensive than an abandoned fluvial channel.

Analogue data provides a range of the likely lateral extent for a particular sealing facies. Unfortunately, a consistent thickness to width or areal extent relationship does not apply to any of the sealing facies represented in the study area with the exception of abandoned fluvial channel facies. However, an average lateral extent of most sealing facies can be calculated from analogue data. The effectiveness of the seal

geometry is expressed as the ratio of the area of the sealing unit versus the area of the three-way enclosure represented in the study area.

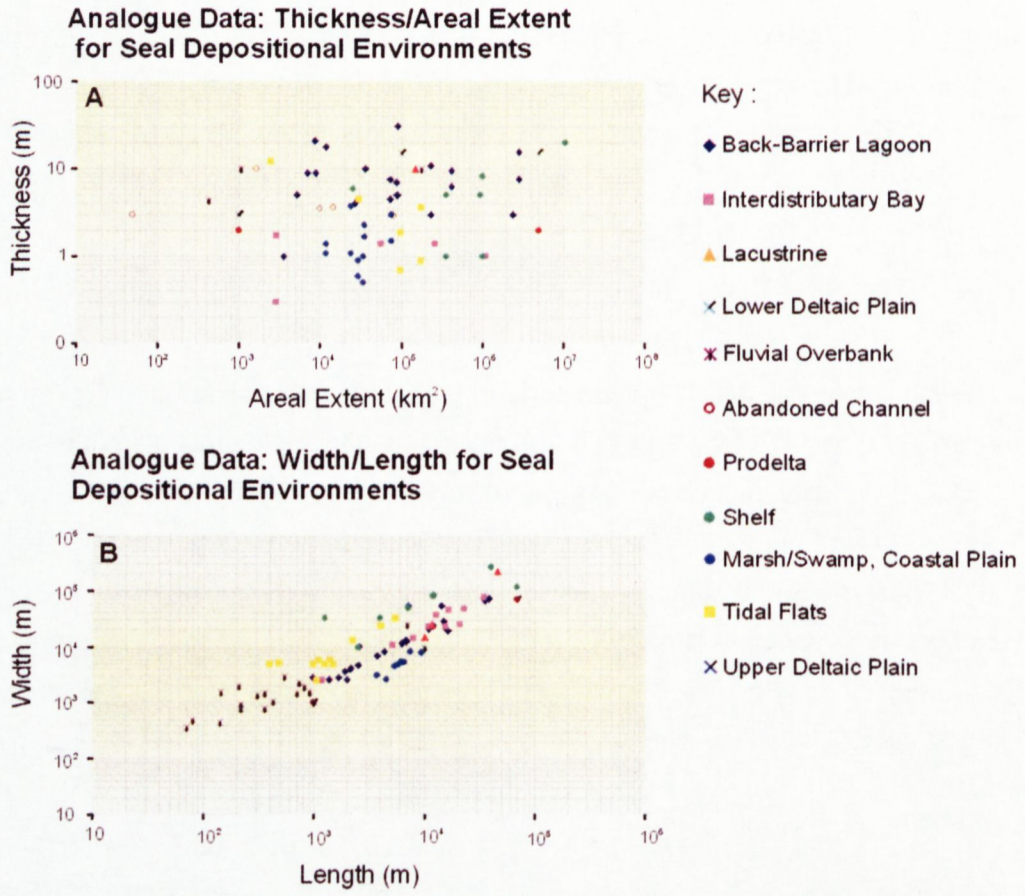

Figure 5.1—Typical geometry of sealing facies represented in the study area. Thickness versus areal extent (A) and width versus length (B) plots are provided.

Though difficult to quantify, it is also useful to incorporate the idea of preservation potential in the evaluation of seal geometry. Sealing units that were deposited as laterally extensive depositional elements are commonly partially eroded, which reduces their effective lateral extent. For example, fluvial channels commonly cut through fine-grained floodplain deposits. The susceptibility to erosion after deposition is largely a function of the ratio of accommodation creation (relative sea level and base level) to sediment supply during deposition. As a result, the stratigraphic position of sealing facies will play an important role in assessing their susceptibility to erosional alteration after deposition. In general, sealing facies in the lowstand systems tract and late highstand systems tract have limited potential to be fully preserved without subsequent erosion. However, sealing facies deposited in the

transgressive and early highstand systems tract have a better chance of being wholly preserved.

SEAL INTEGRITY

No experimental data is available at present on the mechanical properties of the sealing lithologies in the study area. However, some assumptions regarding the mechanical properties of the sealing lithologies represented in the study area may be made based on published relationships between lithology and mechanical properties.

Results

Several different sealing lithologies are present in the study area that act as regional seals, or as intra-reservoir/aquifer sealing units. These include:

- Lakes Entrance Formation (seismically mapped)
- Gurnard Formation (mapped through wireline correlation)
- Marlin/Turrum Submarine Canyon Fill (seismically mapped)
- Latrobe Group intraformational seals (below seismic resolution and commonly cannot be correlated with confidence between wells).

All but the Latrobe Group intraformational seals can be mapped seismically or by wireline log correlations. The spatial distribution of mappable sandstones is provided in Figure 5.2.

The Lakes Entrance Formation is everywhere present in the study area and overlies the Turrum and the Gurnard Formations. The Gurnard Formation is mapped based on its character on wireline logs and its distribution between wells is inferred. The Marlin Canyon, filled by the Turrum Formation, is important as both a top seal and a lateral seal. It truncates reservoir units in the east of the study area and consequently is likely to prevent eastward migration of CO_2. The seal capacity, geometry, and integrity were evaluated for each of the sealing facies represented in the study area.

Seal Capacity

Mercury intrusion graphs for all of the samples used in this study are provided in Figures 5.3 – 5.9. The interpreted threshold pressures are indicated on the graphs and were interpreted using the techniques outlined by Dewhurst *et al.* (2002).

Seal capacity is dependent not only on the rock properties but also on the reservoir conditions. The salinity and density of the formation water, and the reservoir/aquifer temperature and pressure affect the calculation of the SC CO_2 column height that can be supported by a seal. The temperature and reservoir conditions vary for each sample, but average conditions are as follows: temperature ~80°C; pressure ~13 MPa; formation water density ~0.95 g/cm^3, and; SC CO_2 density ~0.44 g/cm^3. The seal capacity is also dependent on the capillary properties of the reservoir/aquifer underlying the seal unit. Several sandstone samples were run to ascertain reasonable values for reservoir/aquifer threshold pressure. Threshold pressures of 2 – 10 psia were typical for fairly high permeability upper Latrobe Group sandstones, and up to 20 psia for very fine-grained, tight sandstones.

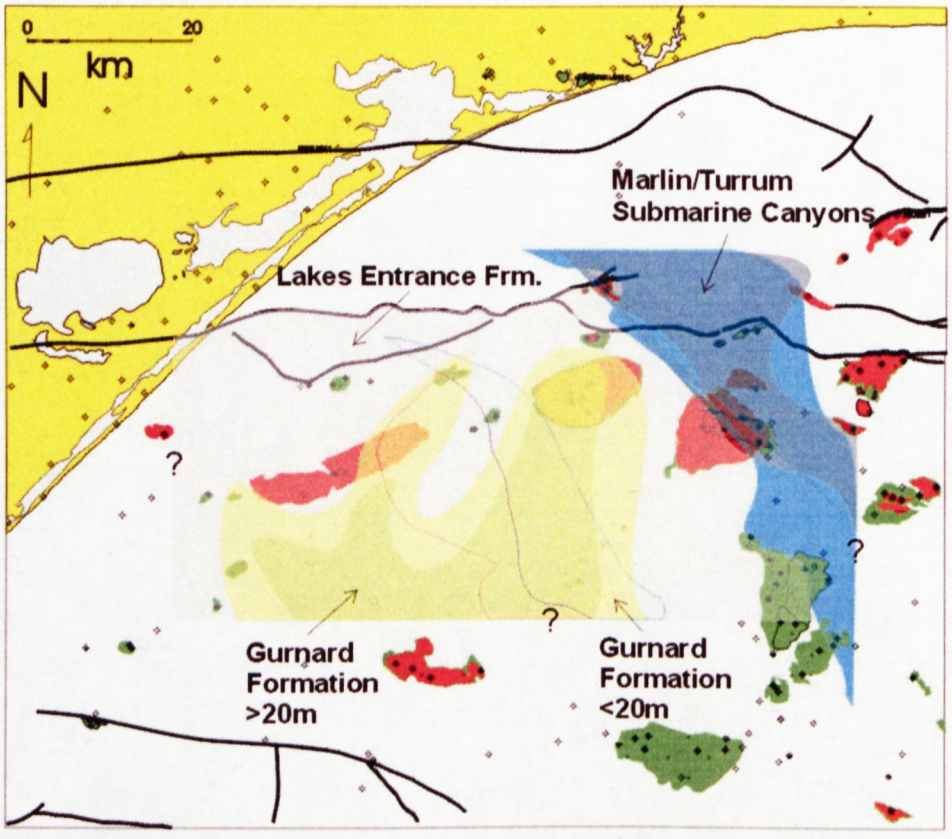

Figure 5.2—Map of regional sealing facies: Lakes Entrance Formation, Marlin Canyon and the Gurnard Formation. The thin blue and red lines represent the approximate positions of Miocene submarine canyons.

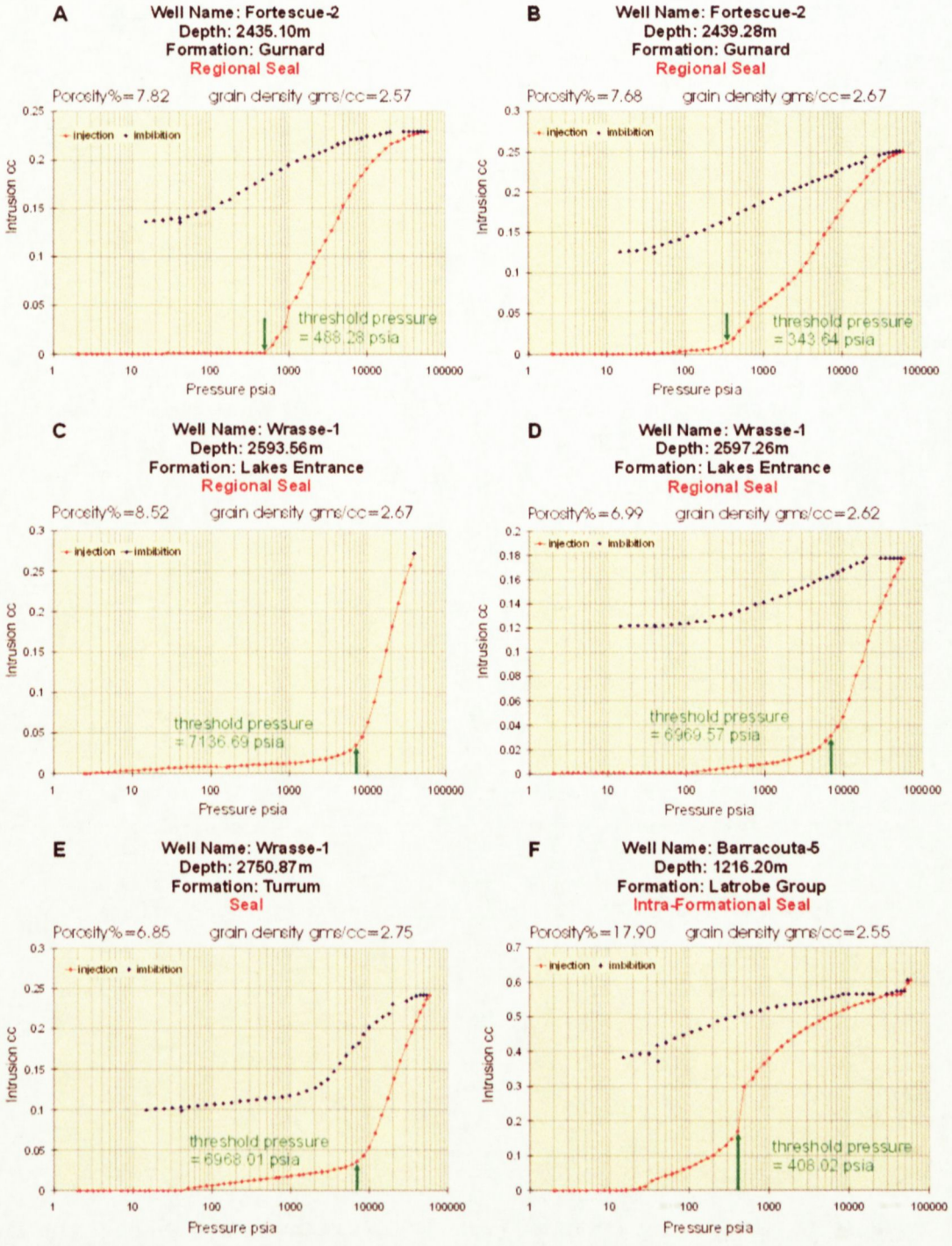

Figure 5.3—MICP curves plot intrusion in cubic centimetres of mercury against pressure shown on a log scale. The threshold pressure is indicated on each diagram. MICP curves for regional sealing facies are primarily shown (A-E). The Lakes Entrance (C & D) and Turrum Formations (E) have relatively high threshold pressures. Gurnard Formation samples have significantly lower threshold pressures (A & B).

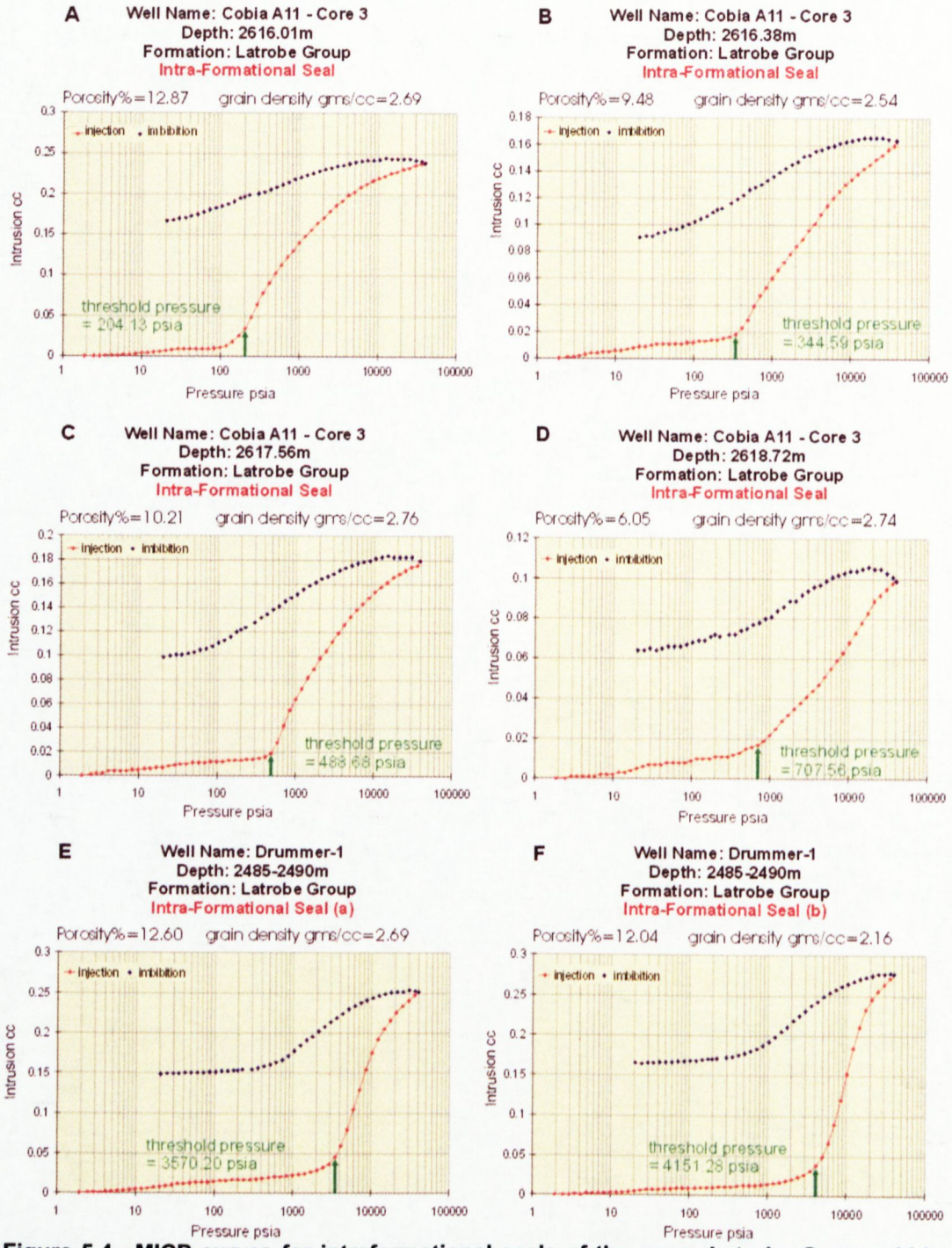

Figure 5.4—MICP curves for intraformational seals of the upper Latrobe Group within the study area. Threshold pressure range is considerable—from 204.13 psia (A) to 4151.28 psia (F).

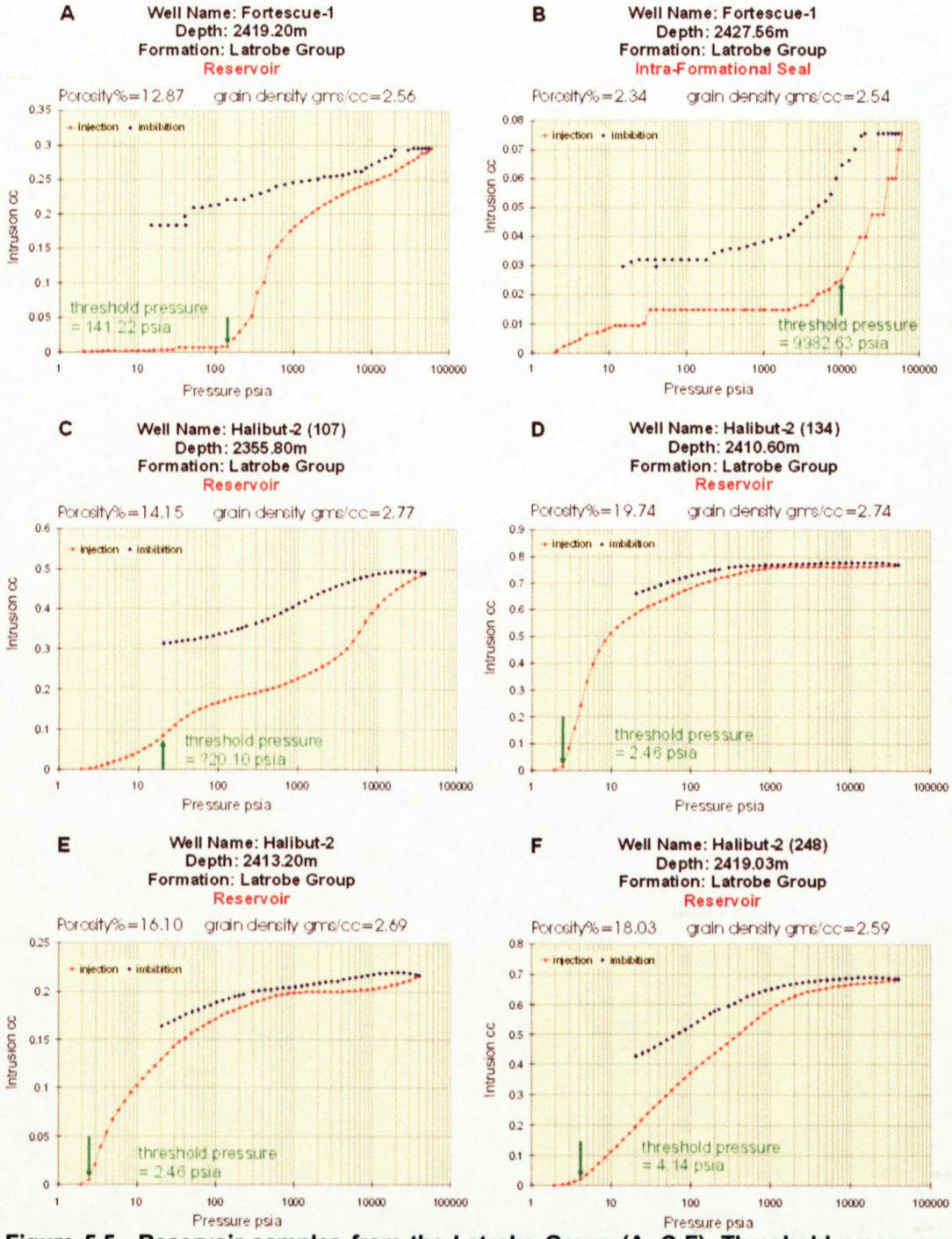

Figure 5.5—Reservoir samples from the Latrobe Group (A, C-F). Threshold pressures are generally low and may be difficult to interpret (C). 'B' is an intraformational seal sample, the 'stepped' character of the MICP curve may be an artifact of incremental pressure increase.

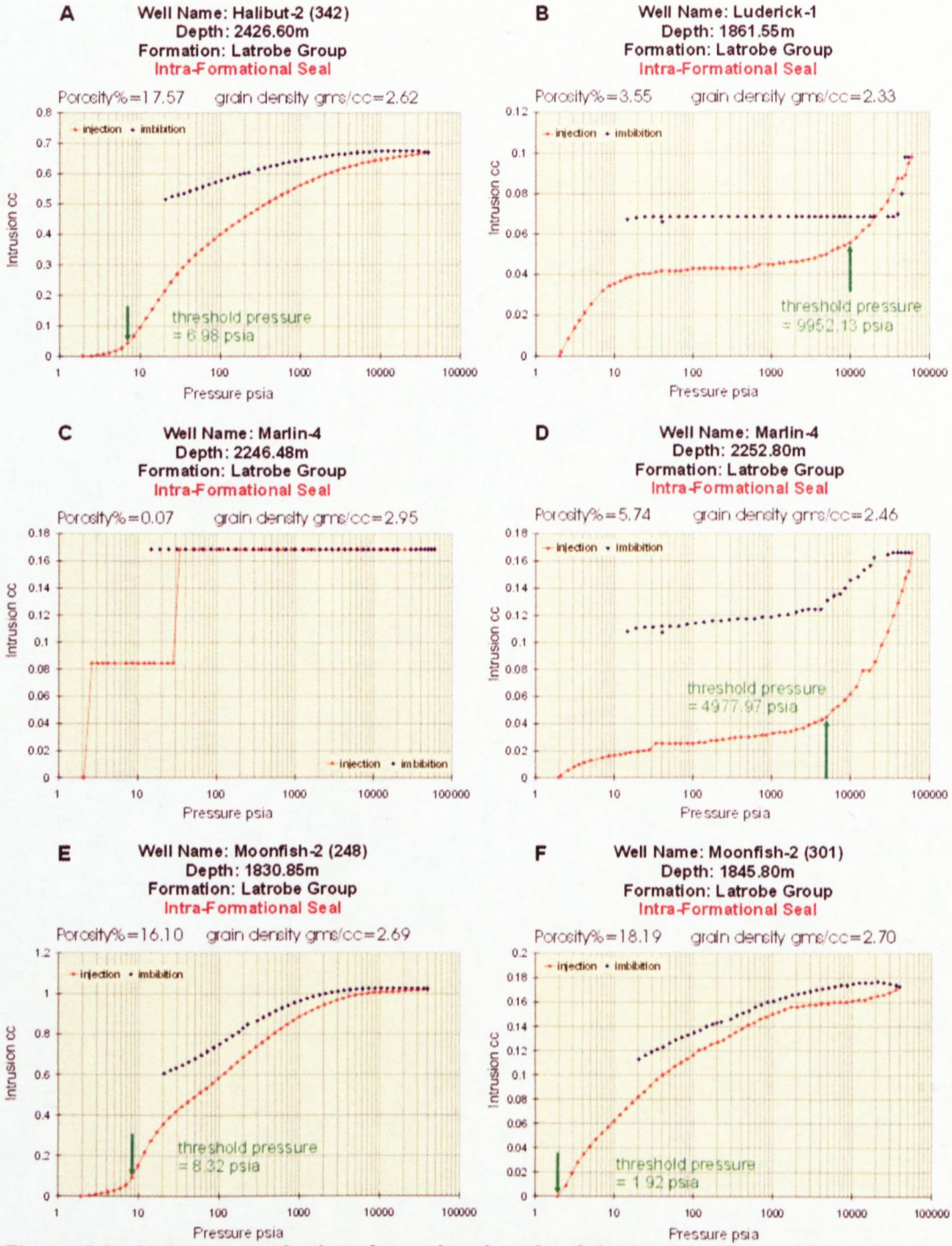

Figure 5.6—MICP curves for intraformational seals of the Latrobe Group. C is a heavily carbonate cemented sample associated with the damage zone of a fault. The MICP curve may suggest that mercury never entered the pore network of the sample due to the intensity of cementation. The seal/reservoir distinction for samples A, E & F were made from wireline logs, as the original samples were not available. The MICP curves (low threshold pressures and high intruded volumes of mercury) suggest that A & E may represent coarse-grained beds (sandstone or siltstone?) interbedded in a finer grained succession.

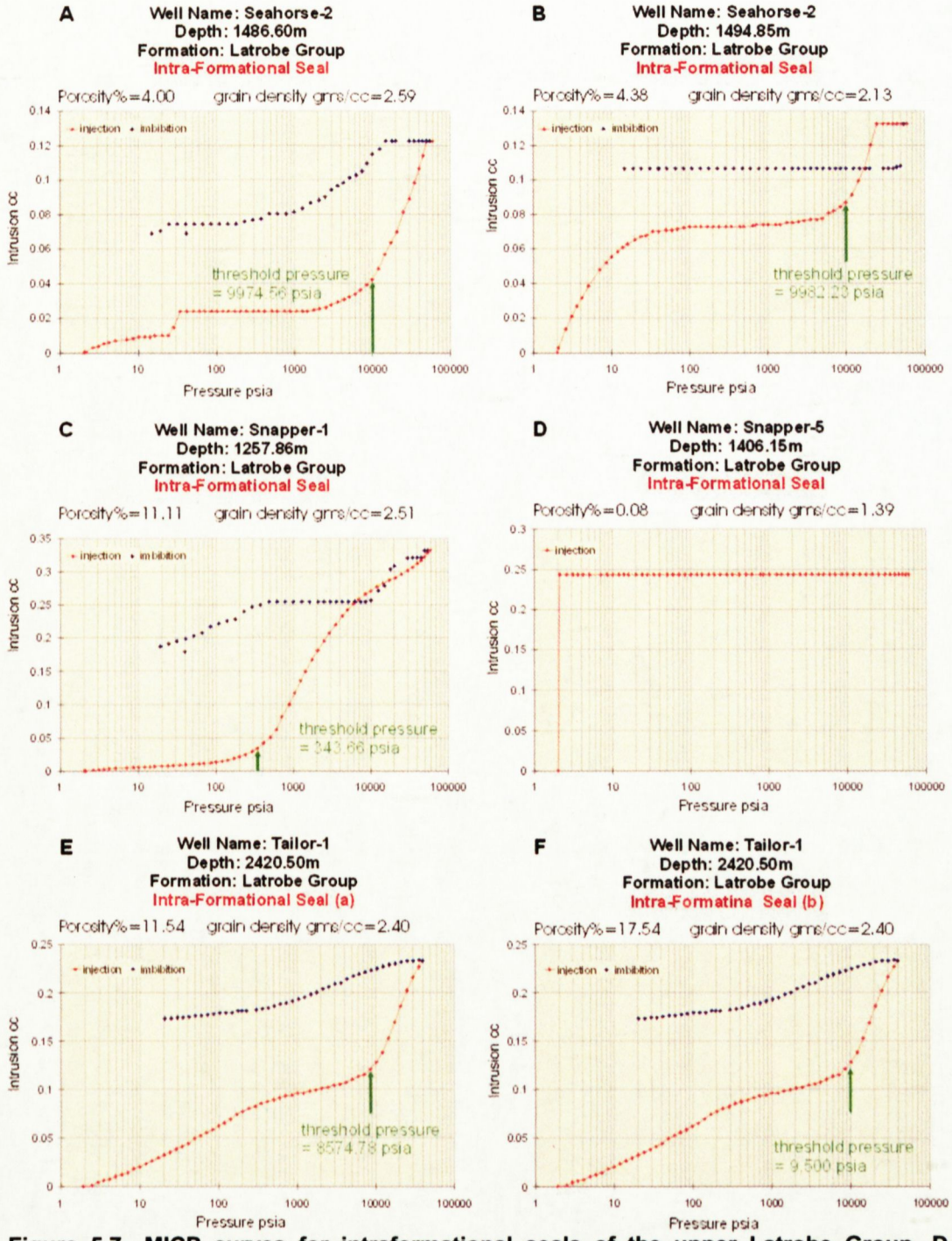

Figure 5.7—MICP curves for intraformational seals of the upper Latrobe Group. D represents a highly carbonaceous mudstone. The high proportion of extremely fine-grained carbonaceous material prevented mercury intrusion into the pore network.

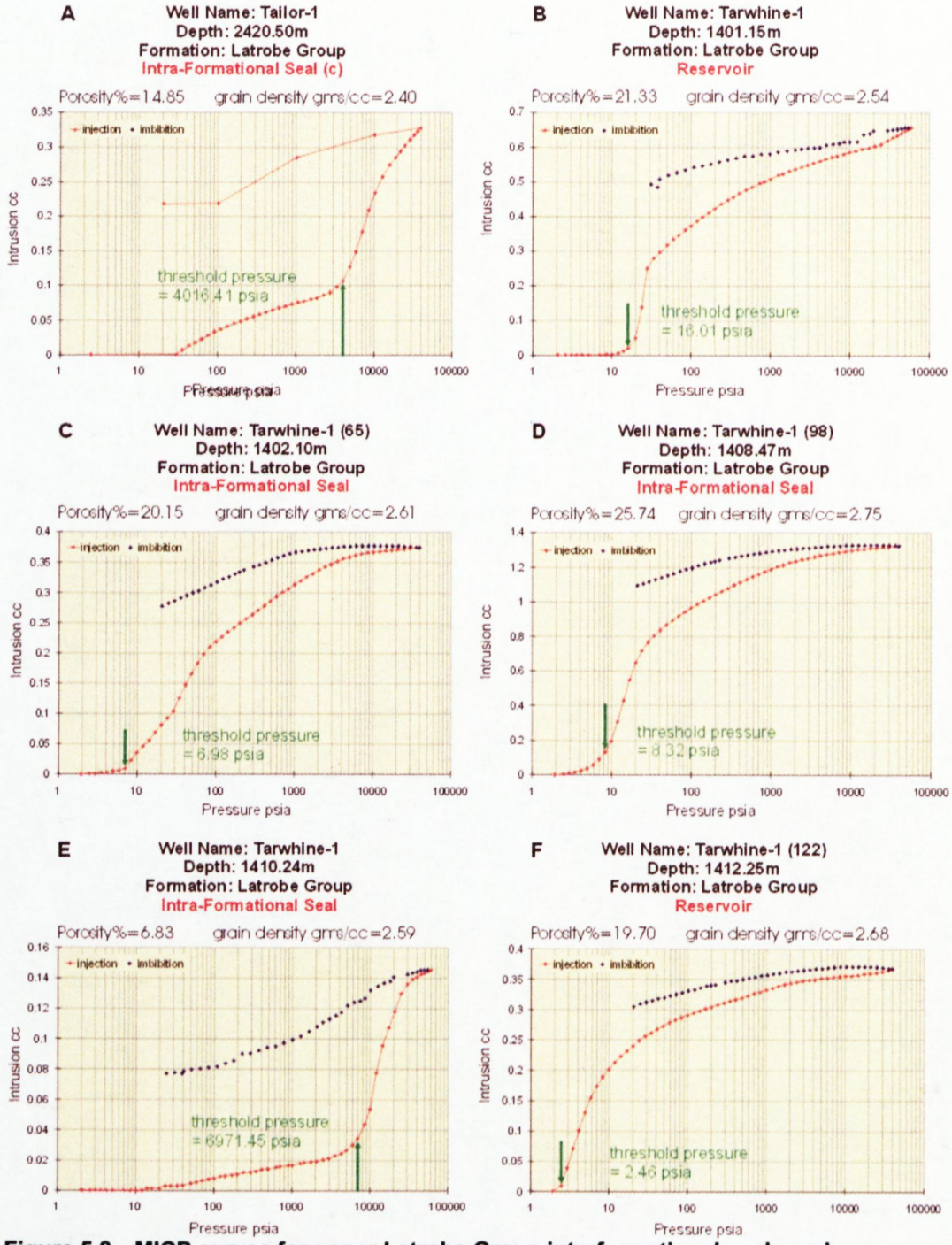

Figure 5.8—MICP curves for upper Latrobe Group intraformational seals and reservoirs.

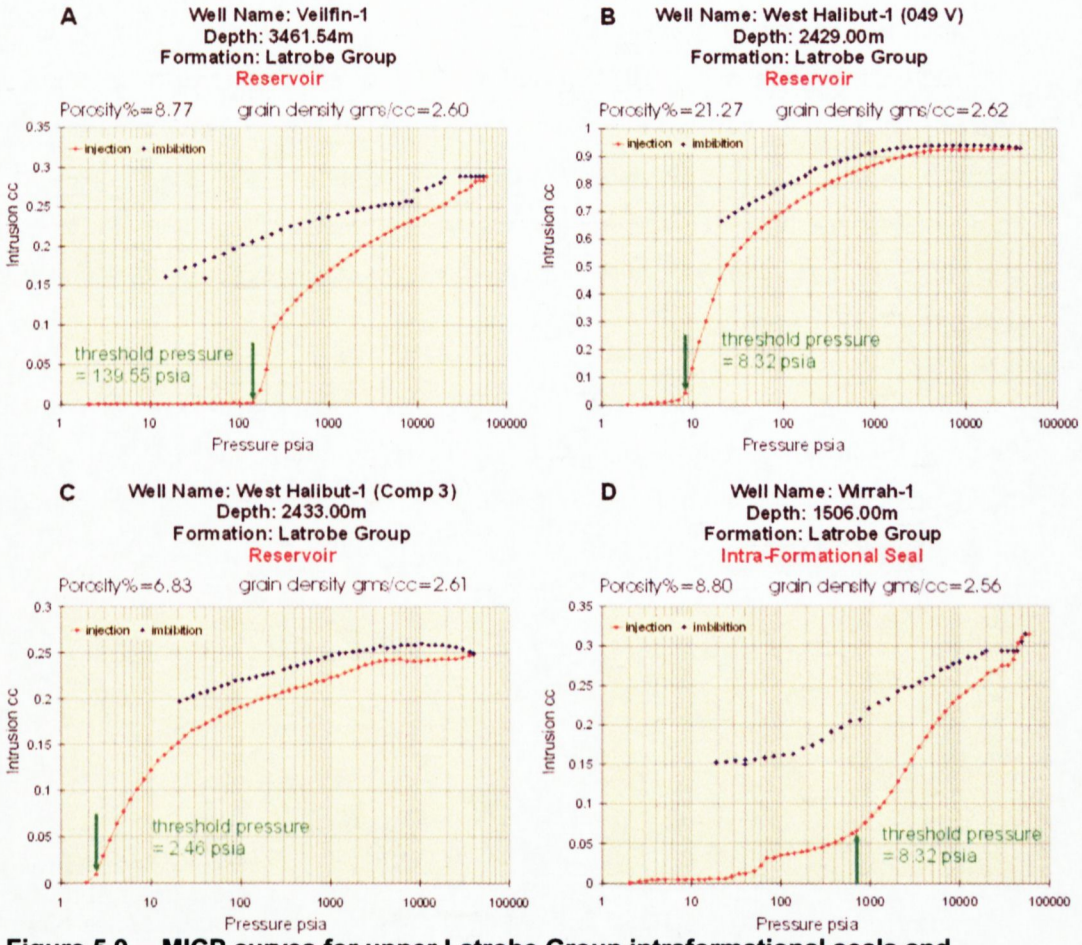

Figure 5.9— MICP curves for upper Latrobe Group intraformational seals and reservoirs.

The threshold pressures for the sealing lithologies represented in the study area are plotted against stratigraphic units in Figures 5.10 and 5.11. Samples from the Lakes Entrance and Turrum formations are associated with high threshold pressures, both equivalent to column heights of ~750 m of SC CO_2 (Table 5.1). Conversely, the Gurnard Formation is characterised by considerably lower seal capacity, and is likely to hold back column heights of a few ~10s of metres suggesting that it may behave as a 'waste zone' rather than a true seal.

Limited data was available for the regional sealing lithologies because seals are rarely sampled and full-hole core of sealing intervals is uncommon. Consequently, it is difficult to assess heterogeneity of regional sealing units and possible lateral variation in seal capacity. However, for fully marine facies deposited in shelfal environments significant lateral variations in rock texture are unlikely.

Considerably more data is available for intraformational sealing facies by comparison with regional sealing facies. MICP threshold pressures suggest a range from ~150 psia to ~10,000 psia, which are equivalent to SC CO_2 column heights of between ~10 m and ~1000 m. The high variability in threshold pressures stems from textural and compositional variation in intraformational sealing lithologies. A couple of factors may contribute to the high variability including diagenetic cementation and different environments of deposition.

Intraformational seal samples that had high threshold pressures were commonly associated with diagenetic cementation. Highly cemented samples in the vicinity of faults particularly are interpreted to have threshold pressures that exceeded the maximum MICP pressure of 50,000 psi.

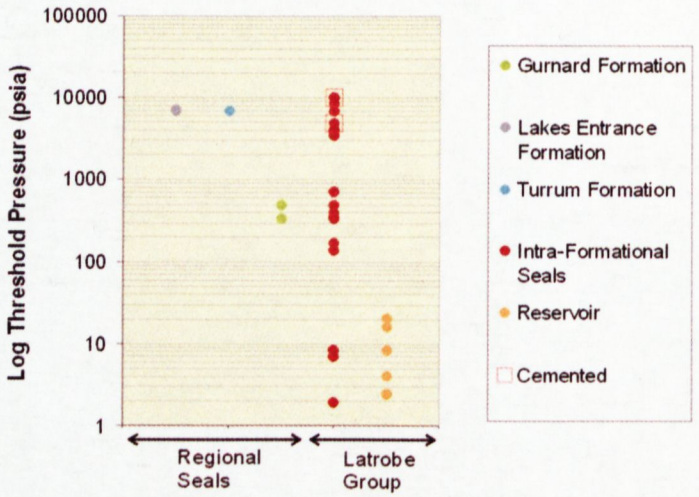

Figure 5.10—Threshold pressures plotted against facies type.

The environment of deposition also has an influence on the seal capacity of intraformational seals (Fig. 5.11). Lower shoreface and back barrier lagoon facies represent the best sealing units in terms of threshold pressures. Fine-grained samples with high carbon content were also characterised by high threshold pressures; however, highly carbonaceous rocks such as coals would likely also be characterised by very poor seal integrity as they are typically very brittle. Samples from floodplain facies and tidal flat facies have the lowest seal capacity. Generally, samples form more distal depositional settings have better seal capacity. The trend appears geologically reasonable because silt and sand, which degrade seal capacity, are less likely to be transported to distal environments. The three regional facies identified in this study may be ranked in terms of seal capacity from best to poorest as follows: lower shoreface-shelf, nearshore, and alluvial-coastal plain facies.

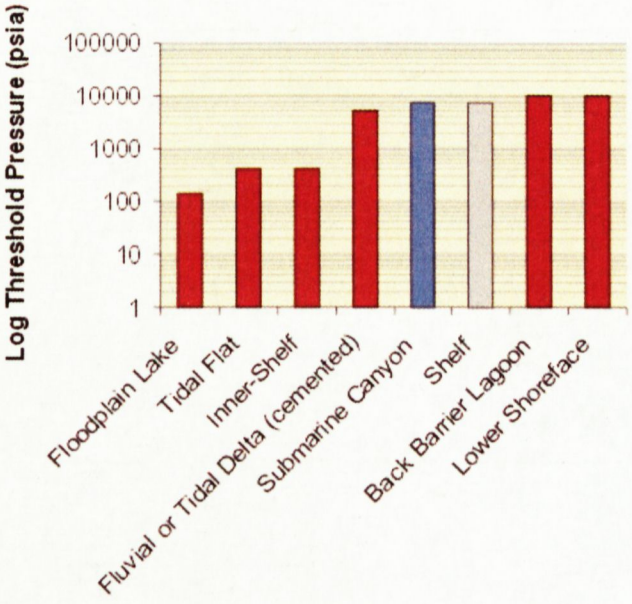

Figure 5.11—Threshold pressure for different depositional facies represented in the study area. The highest threshold pressures are associated with shales deposited in a lower shoreface environment.

In the absence of four-way structural closure, the typical behaviour of SC CO_2 is to concentrate and spread under impermeable sealing layers. Consequently, where a migration/residence time trap strategy is employed, the maximum SC CO_2 column height will probably be equivalent to the height of localised four-way structural closure beneath the regional seal. Four-way structural closures in the study area are generally associated with hydrocarbon accumulations at present (e.g. Barracouta, Snapper, Marlin fields). The maximum height of structural closure along the expected migration path of the CO_2 is no more than 200 m – 300 m. As a result, the seal capacity can be expressed quantitatively as a ratio of the maximum required SC CO_2 column height to the maximum SC CO_2 column that can be supported by a particular sealing facies.

Table 5.1: CO_2 column heights calculated from MICP data for depositional facies in the study area.

Seal Facies	Threshold Pressure (psia)	CO_2 Column (m)
Fluvial Overbank	140	15
Tidal Flat	408	44
Back-Barrier Lagoon	9967	1070
Fluvial or Tidal Delta (cemented)	4978	534
Peat Swamp (Coastal Plain)	(no intrusion)	(high)
Lower Shoreface	9979	1072
Gurnard Formation	416	45
Marlin/Turrum Channel Complex	6968	748
Lakes Entrance	7053	757

Seal Geometry

The geometry of relative thick regional sealing units can be measured through seismic mapping. The Lakes Entrance and Turrum formations are above seismic resolution so their lateral extent was measured directly. The Gurnard Formation is easily identifiable on wireline logs so its lateral extent was estimated from wireline correlation between wells. However, the lateral extent of intraformational seals cannot be directly measured and was estimated based on analogue measurements of fine-grained units that are interpreted to represent the same depositional facies instead (Fig. 5.12 and Appendix II).

The seal geometry can be expressed as a ratio of the estimated lateral extent of the sealing facies and the area of 3-way closure associated with the regional anticline in the study area. The area of structural closure is (~1200 km^2), and is defined from the western edge of Barracouta Field to the eastern spill point of the anticline at the Marlin Canyon feature. For example, the Lakes Entrance Formation is assigned a value of one (1200 km^2 / 1200 km^2), whereas the Gurnard Formation is interpreted to exist over approximately one quarter of the area of structural closure, so is assigned a value of 0.27 (~ 320 km^2 / 1200 km^2).

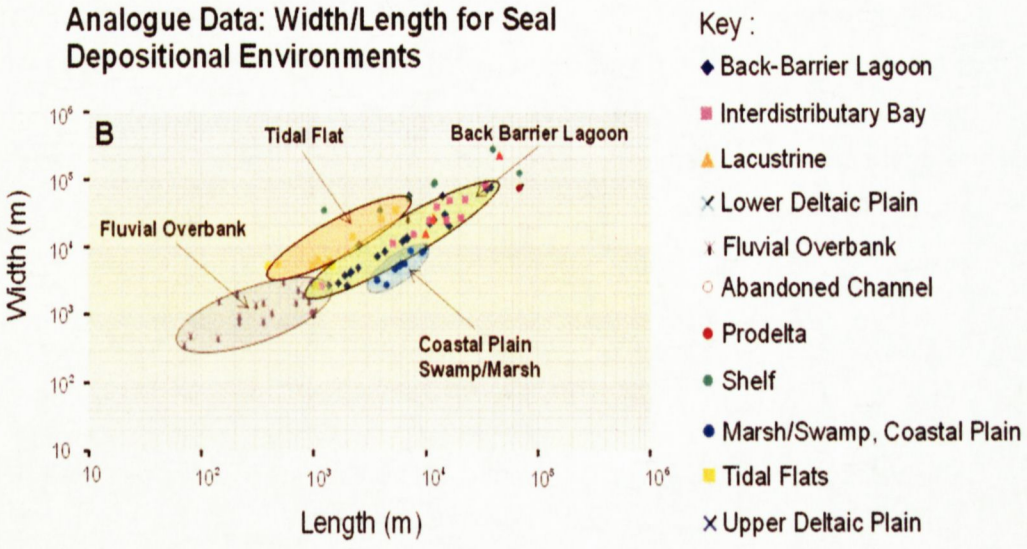

Figure 5.12—Analogue data of lateral extent for fine-grained facies of various depositional environments.

The areal extent of sealing facies from different depositional environments is derived from analogue data, as discussed previously. Quantifying the contribution to seal potential made by sealing facies where the lateral extent is estimated from analogue data is associated with uncertainty because:

- Analogue measurements commonly vary for a particular depositional environment by more than an order of magnitude.
- The spatial position and orientation of the sealing facies is not known relative to the area of closure except at well intersections.

Despite the variability of measurements derived from analogues, they remain useful because areal extent does vary significantly between depositional environments despite the high variation of areal extent within a single environment. Consequently, analogue measurements can be used to compare the relative effectiveness of different kinds of sealing facies. An arithmetic mean of analogue measurements is used to calculate the ratio of areal extent of closure to areal extent of sealing facies.

There is a chance that a sealing facies may be positioned partially outside structural closure so that only a percentage of its total areal extent may be useful for sealing. For example, the total areal extent of the Gurnard Formation in the Gippsland Basin exceeds the areal extent of structural closure at the ESSCI site, but the Gurnard Formation fills only 27% of the area within structural closure at the ESSCI site. If

seals cannot be deterministically mapped the probability that they will exist partially outside structural closure must be calculated and applied to the seal geometry rating, so that they are compared with the regional sealing facies in an unbiased way. The ratio used to evaluate seal geometry for analogue seals, where the lateral position of the seal cannot be seismically mapped or correlated reliably between wells can be simplistically described as:

$$Seal\ Geometry\ Ratio = (\pi(r_{As} + r_{Af})^2 - As)\,Af$$

...where *As* is the area of structural closure, r_{As} is the radius of a circle of area *As*, *Af* is the average area of the seal facies, and r_{Af} is the radius of a circle of area *Af*.

Table 5.2: Lateral extent of sealing units in the study area.

Seal Facies	Min. Areal Extent (km^2)	Max. Areal Extent (km^2)	Areal Extent (km^2)	Ratio
Regional Seal Facies				
Lakes Entrance	n/a	n/a	1200	1.000
Marlin/Turrum Channel Complex	n/a	n/a	274	0.230
Gurnard Formation	n/a	n/a	320	0.270
Intraformational Seal Facies				
Back-Barrier Lagoon	2.50	3000.00	369	0.154
Lower Shoreface	9.00	4900.00	297	0.124
Peat Swamp (Coastal Plain)	10.50	79.90	73	0.030
Tidal Flat	1.60	17.82	11	0.005
Fluvial Overbank	0.28	2.70	2	0.001

Figure 5.13 summarises the effectiveness of various sealing facies in terms of their geometry based on data provided in Table 5.2. Predictably, regional extensive, seismically mappable units rank highest, like the Lakes Entrance Formation. In terms of seal facies that could not be deterministically mapped, back-barrier lagoon and lower shoreface facies rank the highest because they are typically very laterally extensive as indicated by analogue measurements (Fig. 5.12).

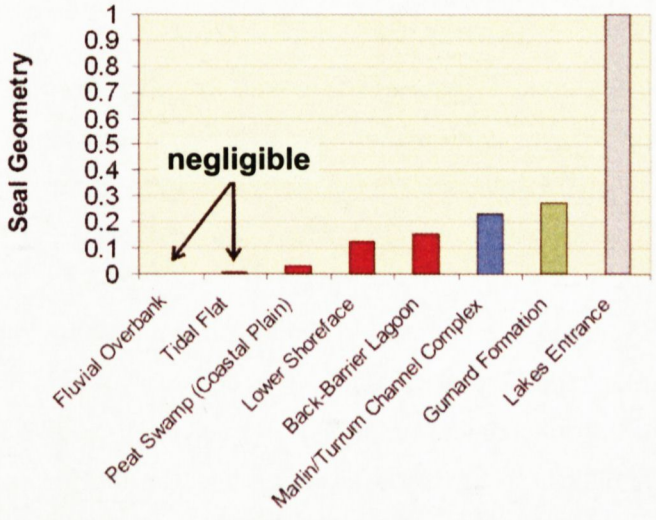

Figure 5.13—Comparison of seal geometry for different sealing units of the study area.

SEAL INTEGRITY

Seal integrity is a function of rock compressibility and ductility (Kaldi & Atkinson 1997). Values for seal integrity were assigned based on published relationships between lithology, and compressibility and ductility (Fig. 5.14).

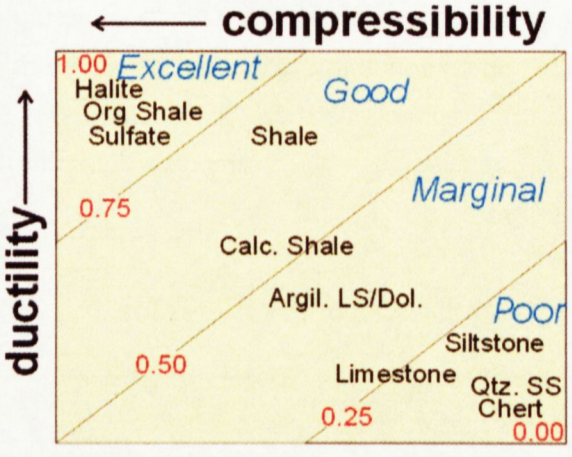

Figure 5.14—Rock compressibility and ductility for different lithologies. Figure modified from Kaldi and Atkinson (1997).

Significant lithological factors that influenced the values assigned to seal facies for assessing seal integrity included:

- Proportion of calcareous material
- Proportion of siltstone and sandstone

- Proportion of carbonaceous material.

For example, the seal integrity of the Lakes Entrance Formation was downgraded because it consists in part of marl. Small-scale faults within the Lakes Entrance Formation are an indication of brittle deformation in parts of the formation, while surrounding sealing units appear to have deformed ductilly (Fig. 3.7).

The calcareous component of sealing lithologies may also be important in the context of chemical reactions induced by CO_2. The possibility exists that chemical reaction could change the mechanical properties of sealing lithologies over geological time. However, it is difficult to envisage a unit as thick as the Lakes Entrance Formation being significantly chemically altered by CO_2. Large-scale flow of CO_2 through the Lakes Entrance Formation is unlikely, as indicated by its seal capacity, so the amount of rock available for reaction would be limited. Glaucony in the Gurnard Formation may also induce chemical reaction with CO_2. The prospect of large-scale alteration of mechanical properties appears more likely with the Gurnard Formation because of relatively low seal capacity.

Environments where fine-grained rocks are commonly characterised by mixed or interbedded coarser grained siltstone and sandstone are also downgraded in terms of seal integrity. For example, siltstone and sandstone interbeds in fine-grained samples from fluvial overbank and tidal flat environments are common. Fine-grained facies from depositional settings high in carbonaceous material, resulting in a high proportion of carbonaceous mudstone, are likely to have better seal integrity than facies from settings characterised by pure siliciclastic input.

Table 5.3: Seal integrity for different sealing facies of the study area.

Seal Facies	Integrity Value	Comments
Fluvial Overbank	0.375	Silt and sand size grains are common.
Tidal Flat	0.375	Silt and sand size grains are common.
Back-Barrier Lagoon	0.75	Carbonaceous shale is common.
Fluvial or Tidal Delta (cemented)	0.25	Pervasive cementation in the samples used in this study is likely to reduce integrity.
Peat Swamp (Coastal Plain)	0.75	Carbonaceous shale is common.
Lower Shoreface	0.375	Silt and sand size grains are common.
Gurnard Formation	0.625	Relatively good integrity.
Marlin/Turrum Channel Complex	0.5625	Marl reduces overall integrity.
Lakes Entrance	0.5625	Marl reduces overall integrity.

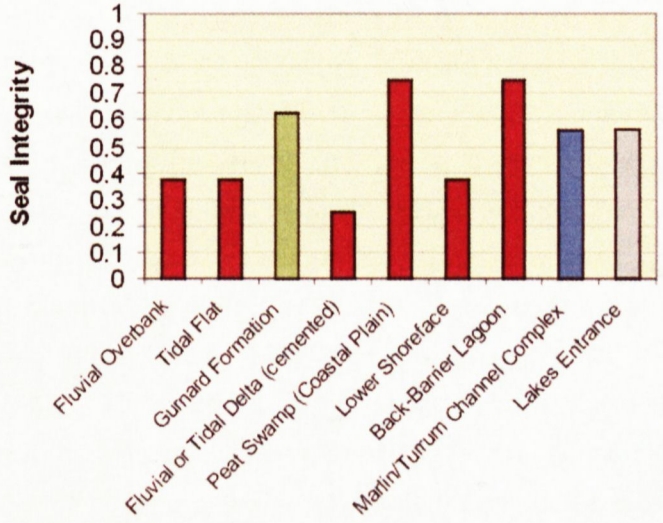

Figure 5.15—Comparison of seal integrity for different sealing units of the study area.

The three component properties of seal potential—capacity, geometry and integrity—can be combined to yield a semi-quantitative ranking of seal potential for all sealing facies represented in the study area (Fig. 5.16).

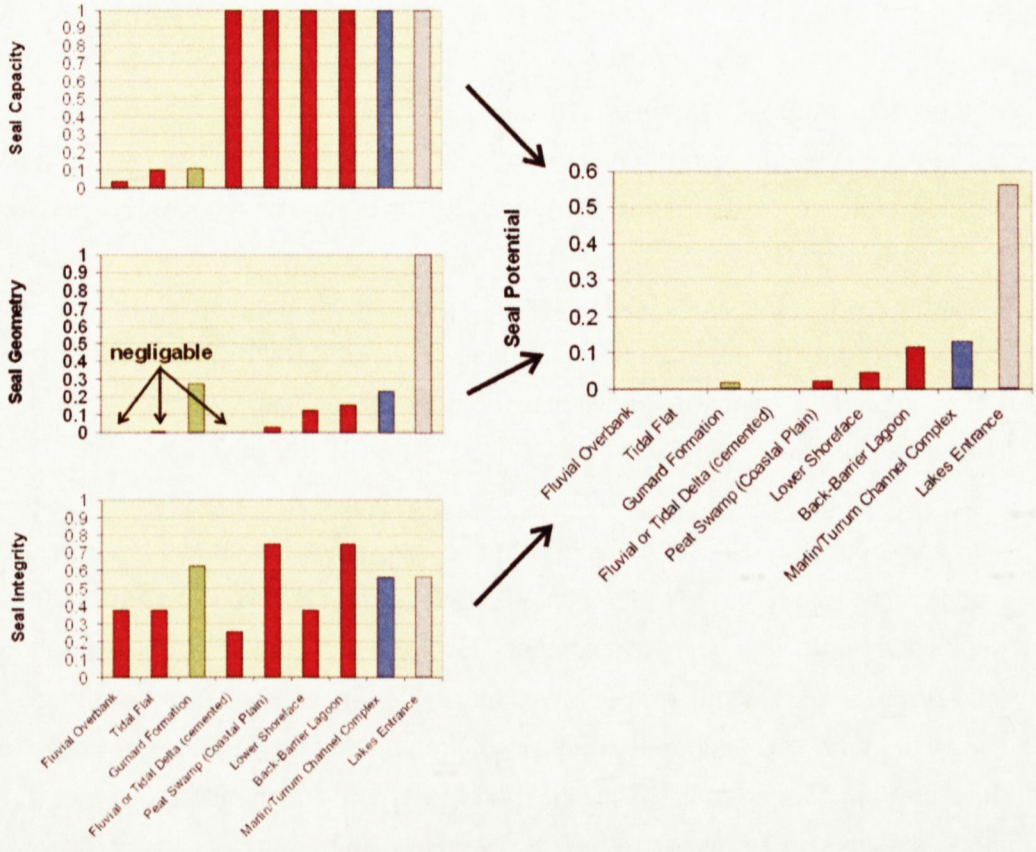

Figure 5.16—Values for seal capacity (A), seal geometry (B), and seal integrity (C) are multiplied to calculate seal potential (D). The Lakes Entrance Formation has the best seal potential in the study area.

Discussion of Seal Potential

The semi-quantitative approach to evaluating top seal potential used here provides an unbiased method for comparison of different sealing units. The good seal potential Lakes Entrance Formation is not an unexpected result, however, the process of quantitative evaluation provides confidence that all of the component aspects of seal potential have been assessed. The presence of several hydrocarbon accumulations in the study area, sealed by the Lakes Entrance Formation, provides additional confidence in its good seal potential. The seal potential of the Lakes Entrance Formation is the over-riding issue in the context of CO_2 storage in the Gippsland Basin ESSCI because it is everywhere present within the study area and because all other seal facies exist below the Lakes Entrance Formation.

The sealing facies below the Lakes Entrance Formation remain important despite the fact that the Lakes Entrance Formation is the most critical unit in terms of regional seal potential. Intraformational sealing facies will influence the subsurface behaviour of SC CO_2. The importance of intraformational seals is illustrated by CO_2 injection at Sleipner-Vest Field in the North Sea (see Chapter 1). A similar scenario to the one observed at Sleipner-Vest may occur in the Gippsland Basin where SC CO_2 flattens and spreads under intraformational sealing units due to gravity effects as it migrates up-section. The spreading behaviour of SC CO_2 is important in terms of improving storage efficiency and in terms of reducing the migration rate of SC CO_2 by inducing a tortuous migration path. Consequently, the presence of intraformational seals will probably be beneficial for CO_2 storage, provided sealing units do not result in pressure compartmentalisation. In the case of the Gippsland Basin ESSCI, pressure data suggest that compartmentalisation does not occur within the area and interval of interest (Root *et al.* 2004).

The seal potential evaluation has shown that intraformational seals are likely to have significantly different seal potential depending primarily on the environment of deposition and diagenetic cementation. Back-barrier lagoon and lower shoreface intraformational sealing facies have much better sealing qualities than fluvial overbank, tidal flat, tidal delta, and swamp/marsh sealing facies. The implication is that intraformational seals in lower shoreface-shelf and nearshore facies may be more effective in terms of reducing the migration rate and possibly in terms of improving storage efficiency than seals in the coastal-alluvial plain facies.

Fault Seal Potential—Empirical Evaluation

The evaluation of seal potential can be partially evaluated through empirical geophysical methods. Side aperture radar and SNIFFER surveys have been carried out by Geoscience Australia in the Gippsland Basin. Airborne side aperture radar surveys can detect slicks on the sea surface and SNIFFER surveys conduct geochemical analysis of seawater near the seabed. Hydrocarbon leakage from the subsurface may be associated with hydrocarbon in the water column or hydrocarbon slicks at the sea surface.

Trap breach due to fault seal failure appears to be limited in the Gippsland Basin based on previous literature. However, 'leaky faults' are mentioned with reference to Snapper Field (Glenton 1988; Fig. 5.17), and Roder & Sloan (1986) conclude that the N – S-trending fault that bisects Barracouta Field has not sealed to gas over geologic time (Fig. 5.18). Both Snapper and Barracouta fields are characterised by faults that cut the BaseSeal surface and are associated with large displacement relative to other faults of the study area. In general however, the central deep area is characterised by good trap integrity regionally—most faults associated within hydrocarbon charged structural closure appear to have sealed over geologic time.

Like the faults at Barracouta and Snapper fields that may have leaked in the geologic past, normal faults in the west of the study area, near Tarwhine-1, and to the south-south-west of the Swordfish-1, Salmon-1, and Veilfin-1 area also cut the BaseSeal surface and are associated with relatively large displacement (Fig. 5.19). Additionally, faults situated near the basin margins or towards landfall (northern and western parts of the study area) are more likely to cut the BaseSeal surface and are associated with more displacement than other faults mapped in the study area.

SNIFFER survey data suggest that hydrocarbon leakage is associated primarily with the Rosedale Fault system, north of the ESSCI structural closure. Within the study area only the Seahorse and West Seahorse areas and areas northeast of Marlin/Turrum fields show evidence of hydrocarbon in the water column (Fig. 5.20). There is no evidence of present day hydrocarbon leakage associated with faults along the expected flow path for CO_2 in the study area.

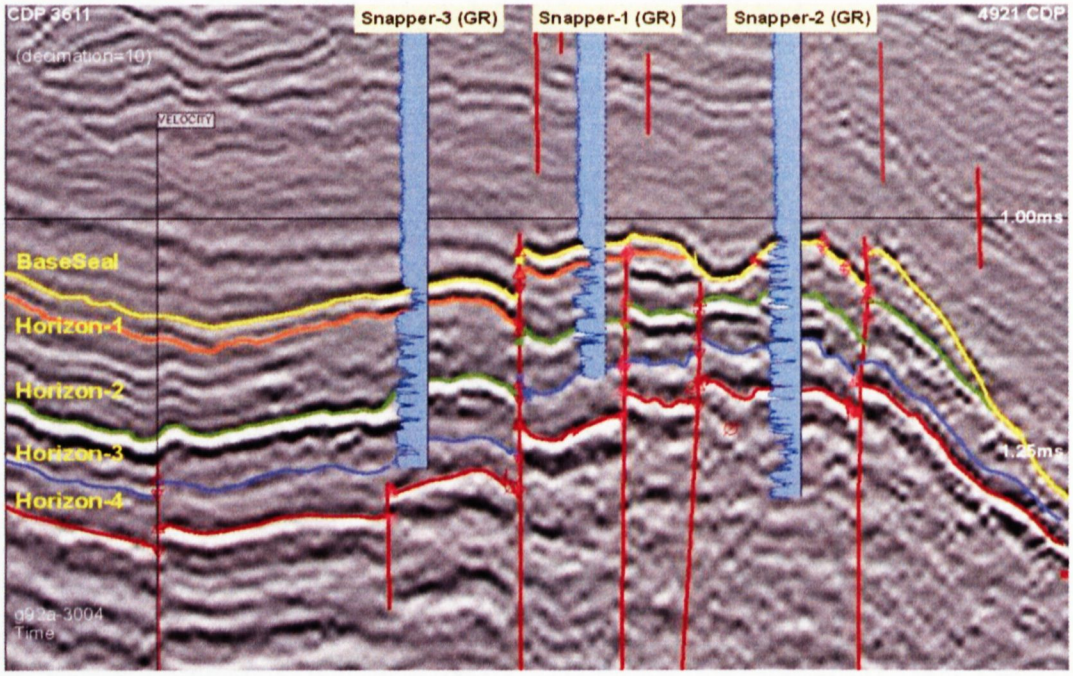

Figure 5.17—West to east seismic line at Snapper Field.

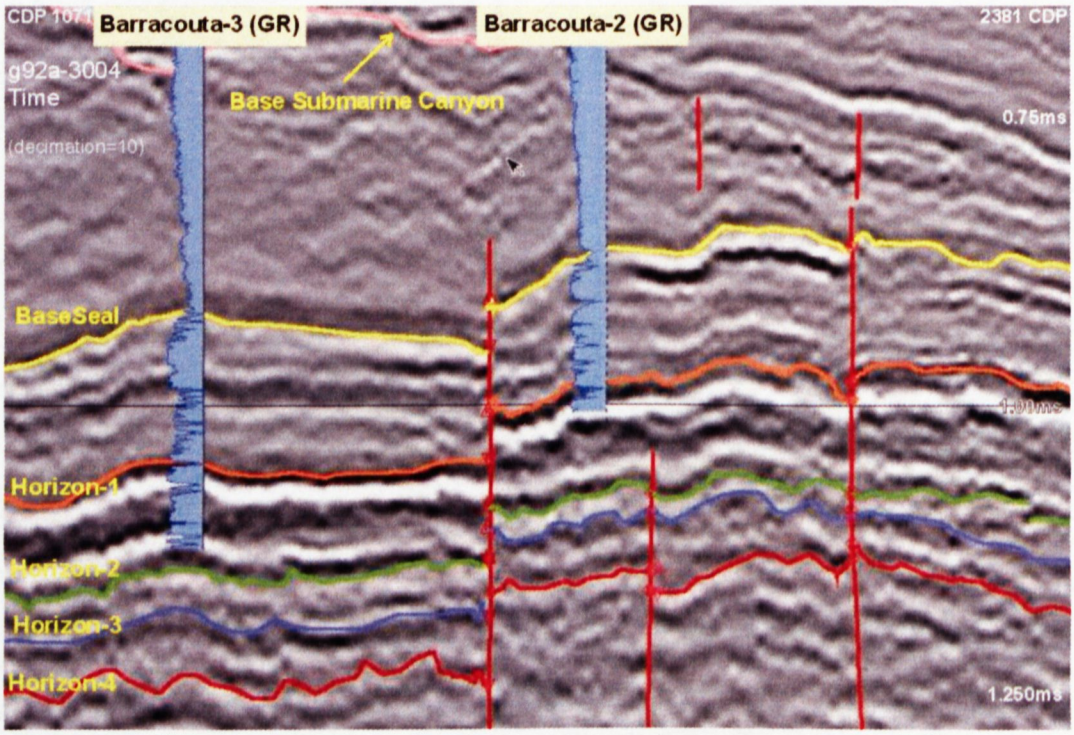

Figure 5.18—West to east seismic line at Barracouta Field. The fault cutting the Barracouta structure (between Barracouta-2 & Barracouta-3) may not have sealed to gas over geologic time.

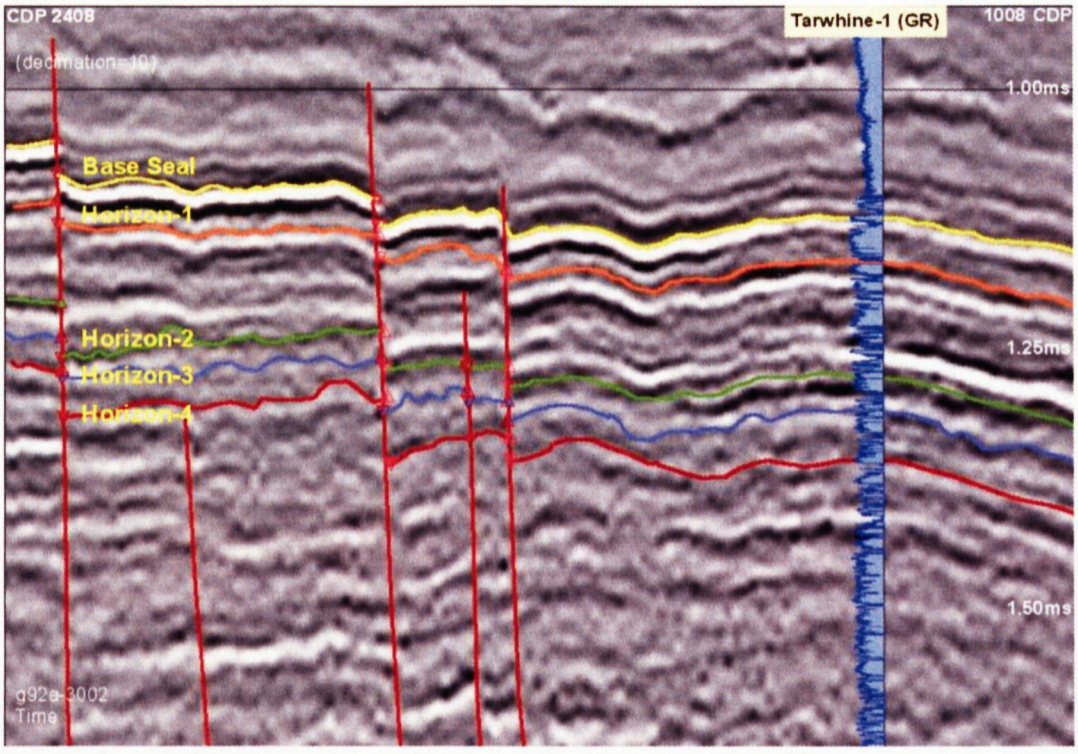

Figure 5.19—Southwest to northeast seismic line in the area near Tarwhine-1. The faults west of Tarwhine are associated with significant displacement and cut the BaseSeal surface.

The likelihood of fault seal failure is a function of the *in situ* stress conditions relative to the geometry, dip and orientation of the fault, the nature of the fault rock and pore pressure. A geomechanical study was carried out in parallel with this study that evaluates the fault seal potential (Streit 2003, Root *et al.* 2004; see Appendix I).

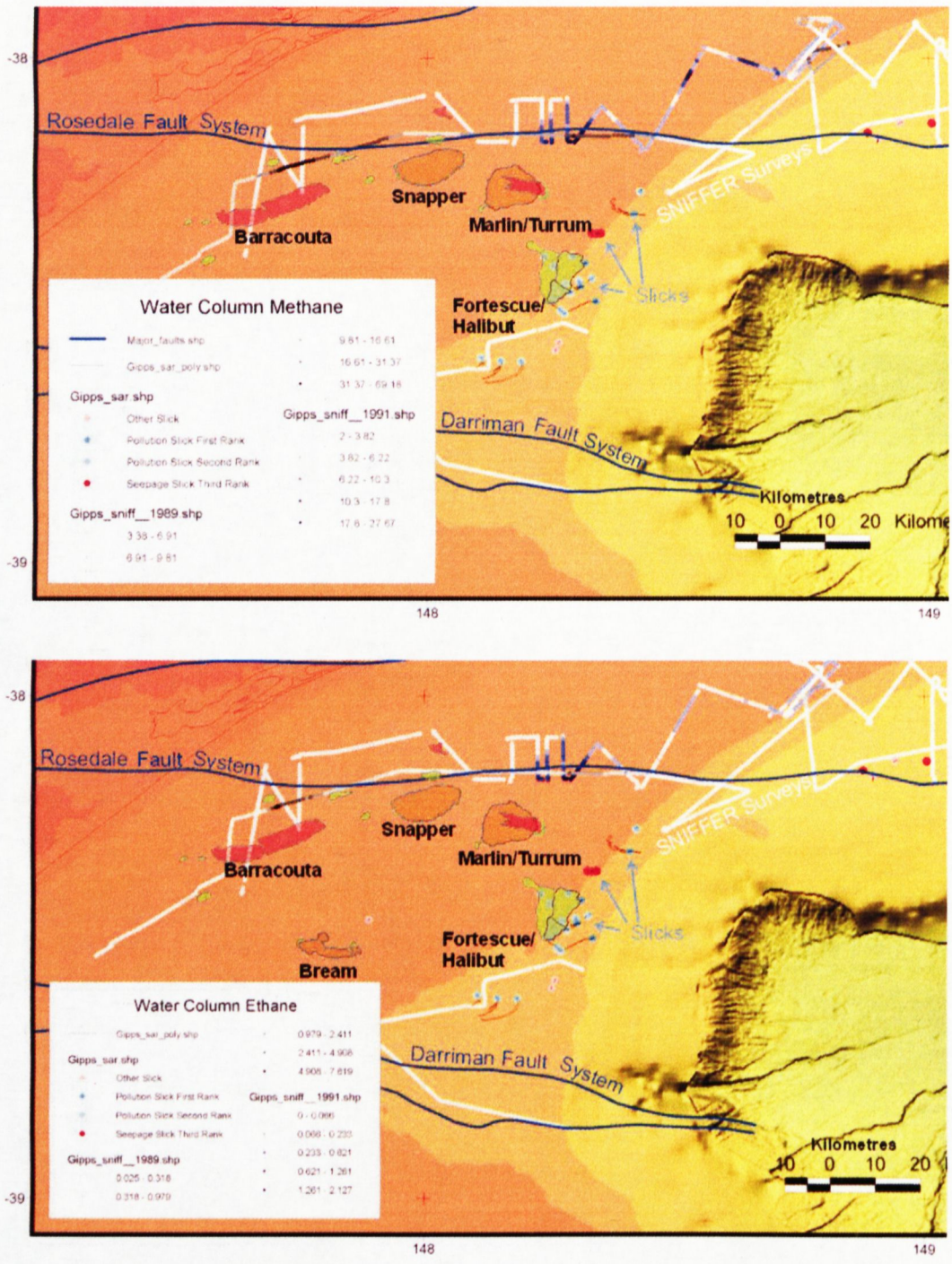

Figure 5.20—Modern day Gippsland bathymetry with SNIFFER survey and SAR data. Methane (above) and ethane (below) in the water column is shown. Leakage of hydrocarbon may be occurring associated with the Rosedale Fault System to the north of the study. Areas of relatively high hydrocarbon leakage can be identified northeast of Marlin/Turrum fields and north of Barracouta Field in the area of Seahorse and West Seahorse fields.

Chapter 6—Geological Model Construction

Abstract

A cellular geological model of the Gippsland Basin 'central deep' area was constructed for flow simulation of CO_2 injection and storage. Features of the geological model such as large-scale zone geometry, grid cell size, and layering style represent the structure and stratigraphic architecture in the study area. Other important subsurface features such as porosity, permeability and facies as well as pressure/temperature conditions are represented in the geological model by attributes, which are values assigned to the grid cells. Attributes were populated in the geological model using a combination of deterministic and stochastic techniques. Sequential gaussian simulation and co-located gaussian co-simulation were used to populate porosity and permeability, respectively, using facies as a classifying attribute.

Based on the geological model, an injection strategy was proposed and estimates of CO_2 capacity were made. The most effective strategy for CO_2 injection and storage may be injection in the structurally low Salmon-1/Swordfish-1/Conger-1 area with long-distance migration (>50 km) due primarily to buoyancy effects, up-dip and up-stratigraphy northeast towards Marlin/Turrum fields, then west-south-west through Snapper Field to Barracouta Field. The strategy leverages four-way structural closures along the expected migration path of the CO_2, which is the key short-term trapping mechanism (10s – 100s of yrs), and CO_2 dissolution into formation water, which is the key long-term trapping mechanism (1000s of yrs). However, irreducible CO_2 along the migration path, localised structural and stratigraphic traps due to reservoir heterogeneity, and mineralogical trapping are also likely to make a contribution to total capacity.

CO_2 capacity estimates suggest that a 'most likely' estimate of 26 tcf of CO_2 could be stored within structural closures in the study area. Additional storage capacity is likely to result from unconventional trapping techniques like dissolution, gas trapping and mineralogical trapping (P10 = 26 tcf; P50 = 36 tcf; P90 = 48 tcf). The most important limit on capacity is structure and the associated risk of filling Barracouta Field beyond spill point, which would result in CO_2 migration towards onshore aquifers, bubble point pressure/temperature conditions, and the zero edge of regional sealing facies.

Introduction

A key benefit of the geological model is that it provides a spatial framework for integrating a large amount of subsurface information stemming from reservoir characterisation. In the case of the Gippsland Basin ESSCI, sedimentological (Chapter 2), structural and stratigraphic (Chapter 3), as well as geostatistical data (Chapter 4) are integrated in the geological model in addition to petrophysical, pressure, temperature and salinity data, which are discussed in this chapter. The capillary properties of fine-

grained sealing facies (Chapter 5) are not directly integrated into the model at the geological model building stage, but are useful in assessing flow simulation results. For example, if a particular scenario resulted in large CO_2 accumulations where column heights approached critical values near the maximum seal capacity for a particular sealing unit, the injection and storage strategy would have to altered.

Attributes, which are values assigned to grid cells in the geological model, are used to represent reservoir/aquifer properties like facies, permeability and porosity. The values assigned for these properties at the wells stem from an understanding of the sedimentological and petrophysical characteristics of the rock. The way in which the properties are spatially populated between wells is primarily a function of the geometry, orientation and distribution of depositional features in the subsurface, and the statistical models used to describe their spatial continuity. Diagenesis alters primary reservoir/aquifer properties, so the impact of diagenetic events must also be captured in the geological model as well.

In addition to attributes, the grid cells, layers, zones and faults in the geological model, must accurately represent the shape and compartmentalisation of the aquifer/reservoir. These characteristics of the geological model provide the framework into which attributes are populated. In this chapter, the construction of the Gippsland Basin ESSCI geological model is described with reference to its constituent parts: grid cells, layers, zones, and attributes.

Methodology

PETROPHYSICS

Petrophysical evaluation of 20 wells in the study area was done by Tim O'Sullivan (Saros Group). Permeability (k), porosity (∅), shale volume (Vsh), water saturation (Sw) logs and a coal flag were produced for each well. The petrophysical data is provided in O'Sullivan (2002).

Wireline log suites from the following 20 wells were used for petrophysical analysis: Barracouta-1, Barracouta-5, Conger-1, Emperor-1, Fortescue-1 Fortescue-2 Halibut-1, Luderick-1, Marlin-2, Marlin-4, Moonfish-2, Salmon-1, Seahorse-2, Snapper-2, Snapper-

5, Swordfish-1, Tarwhine-1, Whiting-1, Wirrah-1, and Wrasse-1. Wells were selected for petrophysical evaluation based on the spatial position of the well, the quality of wireline data, and the availability of routine and special core analysis including MICP over the interval of interest.

The majority of wells had a limited wireline log suite, so a deterministic methodology was used for petrophysical analysis. Wireline log suites were quality controlled and environmentally corrected prior to analysis. Where possible, petrophysical analysis was carried out with reference to mudlogs, cuttings descriptions and core analysis. The specific methodology employed for petrophysical analysis is described in O'Sullivan (2002).

Model Geometry

Among the first order controls on the behaviour of a fluid in the subsurface is the shape and volume of the 'container' in which the fluid is stored. In the case of a geological model the shape of various containers at different scales is defined by grid cells, layers, and zones. These are represented in a cellular geological model that was constructed using the GeoVisual GeoCard geological modeling software.

GRID CELL SIZE

The selection of grid size is influenced by the desire to represent realistic reservoir heterogeneity and by computational limitations. Reservoir heterogeneity is virtually a scaleless characteristic ranging from pore-scale heterogeneity (~10^{-5} m -10^{-3} m) to regional heterogeneity that stems from large-scale basin structure and stratigraphy (~10^{4} m -10^{5} m). Conceptually, increasingly detailed grids more accurately represent 'real' reservoir heterogeneity to an extremely detailed lower threshold. However, practical computational restrictions generally limit grid size to several million cells for the geological model* and ideally, a few hundred thousand cells for the simulation model. Consequently, some reservoir heterogeneity will always be 'lost' by representing real

* Deutsch (2002) and Liu *et al* (2000) identify 100 million cells as the upper practical limit in the petroleum industry; however, computational limitations for this study are considerably greater.

rock in a cell-based model. However, an understanding of the amount of heterogeneity that is lost and the areas of the geological model that will be most affected is useful.

Moving from the relatively detailed geological model to the simulation model is an up-scaling and up-gridding problem that is further discussed later in this chapter. However, even the grid cell size in a geological model prior to up-scaling and up-gridding has a lower threshold that is also governed by computational limitations; extremely detailed models are expensive to store and slow to visualise and manipulate. On the other hand, overly simplistic geological models have often lead to failed predictions in the petroleum industry (Chambers 2000), and consequently, are likely to lead to failed predictions for CO_2 geosequestration as well. In the case of CO_2 geosequestration, extremely large areas must be modeled so the problem of initial grid cell size is more pressing than it would be in a typical hydrocarbon development/production or natural gas storage scenario.

The lateral extent of grid cells in geological models is characteristically much greater than the thickness of grid cells as a result of the typical disparity of vertical to horizontal anisotropy in sedimentary rocks (Chapter 4). However, the areal extent to thickness ratio of the grid cells should be sufficient to accurately model the flow units (e.g. depositional facies) represented in the geological model. This point is relevant in the context of models for CO_2 geosequestration, because typically, where a residence/migration time trap is used a very thin but laterally extensive geological model must be built. This is because CO_2 will concentrate under low permeability units and migrate laterally over long time frames and large areal distances in most settings. As a result, it is convenient to reduce computational expense by using thin, very laterally extensive grid cells. However, there is a point at which reservoir heterogeneity can no longer be accurately represented; few naturally occurring flow units will have an aspect ratio similar to a sheet of paper.

In terms of both thickness and lateral extent grid cell size in excess of the size of depositional elements will result in the loss of geological detail. Below an algorithm is used to calculate the optimum gird cell size for the Gippsland ESSCI geological model based on the total volume of the model. The resulting grid cell size is then compared to the dimensions of flow units that need to be represented in the model.

The total volume that must be represented by the Gippsland ESSCI geological model is:

$$X \times Y \times Z = 72000 \times 40000 \times 2000 = 5.76 \times 10^{12} m^3$$

The optimum grid cell size is given by (Deutsch 2002):

$$\frac{72000}{da} \times \frac{40000}{da} \times \frac{2000}{ds} = gc$$

...where *da* is the areal extent of an individual grid cell, *ds* is the minimum grid cell thickness required to capture reservoir heterogeneity and *gc* is the number of grid cells. Solving for *da* using 5m for *ds*, and 2M for *gc*, yields an areal grid size of 1157m (~1km). The number of cells in the model is 2.1M with a cell geometry of 1000m × 1000m × 5m; however, only ~250 000 of the 2M cells are active* (Fig. 6.1).

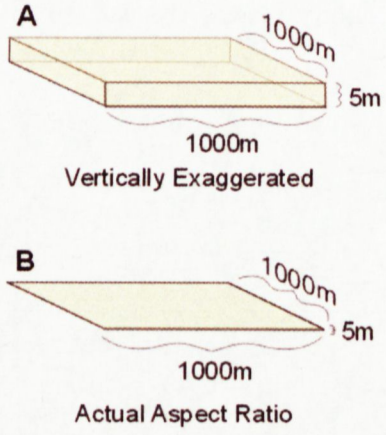

Figure 6.1—Grid cell size used in the geological model. The actual aspect ratio is included to illustrate the balance between using large grid cells due to computational limitations and accurately representing reservoir heterogeneity. Note that larger grid cells are used in the Seal zone and Lower *M. diversus* & *L. balmei* zone (base and top of the model).

One km^2 in the horizontal plane is near the upper areal limit for representing reservoir heterogeneity according to measurements taken from analogue data from similar depositional environments to those represented in the Gippsland Basin. Figures 6.2 & 6.3 plot typical geometry of depositional elements that are likely to act as flow units in the study area (e.g. channels, barrier islands etc...) versus grid cell size used in the model.

* Some parts of layers that are associated with truncation, pinch-out, and down-lap have cells of zero thickness, which are made inactive.

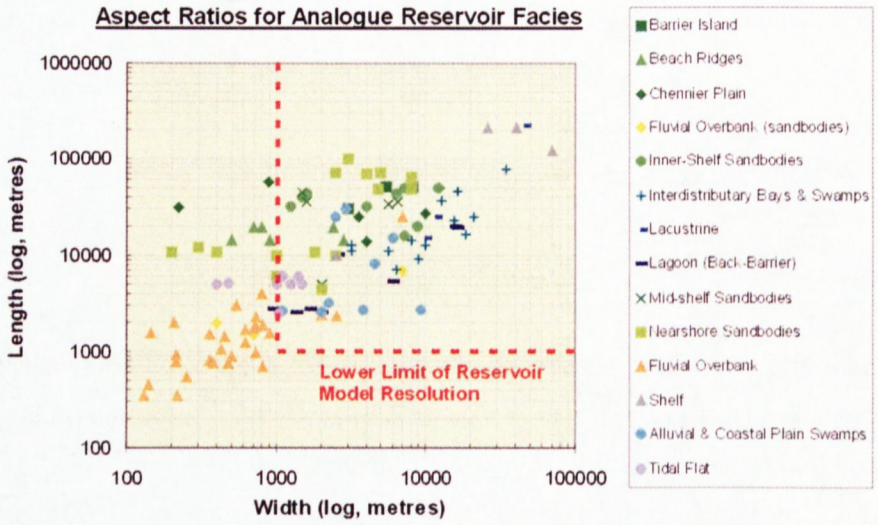

Figure 6.2—Comparison of grid cell size and width to length aspect ratios of depositional facies. The aspect ratios were derived from depositional analogues for facies that are interpreted to be represented in the study interval. Some facies are likely to be below the resolution of the model (e.g. fluvial overbank facies-orange triangles). Data and sources are provided in Appendix II.

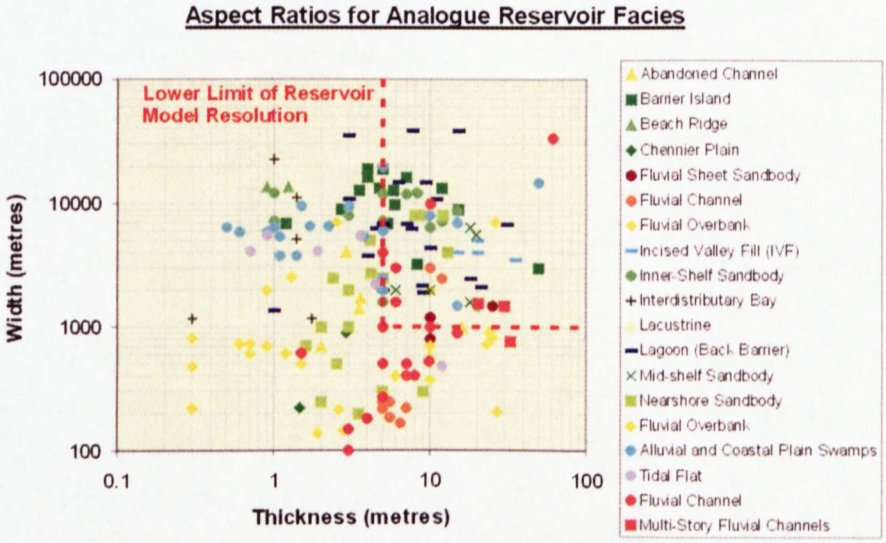

Figure 6.3—Comparison of grid cell size and thickness to width aspect ratios of depositional facies. The aspect ratios were derived from analogues for facies that are interpreted to be represented in the study interval. The graph suggests that some heterogeneity may be lost—particularly in fluvial/alluvial depositional settings—because of the relatively thick grid cells that are used in the model. Data and sources are provided in Appendix II.

Figure 6.2 and 6.3 give an indication of the geological detail that will be sacrificed by using a grid cell size of 1000 m × 1000 m × 5 m. The lateral extent of the grid cells is sufficient to represent most nearshore features, but fluvial features are commonly less extensive than the grid cell size.

The artificial reduction of reservoir heterogeneity that is induced by using a relatively coarse grid size will impact fluvial/alluvial depositional environments more than it will impact other depositional environments that occur in the study area (Figs 6.2 & 6.3). This is because significant depositional elements in fluvial/alluvial depositional environments like fluvial channels, crevasse channels and splays and levees are relatively thin and laterally restricted. By comparison, nearshore marine depositional elements such as barrier islands, chennier plains, back-barrier lagoons and shoreface deposits are more aerially extensive and are also appreciably thicker. However, both fluvial and nearshore features are commonly less than 5 m in thickness, which introduces a vertical resolution challenge as well.

Techniques for sampling reservoir/aquifer properties from the wells and assigning them to the grid cells in order to reduce the impact of the thickness disparity are discussed later in this chapter. The lack of small-scale heterogeneity represented in the geological model is not likely to significantly impact estimates of capacity or migration rate at large scales provided the effective porosity and permeability that are assigned to the relatively coarse grid cells is reasonable. However, detailed flow patterns and the shape of the flow front will be inaccurate at small scales. The 1000 m × 1000 m × 5 m grid cell size pushes the boundaries of the hardware that is available for this study and is considered an acceptable trade off in the sense that investigating the small-scale details of CO_2 flow behaviour is not one of the primary objectives of this study.

Grid Orientation

The orientation of the grid was determined by the expected initial direction of flow of the CO_2 and by the orientation of faults within the geological model. The direction of flow must be considered when selecting the orientation of the grid because fluid flow through a grid cell is through the face of the cell and not through the corners of the cell at the intersection of cell faces. Consequently, natural subsurface flow is best represented

when the faces of a grid cell are perpendicular to the direction of flow. If the faces of grid cells are generally oblique to the direction of flow, unrealistic rugosity may be imparted to the flow paths (Fig. 6.4).

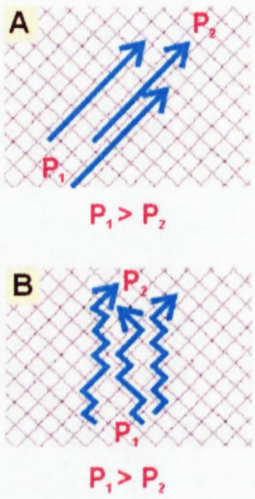

Figure 6.4—Conceptual flow lines showing flow paths parallel to the orientation of grid cell faces (A) and oblique to the orientation of grid cell faces (B).

The orientation of faults is important when selecting the orientation of the grid because faults can only be modeled along I or J in the horizontal plane. Fortunately, the expected initial direction of flow is oriented at approximately 90° to the strike of the main fault set in the study area so an optimum grid orientation was easily achieved.

New 'model axes' are defined by the orientation of the grid that are called I, J, (horizontal) and K (vertical). In the case of the Gippsland Model, I and J are offset by ~45° to the X and Y of 'normal' (Cartesian) space (Fig. 6.5). K and Z are coincident.

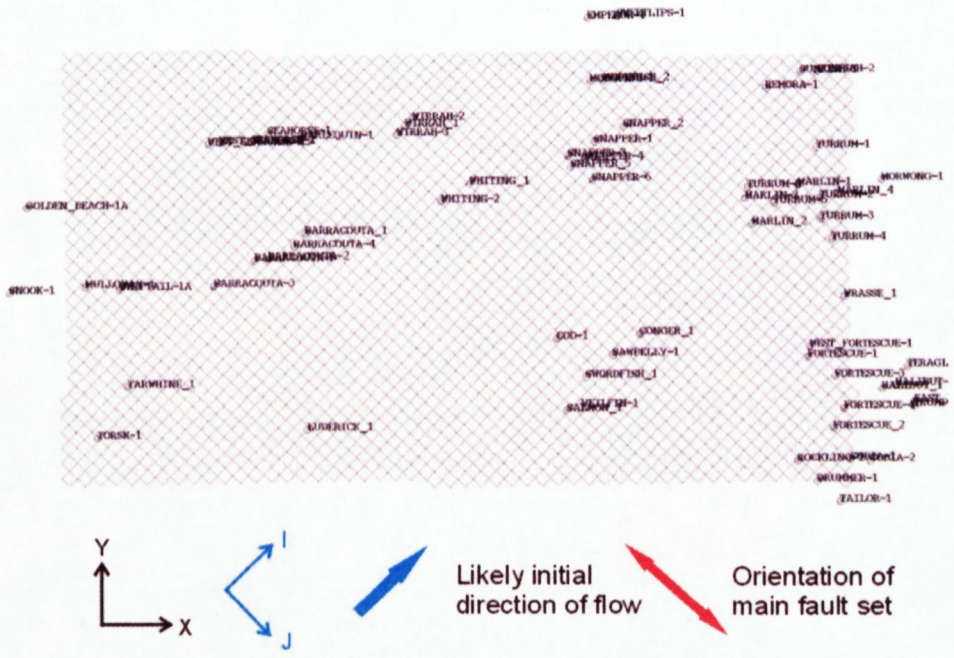

Figure 6.5—Geological model grid orientation. The grid is oriented at ~45° so that cells are both oriented parallel to the likely initial flow direction, and oriented parallel to the strike of the main fault set.

ZONES

Zones are defined by the five mapped seismic surfaces (Horizons 1 – 4 and BaseSeal) as well as copies of the seismic horizons 'phantomed' up or down. For example, the uppermost reservoir zone is called 'Middle & Upper *N. asperus*' and is defined by the seismic surfaces Horizon 1 and BaseSeal.

Zones are important features in the geological model because they reflect the structure characterised by the seismic interpretation. The layering style can be changed within each zone to represent smaller scale stratigraphic architecture. Table 6.1 lists the six zones used in this study and the surfaces that define them. The layering style and layering thickness for each zone is also provided.

Table 6.1: Zones and surfaces in the Gippsland Basin ESSCI geological model.

Zone Name	Colour	Upper Bounding Surface	Lower Bounding Surface	Layering style	Layer Thickness
Seal	Dark Green	BaseSeal – 50m (phantom)	BaseSeal	Proportional	10 m
Middle & Upper *N. asperus*	Yellow	BaseSeal	Horizon1	Parallel to base	5 m
Lower *N. asperus*	Light Green	Horizon1	Horizon2	Parallel to base	5 m
P. asperopolus	Red	Horizon2	Horizon3	Parallel to top	5 m
Mdl and Upr *M. diversus*	Light Blue	Horizon3	Horizon4	Parallel to top	5 m
Lwr *M. diversus* & *L. balmei*	Brown	Horizon4	Horizon4 + 100m (phantom)	Proportional	10 m

LAYERS

Layering represents the internal stratigraphy of each zone. The style of layering will significantly affect the flow behaviour of SC CO_2 because the geometry of the layers determines in part the spatial distribution of attributes within the model. An attribute sampled within a particular layer at a well location can only influence the values of attributes in grid cells of the same layer away from the well.

One of three different layering styles can be applied to a particular zone in the model. The layering styles are: 'parallel to the base of the zone', 'parallel to the top of the zone', and 'layers of proportional thickness' (Fig. 6.6). Each layering style can represent a different stratigraphic style. For example, 'parallel to base' will result in the truncation of layers at the top of the zone, suggesting an erosional unconformity. 'Parallel to top' will cause layers to down-lap onto older units. Proportional layering is good for representing stratigraphic continuity and causes lateral variation in layer thickness, which may be appropriate for a scenario involving syntectonic deposition, for example.

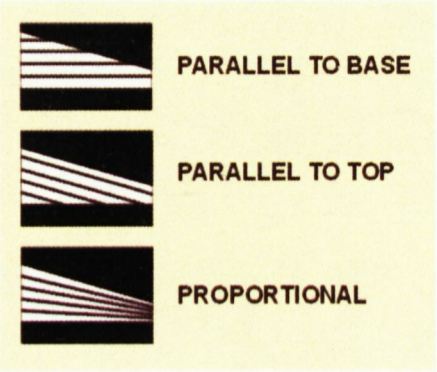

Figure 6.6—One of three layering styles can be applied to each zone in the geological model. These are parallel to the base of the zone, parallel to the top of the zone, and proportional layering.

A limiting aspect of layering style is that only one layering style may be applied to a single zone. Seismic interpretation suggests that bedding within the *P. asperopolus* zone is characterised by both downlap onto older units and truncation by the top Latrobe unconformity. In practice, the layering style that will have the greatest impact on flow behaviour is chosen.

The stratigraphic architecture of the Gippsland Basin ESSCI area is described in Chapter 3, and is expected to be important in terms of impact on the flow behaviour of SC CO_2. Therefore, it is important to represent the stratigraphic architecture realistically in the geological model. The Middle & Upper *N. asperus* zone and Lower *N. asperus* zone have layering parallel to base so that the truncation of layers by the top Latrobe unconformity is represented. The *P. asperopolus* zone and the Middle & Upper *M. diversus* zone have layering proportional to top so that downlap onto older units is represented. Layering style in the Lower *M. diversus & L. balmei* zone is proportional as is suggested by the geometry of seismic reflectors. The Seal zone is also proportionally layered. Both the Lower *M diversus & L. balmei* zone and the Seal zone were assigned thicker layers (10 m) than the rest of the model as large-scale flow of SC CO_2 is not likely to occur in these zones.

An unwanted result of the parallel to base layering style in zone Lower *N. asperus* is that it implies the existence of an erosional unconformity at the base of the overlying Middle & Upper *N. asperus* zone (Fig. 6.7A). However, the surface defining the base of the Middle & Upper *N. asperus* zone is interpreted to be a flooding surface, which is not associated with erosion. This incorrect representation of stratigraphic geometry is a

trade-off for correctly representing the truncation of layers in zone Lower *N. asperus* by the top Latrobe unconformity (base of Seal zone) in more distal parts of the study area, which is considered to be the more important stratigraphic relationship in terms of simulating CO_2 geosequestration.

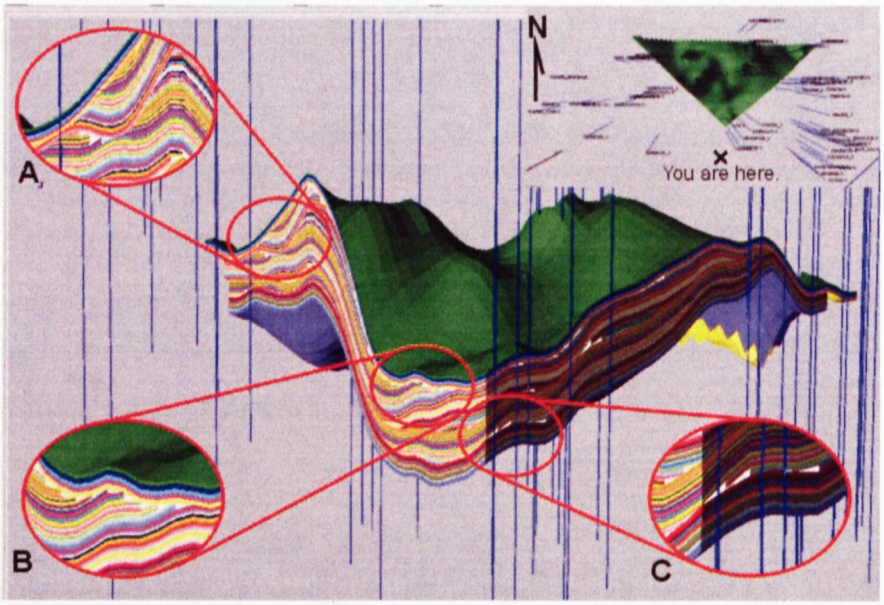

Figure 6.7—The grid is sliced along NE and SW trending axes to provide a view of its internal structure that results from the layering styles in the various zones. Truncation of reservoir units by the top Latrobe unconformity is shown (A & B). 'A' also shows truncation of the Lower *N. asperus* zone by the base of the overlying Middle & Upper *N. asperus* zone. 'C' shows downlapping stratigraphic relationships.

Attributes

Several attributes need to be represented in the geological model to characterise the subsurface behaviour of SC CO_2 through flow simulation. These are listed in Table 6.2.

Table 6.2: Attribute data included in the Gippsland Basin ESSCI geological model.

Attribute	Name	Units	Description
Capacity	CO2capacity	metres cubed	estimate of capacity for each grid cell; calculated from porosity, CO2 expansion factor and volume
Depth	CentreDepth	metres	true vertical depth to the centre of a grid cell
Expansion Factor for CO_2	CO2ExpansionFactor	scf/scf	expansion factor for CO2 from normal pressure temperature conditions to reservoir

Attribute	Name	Units	Description
			conditions
Facies	Template	1,2,3...n	categorical variable of facies type
Fault proximity	FaultProximity	metres	distance to nearest fault surface
Geothermal gradient	GeoGradient	deg. C/km	used to calculate temperature
Hydraulic head	HydroHead	pounds per square inch	present day hydraulic head in the study area
Permeability	KatWell_Arith	millidarcies	permeability at the wells only (derived from arithmetic mean of petrophysical measurements)
Permeability	KatWell_Harm	millidarcies	permeability at the wells only (derived from harmonic mean of petrophysical measurements)
Permeability	cosim_Karith_8000	millidarcies	permeability co-simulated from KatWell_Arith, using porosity as a secondary attribute and facies as a classifying attribute. Values over 8000 mD were not acceptable (six realisations)
Permeability	cosim_Kharm_8000	millidarcies	permeability cosimulated from KatWell_Harm, using porosity as a secondary attribute and facies as a classifying attribute; values over 8000 mD were not acceptable (six realisations)
Porosity	PhiAtWell	percent	porosity at the wells only (derived from petrophysical evaluation)
Porosity	SGS_Phi	percent	porosity populated in the geological model using SGS (six realisations)
Pressure	Pressure_MPa	megapascals	present day pressure in the study area
RMS amplitude	RMS_Amp	hertz	root mean square of seismic amplitude in zones; used for facies mapping
Salinity	Salinity	ppm (NaCl equivalent)	petrophysical estimates of salinity
Structural Closure	StructClosure	n/a	defines areas of 4-way structural closure along the expected migration path; used for capacity estimation
Water Saturation	Sw_Perm_High	percent	S_w populated using a logarithmic relationship with the cosim_Karith_8000 attribute
Water Saturation	Sw_Perm_Low	percent	S_w populated using a logarithmic relationship with the cosim_Kharm_8000 attribute
Water Saturation	Sw_Phi	percent	S_w populated using an exponential relationship with the SGS_Phi attribute
Temperature	Temperature	degrees centigrade	Horner plot temperature
Volume	Volume	metres cubed	volume of grid cell

The following sections describe each attribute type, discuss how the attribute was derived, and describe how the attribute was populated in the geological model. Some attributes require geostatistical models for realistic spatial population in the geological model. Understanding and describing the spatial continuity of a regionalised variable with semi-variogram and madogram models is addressed in Chapter 4.

Depth

A depth attribute was generated in the geological model called the 'CentreDepth' attribute, which is the true vertical depth at the centre of each grid cell in the geological model (Fig. 6.8). Depth is an implicit property in the geological model, however, depth as an attribute associated with each grid cell is important for generating other attributes. For example, temperature and pressure attributes are generated with functions using the CentreDepth attribute.

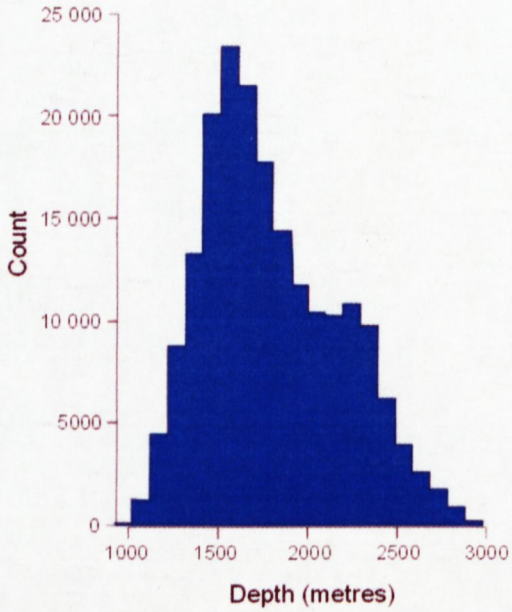

Figure 6.8—Histogram of the CentreDepth attribute that gives the depth to the centre of each grid cell in the model. The histogram shows that the majority of grid cells in the model exist between 1300 and 2400 metres.

Volume

The 'volume' attribute provides the volume in metres cubed of each of the grid cells in the geological model. Most cells have a volume of ~5.0 × 10^6 m^3 (1000 m × 1000 m × 5 m), however, some cells must be deformed to accommodate the geometry and layering

styles of the zones. Grid cells in the Lower *M. diversus & L. balmei* zone and the Seal zone have a volume of 1.0×10^7 m^3 (1000 m × 1000 m × 10 m). Unusually small grid cells are most common at zone boundaries, such as in areas where zones pinch out or are truncated (Fig. 6.9). Like the CentreDepth attribute, the volume of grid cells is implicit in the geological model, but is required to calculate other attributes (e.g. 'CO2VolumeExapansion') and is particularly useful for volumetric calculations.

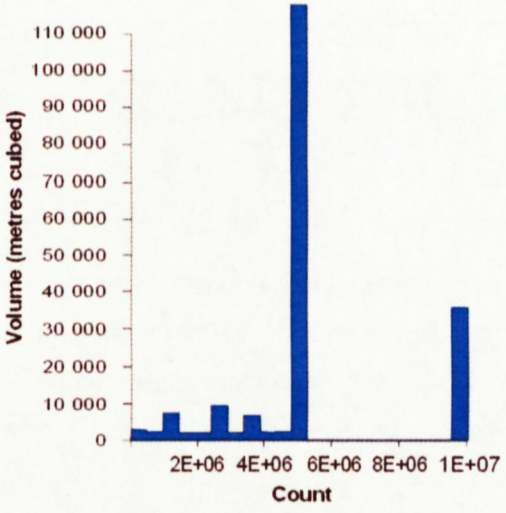

Figure 6.9—Histogram of cell volume attribute showing the volume of each active cell in the geological model.

FACIES

Facies maps for reservoir intervals Middle & Upper *N. asperus;* Lower *N. asperus; P. asperopolus;* Middle & Upper *M. diversus;* and Lower *M. diversus & L. balmei* were constructed from full-hole core, wireline logs and RMS amplitude maps (Chapter 3). Categorical variables representing lower shoreface-shelf, nearshore and alluvial-coastal plain facies were assigned to specific areas in each zone based on the facies maps (Fig. 6.10)

The categorical variables were assigned by constructing polygons that enclosed areas represented by a particular facies. Three polygons were applied to each zone (except the Seal zone and the Lower *M. diversus & L. balmei* zone) and numbers representing facies type were applied within the polygons.

Categorical variables are a representation or a label for facies type, so the numeric value of the categorical variable is of no consequence. However, the geological modeling software required that categorical variables are sequential. Each facies type in each stratigraphic unit of the geological model is assigned a different number (see Table 6.3).

Table 6.3: Categorical facies attributes in the Gippsland Basin ESSCI geological model.

CATAGORICAL FACIES VARIABLES	*Mdl & Upr* N. asperus	Lower *N. asperus*	*P. asperopolus*	*Middle & Upper M. diversus*	Lwr *M. diversus & L. balmei*
Lower Shoreface-Shelf	1	3	6	9	n/a
Nearshore	2	4	7	10	n/a
Alluvial-Coastal Plain	n/a	5	8	11	12

The categorical facies variable was used primarily to spatially constrain the population of other attributes such as porosity and permeability. However, the categorical facies may have further utility, primarily because facies are associated with compositional differences. The textural variation between different facies is largely dealt with by porosity and permeability attributes, but in the context of CO_2 geosequestration, compositional changes may also be important. The composition of alluvial-coastal plain facies suggests that it will be more chemically reactive with CO_2 than nearshore or lower shoreface-shelf facies (Chapter 2). The categorical facies attribute groups grid cells representing alluvial-coastal plain facies (categorical facies attribute = 2, 4, 7, and 10), so they can be identified and manipulated for simulation to account for increased likelihood of chemical reaction.

As previously discussed, the loss of geological detail that stems from the use of relatively coarse grid cells in the geological model will impact the alluvial-coastal plain facies to a greater degree than nearshore and lower shoreface-shelf facies. Consequently, the categorical facies variables representing alluvial-coastal plain facies (5, 8, 11, and 12) highlight areas where small-scale reservoir heterogeneity is likely to be more poorly represented in the geological model.

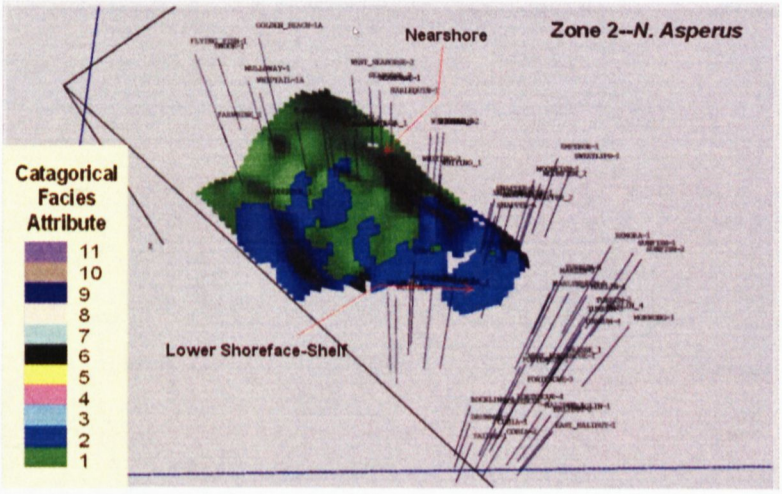
Zone 2--N. Asperus
Nearshore
Lower Shoreface-Shelf
Catagorical Facies Attribute
11
10
9
8
7
6
5
4
3
2
1

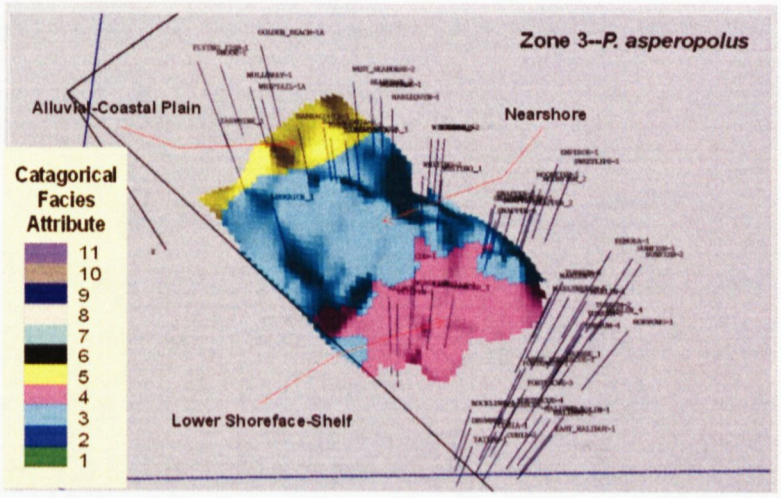
Zone 3--P. asperopolus
Alluvial-Coastal Plain
Nearshore
Lower Shoreface-Shelf
Catagorical Facies Attribute
11
10
9
8
7
6
5
4
3
2
1

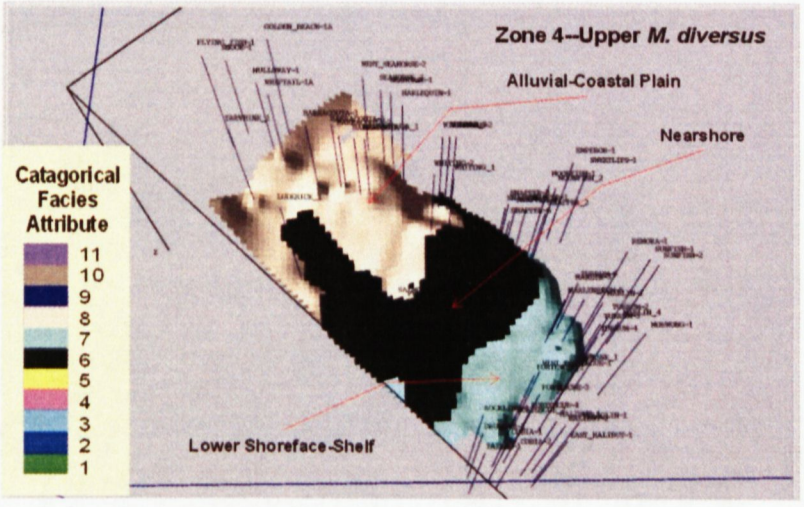
Zone 4--Upper M. diversus
Alluvial-Coastal Plain
Nearshore
Lower Shoreface-Shelf
Catagorical Facies Attribute
11
10
9
8
7
6
5
4
3
2
1

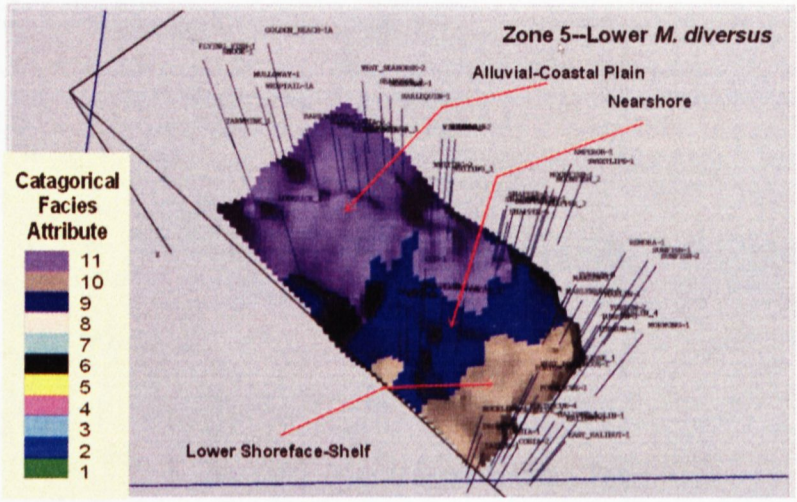

Figure 6.10—Categorical facies attribute represents lower shoreface-shelf, nearshore, and alluvial-coastal plain facies tracts in each zone of the geological model. The attribute is assigned arbitrary sequential values that represent a particular facies within a particular zone. A transgressive stacking pattern is evident through time. Facies tracts occur in more landward positions in progressively younger zones.

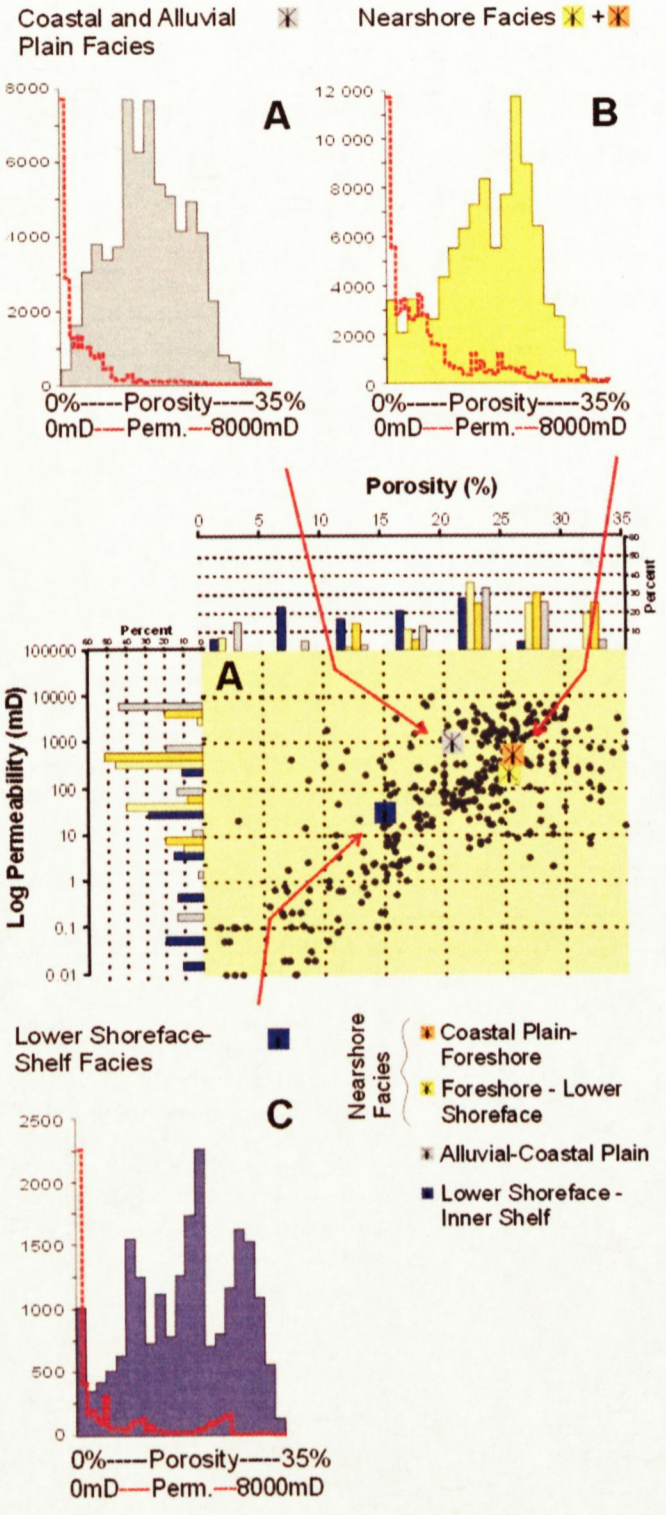

Figure 6.11—Scatter plot and histograms of porosity and permeability for facies measured from routine core analysis compared with histograms of porosity (coloured) and permeability (red line) of facies from attributes in the geological model. Histograms are provided for coastal and alluvial plain facies (A), nearshore facies (B), and lower shoreface to shelf facies (C).

The spatial distribution of facies in the model reflects the retrogradational, transgressive stratigraphy. As a result, facies tracts back-step towards the west and northwest, as represented in the geological model (Fig. 6.12). An attribute called 'Facies' was created that groups all grid cells designated alluvial-coastal plain, nearshore, and lower shoreface-shelf, regardless of the zone in which they occur.

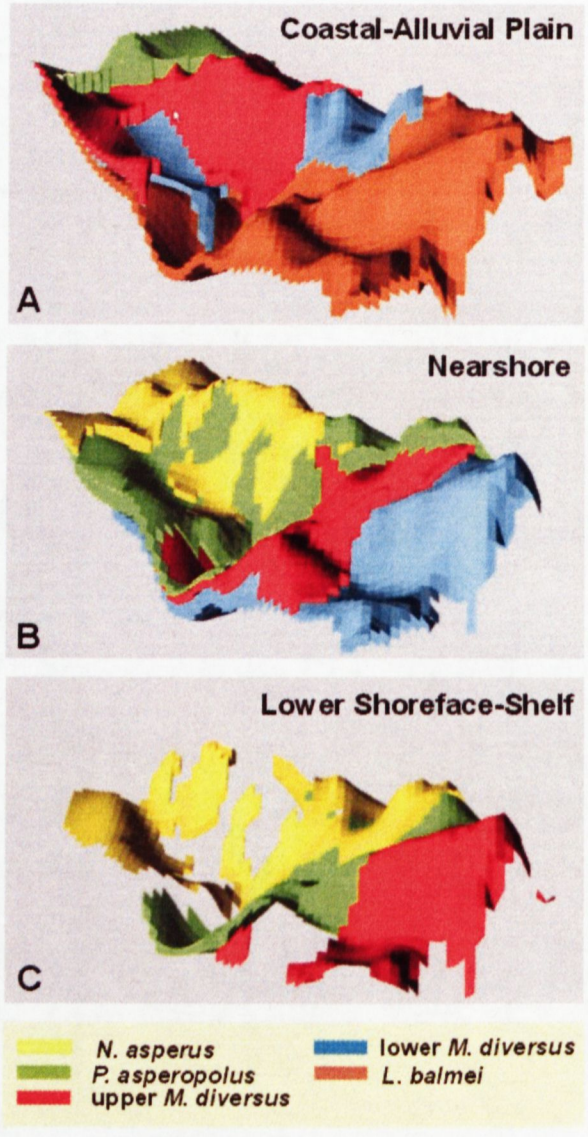

Figure 6.12—Facies used in the geological model, shown with reference to stratigraphic unit. The visible cells represent facies and the colour represents the model zone. View is to the NW.

For example, in A it is evident that the Coastal Alluvial Plain Facies does not exist in the Middle & Upper *N. asperus* zone.

The retrogradational, transgressive large-scale stratal architecture is evident. Coastal and alluvial plain facies exist largely in the lower proximal (W, NW) parts of the study area, and lower shoreface-shelf facies exists primarily in the upper and distal (E, SE) parts of the study area.

POROSITY

Porosity was populated from well locations throughout the geological model using sequential gaussian simulation constrained by the categorical facies attribute. Consequently, data from a cell assigned categorical variable '1' cannot be used to populate a cell assigned categorical variable '2'. This prevents, for example, porosity values from a nearshore setting from being populated in a lower shoreface-shelf setting. Constraining porosity data with the categorical facies variable ensures a geologically realistic distribution of porosity. The distribution for log analysis porosity at well locations is provided in Figure 6.13.

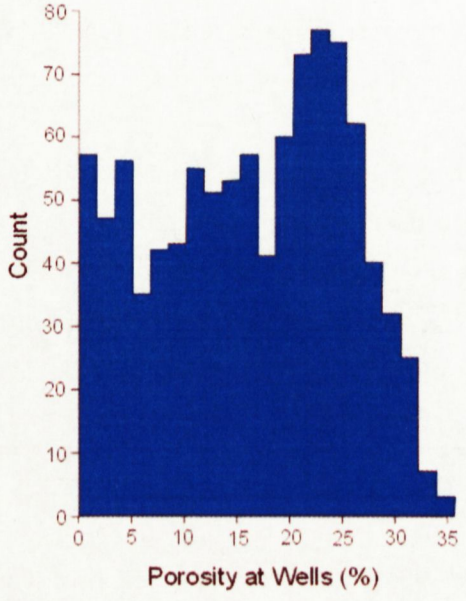

Figure 6.13—Histogram of log analysis porosity at the wells. These data are populated away from the wells throughout the rest of the geological model.

Porosity is assigned to grid cells that are intersected by wells by sampling petrophysical logs at the well bore. The porosity value that is assigned to a particular grid cell is the arithmetic mean of all petrophysical porosity measurements that occur within the grid cell. Between fifteen or twenty petrophysical porosity measurements are averaged per grid cell in general. The porosity attribute at the wells that is generated from petrophysical data is called 'PhiAtWell' and is used as 'hard data' in sequential gaussian simulation.

Representing realistic reservoir heterogeneity is of critical importance in populating both porosity and permeability in the geological model. For this reason gaussian simulation techniques were used to populate both porosity and permeability in the geological model. Sequential gaussian simulation and gaussian co-located co-simulation allow the knowledge of spatial continuity of reservoir properties derived from analogue studies to be incorporated in the geological model (Chapter 4).

Most methods of attribute population described above are fairly simplistic; however, sequential gaussian simulation warrants further explanation. A rigorous mathematical explanation is beyond the scope of this study, but a qualitative understanding of conditional simulation is necessary to appreciate the implications for CO_2 storage. Much of the theoretical basis for kriging and conditional simulation is provided in Chapter 4, where spatial continuity, anisotropy and semi-variograms are discussed.

Stochastic simulation produces alternative equiprobable spatial distributions (realisations), all of which honour specific statistics, for example, histogram and semi-variogram. A description of spatial continuity such as covariance or variogram (2 × semi-variogram) is used for conditional simulation. The variogram (γ) is mathematically related to covariance (C) —another measure of spatial correlation—as follows:

$$C(\vec{h}) = C(0) - \gamma(\vec{h})$$

In kriging and conditional simulation, covariance is used in the calculation of weights, which are utilised to estimate values at unsampled locations. Consequently, the description of spatial correlation for a regionalised variable that is provided by the semi-variogram is included in the kriging or conditional simulation process. This allows the inclusion of geological knowledge in the population of a regionalised variable within the geological model. For example, characteristics of specific depositional environments can be captured in the spatial distribution of various attributes as was discussed in Chapter 4.

Sequential Gaussian Simulation (SGS) is an improvement on kriging, which was originally developed in the mining industry so that geological trends could be

incorporated in maps rather than simple contouring (Chambers 2000). Kriging is a procedure for minimising the estimation variance by altering the weights through a system of linear equations. The way in which the weights are altered is influenced by the covariance (or semi-variogram) and by the spatial distribution of hard data points. A kriged estimate of the value of a regionalised variable at a particular location and the estimation variance is calculated for every grid cell. It is significant that the variance of each estimated value can be calculated.

An important implication of kriging is that the resulting spatial distribution of data results in the correct covariance (i.e. the correct variogram) between hard data and estimated values. However, kriging does not result in the correct covariance between estimated values. This results in the 'smoothed' appearance, typical of kriged maps, which is particularly noticeable with increasing distance from hard data points. The smoothed appearance results from weights being set to zero away from hard data points (beyond the range of the semi-variogram).

Ideally, the heterogeneity represented by the semi-variogram model should be preserved in all areas of the geological model including those areas characterised by sparse hard data points. In other words, the variance between hard data points and estimated data points should be correct and the variance between estimated points should be correct. Conditional simulation approaches can fix the 'missing' variance problem that is characteristic of kriged data, resulting in a more realistic representation of heterogeneity. Largely for this reason, conditional simulation approaches, and particularly SGS, are commonly used for the population of geological models in the petroleum industry (Deutsch 2002). The need to preserve reservoir heterogeneity in areas of sparse hard data may be even more critical in the case of geological models for CO_2 geosequestration for two reasons:

- Models representing very large areas are required to simulate CO_2 storage so areas of sparse data, which are not handled well by kriging, are likely to be common.
- Reservoir heterogeneity has a significant impact on the flow behaviour, migration rate and storage efficiency of SC CO_2 so realistic reservoir heterogeneity should be represented.

SGS corrects the covariance between kriged values by using previously estimated points as 'pseudo-hard data' during population of the geological model. As discussed previously, estimation variance can be calculated for all estimated points. Consequently, the variance for an estimated point can be corrected by adding a value with the correct variance for that point and a mean of 0.

The general SGS process is as follows. All data is transformed to a normal distribution. Grid cells in the geological model are generally visited in random order ('random walk') and the independent residual is randomly drawn (Monte Carlo simulation) from a normal distribution that has a mean of 0 and a variance equal to the kriged variance. Different realisations result from using different seed values for drawing the independent residuals. The result of adding the kriged estimate and the random residual is a new simulated value. The simulated value is added to the set of data from which the random residual is drawn. Simulated values are treated as 'pseudo-hard data' because they are used in the calculation of the next simulated value. Using simulated values in subsequent calculations ensures that the covariance (variogram) remains correct between all values, whether they are hard data or simulated.

When all points in the area of interest are populated with simulated values, the data is back transformed to its original distribution. The result is a simulated distribution where the spatial continuity, or reservoir heterogeneity implied by the semi-variogram model is represented throughout the model.

While SGS results in a spatial distribution of regionalised variables that are conceptually more suitable for the simulation of CO_2 storage, the use of SGS adds complexity to the process of populating a geological model in two ways. First, sequential gaussian simulation induces maximum spatial disorder at points beyond the influence of the variogram model. So the SGS simulation may result in greater heterogeneity than is actually represented in the reservoir/aquifer. This implies that there is no potential to simulate connected paths of extreme values beyond the range of the semi-variogram. In the context of CO_2 flow behaviour particularly, areas of connected low or high permeability and porosity values, which may represent flow baffles or high permeability layers, are important features of reservoir heterogeneity.

The second way in which SGS adds complexity is that data that cannot be transformed properly to a normal distribution may cause anomalous simulation results. The global histogram for the simulated values may be significantly different than the global histogram for the hard data if the data is not properly prepared prior to simulation. For example, permeability data used in this study had to be 'de-spiked' before acceptable simulation results could be achieved. Additionally, normal scores transforms were performed within the zones of the model during SGS and were performed manually on the whole data set prior to SGS. Transforming and back-transforming data sets twice appears to reduce the problems that are characteristically associated with spiky data sets and does not induce unwanted effects. For example, the semi-variogram and histogram are still honoured in the simulation result.

Figures 6.14 – 6.15 show the spatial distribution of porosity in the geological model at different layers. Bands of low and high porosity can be seen trending NE – SW in upper parts of the model and NNE – SSW in lower parts of the model. The orientation of the bands of high and low porosity approximates the interpreted orientation of facies tracts across the study area. These trends in porosity distribution are captured through utilisation of both facies maps (the categorical facies attribute is used as the classifying attribute in SGS) and through the utilisation of geostatistical models that honour the expected facies distribution based on the geological interpretation.

Figure 6.15 shows several realisations of porosity in the geological model. Multiple realisations give an appreciation of the variability that may exist between wells. The figure also illustrates an undesirable aspect of deterministically mapping facies tracts within the model. At some locations within individual zones boundaries between facies tracts are characterised by abrupt changes in porosity values. A more gradual change in porosity or an interfingering geometry between facies tracts would be more geologically realistic.

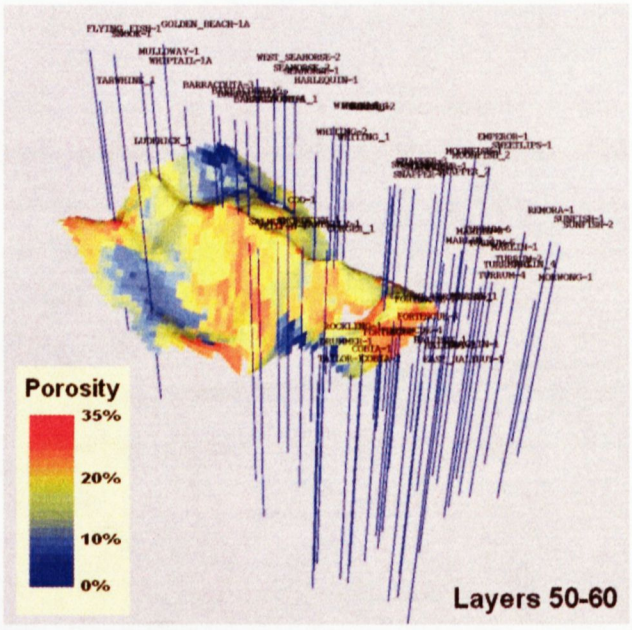
Porosity
35%
20%
10%
0%
Layers 50-60

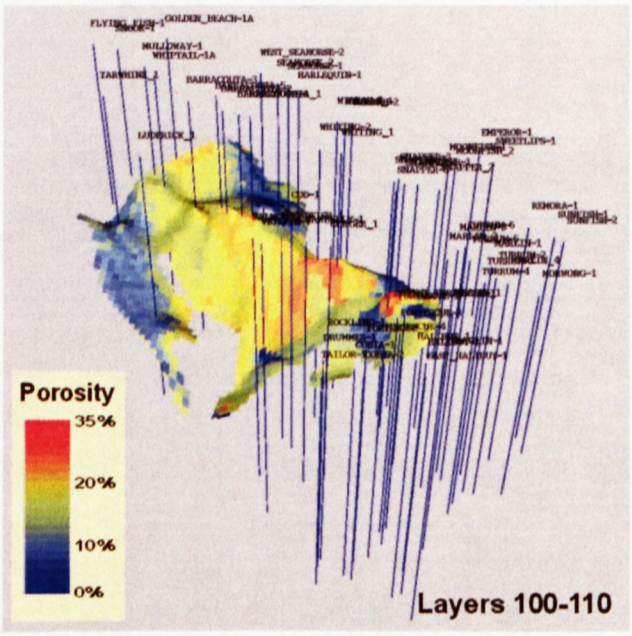
Porosity
35%
20%
10%
0%
Layers 100-110

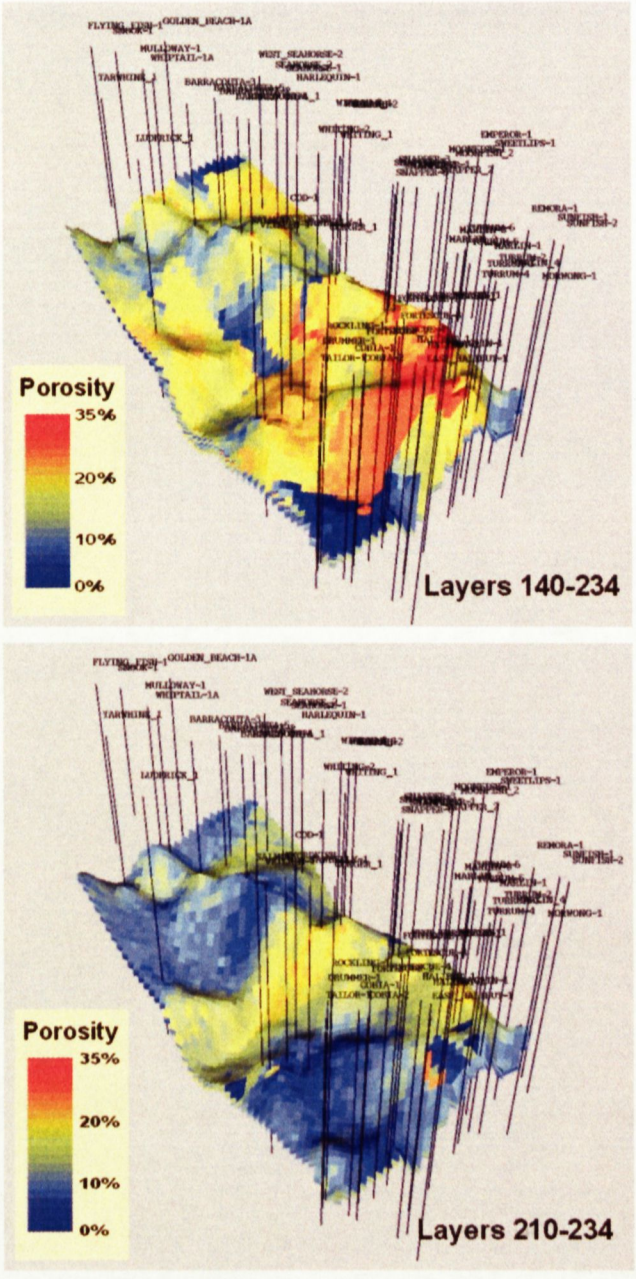

Figure 6.14—Spatial distribution of porosity at various layers in the geological model. Bands of relatively high porosity trending NNE to SSW represent nearshore sandstones oriented parallel to the palaeo-shorelines. Another pattern is an overall reduction in porosity with depth. View is to the NW.

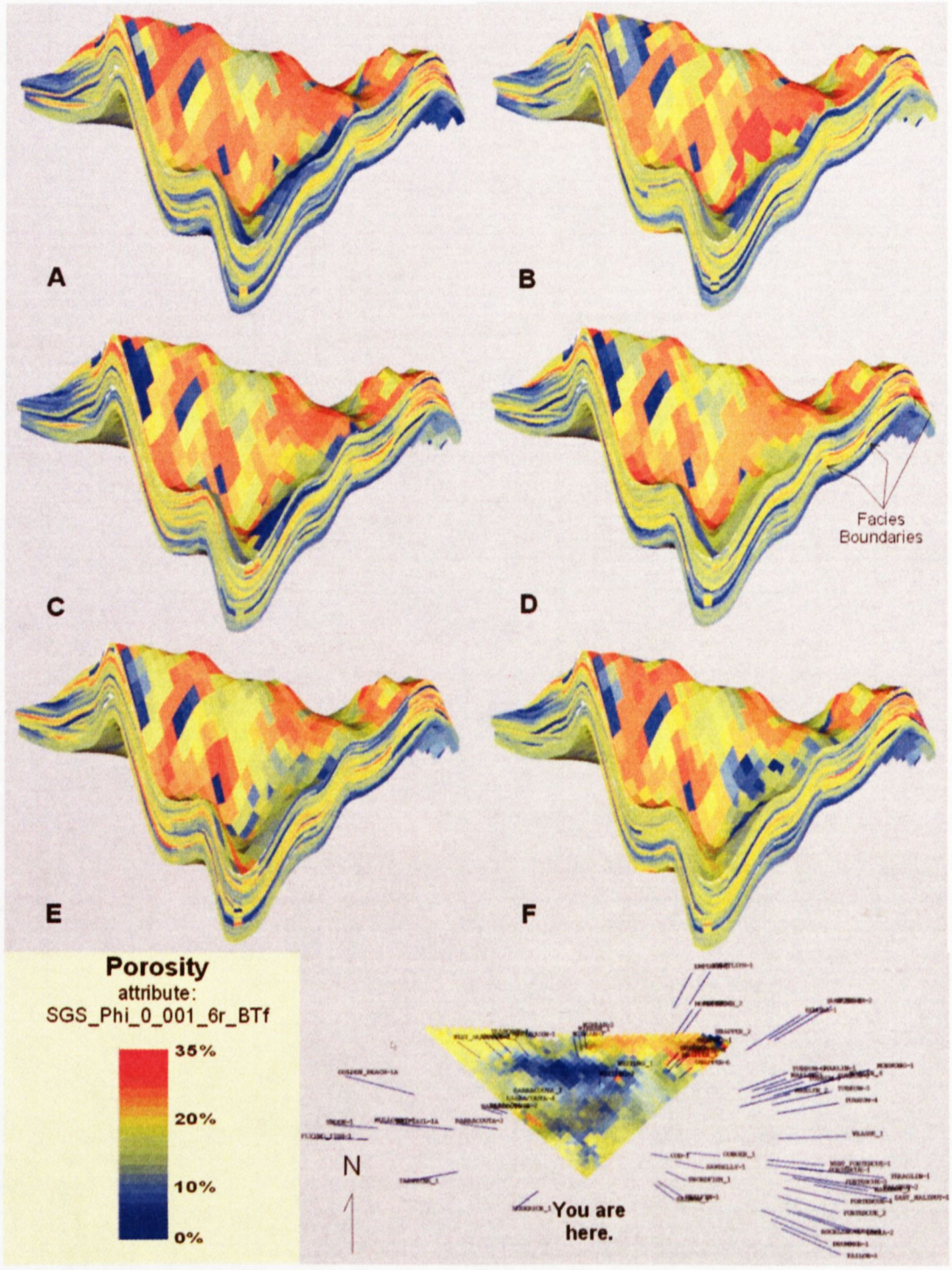

Figure 6.15—Six realisations of porosity (A-F) with the grid sliced along NE and NW trending axes. Some areas are associated with relatively abrupt porosity changes that represent a facies boundary (D). Ideally, an interfingering geometry of a more gradual porosity change would be represented at facies boundaries.

PERMEABILITY

In a similar fashion to the porosity attribute, permeability data was sampled from petrophysical logs at the wells to produce the hard data for conditional simulation. The resulting attribute, 'KatWell' had an unusually high mean (1498.5 mD) that corresponded poorly with routine core analysis data. The unusually high mean value for permeability resulted largely from the fact that permeability has a logarithmic distribution and that relatively thick grid cells were used in the model (5 m). An arithmetic average of between 15 to 20 permeability values was used to calculate the permeability attribute of individual grid cells. Unusually high values, which are characteristic of a logarithmic permeability distribution, bias the resulting value of the KatWell attribute towards the higher permeability values.

An alternative to the KatWell generated from an arithmetic mean of petrophysical data is a KatWell attribute generated from the harmonic mean of petrophysical data. The equation for calculating the harmonic average of permeability is provided below:

$$KatWell_{harm} = \left(\frac{1}{n} \sum_{i=1,2..n}^{n} \frac{1}{k_i} \right)^{-1}$$

The correct permeability value assigned to the grid cells is an up-scaling problem because the grid thickness is considerably greater than the individual beds of different permeability that are represented. One value of effective permeability must be assigned to a single grid cell representing perhaps tens or hundreds of lithologic units (beds and laminae) that have different fluid flow properties. In theory, the harmonic mean gives the correct effective permeability for series flow (flow perpendicular to bedding) and the arithmetic mean gives the correct effective permeability for parallel flow (flow parallel to bedding). Consequently, the harmonic mean and the arithmetic mean of permeability are theoretically the upper and lower bounds of effective permeability (Fig. 6.16). As a result two permeability attributes were generated at the well and populated in the geological model: $KatWell_{arith}$ and $KatWell_{harm}$. The permeability attributes are unrealistically high and low respectively, however, the correct effective permeability is very likely to be between the two results. Interestingly, the routine core analysis data agree more closely

with $KatWell_{harm}$, which may suggest that the true effective permeability is likely to be represented in the lower part of the spectrum bounded by $KatWell_{arith}$ and $KatWell_{harm}$.

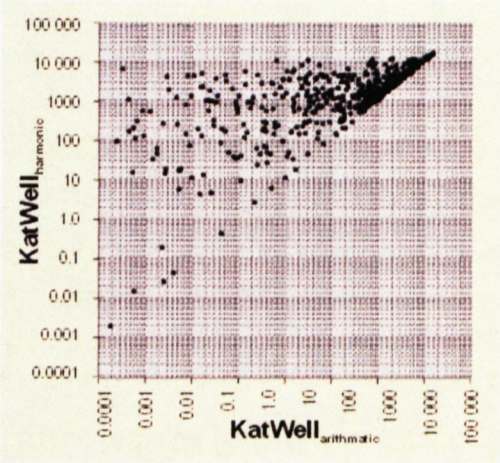

Figure 6.16—Scatter plot of attributes $KatWell_{arithmetic}$ and $KatWell_{harmonic}$. Where data points occur along a straight line with a slope of one, arithmetic and harmonic averages at the grid cell return the same value. However, many gird cells are characterised by a significant difference in arithmetic and harmonic permeability averages.

Permeability is dependent on porosity in the sense that high permeability is rarely associated with low porosity in nature. Routine core analysis and petrophysical data both show a fairly highly correlated, positive relationship between porosity and permeability in rocks of the Gippsland Basin (Fig. 6.11 & 6.17). Consequently, it is desirable to populate the permeability attribute in the geological model with respect to the pre-existing porosity attribute.

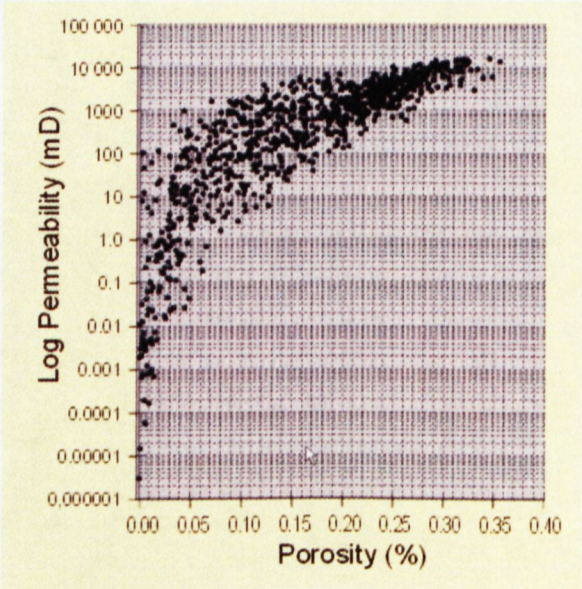

Figure 6.17—Scatter plot of log permeability versus porosity at the wells (i.e. hard data).

In order to maintain the correct relationship between porosity and permeability in the geological model, permeability was populated with gaussian co-located co-simulation, using permeability as the primary attribute and porosity as the secondary attribute. The spatial distribution of permeability in the study area is illustrated in Figure 6.18.

The process for attribute population in the geological model is similar to sequential gaussian simulation, described previously, but with co-located co-simulation two sets of weights are used to calculate the estimated value. The first set of weights used in gaussian co-located co-simulation is derived via the traditional kriging method described previously, which uses covariance/semi-variogram models. The second set of weights is derived from the value of the secondary attribute (porosity) at the point where the primary attribute (permeability) is being estimated. The value of weights belonging to the second set is a function of the covariance between the primary and secondary variables (i.e. the strength of the relationship between porosity and permeability). The relationship between porosity and permeability represented in the study area that is evident from routine core analysis can be preserved in the geological model using gaussian co-located co-simulation.

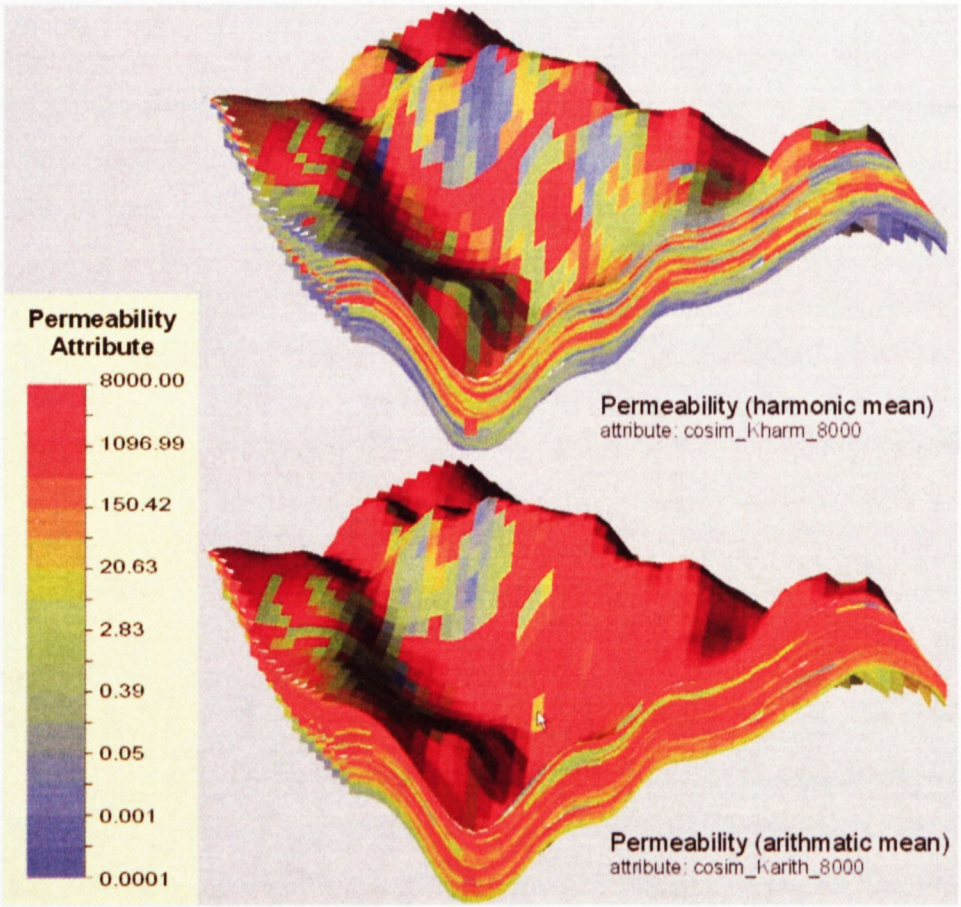

Figure 6.18—Realisations of permeability distribution in the geological model using absolute permeability attributes generated from the harmonic mean (A) and arithmetic mean (B) of petrophysical permeability measurements at the wells. The two permeability realisations theoretically represent the upper and lower thresholds of effective permeability in the study area. The 'real' absolute permeability probably exists somewhere between the two realisations shown. Model is sliced along its NE trending axis. The slice is approximately along the expected initial flow path of the CO_2. View is to the WNW.

WATER SATURATION

Water saturation is an attribute that is associated with considerable uncertainty in the context of CO_2 geosequestration because there is limited analogue or experimental data available for CO_2 saturation in subsurface reservoirs and aquifers. In Chapter 1 the uncertainty associated with the ability of supercritical CO_2 to displace water from pores space is addressed. Where CO_2 is more likely to bypass water molecules rather than displace them high S_w is expected and the capacity of reservoirs and aquifers to store CO_2 is reduced. For example, flow simulations by van der Meer (1995) showed that CO_2

may only occupy a small percentage of the pore space within a structural closure if injected near the crest of the structure.

Despite some simulation results suggesting poor storage efficiency, empirical evidence from hydrocarbon fields suggests that natural gas, which has fluid properties less favourable for displacing water than CO_2, can fill structural closures very efficiently resulting in very low water saturation. Petrophysical analysis suggests that gas fields within the study area are commonly associated with S_w of < 10% (Fig. 6.19).

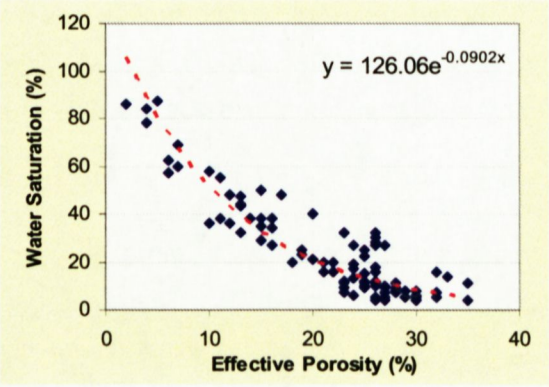

Figure 6.19—Scatter plot of effective porosity and water saturation based on quantitative log analysis from wells in the study area (Barracouta 5, Marlin 2 & 3, Snapper 5 & 6, and Turrum 2).

The key distinction between simulation results indicating high S_w and empirical evidence from hydrocarbon fields associated with low S_w is likely to be the way in which the structural closures are filled. Where fluid is injected at high pressures directly into structural closures formation water is more likely to be bypassed than displaced, resulting in high S_w. Alternatively, where fluid trickles into geological structures over geological time the displacement of formation water is much more efficient resulting in low S_w.

There are a couple of reasons that S_w resulting from CO_2 geosequestration in this study is more likely to be analogous to S_w observed in hydrocarbon fields rather than S_w calculated from some flow simulations of CO_2 injection. First, the mechanism for filling structural closures along the expected migration path of CO_2 is much more analogous to hydrocarbon charge than direct injection of CO_2 into a structural closure. The geosequestration strategy proposed for the Gippsland Basin involves injection of CO_2 in a structurally low area to allow migration under gravity forces towards structural closures.

Because the point of injection is likely to be a considerable distance from the first hydrocarbon field encountered, the structure is likely to fill relatively slowly, through gravity forces rather than pressure driven viscous flow.

The second reason that low S_w is expected is that hydrocarbon and water will have already been produced from the structural closures along the expected migration path so structural closures are likely to be pressure depleted, particularly in the case of the hydrocarbon fields that are initially encountered by CO_2. Because of relatively high permeability and reservoir/aquifer connectivity in the study area, pressure equilibration may occur relatively quickly in depleted hydrocarbon fields resulting in rapid water intrusion from the aquifer leg into the depleted field. Consequently, it is possible that water intrusion and pressure equilibration will occur in some fields before CO_2 reaches them.

The fact that the structural closures along the migration path represent depleted hydrocarbon fields also adds complexity to the estimation of S_w. There will be both residual water and residual hydrocarbon in the pore space within structural closure resulting in a three-phase system with the introduction of CO_2. The effect of the residual hydrocarbon is likely to impact not only S_w, but also relative permeability and the chemical behaviour of CO_2 (e.g. CO_2 is miscible in oil). Understanding detailed physical and chemical interactions of CO_2, hydrocarbon and water is beyond the scope of this study, but is highlighted as an area in which further research is needed. Given the dearth of data addressing three-phase CO_2-hydrocarbon-water systems, sensitivity to wide ranges of relative permeability and capillary properties should be assessed during flow simulation.

Two approaches were used for estimating S_w and populating it as an attribute in the geological model. The key challenge was that there is no publicly available data specifically addressing S_w in CO_2 accumulations, either within the study area or from analogue reservoirs/aquifers. First, a highly qualitative approach was used to estimate S_w for CO_2 accumulations: notional water saturations for rocks of specific permeability were solicited from reservoir engineers and development geologists based on their intuition and experience; a logarithmic trend was fitted to the resulting estimates. For example, one might expect relatively low S_w, on the order of ~15%, in a rock of Darcy

permeability, whereas in rock of 1 mD S_w is likely to be much higher, perhaps 50%. Water saturation was populated in the geological model based on the logarithmic relationship defined (S_w = -5.14 × Ln(k) + 53.3). A high and low S_w estimate was generated because of the high and low permeability data sets that were created at the wells from two alternative approaches for sampling the high vertical resolution petrophysical permeability data, discussed previously. The resulting distributions of S_w in the geological model were used primarily for comparison with the distributions resulting from more quantitative techniques for deriving S_w.

The second approach for estimating S_w was based on log analysis data from wells in the study area intersecting hydrocarbon accumulations. Sufficient data was not available to compare permeability and S_w, however, data was available to compare effective porosity and S_w (Fig. 6.19). The data indicate that water saturation is generally below 20% in hydrocarbon charged rock of relatively high porosity (>20%). Water saturation was populated within structural closures represented in the geological model based on the relationship between effective porosity and S_w (i.e. $S_w = 126.06e^{-0.0902(\phi)}$).

The distributions of S_w resulting from the approaches to populating S_w described above are provided in Figure 6.20. The graphs represent the theoretical distribution of S_w within structural closures represented in the geological model if the structural closures were CO_2 charged. S_w distributions resulting from the qualitative approach using permeability are characterised by a large number grid cells with very low S_w (<10%). Additionally, a large number of grid cells characterised by unusually high S_w (>50%) result from using the low permeability distribution to populate S_w. The S_w distribution resulting from the empirical relationship between S_w and effective porosity is more realistic because most S_w values are between 10% and 30%, as might be expected in relatively high quality reservoir rock, and very few values have S_w in excess of 50%.

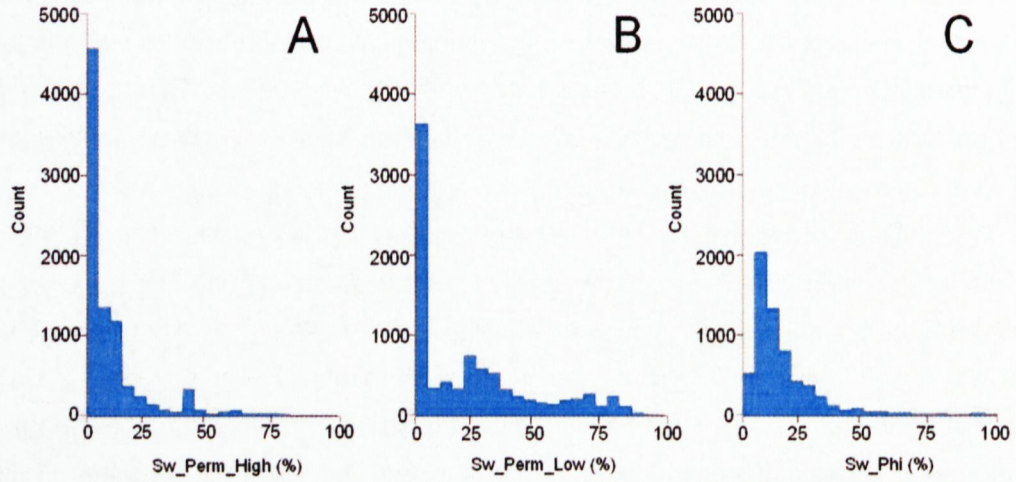

Fig. 6.20—Histograms of expected water saturation within structural closures in the study area assuming CO_2 charge. A and B represent S_w distributions resulting from a qualitative approach using high (A) and low (B) permeability attributes. C represents a S_w distribution calculated using the relationship between measured S_w from hydrocarbon accumulations and effective porosity observed in the study area.

The approaches to populating S_w outlined above neglect the existence of a transition zone at the base of a theoretical CO_2 column. The transition zone is a zone of systematic vertical change between an area 100% S_w below a hydrocarbon or CO_2 column to an area characterised by irreducible water saturation within the hydrocarbon or CO_2 column. The characteristics of the transition zone are a function of the rock and fluid properties. The thickness of the transition zone, for example, is typically very thin for hydrocarbon gas accumulations where the density difference between natural gas and formation water is very large. Conversely, the transition zone is relatively thick for oil accumulations where the density difference between oil and water is fairly small by comparison with the density difference between gas and water.

The height above free water level (h) can be used to approximate the thickness of the transition zone. The difference in density between formation water and CO_2 ($\Delta\rho$), as well as capillary pressure (P_c) control h, is described as $(144 \times P_c)/\Delta\rho$. The largest height above the free water level would occur in facies of relatively poor fluid flow properties, characterised by fairly high capillary pressure. The average density difference between supercritical CO_2 and water at reservoir/aquifer pressure and temperature conditions was estimated to be ~ 0.3 g/cm^3. Even if one were to assume a relatively high capillary pressure for rocks in the study area (10 psi) the calculation suggests that height above

free water level in excess of ~20 m is unlikely to occur. By comparison with the range of structural uncertainty the transition zone of the CO_2 column will have a negligible impact of volumetric calculations and consequently, is excluded from the volumetric estimates.

TEMPERATURE

Several important aspects of CO_2 storage are dependent on the pressure and temperature conditions of the aquifer/reservoir as well as the rock properties. For example, the compressibility of CO_2 is a function of the pressure/temperature conditions as well as rock properties, like porosity.

The temperature attribute was populated in the geological model by creating a surface from gridding geothermal gradients in the study area. Geothermal gradients were calculated from Horner plot temperatures in well completion reports using the relationship:

$$gg = \frac{T - t_0}{z}$$

... where gg is geothermal gradient, T is temperature, t_0 is surface temperature (calculated using 9.2°C), and z is depth in metres. A linear geothermal gradient was assumed. Table 6.4 and Figure 6.21 show the temperature data that was used to populate the geological model.

Table 6.4: Temperature data.

WELL NAME	Surface Temperature (°C)	Depth (m)	Horner Temp (°C)	Geothermal Gradient (°C/km)
CONGER-1	9.2	2957.00	132.00	42.3
LUDERICK-1	9.2	2489.00	110.00	40.5
MOONFISH-2	9.2	2033.00	105.90	47.57
MULLAWAY-1	9.2	1712.00	75.00	38.43
SAWBELLY-1	9.2	3065.00	91.00	29.69
SEAHORSE-2	9.2	2121.00	83.40	34.98
SNAPPER-4	9.2	1513.00	78.50	45.80
SNAPPER-5	9.2	2516.00	108.40	39.43
SNAPPER-6	9.2	2971.00	133.00	41.67
SUNFISH-2	9.2	2644.00	119.00	41.53

WELL NAME	Surface Temperature (°C)	Depth (m)	Horner Temp (°C)	Geothermal Gradient (°C/km)
TARWHINE-1	9.2	1582.00	70.95	39.07
TERAGLIN-1	9.2	3373.00	131.50	36.26
TURRUM-4	9.2	2750.00	111.70	37.27
VEILFIN-1	9.2	3317.00	127.00	35.51
WHIPTAIL-1A	9.2	2007.00	86.00	38.27
WHITING-1	9.2	3013.00	146.50	45.57
WIRRAH-2	9.2	3081.00	111.00	33.04
WIRRAH-3	9.2	2430.00	91.70	33.95

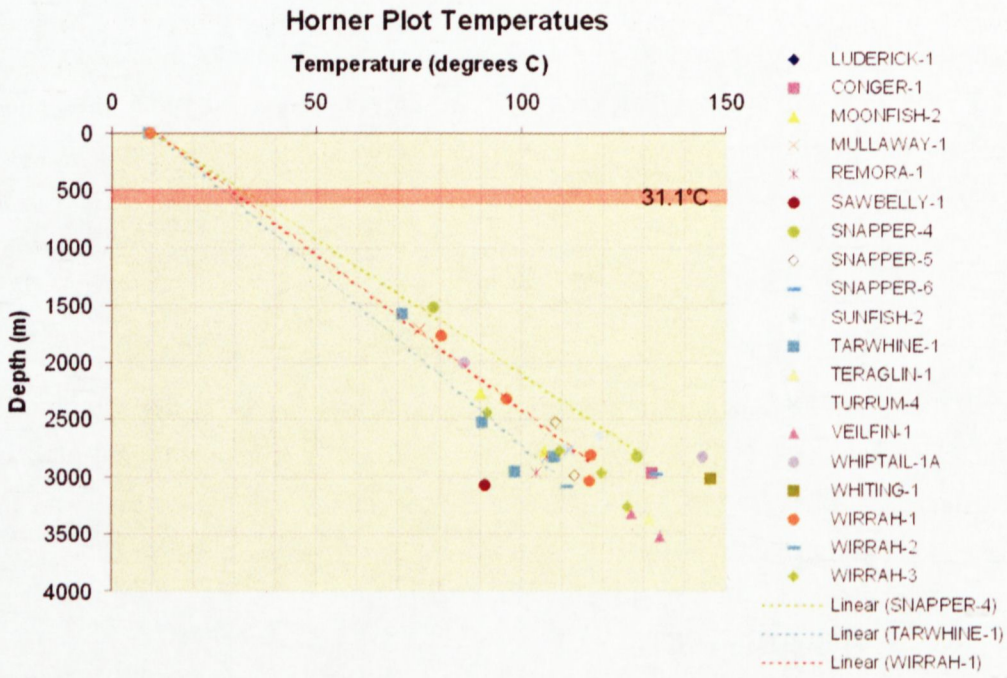

Figure 6.21—Horner plot temperatures plotted against depth for wells within the study area. The range of temperature gradients suggests that 31.1°C will occur between depths of 500 m and 610 m within the study area.

An attribute was created from the gridded surface of geothermal gradients and converted to an attribute called 'GeoGradient' in the geological model. The GeoGradient attribute was multiplied by the CentreDepth attribute, which is true vertical depth to the centre of every grid cell. The resulting spatial distribution of temperature is shown in Figure 6.22.

The area with the highest geothermal gradient is the northeastern part of the study area. Clearly, however, the highest temperatures are represented in the deepest parts of the model. The temperature at target reservoir/aquifer depths is well above the threshold temperature of 31.1°C at which the phase shift between gaseous and supercritical CO_2 occurs.

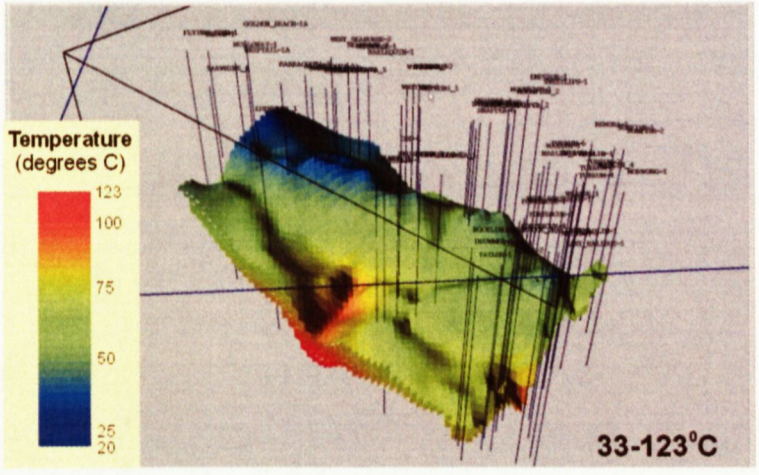

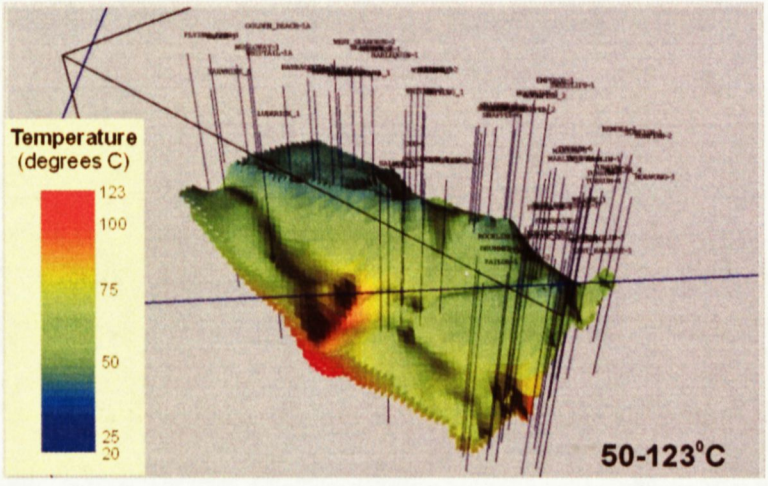

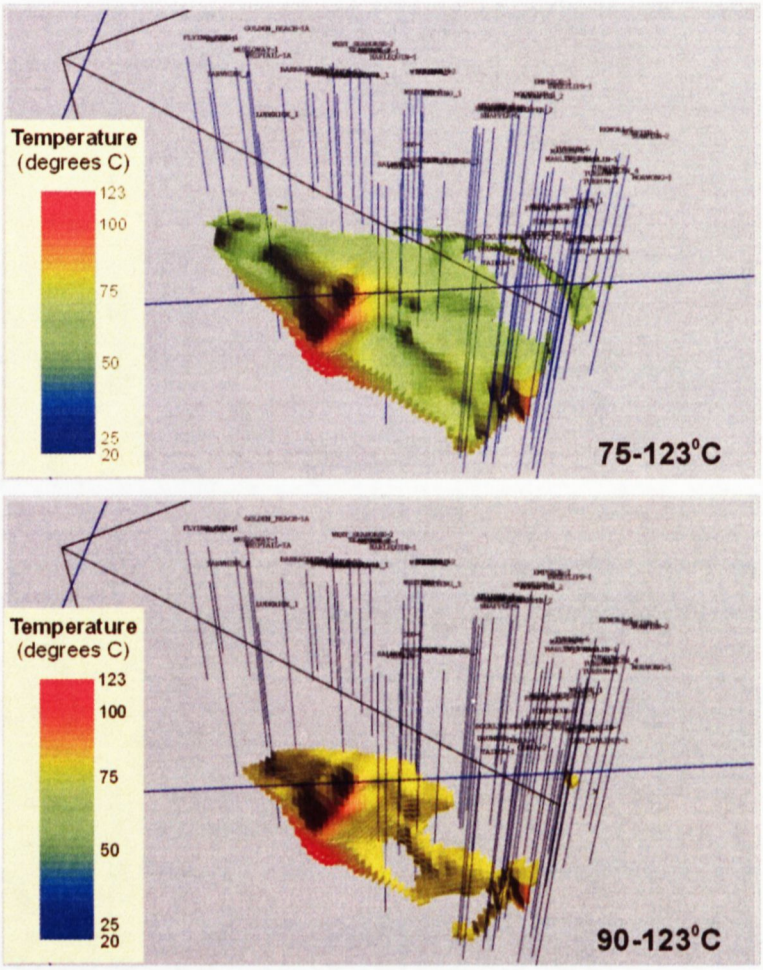

Figure 6.22— Spatial distribution of temperature attribute within the geological model. The lowest and highest temperatures are consistent with the shallowest and highest parts of the geological model—in the northwestern and southern, central parts of the study area, respectively. View is from the SE.

PRESSURE

Hydraulic head maps for each stratigraphic interval of the geological model were produced by Jim Underschulz, Valorie Roy and Claus Otto at CSIRO, Perth. Repeat Formation tests (RFT), Formation Interval Tests (FIT), Drill Stem tests (DST) and production data in well completion reports were used to calculate hydraulic head (Root *et al.* 2002). The most recent pressure measurements were used in order to represent the present day pressures in the Gippsland Basin in the geological model as accurately as possible.

Surfaces were produced from gridding hydraulic head measurements at the wells. A hydraulic head attribute called 'HydroHead', was produced for each stratigraphic interval in the geological model. Pressure in megapascals was calculated by multiplying HydroHead by the CentreDepth attribute and converting units (HydroHead × depth × 0.006897 = pressure [MPa]).

The present day pressure of the Gippsland Basin was incorporated in the reservoir because pressure depletion at producing fields may influence the migration rate and direction of CO_2. Pressure is also a key factor in estimating the compressibility of CO_2 at reservoir/aquifer conditions for volumetric estimates. Present day pressure data may also provide an opportunity to broadly check the validity of the geological model. For this study however, the absence of detailed publicly available production data, and the size of the geological model made a history matching exercise impossible to undertake.

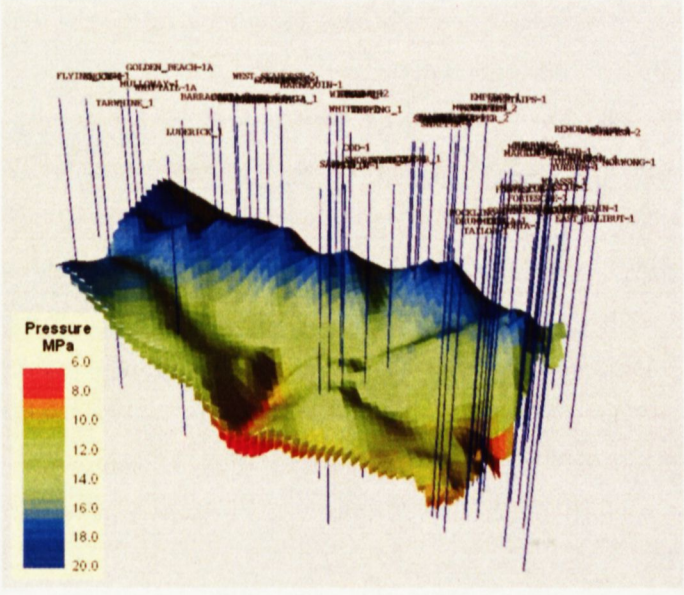

Fig. 6.23—Spatial distribution of pressure attribute within the geological model.

In general, producing fields in the Gippsland Basin are characterised by a strong water drive, so pressure depletion from production is generally short-lived. However, significant pressure depletion in the Fortescue-Cobia-Halibut area in the southeast of the study area, and near Moonfish in the northern part of the study area, suggest sufficient pressure compartmentalisation in these areas to maintain non-hydrostatic gradients for

short periods of time at least. Production induced pressure depletion in these areas is relevant in the context of altering the flow behaviour of the regional aquifer, but is not relevant in the context of trapping SC CO_2 or unforseen pressure increases at injection wells due to the location of the proposed injection site.

The pressures expected in target reservoirs/aquifers are sufficient to maintain CO_2 in a supercritical state. Consequently, in terms of both pressure and temperature no unexpected phase changes are likely to occur along the anticipated migration path.

SALINITY

Salinity attribute was created from salinity data from quantitative log analysis reports (Fig. 6.24). The salinity attribute was populated separately for each zone in the geological model because differing flow properties can result in different spatial distributions of salinity. A surface was created from gridding salinity (ppm NaCl-equivalent) in each zone. An attribute was then generated from the resulting surfaces in each zone of the geological model. Limited data for the zone Middle & Upper *N. asperus* resulted in unknown salinity values for the easternmost part of the zone. In this area of the Middle & Upper *N. asperus* zone the salinity attribute was manually added in keeping with the general spatial salinity trend of the zone. The resulting salinity distribution in the model suggests a range of water compositions, most of which are less saline than seawater (Fig. 6.25).

Salinity data from water samples taken during repeat formation tests (RFT), formation interval tests (FIT), and drill stem tests (DST) were available in addition to the quantitative log analysis data. Salinity data from quantitative log analysis was used in preference to water sample data because the quantity of data was much greater for the former. However, it should be noted that titrated Cl^- from water samples shows a relatively poor correlation with salinity from quantitative log analysis. Additionally, salinity data from water samples does not appear to substantiate freshwater flushing in the proximal parts of the Gippsland Basin (NW part of the study area), which is a well-documented trend (Glenton 1988). It is possible that the pattern of freshwater flushing would be borne out if more salinity data from water samples were available. It is also possible that many water samples were contaminated with mud filtrate. The spatial distribution of salinity in the geological model is illustrated in Figure 6.26.

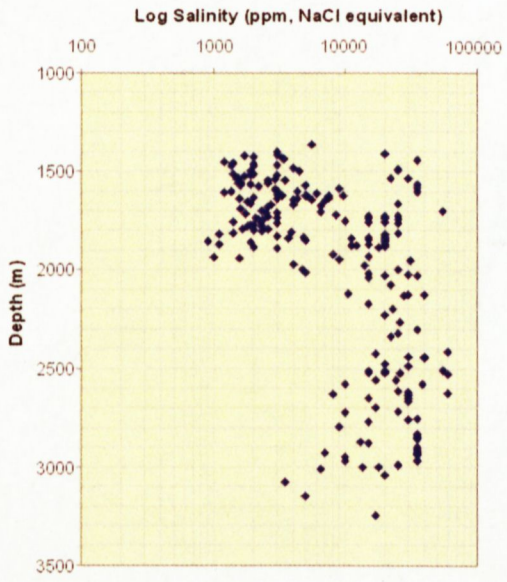

Figure 6.24—Quantitative log analysis salinity (NaCl equivalent) versus depth in the upper Latrobe Group. The majority of the geological model exists between 1500 m and 2500 m, characterised by brackish water and saline water as well as some fresh water.

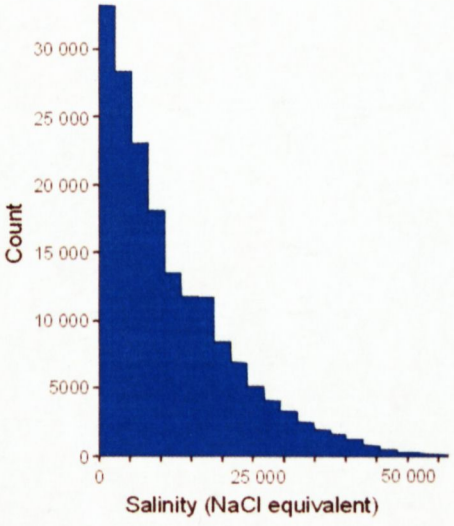

Figure 6.25—Histogram of salinity attribute (NaCl equivalent). Most of the formation water in the study area is relatively fresh because of the 'fresh water wedge' that encroaches into the study area from onshore aquifers to the northwest of the study area.

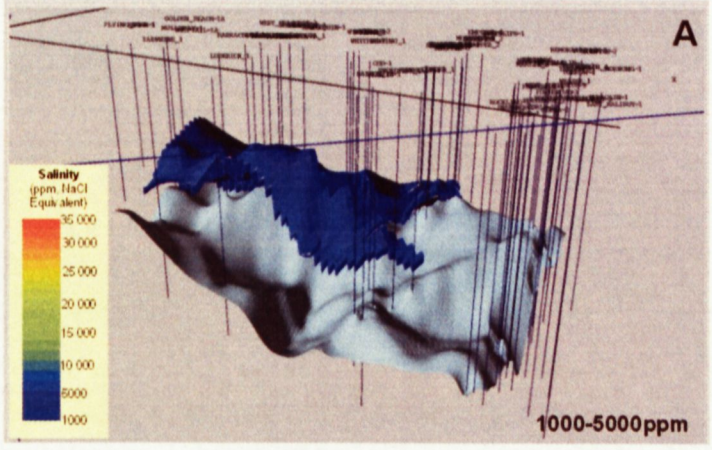

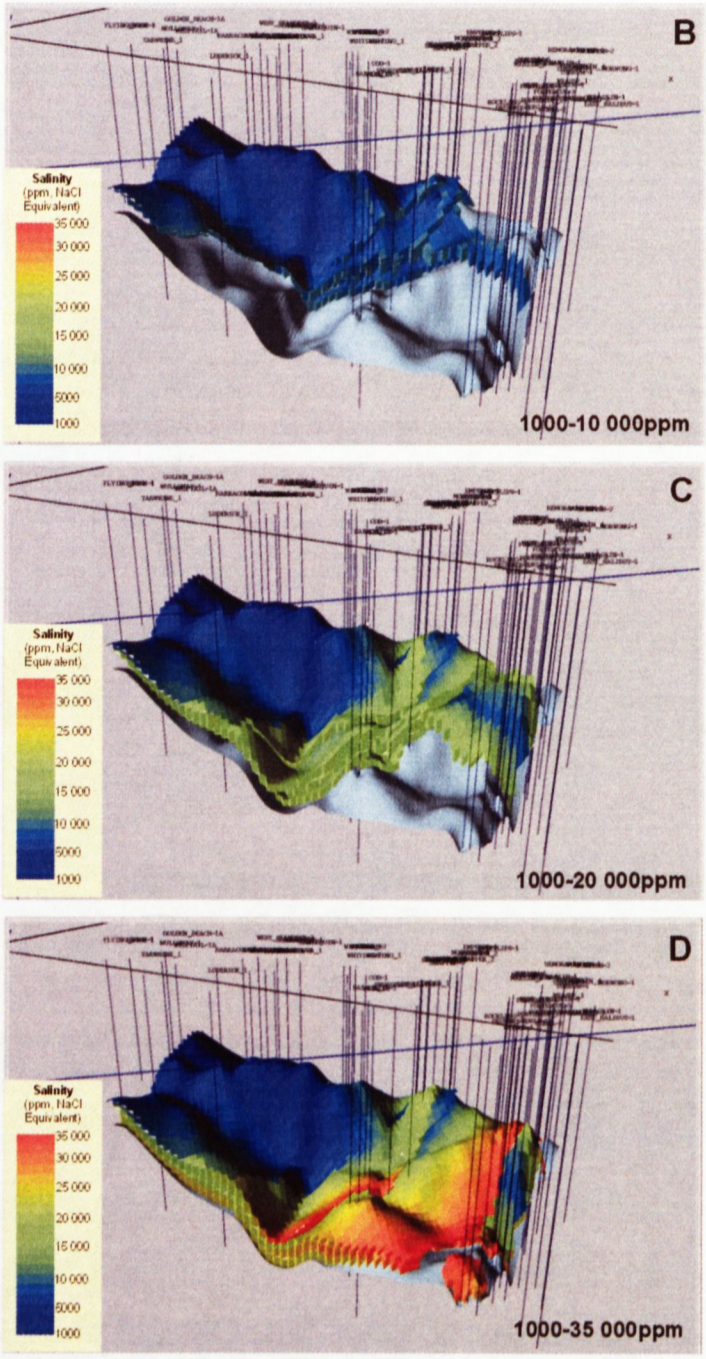

Figure 6.26—Various ranges of salinity displayed in the geological model with the BaseModel Surface shown for reference [1000 – 5000 ppm (A); 1000 – 10 000 ppm (B); 1000 – 20 000 ppm (C); 1000 – 35000 ppm (D)]. A 'wedge' of fresh water encroaches into the study area from fresh water aquifers to the NW. Only a small parts of the study area in the SE and NE are characterised by salinity greater than or equal to sea water (35000 ppm). View is from the SSE.

FAULT PROXIMITY

All of the faults identified by seismic interpretation could not be utilised in the geological model as they would prohibitively increase the complexity and computational cost of the model. As a result, only selected faults were modeled and some simplifying assumptions were made, described previously in this chapter. The faults that were utilised in the study were selected based on the following criteria:

- The faults must occur within the area of interest and along the likely flow-path of the CO_2
- The faults must be associated with displacement greater than ~30 m
- The faults must propagate into regional sealing units (i.e. Gurnard, Lakes Entrance, Marlin, Turrum, Flounder formations).

Based of the criteria listed above nine faults were selected from the ~40 faults that were seismically mapped and correlated (Fig. 6.27). Most faults were not selected for inclusion in the geological model because they did not propagate into regional sealing lithologies. Many faults occurred primarily below the geological model and showed little displacement within the geological model area itself. Simplifying assumptions had to be made about the nine faults selected for modeling because of limitations of the modeling software. These assumptions were:

- The faults are vertical
- The faults are parallel with either the I or J axes of the model.

The assumption that faults are vertical is allowable in the case of the Gippsland ESSCI because faults within the study area are very steeply dipping, though their dip generally shallows at greater depths. By comparison with the assumption that faults are vertical, the limitation of fault orientations to the I and J axes of the model has greater impact. The greater impact stems from the existence of two fault sets of varying orientations in the study area (NE – SW & ENE – WSW). Because the average orientation of the two fault sets differs by 20° – 25°, it is not possible to incorporate both fault sets in the geological model realistically. However, faults of the dominant NE – SW-trending fault set represent eight of the nine faults included in the geological model, so most of the faults in the model are relatively realistically represented.

Carbonate cementation appears to be commonly associated with faults in the study area (Chapter 2 and 3). In the absence of other information, carbonate cementation is considered characteristic of fault damage zones in the study area, so permeability in the geological model was reduced to 0.0001 mD where FaultProximity attribute is <400 m. The average value of permeability that appropriately characterises fluid flow behaviour in proximity to faults is difficult to determine. Based on samples of fault damage zones from core on which MICP analysis was conducted there would be no fluid movement through heavily cemented fault rock, even under considerable pressure gradients. However, the assumption that the entire area of every fault plane is sufficiently cemented to negate all fluid flow is perilous, so a permeability of 0.0001 mD was assigned. Sensitivity of CO_2 flow behaviour to fault transmissibility should be evaluated through flow simulation.

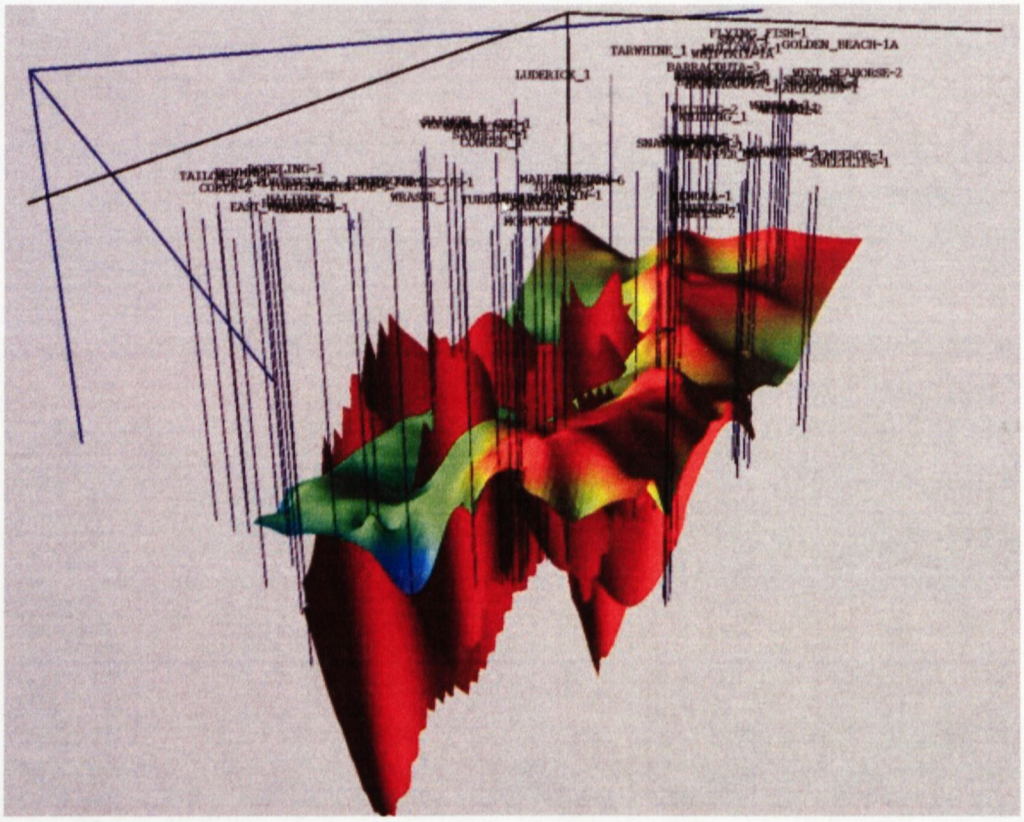

Figure 6.27—Fault planes from which the proximity to fault attribute was calculated. View is from the NE.

CO_2 Compressibility and Expansion

In order to calculate the volumetrics of an ESSCI, the compressibility of CO_2 must be calculated as a function of aquifer/reservoir pressure and temperature conditions. It is useful to express the volume of CO_2 that can be stored in an ESSCI in terms of pure CO_2 volume at normal pressure and temperature conditions. Therefore, the real gas deviation factor for pure CO_2 was used to estimate the magnitude of fluid compression at reservoir/aquifer conditions.

In the geological model for the Gippsland Basin ESSCI, the volume of CO_2 that can be stored in a particular pore volume at a specific temperature and pressure is expressed by multiplying pore volume by an attribute called 'CO2ExpansionFactor.' CO2ExpansionFactor is a function of the pressure and temperature represented in a particular grid cell and the real gas deviation factor, or 'Z-factor', for CO_2. The method for deriving CO_2 Z-factors is based on the Span & Wagoner (1996) equation of state for pure CO_2, which defines standard pressure temperature conditions at 15°C and 0.101325 MPa (14.7 psi). The Z-factor, and consequently the fluid compressibility, will change depending on the exact composition of the injected fluid stream. Realistically, 100% CO2 in the fluid stream to the injection wells is unlikely; some impurities (e.g. CH_4, H_2S, NO_2) are likely to exist depending on the source of CO_2 (e.g. power stations, hydrocarbon fields).

The formation volume factor describes how fluid expands and contracts under reservoir/aquifer conditions:

$$B_g = C\frac{zT}{P}$$

Where B_g is the fluid formation volume factor, C is a constant (0.02827 for B_g in ft^3/scf), z is the Z-factor, T is temperature in Rankine, and P is pressure in psia.

The variation of the Z-factor for CO_2 with pressure and temperature cannot easily be mathematically described by using a script in the geological model, so calculation of the Z-factor as a smooth function of pressure and temperature was not possible. Instead, discrete values for CO2_Z-factor and discrete CO2ExpansionFactor values are applied to specific ranges of pressure and temperature. The range increment for pressure is

~0.85 MPa and for temperature is ~5°C. The pressure and temperature increments were sufficiently small that a smoothly varying attribute was at least approximated (Fig. 6.28). The Z-factor and CO2ExpansionFactor values applied to each increment of pressure and temperature are provided in Table 6.5.

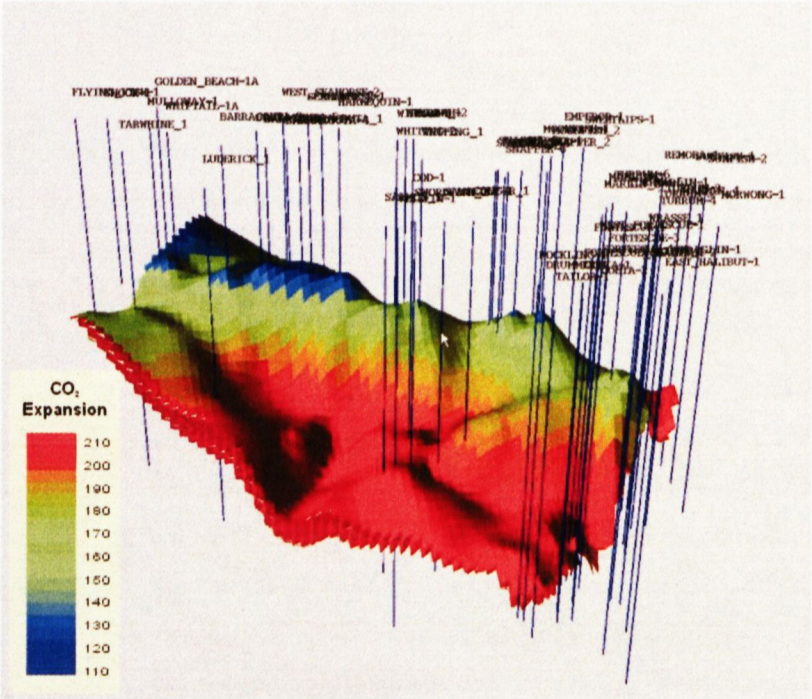

Figure 6.28—Spatial distribution of CO2ExpansionFactor attribute within the geological model. The degree of CO_2 compression in target reservoir/aquifers varies between 115 and 180 times the CO_2 volume at standard pressure/temperature conditions. View is from the SSE.

Results indicate that between 115 and 220 times the amount of CO_2 that can be stored at ambient pressure/temperature conditions will be stored at aquifer/reservoir conditions in the study area. The relatively high expansion factors represented in the geological model stem from the phase shift that occurs from gaseous CO_2 to supercritical CO_2 at 31.1°C and 7.28 MPa.

Table 6.5: Z-factors and gas expansion factors applied to the Gippsland Basin ESSCI geological model.

Pressure (MPa)		Temperature (deg. C)		Average Pressure (MPa)	Average Temp. (deg. C)	CO_2 Z-Factor	CO_2 Volume Expansion
high	low	high	low				
6.700	7.550	35.000	40.063	7.125	37.531	**0.561**	**115.594**
7.550	8.400	40.063	45.125	7.975	42.594	**0.527**	**135.523**
8.400	9.250	45.125	50.188	8.825	47.656	**0.504**	**154.266**
9.250	10.100	50.188	55.250	9.675	52.719	**0.493**	**170.147**
10.100	10.950	55.250	60.313	10.525	57.781	**0.492**	**182.628**
10.950	11.800	60.313	65.375	11.375	62.844	**0.498**	**192.142**
11.800	12.650	65.375	70.438	12.225	67.906	**0.508**	**199.393**
12.650	13.500	70.438	75.500	13.075	72.969	**0.521**	**204.993**
13.500	14.350	75.500	80.563	13.925	78.031	**0.535**	**209.396**
14.350	15.200	80.563	85.625	14.775	83.094	**0.551**	**212.923**
15.200	16.050	85.625	90.688	15.625	88.156	**0.567**	**215.799**
16.050	16.900	90.688	95.750	16.475	93.219	**0.583**	**218.186**
16.900	>17.75	95.750	>100.813	17.325	98.281	**0.599**	**220.195**

Volumetrics

A key part of a technical evaluation for CO_2 geosequestration is characterising the amount of CO_2 that can be stored (CO_2 capacity) for a given CO_2 injection and storage strategy. The generalised equation for estimating hydrocarbon gas in place can be described as follows and need not be varied to estimate a 'base case' CO_2 volume within traditional structural closures:

$$\frac{GRV \times \phi \times (1 - Sw) \times NTG}{B_g}$$

Where *GRV* is the gross rock volume, ϕ is porosity, S_w is water saturation, *NTG* is net to gross and B_g is the formation volume factor.

The parameters for estimating and populating the volumes used in volumetric calculations in the geological model have been discussed previously. Gross rock volume is equivalent to the 'volume' attribute within four-way structural closure in the geological model and the formation volume factor is the inverse of the 'CO2 expansion factor' attribute (i.e. $1/B_g$). The porosity variable is equivalent to 'SGS_Phi' and there are three attributes representing the water saturation variable: 'Sw_Perm_High'; 'Sw_Perm_Low'; and 'Sw_Phi'.

In the geological model the net to gross (NTG) term is incorporated with a porosity cut-off at 7%. The cut-off at 7% was based on the assumption that the permeability and capillary properties of rock with permeability <7% are such that they will prohibit fluid flow into the rock. Routine core analysis suggests that rocks of <7% porosity are generally associated with permeability of less than 1 mD. The NTG cut-off assumption is relatively conservative in the sense that 1 mD is a common cut-off for oil reservoirs and SC CO_2 is more mobile than oil.

Volumetric estimates for CO_2 capacity were made in a couple of different ways. First, capacity was deterministically calculated directly from the geological model, and second, distributions were assigned to the parameters controlling gas in place to probabilistically estimate CO_2 capacity resulting in a P10-P50-P90 estimate using CrystalBall. The volumetric estimate from the geological model can be considered a deterministic base case or 'most likely' estimate because ranges of uncertainty are not incorporated and because only conventional trapping mechanisms (i.e. structural trapping) are included in the estimate. Unconventional trapping mechanisms such as trapped/residual CO_2, mineralogical trapping and dissolution in formation water are only integrated in the probabilistic volumetric estimate.

As mentioned previously, three methods for calculating S_w were used when S_w was populated in the geological model resulting in three different volumetric estimates for CO_2 capacity: 2.13E+13 scf (21 tcf); 2.57E+13 scf (26 tcf), and; 2.63E+13 scf (26 tcf). The lower and upper estimates used the low and high permeability attributes in the geological model in the calculation of S_w, respectively. The middle estimate used the porosity attribute in the calculation of S_w, which resulted in the more realistic distribution of S_w. The range represented by the three attributes is not particularly meaningful in the sense of capturing uncertainty, but may improve confidence in the S_w values used because two different techniques resulted in fairly similar volumetric estimates.

CO_2 capacity can be visualised within the geological model, which lends insight into areas in which CO_2 can be most efficiently stored (Fig. 6.29). The CO_2 capacity is a measure of the amount of CO_2 that can be stored per model grid cell. Groups of cells associated with high CO_2 capacity approximate the interpreted positions of high porosity N – S and NE – SW trending amalgamations of nearshore sand bodies. The

easternmost part of the study area is characterised by relatively unfavourable rock properties and CO_2 capacity is generally low.

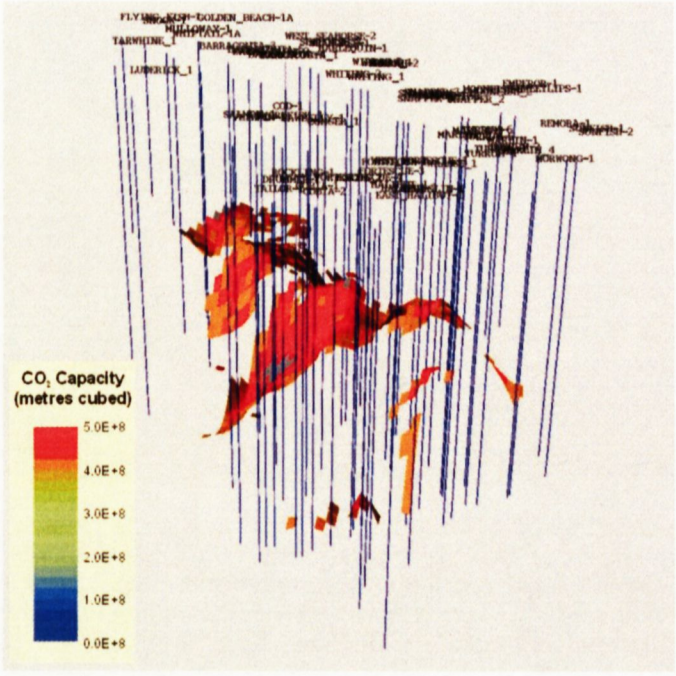

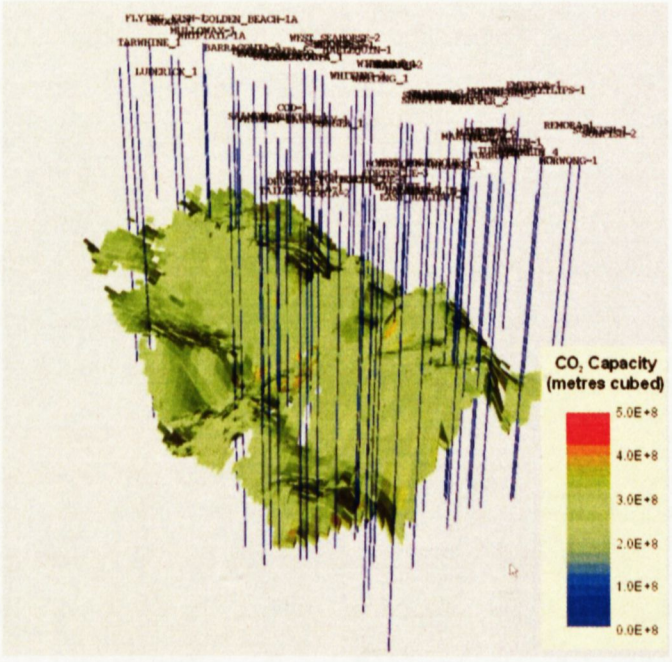

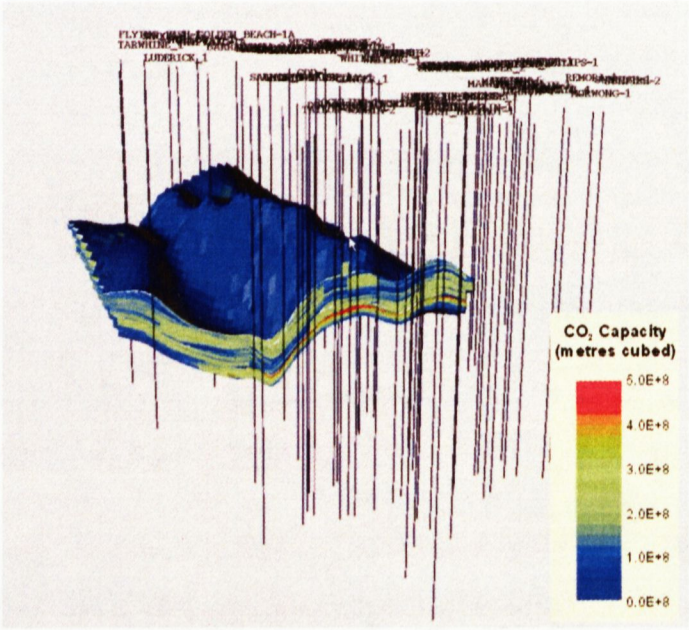

Figure 6.29—Spatial distribution of the CO_2 capacity attribute within the geological model. CO_2 capacity is a function of pressure, temperature, cell volume, porosity, and water saturation. Major areas of very high CO_2 capacity are associated with the stratigraphic architecture of the study—facies tracts of backstopping nearshore facies tend to be associated with high CO_2 capacity.

The deterministic volumetric estimate made from the geological model is based on the assumption that CO_2 is only trapped structurally. In fact, there are several ways in which CO_2 can be stored geologically, including CO_2 within structural closure, residual immobile CO_2 along the migration path, mineralogically trapped CO_2, and CO_2 dissolved in formation water. Each type of geological storage is associated with different volumes of CO_2 and a different degree of uncertainty. Additionally, some mechanisms of geological storage are rate dependant (i.e. time dependent). For example, dissolution into formation water and mineralogical trapping are constrained by the rate of dissolution and the rate of chemical reaction with formation rock.

The estimate of total volume of CO_2 that can be stored in a particular ESSCI scenario is best made when constrained by simulation results, particularly given the uncertainty regarding the rate of CO_2 dissolution into formation water. Each mechanism for geological storage of CO_2 is described below.

STRUCTURAL TRAPPING

Traditional four-way structural closures along the expected migration path probably represent the most important type of geological storage in the Gippsland Basin ESSCI for short time-frames. Hypothetically, the volume of structural closure along the expected CO_2 migration path would fundamentally govern the amount of CO_2 injected into the ESSCI, initially at least. If a greater volume of CO_2 is injected than can be stored in four-way structural closures along the CO_2 migration path, there is a risk of migration west-north-west from the Barracouta structure, towards bubble point depth, towards onshore aquifers, and towards the zero edge of the regional seal. Consequently, the volume of CO_2 that can be stored as a result of other types of geological storage are estimated as a percentage of the CO_2 capacity of structural closure along the migration path.

The major four-way closures along the expected migration path of CO_2 are hydrocarbon fields: Marlin/Turrum, Snapper and Barracouta fields. The CO2Capacity attribute was summed for all grid cells within structural closure.

Uncertainties that could affect CO_2 storage capacity within structural closures along the expected migration path include unproduced hydrocarbon assets and uncertainty regarding the top structure of the four-way closures. Clearly, estimates of the time required for CO_2 to reach existing hydrocarbon fields from numerical flow simulation are likely to prove important as the hydrocarbon fields are presently under production.

A wide range of uncertainty regarding top structure in the Gippsland Basin ESSCI results primarily from complications with depth conversion of the time structural interpretation (Chapter 3). However, well control is good in the Marlin, Snapper and Barracouta areas, so the volume of structural closure is partially constrained. Structural uncertainty was captured in the probabilitistic CO_2 capacity estimate by varying the gross rock volume term by approximately ±30% (Table 6.6).

GAS TRAPPING / RESIDUAL CO_2

Relative permeability and capillary properties of the rock fluid system suggest that some of the SC CO_2 will be trapped behind the mobile SC CO_2 plume as a residual phase. The amount of SC CO_2 trapped is dependent on the length of the migration path and the

shape of the SC CO_2 front. Relative permeability and capillary pressure behaviour are also key parameters controlling the amount of residual gas trapping that might occur. However, with a sufficiently long migration path the whole plume would 'spend' or 'cannibalise' itself. The length of the SC CO_2 migration path is not purely a function of straight-line distance between injection point and structural closure. The degree of reservoir heterogeneity may also significantly increase the effective length of the migration path.

Flow simulation for geosequestration utilising residence/migration time traps suggest that a relatively high proportion of CO_2 could be trapped as a residual phase (20 – 30%; Ennis-King and Paterson 2001, Flett *et al.* 2003) within a production time scale (a few tens of years). Because the process of gas trapping is fairly poorly understood for SC CO_2, due primarily to an absence of experimental data, a range of 5% – 20% of the injected CO_2 volume was used to account for gas trapping in probabilistic capacity estimates.

Mineralogical Trapping

As discussed previously, some mineralological compositions in the Gippsland Basin are appropriate for mineralogical trapping. However, SC CO_2-mineral reaction kinetics are poorly understood. In the short term, mineralogical trapping may not play an important role in storage capacity. For the purpose of probabilistic capacity estimates, an estimate between 0% and 10% of the injected CO_2 volume was used.

Dissolution

In the long term (1000s of years) dissolved CO_2 in the formation water is likely to be the dominant form of storage. Hypothetically, one of the primary issues that would govern the amount of injected CO_2 in the Gippsland Basin ESSCI is the rate of migration versus the rate of dissolution, which will be estimated through flow simulation. The capacity of the Gippsland Basin ESSCI may be dramatically increased if a high percentage of CO_2 is dissolved into the formation water (or trapped) before the Barracouta structure is filled. Given the uncertainty regarding rate of dissolution, the estimated range of the contribution of dissolved CO_2 to total capacity is relatively wide: 5% – 25%. For probabilistic CO_2 capacity estimates, reasonable distributions of the average values of key parameters are required. In general, triangular distributions were used that are

defined by upper and lower limits as well as a mid point. Distributions for variables that affect CO_2 capacity are provided in Table 6.6.

Table 6.6: Ranges for probabilistic CO_2 capacity estimates.

INPUTS				
Variable	Low	Mid	High	Comments
Conventional Volumetric Variables				
Gross Rock Volume (GRV)	1.66E+12 scf	2.66E+12 scf	3.66E+12 scf	Wide range due to limited time depth data for depth conversion.
Porosity (ϕ)	0.14%	0.17%	0.19%	From log analysis data.
Water Saturation (S_w)	0.60%	0.30%	0.20%	Wide range due to uncertainty regarding the efficiency of CO_2 displacing brine.
Net to Gross (NTG)	0.60%	0.75%	0.80%	No porosity cut-off was used for probabilistic volumetric estimates.
Formation Volume Factor ($1/B_g$)	110 scf/scf	130 scf/scf	150 scf/scf	Range stems from uncertainty regarding the exact composition of the CO_2 stream.
CO_2-Specific Volumetric Variables				
Dissolution	0.05%	0.15%	0.25%	Applicable to production time-frame only—larger percentages of dissolved CO_2 expected over longer times.
Gas Trapping	0.05%	0.10%	0.20%	Applicable to production time-frame only.
Mineralogical Trapping	0.00%	0.05%	0.10%	Significant proportion of mineralogically trapped CO_2 over production time-frames considered unlikely.

Unlike the deterministic CO_2 capacity estimate from the geological model, the probabilistic estimate does not use a porosity cut-off so a net-to-gross term is required. Average net-to-gross is estimated to range between 60% – 80% within structural closures in the study area based on petrophysical interpretation.

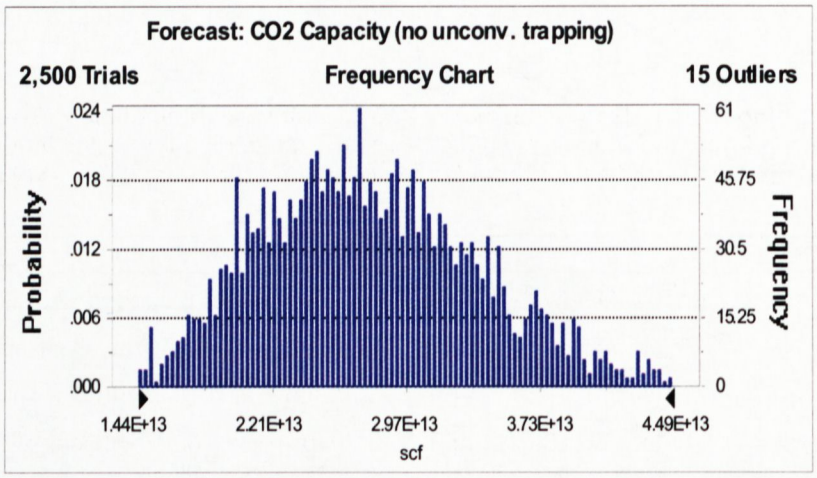

Figure 6.30—Probabilistic distribution of CO_2 capacity with no contribution from unconventional trapping mechanisms (dissolution, gas trapping & mineralogical trapping): P10 = 1.99E+13 scf (20 tcf); P50 = 2.72E+13 scf (27 tcf); P90 = 3.62E+13 scf (36 tcf).

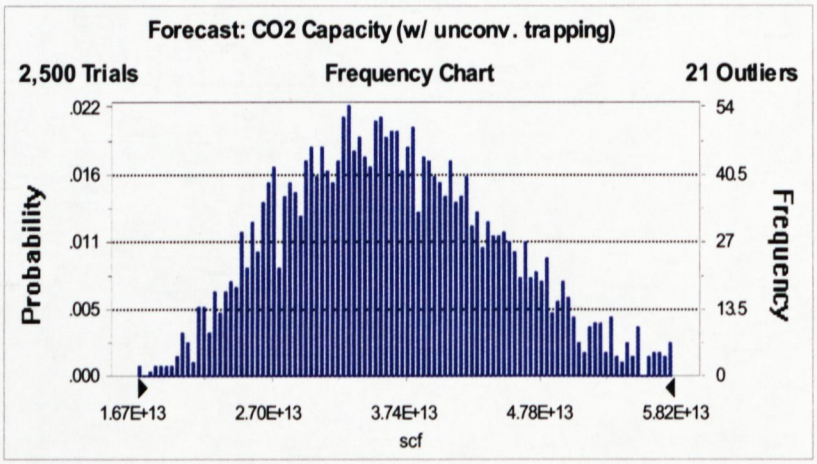

Figure 6.31—Probabilistic distribution of CO_2 capacity with estimated contributions from unconventional trapping mechanisms (dissolution, gas trapping & mineralogical trapping): P10 = 2.59E+13 scf (26 tcf); P50 = 3.59E+13 scf (36 tcf); P90 = 4.78E+13 scf (48 tcf).

The results of the probabilistic estimate of CO_2 capacity in the study area are provided above. The distributions resulting from 2500 trial Monte Carlo runs are provided for traditional capacity estimates in Figure 6.30 and distributions for CO_2-specific capacity estimates incorporating unconventional trapping mechanisms (dissolution, gas trapping, and mineralogical trapping) are provided in Figure 6.31. Distributions are traditionally described by the P10, P50 and P90 values. For the traditional volumetric estimate, excluding unconventional trapping mechanisms, the results are:

- P10 = 1.99E+13 scf (20 tcf)
- P50 = 2.72E+13 scf (27 tcf)
- P90 = 3.62E+13 scf (36 tcf).

For the CO_2-specific volumetric estimate, including unconventional trapping mechanisms, the P10, P50 and P90 results are:

- P10 = 2.59E+13 scf (26 tcf)
- P50 = 3.59E+13 scf (36 tcf)
- P90 = 4.78E+13 scf (48 tcf).

The close correspondence between the of the probabilistic P50 estimate (27 tcf) and the deterministic estimate from the geological model (26 tcf) suggests that the geological model is a reasonably 'well centred' model and therefore improves confidence that the resulting forecasts from numerical flow simulation represent average or 'most likely' outcomes for subsurface CO_2 behaviour. However, the two estimates are not independent so a degree of correspondence is engineered; for example, the GRV estimates are based on the static model in both cases. Additionally, the wide range in the probabilistic distribution of CO_2 capacity is also a useful reminder not to anchor too heavily on 'most likely' outcomes in terms of capacity estimates or CO_2 flow behaviour. There are several key areas associated with considerable uncertainty that markedly affect CO_2 capacity in the study area and are likely to affect CO_2 flow behaviour as well.

It is useful to test the sensitivity of CO_2 capacity to individual variables (Fig. 6.32). Significant uncertainty (±>10 TCF) in volumetric estimates in the Gippsland Basin ESSCI stem from the following five areas (listed in order from greatest to least potential impact on capacity estimates):

- structure and gross rock volume (GRV)
- water saturation
- CO_2 dissolution
- formation volume factor
- gas trapping.

All sources of uncertainty listed above have been discussed previously. In Chapter 7 further work to reduce the range of uncertainty in key areas to improve forecasts and predictions is discussed.

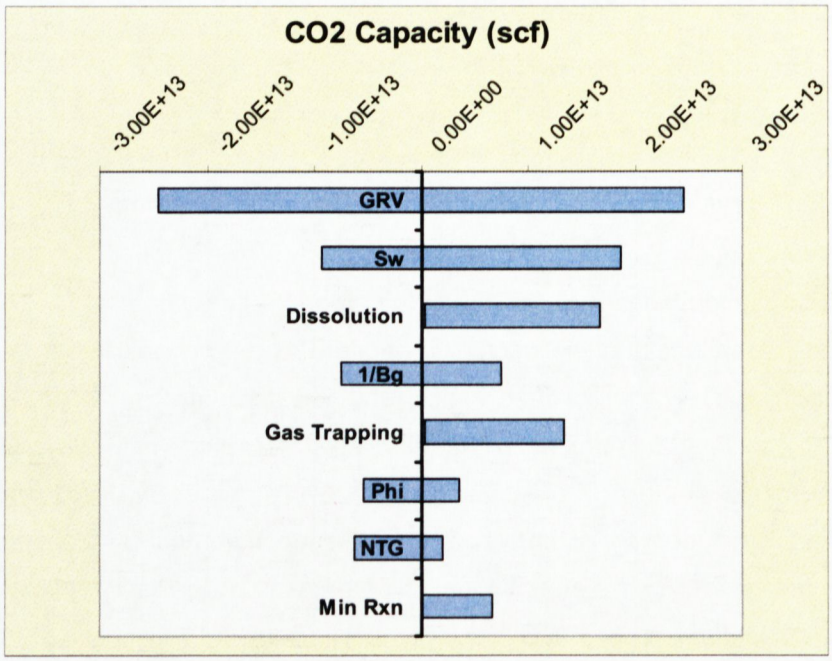

Figure 6.32—Tornado plot showing the impact of uncertainties on CO_2 capacity based on probabilistic estimates.

Chapter 7—Conclusions and Recommendations

Abstract

Numerical flow simulation shows that CO_2 injection at 10 MT/yr (200 bcf) for 20 years at a structurally low injection point near Salmon-1, Conger-1 and Cod-1 wells in the 'central deep' area of the offshore Gippsland Basin will result in up dip migration of CO_2 towards the NNE towards Marlin/Turrum field and then WSW into Snapper field. The expected arrival of CO_2 at Marlin/Turrum field may vary between ~20 years and >200 years after injection ceases depending primarily on permeability heterogeneity and relative permeability behaviour of the CO_2 plume. The key trapping mechanisms are identified as localised structural trapping in depleted hydrocarbon fields along the migration path of the CO_2, residual gas trapping and, in the long term, dissolution of CO_2 into formation water. Numerical flow simulation at a proof of concept level suggests that the CO_2 injection strategy proposed would be technically feasible.

Several conclusions are drawn from work completed in this study related to the feasibility of CO_2 geosequestration in the Gippsland basin and related to geological modeling for geosequestration generally. This study suggests that geosequestration strategies that maximise conventional structural and stratigraphic trapping as well as unconventional trapping mechanisms including CO_2 dissolution in formation water and residual gas trapping behind the CO_2 plume significantly increase the available subsurface storage capacity. A degree of permeability heterogeneity in the target aquifers/reservoirs is useful for reducing CO_2 migration rate and maximising the amount of trapped immobile CO_2. However, over the long term (>1000 yrs) regional structure, particularly at the base of regional sealing units, is likely to be the key control on the spatial distribution of CO_2. Effective strategies for CO_2 geosequestration are significantly different from strategies for traditional hydrocarbon developments or natural gas storage because the CO_2 does not have to be recovered from the subsurface in the foreseeable future and because of the very large volumes of fluid that will typically have to be injected.

Another related difference between traditional hydrocarbon developments and CO_2 geosequestration projects is that very large areas are typically modeled for CO_2 geosequestration, commonly utilising old and inconsistent data sets. Some techniques for managing challenging data sets are proposed specifically pertaining to selecting effective model and grid cell sizes, and geostatistical approaches are suggested for dealing with spatial distribution of data that is unfavourable for stochastic modeling.

Recommendations for additional work stem from key sources of uncertainty in this study and include: developing a probabilistic suite of models for simulation to investigate 'end member' outcomes of geosequestration in the Gippsland Basin; optimisation of the structural interpretation utilising additional time-depth data for depth conversion or interpretation of newly acquired regional 3D seismic data sets; additional research into CO_2-brine-hydrocarbon-rock systems focusing on residual saturations and relative permeability effects, and; further investigation of existing well penetrations and faults in the study area in terms of CO_2 containment in the subsurface.

Introduction

After reservoir characterisation studies and construction of the geological model were completed the model and accompanying data were passed on to reservoir engineers for numerical flow simulation of CO_2 injection and storage in the Gippsland Basin ESSCI. The results of the simulation work are discussed in detail in Ennis-King and Paterson (2003), however, a high level summary is provided herein as the results of numerical flow simulation are necessary for drawing conclusions from this study.

Conclusions stemming from this study are grouped according to:

- Conclusions relating specifically to CO_2 storage in the Gippsland Basin
- Conclusions relating to geosequestration of CO_2 in general
- Conclusions relating to reservoir characterisation and geological model Construction for CO_2 storage.

Summary of Numerical Flow Simulation

Numerical simulation of CO_2 injection and storage was carried out using the reservoir characterisation information and the geological model described previously. The simulation code used was Tough 2, version 2, which can simulate isothermal, multicomponent, multiphase flow and compares well with commercially available simulation codes such as Eclipse and CMG-GEM. A number of 2D and 3D models were simulated to evaluate sensitivity of CO_2 behavior to changes in various technical parameters.

The CO_2 injection and storage strategy employed involved CO_2 injection at a rate of 10 Mt/yr (~200 bcf) for 20 years in the structurally low area near wells Salmon-1, Conger-1 and Cod-1 approximately 25 km down dip from Marlin/Turrum field. The CO_2 volume and the rate of injection were selected to simulate a realistic CO_2 sequestration project. The rationale for the proposed injection location for CO_2 injection is described in greater detail previously in Chapters 3 and 6. The CO_2 stream is injected from a single well with a maximum injection pressure of 30 MPa (~4350 psi). Key sensitivities to the subsurface flow behavior of CO_2 were also investigated through flow simulation. The key outcomes of numerical flow simulation carried out by Jonathan Ennis-King and Lincoln Paterson are summarised below.

Overall flow simulation suggests that the subsurface flow behavior of CO_2 will be as expected: the initial direction of CO_2 migration is NNE, up structural dip towards Marlin/Turrum field and later WSW towards Snapper and Barracouta fields (Fig. 7.1). The key control on the long term (1000's of years) distribution of CO_2 is the structure at the base of regional sealing units, however, permeability heterogeneity and relative permeability behavior are important affects on CO_2 migration rate and distribution over shorter time intervals (10's – 100's of years). Key CO_2 trapping mechanisms are localised structural trapping (primarily in depleted hydrocarbon fields), residual gas trapping, and in the long term dissolution of CO_2 into formation water.

All simulation cases showed that CO_2 has not reached Barracouta field after 2000 years. Consequently, there appears to be little risk of CO_2 migrating to onshore freshwater aquifers, depths of bubble point pressure/temperature conditions or the zero edge of regional seal units with the injection and storage strategy suggested in this study (assuming roughly equivalent rates of CO_2 injection). The shortest arrival time of SC CO_2 at Marlin/Turrum field was ~20 years after injection ceases, which is well after forecasted field abandonment (Ennis-King and Patterson 2003). The 20 year arrival time of CO_2 at Marlin/Turrum field resulted from use of a homogenised 'base case' model, where average flow properties were applied to the various zones in the model. In other words, negligible reservoir/aquifer heterogeneity was represented, which expedites the rate of SC CO_2 migration; a useful 'end member' case though somewhat unrealistic.

As expected, the introduction of reservoir/aquifer heterogeneity to the model resulted in a reduced rate of up dip CO_2 migration due to a more tortuous migration path. Some realisations of permeability heterogeneity resulted in arrival times of CO_2 at Marlin/Turrum field in excess of 200 years. Over longer time periods the migration rate and direction of CO_2 is less sensitive to permeability heterogeneity. At 2000 years the distribution of CO_2 was similar for all simulation cases regardless of permeability heterogeneity. However, in the long term higher permeability heterogeneity decreases the amount of CO_2 dissolution into formation water, presumably because lateral migration is more restricted so contact between the CO_2 plume and formation water is reduced overall (Fig. 7.2).

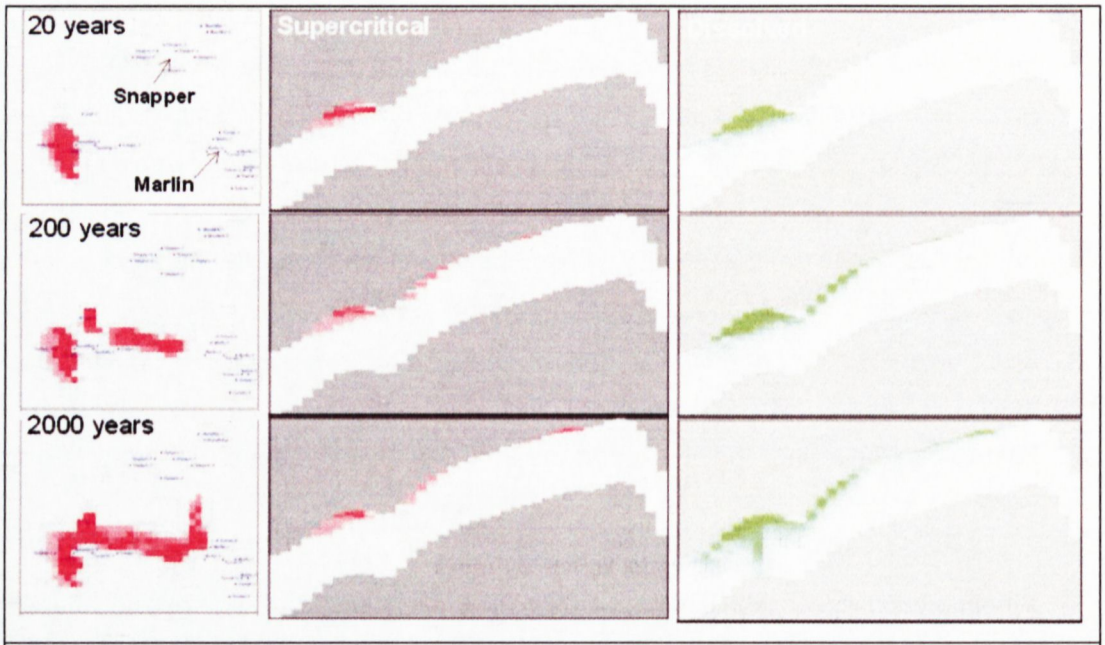

Figure 7.1—One realisation of a reservoir flow simulation of the upper Latrobe Group ESSCI for 20 years, 200 years and 2000 years after CO_2 injection ceases. (a) Plan view of gas saturation in the topmost layer of the grid. (b) Vertical cross-section of gas saturation along an up dip line between Salmon-1 and Marlin-1. (c) Vertical cross-section of the mass fraction of dissolved CO_2 along an up dip line between Salmon-1 and Marlin-1. Figure from Root *et al.* (2004).

The ratio of horizontal to vertical permeability (k_v/k_h) was also varied between 0.1 and 0.01 to evaluate the affect on CO_2 flow behavior. Lower values of k_v/k_h retarded the arrival of CO_2 at the base of the regional seal and consequently, decreased the rate of up dip CO_2 migration.

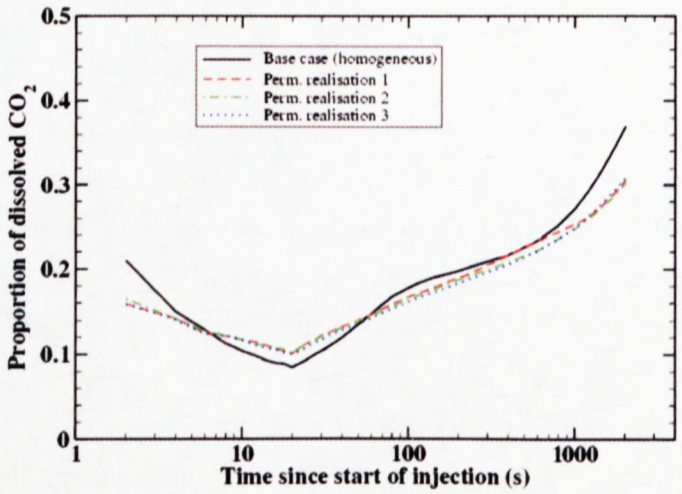

Figure 7.2—Proportion of dissolved CO_2 over time for the base case model and three different permeability realisations. Figure from Ennis-King and Paterson (2003).

The flow behavior of SC CO_2 was also influenced by the choice of relative permeability and capillary pressure curves. Relative permeability and capillary pressure behavior are key controls on the residual CO_2 saturation left behind the SC CO_2 plume and also influence the rate of SC CO_2 dissolution into the formation water. A comparison was made between the 'base case' model characterised by 20% residual CO_2 saturation (S_{gr}) and 20% residual water saturation (S_{wr}) and an alternative model characterised by 5% S_{gr} and 11% S_{wr}. The alternative model results in less rapid lateral migration of SC CO_2 in the short term (0 – 20 yrs) which is probably attributable to two effects: more SC CO_2 can be stored in a smaller rock volume due to lower S_{wr}, and; relative permeability to gas at low water saturations is less than in the base case model. As a result of less rapid lateral migration the arrival time of SC CO_2 at Marlin/Turrum field is later than in the base case model (~60 years after CO_2 injection ceases).

The use of alternative relative permeability and capillary pressure curves in one case resulted in an alternative migration path for some of the SC CO_2, which flowed NNW from the injection point towards Whiting field rather than directly up dip towards Marlin/Turrum field. The alternative migration path is thought to be a consequence of lower S_{gr}, which has the effect of allowing the SC CO_2 plume to spread farther over the longer term (200 – 2000 yrs). In addition to the alternative migration path, the low S_{gr} model showed a higher percentage of dissolved CO_2 than the base case model at 2000 years (44% versus 37% respectively) due to the greater lateral spread of the SC CO_2 plume. The inferred time for complete dissolution of the SC CO_2 plume is thousands of years at least.

The migration of the SC CO_2 plume induced by down dip injection was important for a few reasons. First, the up dip migration of SC CO_2 resulted in residual gas saturation behind the SC CO_2 plume, which is immobile and effectively trapped. Second, up dip migration of SC CO_2 induced contact between the SC CO_2 plume and large volumes of formation water, which increased the rate of dissolution. Flow simulation showed that both residual gas trapping and dissolution were key trapping mechanisms in addition to conventional structural trapping along the migration path. A third reason that the down dip injection location is important is that it provides a stand off from producing hydrocarbon fields and would probably allow sufficient time to complete field development and abandonment.

The sensitivity of SC CO_2 flow behavior to changes in injector well location of a few kilometres was also evaluated. In general small shifts in the injector well location had little impact on SC CO_2 migration rate and direction. However, there is a small localised structural high in the proposed injection area so an injector location too near the spill point (e.g. Sawbelly-1 area) could result in a more rapid arrival of SC CO_2 at Marlin/Turrum field than was observed in the base case. Additionally, it can be qualitatively observed based on the base seal structure that shifting the injection location too far west and/or north could result in an alternative migration path (NNW) for some of the injected CO_2; this was observed in the simulation run using an alternative relative permeability curve.

A degree of flexibility in the injection location is useful due to faults in proximity to the injection location. It may be advantageous to optimise the injection site to minimise pore pressure increase at some faults in the study area to reduce risk of geomechanical reactivation and associated leakage (Root *et al.* 2004). Presently, the *in situ* stress tensor in the study area is not sufficiently well constrained to estimate maximum sustainable pore pressure at faults due to limited data. Further geomechanical work would be useful to help optimise injector well locations and constrain maximum injection pressures.

An important observation from flow simulation was that a relatively small amount of SC CO_2 was structurally trapped at Marlin/Turrum field and consequently, SC CO_2 migration WSW towards Snapper field occurred sooner than expected. It is thought that the Marlin/Turrum field structure represented in the geological may be unrealistically small due primarily to complications with depth conversion of the seismic interpretation (Chapter 3). Hydrocarbon reserve estimates for Marlin/Turrum field may suggest a larger structure than is represented in the geological model (Ennis-King and Paterson 2003). As previously discussed (Chapter 6), structure (GRV) is identified as the uncertainty with the greatest potential impact on CO_2 capacity in the study area. Some options are suggested later in this chapter for addressing this uncertainty.

There are a few aspects of the Gippsland Basin ESSCI that were not investigated through numerical flow simulation. These include: the salinity gradient in the study area, the effect of regional hydrodynamic flow, residual hydrocarbon saturation in depleted fields and mineralogical trapping. Both the effects of hydrodynamic flow and salinity are likely to be less important than the other effects that were evaluated

through numerical flow simulation, but remain interesting and may be locally important.

The result of the salinity variations in the study area would have been mainly corresponding variations in the solubility of SC CO_2 in formation water (lower solubility in areas of high salinity). In the simulation models a constant salinity of 25,000 ppm was used. The effect of hydrodynamic flow on storage is an interesting area of research and is further addressed in Root *et al.* (2004) however, Ennis-King and Paterson (2003) point out that it is necessary to hypothesis future production from hydrocarbon fields to make practical predictions. Broadly however, the direction of hydrodynamic flow is the study area is known to be from the onshore to the offshore so qualitatively the impact of hydrodynamic flow might be to somewhat retard the rate of up dip CO_2 migration. Qualitatively however, it is understood that gravity forces will be the dominant force controlling the direction and rate of SC CO_2 migration to the presence of appreciable dip of sealing units due to the significant density contrast between SC CO_2 and water.

The influence of residual hydrocarbon saturation in depleted fields and mineralogical trapping are presently too complex to investigate through numerical flow simulation and some possible effects have been discussed previously in this report. The salinity, pressure and mineralogical information provided in this study may form the basis for more detailed studies in the future.

Another aspect of CO_2 geosequestration not addressed through the numerical flow simulation is the impact of viscous flow on CO_2 behaviour. Tough 2 does not have provisions for non-Darcy flow so viscous flow behavior of CO_2 was not represented in the simulations. However, with the CO_2 injection and storage strategy selected the dominant flow behaviour will result from gravity forces as CO_2 migrates up structure. Non-Darcy effects would only be expected in proximity to the injection site and would drop off as pressure decreases away from the injector. For the relatively long-distance migration path scenario proposed herein, the impact of viscous flow is expected to be minimal. However, future work should address flow behaviour in close proximity to the injection site with simulators capable of representing non-Darcy flow utilising detailed geological models focusing locally around the injection site.

At a 'proof of concept' level reservoir characterisation, geological modeling and numerical flow simulation suggest that the proposed strategy for geological CO_2

storage in the Gippsland Basin central deep area is technically feasible. However, there are several technical areas that would require further work, which are discussed below.

Conclusions Relating to Geological Storage of CO_2 in the Gippsland Basin

- Based on numerical flow simulation a CO_2 injection and storage strategy involving a combination of traditional structural traps (depleted hydrocarbon fields) and residence time/migration path trapping may be the most effective geosequestration solution. Slow migration of the CO_2 plume up structure and through the depleted hydrocarbon fields will increase exposure of SC CO_2 to fresh water and fresh rock to induce dissolution and possibly mineralogical trapping, adding to the overall capacity of the ESSCI. Additionally, the migration of the CO_2 plume promotes gas trapping behind the CO_2 plume resulting in immobile, residual gas saturation, which also contributes to the overall capacity of the Gippsland Basin ESSCI.

- Down dip injection of CO_2 is an important component of the overall strategy—down dip injection not only promotes dissolution of SC CO_2 into formation water and residual gas trapping, but also provides a stand off between the migrating SC CO_2 and producing hydrocarbon fields. Arrival time of CO_2 at Marlin/Turrum field varies between 20 and more than 200 years, which is thought to be sufficient time to complete the field development and abandonment. Longer arrival time estimates result from the incorporation of realistic permeability heterogeneity in the simulation model, so a later arrival time than 20 years may be the more accurate estimate.

- A deterministic volumetric estimate of the Gippsland Basin ESSCI capacity for CO_2 suggests capacity of 26 tcf, which excludes the contribution of unconventional trapping mechanisms (dissolution, residual gas trapping, and mineralogical trapping). Notional probabilistic estimates that include estimates for unconventional trapping mechanisms indicate considerable extra capacity: P10 = 26 tcf; P50 = 36 tcf, and; P90 = 48 tcf. For the case evaluated through numerical flow simulation, which is thought to incorporate a realistic CO_2 volume and

injection rate (10 Mt/yr [~200 bcf] for 20 yrs), the capacity of the Gippsland Basin ESSCI is more than sufficient.

- Flow simulation of CO_2 injection at 10 Mt/yr for 20 years shows that CO_2 has just reached Snapper field after 2000 years and is not near onshore fresh water aquifers, bubble point depth or the zero edge of regional seal units.

- Due to complications with depth conversion the Marlin/Turrum field structure represented in the geological model is thought to under-represent the full CO_2 capacity of the field. Consequently, the estimated time of CO_2 arrival at Snapper field (~2000 years) is probably unrealistically short.

- Numerical flow simulation suggests that approximately 40% of the injected CO_2 will be dissolved in the formation water at 2000 years after injection ceases. At 2000 years the rate of CO_2 dissolution appears to be constant or increasing. This suggests a reasonable residence time target on the order of several thousand years.

- Structural uncertainty is the key uncertainty affecting the CO_2 capacity of the Gippsland Basin ESSCI concept. Other key uncertainties that could result in more than ±10 tcf of CO_2 capacity include: residual water saturation, dissolution rate of CO_2 into formation water, formation volume factor (dependant on composition of the CO_2 stream) and the amount of residual gas trapping.

- Based on a top seal evaluation addressing seal capacity, seal geometry and seal integrity, the Lakes Entrance Formation represents a sufficient top seal for CO_2 geosequestration. MICP experiments suggest the marl and mudstone of the Lakes Entrance Formation is sufficient to hold back a column of supercritical CO_2 ~750 m in thickness, which is more than twice the height of the largest structural closure along the expected migration path.

- Average pressure and temperature conditions in reservoirs/aquifers units of the target injection area are ~60°C and ~12 MPa (1741 psi), which is more than sufficient to maintain CO_2 in a supercritical state. Under reservoir/aquifer conditions in the target injection area pure CO_2 will be compressed to a volume

~200 times less than at standard pressure/temperature conditions, which significantly improves storage efficiency.

- The stratigraphy of the Eocene Latrobe Group in the Gippsland Basin is broadly characterised by a transgressive, retrogradational stacking pattern reflecting progressive shifts of the shoreline towards the W, NW during deposition. Stratigraphic units have been tilted and dip gently westward resulting in angular truncation at the top Latrobe Group unconformity. The large-scale stratigraphic architecture and truncation at the top Latrobe Group unconformity are the key controls on large-scale stratigraphic architecture.

- Sedimentological interpretation suggests that the rocks of the study area were deposited in a range of depositional environments from fluvial to nearshore marine and offshore shelfal environments. The key reservoir/aquifer targets for CO_2 injection are high porosity and permeability (average: 25% and 100's mD), compositionally mature, nearshore sand bodies located primarily in the *M. diversus* and *P. asperopolus* biozones of the stratigraphy. Individual nearshore sand bodies are expected to have good interconnectivity and are expected to be several kilometres wide and several tens of kilometres long oriented from N-S and NE-SW. Fluvial channels are secondary reservoir targets, which also have excellent flow properties locally, but are characterised by lower compositional maturity and individual sand bodies are likely to be less interconnected.

- Several mineralogical components in sandstone of the study area may react with CO_2 particularly over long time frames and may be involved in reactions resulting in permanent mineralogical trapping of CO_2. Potentially reactive mineralogical components include: carbonate cement; metamorphic and volcanic lithic framework grains; glaucony, carbonate minerals in marl, and; plagioclase framework grains. Sandstone from coastal/alluvial plain facies is characterised by relatively low compositional maturity and has greater potential for mineralogical trapping than sandstone from nearshore facies.

General Conclusions on Geological Storage of CO_2

- Strategies for geological disposal of CO_2 differ fundamentally from traditional petroleum production projects including gas storage because:

- Injected CO_2 does not have to be recovered from the subsurface in the foreseeable future.
- Very large areas will typically have to be utilised due to the large volumes of CO_2 that are likely to be sequestered.
- Both chemically and physically SC CO_2 behaves differently to hydrocarbon gas and liquid. Two key differences are that SC CO_2 is soluble in water and SC CO_2 can chemically react with some mineralogical components in reservoir/aquifer rock.

- Unconventional trapping mechanisms including dissolution of SC CO_2 in formation water, residual gas trapping, and possibly mineralogical trapping are key mechanisms that can be utilised to increase storage capacity of CO_2 in the subsurface.

- Strategies for CO_2 injection and storage that induce migration of the SC CO_2 plume are useful for leveraging unconventional trapping mechanisms because residual gas trapping occurs behind the mobile plume and because contact between the SC CO_2 plume and large volumes of formation water and rock is induced.

- Permeability heterogeneity in target reservoirs/aquifers is useful to reduce the rate of SC CO_2 migration and to more effectively trap SC CO_2 in the subsurface. An ideal reservoir/aquifer target is of sufficient permeability to permit injection at the required rates at minimal cost, but not high enough permeability to result in rapid migration of the SC CO_2 plume, which may reduce residence time in the subsurface.

- Traditional structural and stratigraphic traps are not required provided the projected residence time for subsurface SC CO_2 is sufficient to allow for immobilisation through residual gas trapping and dissolution into the formation water of all of the injected CO_2.

- Permeability heterogeneity and relative permeability behaviour are key parameters controlling SC CO_2 migration and areal distribution over the short term 10's – 100's of years. Over the long term, structure at the base of the regional sealing unit appears to be the most important control.

Conclusion Relating to Reservoir Characterisation and Geological Model Construction for CO_2 Storage

- Geological models representing larger areas than typical field-scale hydrocarbon development models generally need to be constructed for the simulation of CO_2 storage for a number of reasons:
    - Very large volumes of CO_2 are likely to be stored.
    - Traditional structures with four-way closure are limited in terms of total capacity within Australia and in terms of availability due to existing hydrocarbon resources.
    - The most viable ESSCI options in Australia presently are residence time/hydrodynamic traps that are associated with long migration paths.
- Some technical challenges associated with geological model construction specifically for geosequestration of CO_2 stem from the need for very large reservoir models. Additionally, targets for CO_2 injection are commonly aquifers and abandoned hydrocarbon fields that are typically associated with sparse, old and incomplete data sets. Some associated issues may include:
    - Evaluating tradeoffs between grid cell size and computational limitations for geological models. In this study grid cell size was selected with reference to the size of the individual flow units that needed to be represented in the geological model (Chapter 5).
    - Data paucity and data distribution that is not favourable for generating geostatistical models to guide stochastic population of attributes in the geological model. In this study depositional analogues were used to guide the selection of geologically meaningful geostatistical models for the regional population of attributes over very large areas (Chapter 6). Facies maps were also generated from core, wireline and seismic data to regionally constrain geostatistical population of attributes (Chapter 3). The incorporation of seismic data in stochastic attribute population is useful in areas of sparse well control.
    - Models of sufficient size for flow simulation of CO_2 regionally may not have the resolution to resolve detailed flow issues in close proximity to the injection well. Localised grid refinements or detailed sector models around the injection site may be useful for improving understanding at both scales of analysis.
- The emphasis of reservoir characterisation and geological model construction in traditional hydrocarbon production projects is typically on reservoir flow units or

'pay' because the containment is already proven by the existence of hydrocarbon columns. In contrast reservoir characterisation and geological model construction for geological CO_2 storage must put at least as much emphasis on 'non-pay' low permeability seals and flow baffles. The structure, stratigraphic architecture and flow properties of baffle, barrier and seal units required considerable attention.

Recommendations for Further Work

The reservoir characterisation and geological model construction in this study has been referred to as proof of concept level work. Further work would be required if a CO_2 geosequestration project were to be executed in the Gippsland Basin. Below some focus areas for future work are listed.

- The geological model constructed in this study is a deterministic 'most likely' model so simulation forecasts do not capture the full range of possible outcomes for CO_2 injection and storage. For example, although a range of permeability was built into the model only a single porosity model was generated (though multiple realisations are contained within the single model). If further work is undertaken it is recommended that a range of models be developed based on ranges of constituent parameters including petrophysical parameters (porosity, permeability, saturations), structure (multiple depth conversions), and stratigraphic (alternative correlations). This will allow the investigation of critical 'end member' outcomes for geological storage in the Gippsland Basin ESSCI.

- The structural uncertainty associated with the BaseSeal horizon could have a large impact on CO_2 capacity and flow behaviour. It is recommended that the structural uncertainty be reduced if further work is undertaken by acquisition of additional time depth data (particularly more seismic stacking velocities). Due to the complexity of overburden lithologies in the study area and due to the importance of GRV and structural uncertainty, pre-stack depth migration work might be considered, at least over the four-way closures along the CO_2 migration path.

- There is uncertainty associated with fluid and rock properties, which were partially addressed in this study. Areas for further work might include: the effect of residual hydrocarbon saturations in depleted fields on injected CO_2; CO_2-hydrcarbon-brine

relative permeability, and; irreducible water saturations where water is displaced by supercritical CO_2. Additionally, it would be useful to know what impurities are expected in the CO_2 stream and what their impact might be on the physical and chemical behaviour of the CO_2. A number of engineering and simulation studies could be undertaken to narrow the range of uncertainty in these areas.

- The effect of chemically reactive mineralogical components in the study area is only notionally addressed in this study. Flow-through experiments with core from the study area and CO_2 saturated brine as well as coupled geochemical-flow simulation would be useful to understand the impact of CO_2-rock reactions.

- After the seismic interpretation for this study was completed petroleum companies operating in the Gippsland Basin have acquired a large 3D seismic survey over the study area. Interpretation of this data set would represent an improvement over the dense 2D grid comprising surveys of multiple vintages used in this study. Additionally, the stacking velocities associated with this survey would be extremely useful for addressing structural uncertainty.

- Notwithstanding the attenuation effects of thick coal intervals within the study area, a qualitative examination of older vintage full stack 2D data indicates that hydrocarbon gas accumulations are associated with fairly strong amplitude responses. This may suggest considerable scope for investigation of 3D time lapse seismic as a monitoring tool for tracking subsurface CO_2. The existing core and wireline database may be a logical starting point to begin rock physics models and fluid substitution work.

- The recent acquisition of 3D data over the study area also presents opportunities to estimate rock properties from the seismic data. There are numerous approaches available that invert seismic data for any number of rock properties; impedance and porosity are among the more reliable in most areas. Even suites of amplitude extractions from 3D volumes might considerably improve the understanding of reservoir/aquifer and seal architecture in areas of sparse well control.

- Additional numerical flow simulation incorporating salinity variation, pressure variation due to hydrocarbon production, residual hydrocarbon affects, and CO_2-

rock reactions would be useful; however, it is acknowledged that simulations of this complexity may be beyond current technological constraints. Detailed flow simulation in and around the proposed injection site would also be useful to investigate non-Darcy flow effects and may assist in making decisions regarding injector well design, well count and well completion strategy.

- More detailed investigation of faults in the study area is recommended in terms of their potential to act as conduits for the vertical migration of CO_2. Specifically, fault rock composition could be addressed in terms of shale gouge ratio, cataclasis and cementation as well as the potential for chemical reactions between CO_2 and fault rock. Additional work to constrain the *in situ* stress tensor in the study area may also prove useful for estimated maximum sustainable pore pressure increases at faults in the study area.

- The issue of existing well penetrations into the Latrobe Group has not been addressed in this study. The exploration, appraisal and development wells along the expected flow path of the CO_2 represent potential containment risks. Work should be undertaken to ensure all wells on the expected flow path have been identified and appraised in terms of the ability to re-enter them and plug and abandon suitably for CO_2 containment. There may be an opportunity to re-enter some wells and convert them to monitoring or injection wells.

- There are a number of critical areas that would have to be addressed prior to embarking on a CO_2 geosequestration project in the Gippsland Basin including: economic, legal and commercial feasibility studies; facilities planning; environmental studies on oceanic and subsurface flora and fauna, and; CO_2 monitoring to name a few. Though most of these are well beyond the scope of this study, an evaluation of the technical feasibility of geophysical monitoring of subsurface CO_2 in the offshore Gippsland Basin particularly would be a very useful companion piece to the work described herein.

References Cited

Allen, G.P. 1998. *Sedimentation in the Modern and Miocene Mahakam Delta: Field Guide*, TOTAL Centre Scientifique et Technique, St. Remy les Chevreuse, France, 236 p.

Allen, J.R.L. 1982. *Developments in Sedimentology: Sedimentary Structures, their Character and Physical Basis, Volume 1*, Elsevier Scientific Publishing Company, Amsterdam, 593 p.

Allen, J.R.L. 2001. *Principles of Physical Sedimentology*, the Blackburn Press, Caldwell, New Jersey, 272 p.

Bachu, S. 2000. 'Sequestration of CO_2 in geological media: criteria and approach for site selection in response to climate change', *Energy Conservation and Management*, **41**, 953 - 970.

Bachu, S., Gunter, W.D. and Perkins, E.H. 1994. 'Aquifer disposal of CO_2: hydrodynamic and mineral trapping'. *Energy Conservation and Management*, **35**, 4, 269 - 279.

Bachu, S. and Gunter, W.D. 1999. 'Storage Capacity of CO2 in sedimentary basins with application to the Alberta Basin.' *In* Eliasson, B., Riemer, P.W.F. and Wokan, A. (Eds.) *Greenhouse Gas Control Technologies*, Peragamon, Amsterdam, 195 – 200.

Bachu, S., Adams, J.J., Micheal, K. and Buschkuehle, B.E. 2001. 'Acid gas injection in the Alberta Basin: a commercial-scale analogue for CO_2 geological sequestration in sedimentary basins'. *National Energy Technology Laboratory Publications, 2001 Conference Proceedings*, Available: http://www.netl.doe.gov/publications/proceedings/01/carbon_seq/carbon_seq01.html [12 Sept. 2004].

Bahar, A. and Kelkar, M. 1998. 'Journey from well logs/cores to integrated geological and petrophysical properties simulation- a methodology and application,' SPE 39565, *SPE India Oil and Gas Conference and Exhibition Proceedings*, New Delhi, 543-552.

Barwis, J.H. and Hayes, M.O. 1979. 'Regional patterns of modern barrier island and tidal inlet deposits as applied to palaeoenvironmental studies,' *In* Ferm, J.C., Horne, J.C., Weisenfluh, G.A. and Staub, J.R. (Eds.) *Carboniferous Depositional Environments in the Appalachian Region*, University of Southern California, Department of Geology, Columbia, S.C. 472-498.

Benson, S. M. 2003.' Lessons Learned from Natural and Industrial Analogues for Storage of Carbon Dioxide in Deep Geologic Formations', E.O. Lawrence Berkeley National Laboratory, Berkley, California, 135 p. (unpublished).

Bernecker, T. and Partridge, A.D. 2001. 'Emperor and Golden Beach Subgroups: the onset of Late Cretaceous sedimentation in the Gippsland Basin, SE Australia', *In* Hill, K.C. and Bernecker, T. (Eds.) *PESA Eastern Australian Basins Symposium 2001*, The Australasian Institute off Mining and Metallurgy, Carlton, Australia, 371-385.

Bishop, M.G., 2000. 'Petroleum system of the Gippsland Basin, Australia. United States Geological Survey', Open-File Report 99-50-Q [online], Available: http://geology.cr.usgs.gov/energy/WorldEnergy/OF99-50Q/ [6 Nov. 2002].

Bjørlykke, K. 1984. *Sedimentology and Petroleum Geology.* Springer-Verlag, Berlin, 363 p.

Blatt, H., Berry, W.B.N., Brande, S. 1991. *Principles of Stratigraphic Analysis,* Blackwell Scientific Publications, Boston, 512 p.

Bodard, J.M., Wall, V.J. and Cas, R.A.F. 1984. 'Diagenesis and evolution of Gippsland Basin reservoirs', *The APEA Journal*, **24**, 314-335.

Bohacs K. and Suter, J. 1997. 'Sequence stratigraphic distribution of coaly rocks: fundamental controls and paralic examples'. *AAPG Bulletin*, **81**, 10, 1612 – 1639.

Bowker, K.A. and Shuler, P.J. 1991. 'Carbon dioxide injection and resultant alteration of the Weber Sandstone', Rangely Field, Colorado, *AAPG Bulletin*, **75**, 9, 1489 - 1499.

Boyd, R., Dalrymple, R. and Zaitlin, B.A. 1992. 'Classification of coastal depositional environments', *Sedimentary Geology*, **80**, 139 - 150.

Bradshaw, J., Bradshaw, B., Spencer, L. and Mackie, V. 2000. 'GEODISC Project 1: Regional Analysis, Stage 2 Basins, version 2.02, November 2000' (compact disc), GEODISC internal report (unpublished).

Bradshaw, J. and Rigg, A. 2001. 'The GEODISC program: research into geological sequestration of CO2 in Australia'. *Environmental Geosciences*, **8**, 3, 166 - 176.

Bradshaw, B., Simon, G., Bradshaw, J. and Mackie, V. 2002a. 'GEODISC research: carbon dioxide sequestration potential of Australia's coal basins', Geoscience Australia, Canberra, Australia (unpublished manuscript).

Bradshaw, J., Bradshaw, B.E., Allinson, G., Rigg, A.J., Nguyen, V. and Spencer, L. 2002b. 'The potential for geological sequestration of CO_2 in Australia: preliminary findings and implications for new gas field development', *The APPEA Journal*, **42**, 25 - 46.

Busch, D.A. 1971. 'Genetic units in delta prospecting', *AAPG Bulletin* **55**, 8, 1137-1152.

Chambers, R.L. 2000. 'Petroleum geostatistics fo nongeostaticians, part 2'. *The Leading Edge*, June 2000, 593-599.

Coleman, J.M. 1969. 'Brahmaputra River; channel processes and sedimentation', *Sedimentary Geology*, **3**, 129-239.

Collinson, J.D. and Thompson, D.B. 1982. *Sedimentary Structures,* George Allen and Unwin, London, 194 p.

Conybeare, C.E.B. and Crook, K.A.W. 1982. *Manual of Sedimentary Structures. Geology and Geophysics Bulletin 102.* Bureau of Mineral Resources, Australian Government Publishing Service, Canberra, 194 p.

Cook, P.J., Rigg, A. and Bradshaw, J. 2000. 'Putting it back where it came from: is geological disposal of carbon dioxide an option for Australia?' *The APPEA Journal*, **40**, 654 - 666.

Dalrymple, R.W., Zaitlin, B.A. and Boyd, R. 1992. 'Estuarine facies models: conceptual basins and stratigraphic implications', *Journal of Sedimentary Petrology*, **62**, 1030 – 1146.

Demarest, J.M. and Kraft, J.C. 1987. 'Stratigraphic record of Quaternary sea levels: implications for more ancient strata'. *In* Nummedal, D., Pikey, O.H., Howard, J.D. (Eds.) *Sea Level Fluctuation and Coastal Evolution*, SEPM Spec. Pub. **41**, 223 – 239.

Deutsch, C.V. 2002. *Geostatistical Reservoir Modelling*. Oxford University Press, New York, 376 p.

Dewhurst, D.N., Jones, R.M. and Raven, M.D. 2002.'Microstructural and petrophysical characterization of Muderong Shale: application to top seal risking', *Petroleum Geoscience*, **8**, 1-13.

Doughty, C., Benson, S.M., and Pruess, K. 2002. 'Capacity investigations of brine-bearing sands for geological sequestration of CO_2'(poster), *Sixth International Conference on Greenhouse Gas Control Technologies,* Lawrence Berkeley National Laboratory, California, USA.

Downey, M.W. 1984. 'Evaluating seals for hydrocarbon accumulations', *AAPG Bulletin,* **68**, 11, 1752-1763.

Dubrule, O. and Damsleth, E. 2001. 'Achievements and challenges in petroleum geostatistics', *Petroleum Geoscience*, **7**, S1 – S7.

Eliasson, B. 2001. 'Energy in the 21st century, the role of GHG control technologies', *In* Williams, D., Durie, B., McMullan, P., Paulson, C. and Smith, A. (Eds.) *Greenhouse Gas Control Technologies, Proceedings of the Fifth International Conference on Greenhouse Gas Control Technologies*, CSIRO Publishing, Collingwood, Australia, 290 - 295.

Ennis-King, J. and Paterson, L. 2001. 'Reservoir engineering issues in the geological disposal of carbon dioxide', *In* Williams, D., Durie, B., McMullan, P., Paulson, C. and Smith, A. (Eds.) *Greenhouse Gas Control Technologies, Proceedings of the Fifth International Conference on Greenhouse Gas Control Technologies*, CSIRO Publishing, Collingwood, Australia, 290 - 295.

Ennis-King, J., Gibson-Poole, C.M., Lang, S.C. and Paterson, L. 2002. 'Long-term numerical simulation of geological storage of CO_2 in the Petrel Sub-Basin, North West Australia', *Sixth International Conference on Greenhouse Gas Control Technologies* [online], Available: http://www.rite.or.jp/GHGT6/ [6 Nov. 2002].

Ennis-King, J. and Paterson, L. 2003. 'GEODISC Project 3: Long-term reservoir simulation of the geological sequestration of carbon dioxide in the offshore Gippsland Basin', GEODISC Internal Report (unpublished), Adelaide, Australia, 52 p.

Esso Australia Limited, 1988. *The Gippsland Basin. Petroleum in Australia, the First Century*, Australian Petroleum Exploration Association, Sydney, Australia, 174-190 p.

Farrell, K.M. 1987. 'Sedimentology and facies architecture of overbank deposits of the Mississippi River, False River region, Louisiana', *In* Ethridge, F.G., Flores, R.M. and Harvey, M.D. (Eds.) *Recent Developments in Fluvial Sedimentology*, SEPM Spec. Pub. **39**, 111-120.

Fink, P., Adamson, M., Jamal, F. and Stark, C. 2002. 'Seismic to simulation: integrated reservoir model for the Patricia Baleen gas field'. *APPEA Journal*, **43**, 83-111.

Fisher, W.L. 1969. 'Facies Characterisation of Gulf Coast Basin Delta Systems with some Holocene Analogues'. *Gulf Coast Association of Geological Societies Transactions*, **19**, 239 - 261.

Flett, M. Taggart, I., Gurton, R. and Lewis, J. 2003. 'Subsurface sensitivity study of geologic CO2 sequestration in saline formations'. 2nd *annual Conference on Carbon Sequestration, Alexandria, VA, Canada.*

Freund, P. 2001. 'Progress in understanding the potential role of CO_2 storage'. *In* Williams, D., Durie, B., McMullan, P., Paulson, C. and Smith, A. (Eds.) *Greenhouse*

Gas Control Technologies, Proceedings of the Fifth International Conference on Greenhouse Gas Control Technologies, CSIRO Publishing, Collingwood, Australia, 272 - 277.

Gale, J. 2002a. 'Geological storage of CO_2: what's known, where are the gaps and what more needs to be done', *Sixth International Conference on Greenhouse Gas Control Technologies* [online], Available: http://www.rite.or.jp/GHGT6/ [6 Nov. 2002].

Gale, J. 2002b. 'Overview of sources, potential, transport and geographical distribution of storage possibilities', *IPCC Workshop on Carbon Capture and Storage, Intergovernmental Panel on Climate Change*, Regina, Canada, 18-21 November 2002 (unpublished), 13-24.

Geovisual Systems 2000. *Geocard Users Guide*, Geovisual Systems Ltd, Berkshire, UK, 133 p.

Glenton, P.N. 1988. 'The Snapper development, Gippsland Basin', *APPEA Journal*, **28**, 29 - 40.

Gould, H.R. and McFarlan, E.1959. 'Geologic history of the chennier plain, southwest Louisiana', *Gulf Coast Association of Geological Societies Transactions*, **9**, 261-270.

Gunter, W.D and Perkins, E.H. 1993. 'Aquifer disposal of CO_2-rich gases: reaction design for added capacity'. *Energy Conservation and Management*, **34**, 9 - 11, 941 - 948.

Halmann, M.M. and Steinburg, M. 1999. *Greenhouse Gas Carbon Dioxide Mitigation: Science and Technology.* Lewis Publishers, Washington DC, 568 p.

Hawkins, D.G. 2002.' Pass gas: policy implications of leakage from geologic carbon storage sites'. *Sixth International Conference on Greenhouse Gas Control Technologies* [online], Available: http://www.rite.or.jp/GHGT6/ [6 Nov. 2002].

Helby, R. Morgan, R., and Partridge, A.D. 1987. 'A palynological zonation for the Australian Mesozoic', *Memoir of the Association of Australasian Palaeontologists* **4**, 1 – 97.

Hendricks, C.A. and Blok, K. 1993. 'Underground storage of carbon dioxide'. *Energy Conservation and Management,* **34**, 9 - 11, 949 - 957.

Hendricks, C.A. and Blok, K. 1995. 'Underground storage of carbon dioxide'. *Energy Conservation and Management,* **36**, 6 - 9, 539 - 542.

Henzell, S.T., Young, A.A. and Khurana, A.K. 1984. 'Reservoir simulation of the Gippsland Basin'. *APEA Journal*, **27**, 170 -179.

Herzog, H.J. 1999. 'Ocean sequestration of CO2—an overview,' *In* Riemer, P., Eliasson, B. and Wokaun, A. (Eds.) *Greenhouse Gas Control Technologies*, Elsevier Science Publishing, 237 - 242.

Hinton, P.V., Cousins, M.G. & Symes, P.E. 1994. The integration of modern technology in Gippsland's central fields study. *APEA Journal* **34**, 513 - 528.

Hohn, M.E. 1999, *Geostatistics and Petroleum Geology. 2*nd Edition, Kluwer Adademic Publishers, Dordrecht, Netherlands. 235 p.

Holloway, S., Rochelle, C.A., Batemen, K. ,Pearce, J.M., Baily, H.E., Metcalfe, R., Czernichowski-Lauriol, I., Sanjoun, B., Barbier, J., Fabriol, H., Summerfield, I.R., Lindeberg, E., Schwarzkopf, T., Putter, J., Keumbeck, M., Moller, H., Gaida, K.A., Kaarstad, O., Berger, B., Heederik, J.P., van der Meer, L.G.H., van der Straaten, R., Elewaut, E., Koelewijn, D., Cox, H., Harrison, R., and Doherty, P. 1996. *The Underground Disposal of Carbon Dioxide. British Geological Survey, Final Report of the JOULE II (Project No. CT92-0031)*, Holloway, S. (*Ed.*), British Geological Survey, Keyworth, Nottingham, 355 p.

Holloway, S. 1997. 'Safety of the underground disposal of carbon dioxide,' *Energy Conservation and Management* , **38**, s241 - s245.

Holloway, S. 1997. An overview of the underground disposal of carbon dioxide. *Energy Conservation and Management.* **38**, s193 - s198.

Holt, T., Jensen, J.I. and Lindeberg, E. 1995. 'Underground storage of CO2 in aquifers and oil reservoirs,' *Energy Conservation and Management*, **36**, 6 - 9, 535 - 538.

Jenkins, J.J. 1968. *The Geomorphology and upper Cainozoic Geology of south-east Gippsland, Victoria*, Geological Survey of Victoria Memoir **27**, 147 p.

Johnston, P. and Santillo, D. 2002. 'Carbon capture and sequestration: a realistic and responsible approach?' *IPCC Workshop on Carbon Capture and Storage, Intergovernmental Panel on Climate Change*, Regina, Canada, 18 - 21 November 2002 (unpublished), 79 - 83.

Johnstone, E.M., Jenkins, C.C. and Moore, M.A. 2001. 'An integrated structural and palaeographic investigation of the Eocene erosional events and related hydrocarbon potential in the Gippsland Basin,' In Hill, K.C. and Bernecker, T. (Eds.) *PESA Eastern Australian Basins Symposium,* Melbourne, Australia, 403 - 412.

Kaarstad, O. 2002. 'Geological storage, including costs and risks, in saline aquifers,' *IPCC Workshop on Carbon Capture and Storage, Intergovernmental Panel on Climate Change*, Regina, Canada, 18-21 November 2002 (unpublished), 44 - 51.

Kaldi, J.G. and Atkinson, C.D. 1997. 'Evaluating seal potential: example from the Talang Akar Formation, offshore northwest Java, Indonesia,' *In* Surdam, R.C. (Ed.) *Seals, Traps and the Petroleum System, AAPG Memoir* **67**, 85 - 101.

Klara, S.M., Srivastava, R.D. and Mcliuried, H.G. 2003. 'Integrated collaborative technology development program for CO2 sequestration in geologic formations,' *Energy Conservation and Management*, **21**:4, 247 – 253.

Kirste, D.M., Watson, M.N, and Tingate, P.R. 2004. 'Geochemical modelling of CO2-water-rock interaction in the Pretty Hill Formation, Otway Basin,' Department of Earth and Marine Sciences, Australian National University, Canberra, Australia (unpublished manuscript).

Kivior, T., Kaldi, J.G. and Lang, S.C. 2002. 'Seal potential in Cretaceous and late Jurrasic rocks of the Vulcan Sub-Basin, North West Shelf Australia'. *APPEA Journal*, **42**, 203 - 224.

Klusman, R.W. 2003. 'A geochemical perspective and assessment of leakage potential for a mature carbon dioxide-enhance oil recovery project and as a prototype

for carbon dioxide sequestration; Rangely field, Colorado,' *AAPG Bulletin* **87**, 9, 1485 – 1507.

Kraft, J.C. 1971. 'Sedimentary facies patterns and geologic history of a Holocene marine transgression,' *Geological Society of America* **82**, 2131-2158.

Kupfersberger, H. and Deutsch, C.V. 1999.' Methodology for integration analog geologic data in 3-D variogram modelling', *AAPG Bulletin*, **83**, 8, 1262 - 1278.

Lang, S.C., Kassan, J., Benson, J.M., Grasso, C.A. and Avenell, L.C., 2000. 'Applications of modern and ancient geological analogues in characterisation of fluvial and fluvial-lacustrine deltaic reservoirs in the Cooper Basin,' *APPEA Journal*, **40** (1), 393-415.

Lang, S.C., Greck, P., Root, R., Hill, A. and D. Harrison, 2001. 'The application of sequence stratigraphy to exploration and reservoir development in the Cooper-Eromanga-Bowen-Surat basin system,' *Australian Petroleum Production and Exploration Journal*, **41**, 223 – 249.

Lenstra, W.J. and Van Engelenburg, B.C.W. 2001. 'Climate policy, CO_2 storage and public perception,' *In* Williams, D., Durie, B., McMullan, P., Paulson, C. and Smith, A. *Greenhouse Gas Control Technologies, Proceedings of the Fifth International Conference on Greenhouse Gas Control Technologies*, CSIRO Publishing, Collingwood, Australia, 31 - 39.

Lindeberg, E. 1997. 'Escape of CO_2 from aquifers,' *Energy Conservation and Management*, **38**, S235-S240.

Lindeberg, E. 2002. 'The quality of a CO_2 repository: what is the sufficient retention tome of CO_2 stored underground?' *Sixth International Conference on Greenhouse Gas Control Technologies* [online], Available: http://www.rite.or.jp/GHGT6/ [6 Nov. 2002].

Liu, K., Paterson, L., Wong, P. and Qi, D. 2002. 'A sedimentological approach to upscaling,' *Transport in Porous Media*, **46**, 345-372.

Malek, R. and Mehin,K, 1998. *Oil and Gas Resources of Victoria*, Department of Natural Resources and Environment, Petroleum Development [online] Available: http://www.nre.vic.gov.au/web/root/domino/cm_da/nrenmp.nsf/frameset/NRE+Minerals+and+Petroleum?OpenDocument [1 Feb. 2003].

Markewich, H.W., Hacke, C.M. and Huddlestun, P.F. 1992. 'Emergent Pliocene and Pleistocene sediments of southeastern Georgia: an anomalous, fossil-poor, clastic section,' *In* Fletcher, C.H. and Wehmiller, J.F. (Eds.) *Quaternary Coasts of the United States: Marine and Lacustrine Systems*, SEPM Spec. Pub. **48**, 173 - 189.

McCubbin, D.G. 1982. 'Barrier-Island and Strand Plain Facies', *In* Scholle, P.A. and Spearing, D. (Eds.) *Sandstone Depositional Environments*, American Association of Petroleum Geologists, Tulsa.

Megallaa, M. 1993. 'Tectonic evolution of the Gippsland Basin and hydrocarbon potential of its lower shelf,' *APEA Journal*, **33**, 45 - 61.

Miall, A.D. 1996. *The Geology of Fluvial Deposits: Sedimentary Facies, Basin Analysis and Petroleum Geology*, Springer-Verlag, Berlin, 582 p.

National Oceanic and Atmospheric Administration, Global Warming, Frequently Asked Questions, [online] Available: http://lwf.ncdc.noaa.gov/oa/climate/globalwarming.html [9 Sept. 2002].

O'Sullivan, T. 2002. *Petrophysical Analysis of 20 Wells for GEODISC Assessment of the Gippsland Basin, Gippsland Basin, Australia*. Saros Group Report, Brisbane Australia, (unpublished).

Obdam, A., van der Meer, L., May, F. Kervevan, C., Bech, N., & Wildenborg, A. 2002. 'Effective CO_2 storage capacity in aquifers, gas fields, oil fields and coal fields,' *Sixth International Conference on Greenhouse Gas Control Technologies* [online], Available: http://www.rite.or.jp/GHGT6/ [6 Nov. 2002].

Oertel, G.F., Henry, V.J. and Foyle, A.M. 1991.' Implications of tide dominated lagoonal processes on the preservation of buried channels on sediment-starved continental shelf,' *Special. Publication, International. Association of Sedimentologists.* **14**, 379-393.

Pelgrain de Lestang, A, Cosentino, L., Cabrera, J., Jimenez, T., and Bellorin, O. 2002. 'Geologically oriented geostatistics: an integrated tool for reservoir studies,' *SPE Journal* (SPE 74371), 1-10.

Pemberton, S.G., MacEachern, J.A. and Frey, R.W. 1992. 'Trace fossil facies models: environmental and allostratigraphic significance', *In* Walker, R.G. and James, N.P. *Facies Models, Response to Sea Level Change*, Geological Association of Canada, Canada, 47 – 72.

Perry, K.F. 2003. *Gas Storage Technology Applicability to CO2 Sequestration, Final Technical Report*, CO2 Capture Project, Gas Technology Institute, Des Plaines, Illinois (unpublished).

Posamentier, H.W. and Allen, G. P. 1999, *Siliciclastic Sequence Stratigraphy - Concepts and Application*, SEPM Concepts in Sedimentology and Palaeontology, no. **7**, 216 p.

Power, M.R., Hill, K.C., Hoffman, N., Bernecker, T. and Norvick, M. 2001. 'The structural and tectonic evolution of the Gippsland Basin: results from 2D section balancing and 3D structural modelling,' *In* Hill, K.C. and Bernecker, T. (Eds.) *PESA Eastern Australian Basins Symposium 2001*, Melbourne, Australia, 371 - 385.

Rahmanian, V.D., Moore, P.S., Mudge, W.J. and Spring, D.E. 1990. 'Sequence stratigraphy and the habitat of hydrocarbons, Gippsland Basin, Australia,' *In* Brooks, J. (Ed.) *Clastic Petroleum Provinces*, Geological Society Special Publication, **50**, 525 - 541.

Reid, I. and Frostick 1994.'Fluvial sediment transport and deposition,' *In:* Pye, K. (Ed.) *Sediment Transport and Depositional Processes,* Blackwell Scientific, Edinburgh, 89 - 144.

Reineck, H. E. and Singh, I.B. 1975. *Depositional Sedimentary Environments with Reference to Terrigenous Clastics*, Spring-Verlag, New York, 155 p.

Reinson, G.E. 1979. 'Transgressive barrier island and estuarine systems,' *In* Walker, R.G. (Ed.) *Facies Models*, Geoscience Canada Reprint Series 1, 179 - 194.

Rigg, A. and Bradshaw, J. 2001. 'The GEODISC program research into geological sequestration of CO_2 in Australia'. *In* Williams, D., Durie, B., McMullan, P., Paulson, C. & Smith, A. (Eds.) *Greenhouse Gas Control Technologies, Proceedings of the Fifth International Conference on Greenhouse Gas Control Technologies*, CSIRO Publishing, Collingwood, Australia, 254 - 259.

Rigg, A.J., Allinson, G., Bradshaw, J., Ennis-King, J., Gibson-Poole, C.M., Hillis, R.R., Lang, S.C., Streit, J.E. 2001. 'The search for sites for geological sequestration of CO2 in Australia: a progress report on GEODISC,' *The APPEA Journal*, **41**, 711 - 725.

Rochelle, L.A., Pearce, J.M. and Holloway, S. 1999. 'The underground sequestration of carbon dioxide: containment by chemical reactions in the deep geosphere,' *In* Metcalfe, R. and Rochelle, C.A. (Eds.) *Chemical Containment of Waste in the Geosphere*, Geological Society of London, Spec. Pub. **157**, 117 - 129.

Roder, G.H. and Sloan, M.W. 1986. Barracouta: history of exploration and development, and geology of the field. *In* Glenie, R.C. (Ed.) *Second South-Eastern Australia Oil Exploration Symposium*, Petroleum Exploration Society of Australia, Melbourne, 75 – 87.

Root, R.S., Gibson-Poole, C.M., Lang, S.C., Streit, J.E., Underschultz, J. and Ennis-King, J. 2004. 'Opportunities for geological storage of carbon dioxide in the offshore Gippsland Basin, SE Australia: an example from the Upper Latrobe Group,' *Eastern Australian Basin Symposium II*, Adelaide, Australia.

Saucier, R. 1967, *Geological investigation of the Boenf-Tensas basin, Talla-Bena 15 minute quadrangle*. US Army Corp. Engineers, Vicksberg, MS.

Schmidt, V. and McDonald, D.A. 1979. 'Pore geometry and reservoir aspects of secondary porosity,' *In* Scholle, P.A. and Schluger, P.R. (Eds.) *Aspects of Diagenesis*, Society of Economic Palaeontologists and Mineralogists Special Publication **26**, 185 – 207.

Schowalter, T.T. 1979. 'Mechanics of secondary hydrocarbon migration and entrapment,' *AAPG Bulletin*, **63**, 5, 723 – 760.

Shafik, S. Glenn, K.C., Bernecker, T., Gallagher, S.J., Edwards, D.S., Holdgate, G.R., Mehin, K. Chaproniere, G.C.H. and Wollands, M. 1998. *Gippsland Basin Biozonation & Stratigraphy, Chart 18*. Australian Geological Survey Organisation, Canberra, Australia.

Shideler, G.L. 1978, 'A sediment dispersal model for the south Texas continental shelf, northwest Gulf of Mexico,' Marine Geology, **26,** 289-313.

Span, R. and Wagoner, W. 1996. 'A new equation of state for carbon dioxide covering the fluid region from triple-point temperature to 1100k at pressures up to 800 MPa,' *Journal of Physical Chemistry, Ref. Data*, **25**, 6, 1509 - 1596.

Stevens, S.H., Kuuskraa, V.A. and Gale, J. 2001. 'Sequestration of CO_2 in depleted oil and gas fields: global capacity, costs, and barriers,' *In* Williams, D., Durie, B., McMullan, P., Paulson, C. and Smith, A. (Eds.) *Greenhouse Gas Control Technologies, Proceedings of the Fifth International Conference on Greenhouse Gas Control Technologies*, CSIRO Publishing, Collingwood, Australia, 254 - 259.

Streit, J. E. 2003. *Geomechanical Analysis of the Offshore Gippsland Basin, South East Australia. GEODISC Project 4*, GEODISC Internal Report (unpublished), Adelaide, Australia, 33 p.

Studlick, J.R.J., Shew, R.D., Basye, G.L. and Ray, J.R. 1990. 'A giant carbon dioxide accumulation in the Norphlet Formation, Pisgah Anticline, Mississippi,' *In* Barwis, J.H., McPherson, J.G. and Studlick, J.R.J. (Eds.) *Sandstone Petroleum Reservoirs*, Sringer-Verlag, New York, 181 - 203.

The Australian Greenhouse Office [online], Available: http://www.greenhouse.gov.au/ [6 Sept. 2002].

Torp, T.A and Gale, J. 2002. 'Demonstrating storage of CO2 in geological reservoirs: the Sleipner and SACS projects,' *Sixth International Conference on Greenhouse Gas Control Technologies* [online], Available: http://www.rite.or.jp/GHGT6/ [6 Nov. 2002].

United States Department of Energy 2002. Fossil.energy.gov, A US Department of Energy Web Site. [online] Available: http://www.fe.doe.gov/coal_power/sequestration/index.shtml [6 Sept, 2002].

van der Meer, L.G.H. 1992. 'Investigations regarding the storage of carbon dioxide in aquifers in the Netherlands,' *Energy Conservation and Management*, **34**, 611 - 618.

van der Meer, L.G.H. 1995. 'The storage efficiency of aquifers', *Energy Conservation and Management*, **36,** 6-9,513 – 518.

van der Meer, L.G.H., Arts, R.J. and Peterson, L. 2001. 'Prediction of migration of CO2 after injected in a saline aquifer: reservoir history matching of a 4D seismic image with a compositional gas/water model,' *Proceedings of the Fifth International Conference on Greenhouse Gas Control Technologies*, CSIRO Publishing, Australia, 378 – 384.

Van Wagoner, J.C., Mitchum, Jr., R.M., Campion, K.M., and Rahmanian, V.D. 1990. 'Siliciclastic sequence stratigraphy in well logs, cores and outcrops: concepts for high-resolution correlation of time facies', *AAPG Methods in Exploration Series* **7**, 55 p.

Veevers, J.J. 1984. *Phanerozoic Earth History of Australia*. Clarendon, Oxford, 212 p.

Werren, E.G., Shew, R.D., Adams, E.R., and Stancliffe, R.J. 1989. 'Meander Belt Reservoir Geology, Mid-Dip Tuscaloosa, Little Creek Field, Mississippi,' *In* Barwis, J.H., McPherson, J.G., Studlick, J.R.J. (Eds.) *Sandstone Petroleum Reservoirs*, Springer-Verlag, New York, 583 p.

Wildenborg, A.F.B. and van der Meer 2002. 'The use of gas and coal fields as CO_2 sinks,' *IPCC Workshop on Carbon Capture and Storage, Intergovernmental Panel on Climate Change*, Regina, Canada, 18-21 November 2002 (unpublished), 44 - 51.

Wilson, M., Moberg, R., Stewart, B. and Thambimuthu, K. 2001. 'CO2 sequestration in oil reservoirs—a monitoring and research opportunity,' *In* Williams, D., Durie, B., McMullan, P., Paulson, C. and Smith, A, *Greenhouse Gas Control Technologies,*

Proceedings of the Fifth International Conference on Greenhouse Gas Control Technologies, CSIRO Publishing, Collingwood, Australia, 243 - 247.

Wright, L.D. and Coleman, J.M. 1976. 'Variations in morphology of major river deltas as functions of ocean waves and river discharge regimes', *In Modern Deltas, Selected Papers Reprinted from Recent Sediments, Northwest Gulf of Mexico*; AAPG Bulletin; Geometry of Sandbodies, AAPG Reprint Series No. **18**, 226 p.

Zillman, J.W. 2001. The science of climate change: an update. Greenhouse Gas Control Technologies', *In* Williams, D., Durie, B., McMullan, P., Paulson, C. and Smith, A, *Greenhouse Gas Control Technologies, Proceedings of the Fifth International Conference on Greenhouse Gas Control Technologies*, CSIRO Publishing, Collingwood, Australia, 11 - 21.

Appendix I—Eastern Australian Basin Symposium II Conference Paper

Root, R., Gibson-Poole, C. M., Lang, S., Streit, J. E., Underschultz, J., & Ennis-King, J. (2004). Opportunities for geological storage of carbon dioxide in the offshore Gippsland Basin, SE Australia: an example from the upper Latrobe Group *In: Eastern Australasian Basins Symposium II EABS04; 19-22nd November 2004; Adelaide, South Australia. 367-388.*

NOTE:

This publication is included in the print copy
of the thesis held in the University of Adelaide Library.